

ROBERTO ZANETTI FREIRE

**NUMERICAL SIMULATION OF PHOTOVOLTAIC HYBRID
VENTILATION SYSTEMS COMBINED WITH A
WHOLE-BUILDING HYGROTHERMAL MODEL**

CURITIBA, BRAZIL

May, 2010

ROBERTO ZANETTI FREIRE

**NUMERICAL SIMULATION OF PHOTOVOLTAIC HYBRID
VENTILATION SYSTEMS COMBINED WITH A
WHOLE-BUILDING HYGROTHERMAL MODEL**

Thesis submitted to the Mechanical
Engineering Graduate Program of the
Pontifical Catholic University of Parana in
partial fulfillment of the doctoral degree.

Supervisor:
Nathan Mendes

Co-supervisor:
Marc Olivier Abadie

PONTIFICAL CATHOLIC UNIVERSITY OF PARANA - PUCPR

CURITIBA, BRAZIL

May, 2010

Doctoral thesis entitled: “*Numerical Simulation of Photovoltaic Hybrid Ventilation Systems Combined with a Whole-Building Hygrothermal Model*” presented by Roberto Zanetti Freire on May 7th, 2010, in Curitiba city - Parana - evaluated by the following research professors:

Prof. Dr. Nathan Mendes
PPGEM/PUCPR
Supervisor

Prof. Dr. Marc Olivier Abadie
LEPTIAB/University of La Rochelle
Co-Supervisor

Prof. Dr. Paulo Smith Schneider
UFRGS

Prof. Dr. Roberto Lamberts
LABEEE/UFSC

Prof. Dr. Luís Mauro Moura
PPGEM/PUCPR

*This thesis is dedicated to my parents
for their love, endless support
and encouragement.*

Agradecimentos

Aos meus pais, Carlos Dalberto Freire e Loredana Zanetti Freire, pelo amor, carinho e orientação com que conduziram minha formação educacional e profissional, e que me permitiram chegar até aqui. Agradeço também a minha irmã, Giovanna Paula Zanetti Freire, que foi a pessoa da família mais próxima durante o período de realização deste trabalho.

Ao Professor Nathan Mendes que, mais do que orientador, foi também professor, companheiro e amigo. Obrigado pela paciência e dedicação exemplares, responsável por direcionar minha vida profissional a pesquisa científica, exemplo de competência e humildade.

Ao Professor Marc Olivier Abadie, co-orientador deste trabalho, companheiro e amigo, imprescindível para realização e sucesso deste trabalho, um exemplo de competência e dedicação a pesquisa.

Aos Professores Paulo Smith Schneider, Roberto Lamberts e Luís Mauro Moura, por terem aceito participar da banca de avaliação, contribuindo, através de relevantes sugestões, com o resultado final deste trabalho.

Aos amigos e companheiros do Laboratório de Sistemas Térmicos da Pontifícia Universidade Católica do Paraná, em especial ao professores Gerson Henrique dos Santos e Ricardo Coração de Leão Fontoura de Oliveira, e aos amigos Rogério Marcos Barbosa e Walter Mazuroski, todos prontamente dispostos a compartilhar seus conhecimentos.

Agradeço aqui a paciência e o incentivo de todos aqueles que me ajudaram a construir este trabalho e sem os quais o mesmo não se realizaria.

Agradeço em especial à CAPES, Coordenação de Aperfeiçoamento de Pessoal de Nível Superior, pelo auxílio financeiro e suporte a este trabalho.

Contents

List of Figures	p. x
List of Tables	p. xiv
Nomenclature	p. xvi
Abbreviations	p. xxii
Abstract	p. xxiii
Resumo	p. xxiv
1 Introduction	p. 1
1.1 Problem Statement	p. 1
1.2 Motivation	p. 1
1.3 Literature Review	p. 6
1.3.1 Natural Ventilation	p. 7
1.3.2 Renewable Technology Integration	p. 7
1.3.3 Hybrid Ventilation	p. 10
1.3.4 Photovoltaic Hybrid Ventilation	p. 11
1.4 Brief Methodology Description	p. 12
1.5 Escope of the Present Work	p. 12
1.6 Dissertation Structure	p. 13
2 Natural Ventilation: Modeling	p. 16

2.1	State-of-Art	p. 17
2.2	Physical Fundamentals	p. 18
2.2.1	Thermal Buoyancy	p. 18
2.2.2	Wind	p. 20
2.2.3	Combination of Thermal Buoyancy and Wind	p. 21
2.3	Pressure Coefficient Calculation	p. 22
2.3.1	Mean C_P Equation	p. 22
2.3.2	CPCALC Model	p. 23
2.4	Cross-Ventilation	p. 24
2.4.1	Airflow Driven by Thermal Buoyancy through More than One Opening	p. 24
2.4.2	Airflow Driven by Wind	p. 25
2.4.3	Airflow Driven by Wind and Thermal Buoyancy	p. 26
2.5	Single-Sided Ventilation	p. 27
2.5.1	de Gids and Phaff (1982)	p. 27
2.5.2	British Standards (1999)	p. 28
2.5.3	ASHRAE (2005)	p. 28
2.5.4	Larsen (2006)	p. 29
2.6	Implementation	p. 30
2.6.1	Important Considerations	p. 31
2.6.2	Cross Ventilation - Thermal Buoyancy Effect	p. 33
2.6.3	Cross Ventilation - Wind Effect	p. 34
2.7	Chapter Remarks	p. 35
3	Natural Ventilation: Validation Procedures	p. 36
3.1	Experiments	p. 36
3.1.1	Wind Tunnel Experiment	p. 37

3.1.2	On-Site Experiment	p. 37
3.2	Validation Results	p. 40
3.2.1	Wind Tunnel Simulations	p. 40
3.2.1.1	Cross Ventilation	p. 40
3.2.1.2	Single-Sided Ventilation	p. 41
3.2.2	On-Site Simulations	p. 44
3.3	Chapter Remarks	p. 45
4	Comparative Analysis: Natural Ventilation versus Air-Conditioning Systems	p. 46
4.1	HVAC System	p. 49
4.1.1	Primary System Components	p. 50
4.1.1.1	Chiller Model	p. 51
4.1.1.2	Pump Model	p. 53
4.1.2	Secondary System Components	p. 53
4.1.2.1	Mixing Box Model	p. 53
4.1.2.2	Cooling and Dehumidification Coil Model	p. 54
4.1.2.3	Fan Model	p. 54
4.2	Thermal Comfort	p. 55
4.2.1	ASHRAE Thermal Sensation Index (ATS)	p. 55
4.2.2	Predicted Mean Vote (PMV)	p. 56
4.2.3	Acceptability of Air	p. 58
4.2.4	Acceptable Thermal Conditions in Naturally Conditioned Spaces	p. 58
4.3	Mould Growth Risk	p. 61
4.4	Simulation Procedure	p. 63
4.4.1	Building Description	p. 64
4.4.2	HVAC Parameters	p. 65

4.4.2.1	Primary Systems (Plant) with Air Cooled Chiller (SP-AIR)	p. 65
4.4.2.2	Secondary System	p. 65
4.4.3	Simulations and Reports	p. 66
4.5	Results	p. 68
4.5.1	Mould Growth Risk Analysis	p. 69
4.5.2	Thermal Comfort and Acceptability of Air	p. 72
4.6	Chapter Remarks	p. 75
5	Building-Integrated Photovoltaic Systems: Modeling	p. 76
5.1	Solar Energy and Photovoltaic Simulation	p. 77
5.2	Array Modeling	p. 80
5.2.1	Model Parameters	p. 81
5.2.2	Mathematical Description of the Four-Parameter Model	p. 81
5.2.3	Determining Performance under Operating Conditions	p. 82
5.2.4	Calculating $I_{L,ref}$, $I_{o,ref}$, γ , and R_s	p. 83
5.2.5	Module Operating Temperature (Thermal Model)	p. 85
5.2.6	Incident Angle Modifier Correlation	p. 86
5.2.7	Multi-Array Modules	p. 87
5.3	Battery	p. 88
5.3.1	Discharge Calculation Method	p. 89
5.3.2	Charge Calculation Method	p. 90
5.4	Load Calculation	p. 91
5.4.1	General Demand	p. 91
5.4.2	Integration to Central HVAC System	p. 92
5.4.3	Fan Model	p. 92
5.4.4	Load and Building Hygrothermal Model Integration	p. 93

5.5	Integration of Photovoltaic Modules to the Building Structures	p. 96
5.5.1	Energy Model	p. 96
5.5.2	Moisture Model	p. 97
5.6	Chapter Remarks	p. 97
6	Building-Integrated Photovoltaic Systems: Verification Procedures	p. 99
6.1	Photovoltaic System Verification	p. 99
6.1.1	Radiation	p. 99
6.1.2	Array Generation	p. 101
6.1.3	Incident Angle Modifier	p. 102
6.2	Hygrothermal Effects of Photovoltaic Systems Integration	p. 104
6.2.1	Building and Photovoltaic System Description	p. 104
6.2.2	Simulation Parameters	p. 105
6.2.3	Results using a Purely Conductive Heat Transfer Model	p. 106
6.2.4	Results using a Combined Heat and Moisture Transport Model	p. 108
6.3	Chapter Remarks	p. 114
7	Comparative Analysis: Natural Ventilation versus Photovoltaic Hybrid Ventilation	p. 115
7.1	Hybrid Ventilation Systems	p. 116
7.2	Brazilian Potential for Natural Ventilation Applications	p. 117
7.3	Brazilian Potential for BIPV Applications	p. 117
7.4	Ventilation Requirements	p. 118
7.4.1	Ventilation in Dwellings	p. 119
7.4.2	Ventilation in Offices	p. 120
7.4.3	Brazilian Standards for Indoor Air Quality	p. 120
7.5	Hybrid Ventilation Strategy	p. 121
7.6	Case Study	p. 123

7.6.1	Building Description	p. 123
7.6.2	BIPV System Description	p. 124
7.6.3	Simulations Parameters and Reports	p. 126
7.7	Results	p. 126
7.8	Natural Ventilation Comparisons	p. 126
7.9	Chapter Remarks	p. 133
8	Final Remarks	p. 134
8.1	General Overview	p. 134
8.2	Natural Ventilation	p. 135
8.3	Building Integrated Photovoltaic systems	p. 136
8.4	Photovoltaic Hybrid Ventilation	p. 137
8.5	Further Works	p. 137
	References	p. 139
	Annex 1: CPCALC Validation	p. 148
	Annex 2: Equipment Data	p. 164

List of Figures

1.1	The approximate service and residential sector shares of primary energy use of 13 industrialized countries (Schipper and Meyers, 1992).	p. 3
1.2	End use shares of delivered energy use in the service and residential sectors (Schipper and Meyers, 1992).	p. 3
1.3	Dissipation of space conditioning energy in the service and residential sectors (Schipper and Meyers, 1992).	p. 4
1.4	Electricity - Supply according to primary generation source: (a) World (IEA, 2007) and (b) Brazil (EPE, 2009).	p. 4
1.5	Brazilian electricity consumption by sector.	p. 5
2.1	Pressure difference around the neutral plane in a building ventilated only by thermal buoyancy (Larsen, 2006) - case of $T_i > T_e$	p. 20
2.2	Variation of surface-averaged wall pressure coefficients for low-rise buildings (ASHRAE, 2005a).	p. 23
2.3	Cross-ventilation driven by temperature difference only.	p. 25
2.4	Cross-ventilation driven by wind only.	p. 26
2.5	Cross-ventilation driven by wind and thermal buoyancy.	p. 27
2.6	Example of natural ventilation model usage.	p. 32
2.7	Determination of the neutral plane location.	p. 34
3.1	Experiments designs performed into the PowerDomus software for the wind tunnel: (a) cross ventilation case and (b) single-sided ventilation case.	p. 38
3.2	Experiment design performed into the PowerDomus software for the on-site single-sided ventilation case.	p. 38
3.3	Window parts for the on-site experiment.	p. 39

3.4	Comparisons between the experimental and simulation results performed for the wind tunnel - cross ventilation case.	p. 40
3.5	Comparisons between the experimental and simulation results performed into the PowerDomus software for the wind tunnel case with wind speed of 1 m/s - single-sided ventilation case.	p. 42
3.6	Comparisons between the experimental and simulation results performed into the PowerDomus software for the wind tunnel case with wind speed of 3 m/s - single-sided ventilation case.	p. 42
3.7	Comparisons between the experimental and simulation results performed into the PowerDomus software for the wind tunnel case with wind speed of 5 m/s - single-sided ventilation case.	p. 43
3.8	Comparisons between the experimental and simulation results performed into the PowerDomus software for the NOA Building case.	p. 44
4.1	Central cooling system: primary components.	p. 50
4.2	Central cooling system: secondary components.	p. 51
4.3	Acceptable operative temperature ranges for naturally conditioned spaces (ASHRAE, 2004).	p. 60
4.4	Two-storey office building geometric characteristics.	p. 65
4.5	Correlation between PMV and PPD.	p. 68
4.6	Daily mean relative humidity for the indoor roof surface.	p. 69
4.7	Mould growth risk for one year simulation.	p. 70
4.8	Mould growth risk for one year simulation (window open from 8 <i>am</i> to 9 <i>am</i>).	p. 71
4.9	Mould growth risk for one year simulation (window open from 8 <i>am</i> to 10 <i>am</i>).	p. 71
4.10	Mould growth risk for one year simulation (window open from 8 <i>am</i> to 11 <i>am</i>).	p. 72
4.11	Comfort zone using natural ventilation from 8 <i>am</i> to 6 <i>pm</i>	p. 73
5.1	Examples of building-integrated photovoltaic systems.	p. 77

5.2	Equivalent electrical circuit in the four-parameter model.	p. 82
5.3	Incidence Angle Modifier of King <i>et al.</i> , 1997.	p. 87
5.4	Flowchart for PV array model.	p. 88
5.5	Flowchart for the battery model.	p. 89
6.1	Total solar radiation comparisons between PowerDomus, PVSYST and TRNSYS software.	p. 101
6.2	Energy conversion comparisons when incident angle modifier is not considered.	p. 102
6.3	Energy conversion comparisons considering incident angle modifier. . .	p. 103
6.4	PV array representation on the two-storey office building.	p. 105
6.5	Daily-averaged values of temperature at the Zone 2 internal ceiling surface (with and without PV system) considering a purely conductive heat transfer model was adopted.	p. 107
6.6	Daily-averaged values of indoor air temperature of Zone 2 (with and without PV system) considering a purely conductive heat transfer model was adopted.	p. 108
6.7	Daily-averaged values of temperature at the Zone 2 internal ceiling surface (with and without PV system) considering a combined heat and moisture transport model.	p. 109
6.8	Daily-averaged relative humidity at the Zone 2 internal ceiling surface (with and without PV system) considering combined heat and moisture transport model.	p. 110
6.9	Daily-averaged values of indoor air temperature of Zone 2 (with and without PV system) considering combined heat and moisture transport model.	p. 110
6.10	Daily-averaged relative humidity at the Zone 1 internal ceiling surface (with and without PV system) considering combined heat and moisture transport model.	p. 111
6.11	Mould Growth Risk at the internal ceiling surface of ground level. . . .	p. 112
6.12	Mould Growth Risk at the internal ceiling surface of first level.	p. 112

6.13	Daily-averaged values of temperature at the Zone 2 internal ceiling surface for both purely conductive heat transfer and combined heat and moisture transport models.	p. 113
6.14	Daily-averaged values of indoor air temperature of Zone 2 for both purely conductive heat transfer and combined heat and moisture transport models.	p. 113
7.1	Demographic and wind energy potential maps for Brazil.	p. 118
7.2	Brazilian solar atlas - yearly average of the daily global radiation and its percentage variation on horizontal plane (Ordenes <i>et al.</i> , 2007).	p. 118
7.3	Hybrid ventilation algorithm flowchart.	p. 122
7.4	PV array representation on the top of the two-storey office building. . .	p. 123
7.5	Comfort zone using just natural ventilation from 8 <i>am</i> to 9 <i>am</i>	p. 127
7.6	Comfort zone using natural ventilation from 8 <i>am</i> to 9 <i>am</i> and hybrid ventilation when necessary.	p. 128
7.7	Mould growth risk when just natural ventilation is considered.	p. 130
7.8	Mould growth risk when hybrid ventilation is considered.	p. 130
7.9	Daily-averaged values of relative humidity at the internal ceiling surface when just natural ventilation is considered.	p. 131
7.10	Daily-averaged values of relative humidity at the internal ceiling surface when hybrid ventilation is considered.	p. 132
7.11	Simulation results for the first week of July (PV power management). .	p. 132

List of Tables

2.1	Reference values for the wind velocity profile exponent.	p. 24
2.2	Constants C_1 , C_2 and C_3 (Larsen, 2006).	p. 30
3.1	Window dimensions for the on-site experiment.	p. 39
3.2	Opening configuration and mean climatic conditions for single-sided ventilation experiments in the NOA building.	p. 39
3.3	Relative differences (%) for the wind tunnel experiment - cross ventilation case.	p. 41
3.4	Relative differences (%) for the wind tunnel experiment - single-sided ventilation case.	p. 44
3.5	Relative differences (%) for the NOA Building experiment.	p. 45
4.1	Criteria for HVAC system and equipment selection (Haines and Wilson, 2004).	p. 50
4.2	ASHRAE thermal sensation scale.	p. 56
4.3	Mould growth risk index description.	p. 61
4.4	Materials physical characteristics.	p. 64
4.5	Air-cooled chiller simulation parameters.	p. 65
4.6	Air-cooled chiller capacity and efficiency coefficients.	p. 66
4.7	Model parameters for the pumps.	p. 66
4.8	Cooling coil simulation geometric parameters.	p. 67
4.9	Model parameters for the fan.	p. 67
4.10	Percentage of time within the comfort zone for both pressure coefficient calculation methods.	p. 73

4.11	Percentage of time within the comfort zone when air-conditioning system is considered.	p. 74
4.12	Percentage of time within the comfort zone when air-conditioning system is considered (ATS index).	p. 75
5.1	PV module characteristics of standard technologies.	p. 85
6.1	Photovoltaic panel electrical characteristics.	p. 100
6.2	Monthly converted power differences between TRNSYS and PowerDomus when the incident angle modifier correlation is adopted.	p. 103
6.3	Glass characteristics.	p. 105
6.4	Yearly degree-hours of cooling and heating for building zones 1 and 2 when a purely conductive heat transfer through the building envelope model was adopted.	p. 106
6.5	Yearly degree-hours of cooling and heating for building zones 1 and 2 when a combined heat and moisture transport model was adopted.	p. 108
7.1	Minimum ventilation criteria for dwellings.	p. 119
7.2	Minimum ventilation criteria for offices.	p. 120
7.3	Minimum ventilation rates according to the Brazilian Standard NBR 6401-08.	p. 121
7.4	Model parameters for the fan used in the hybrid ventilation strategy.	p. 124
7.5	Percentage of time within the comfort zone without hybrid ventilation.	p. 128
7.6	Percentage of time within the comfort zone when hybrid ventilation is considered (8 <i>am</i> - 6 <i>pm</i>).	p. 129
7.7	Monthly energy demand.	p. 129
7.8	Monthly energy demand from January to June.	p. 131
7.9	Annual energy demand.	p. 131

Nomenclature

Symbols:

A_b - total opening area when the pressure difference is caused by the thermal buoyancy (m^2)

A_o - opening area (m^2)

A_w - total opening area when the pressure difference is caused by the wind (m^2)

A_Z - occupied area (m^2)

C - capacity (Ah)

C_D - discharge coefficient for window opening ($-$)

C_P - pressure coefficient ($-$)

c_P - specific heat ($J/kg K$)

C_V - effectiveness coefficient of the opening ($-$)

d - differentiation

D_T - moisture transport coefficient associated to a temperature gradient $m^2/(s K)$

D_{TV} - vapor phase transport coefficient associated to a temperature gradient ($m^2/(s K)$)

D_θ - moisture transport coefficient associated to a moisture content gradient (m^2/s)

$D_{\theta V}$ - vapor phase transport coefficient associated to a moisture content gradient (m^2/s)

e - thickness (m)

E - power (W)

\dot{E}_t - energy transfer rate that crosses the room control surface (W)

\dot{E}_g - internal energy generation rate (W)

F_A - air flow considering the occupied area ($l/(s m^2)$)

f_{cl} - clothing area factor ($-$)

- g - gravity acceleration (m/s^2)
- G_T - total solar irradiance that reaches a specific surface (W/m^2)
- h - (moist air) enthalpy (kJ/kg)
- H - height above the reference (m)
- h_c - convective heat transfer coefficient (W/m^2K)
- h_m - convective mass transfer coefficient (m/s)
- H_o - opening height (m)
- h_r - radiative heat transfer coefficient ($W/m^2 K$)
- I - current (A)
- I_{cl} - clothing insulation (clo)
- I_L - photocurrent (A)
- I_o - reverse saturation current (A)
- j_v - vapor flow (density) ($kg/(m^2 s)$)
- k - battery constant ($-$)
- L - vaporization latent heat (J/kg)
- L_1 - length of a building exterior surface where the opening is placed (m)
- L_2 - length of a building exterior surface orthogonal to the opening surface (m)
- M - metabolic rate (W/m^2)
- \dot{m} - air mass flow rate (kg/s)
- N - number of modules ($-$)
- N_{cells} - number of individual cells in module ($-$)
- P - air pressure (Pa)
- pad - plan area density (%)
- PLR - part-load ratio ($-$)
- P_{SAT} - water vapor saturation pressure (kPa)
- P_T - local barometric pressure (kPa)

- P_V - partial vapor pressure (kPa)
- P_Z - maximum number of people in the ventilated building zone ($-$)
- Q - chiller cooling capacity (W)
- Q_V - airflow rate (m^3/s)
- R_s - series resistance (Ω)
- R_{sh} - module shunt resistance (Ω)
- sbh - surround building height (m)
- SQ - surface quality ($-$)
- t - time (s)
- T - temperature (K)
- T_{bs} - dry bulb temperature ($^{\circ}C$)
- T_{cl} - mean temperature of the outer surface of the clothed body ($^{\circ}C$)
- t_d - hour rating that the battery is specified against (hours)
- t_h - battery discharge time (hours)
- t_m - time needed for the initial of mould growth in constant temperature (week)
- T_o - operative temperature ($^{\circ}C$)
- T_{rm} - mean radiant temperature ($^{\circ}C$)
- t_v - time needed for the first visual appearance of mould growth (week)
- U_{10} - reference air speed at 10-meter height (m/s)
- U_z - air speed at z -meter height (m/s)
- $U_{z=BH}$ - wind velocity at the building height (m/s)
- v - air speed (m/s)
- V - voltage (V)
- \dot{V} - volumetric flow (l/s)
- V_{room} - building zone volume (m^3)
- w - humidity ratio (kg water/ kg dry air)

W - external work (W/m^2)

W_{mat} - material constant (—)

y_1 - photovoltaic array width (m)

y_2 - photovoltaic array length (m)

∂ - partial-derivative

Greek Letters:

α - absorptance (—)

α_R - wind speed profile (—)

β - wind incident angle ($^\circ$)

γ - empirical photovoltaic curve-fitting parameter (—)

Δ - Difference between two variables (—)

ε - porosity (—)

η - efficiency (—)

θ - volume basis moisture content (m^3/m^3)

λ - thermal conductivity ($W/m^2 K$)

ξ - solar radiation incidence angle ($^\circ$)

ρ - density (kg/m^3)

τ - transmittance (—)

ω - slope of the PV array ($^\circ$)

ϕ - relative humidity (%)

Subscripts:

a - air

A - array

AC, DC - inverter AC or DC

b - battery

c - photovoltaic collector

cd - condenser

ch - charger

comp - compressor

crit - critical

D - demand

diff - diffuse

e - external

eff - effective value

eq - equipment

ev - evaporator

gnd - ground-reflected

i - internal

in - inlet

inf - infiltration

j - *j*-th surface

l - liquid, water

M - averaged value

max - maximum or full load

mp - maximum power

MR - reference (current or voltage) at maximum power

NPL - neutral plane level

out - outlet

rat - rating conditions

ref - reference

sup - upper limit

surf - surface

v - water vapor

vent - ventilation

Abbreviations

ACE - Acceptability of Air Index

ACS - Adaptive Comfort Standard

ASHRAE - American Society of Heating, Refrigerating and Air-Conditioning Engineers

ATS - ASHRAE Thermal Sensation Index

BIPV - Building-Integrated Photovoltaic

CFD - Computational Fluid Dynamics

CPCALC - Algorithm for calculating wind pressure coefficients at specific positions on the envelope of a building

HVAC - Heating, Ventilating and Air-Conditioning

IAM - Incidence Angle Modifier

IAQ - Indoor Air Quality

IEA - International Energy Agency

Mean C_P - expression which calculates a mean pressure coefficient value of a selected surface on a low-rise building associated to the variation of the incidence angle

MGR - Mould Growth Risk

MTDMA - MultiTriDiagonal Matrix Algorithm

NOA - National Observatory of Athens

NOCT - Nominal Operating Cell Temperature

NV - Natural Ventilation

PMV - Predicted Mean Vote

PPD - Predicted Percentage of Dissatisfied

PV - Photovoltaic

Abstract

Air-conditioning systems were in the past considered as the ultimate choice to provide thermal comfort and indoor air quality to building occupants, but today, with a need of reducing energy consumption, alternative solutions have to be developed and implemented. Natural ventilation can be an appropriate choice to save substantial amounts of energy while still providing comfortable and pleasant environments for the occupants. Another attractive solution is using clean renewable energy to power up HVAC (Heating, Ventilating and Air-Conditioning) components as new technologies become more efficient and cheaper.

Based on the Brazilian potential for using natural ventilation and solar energy, this work aims at evaluating the use of both natural and photovoltaic-powered hybrid ventilation by integrating state-of-the-art numerical models in the Brazilian Building Energy Simulation program PowerDomus.

First, natural ventilation physical principles are presented. The implementation of numerical models is then described followed by validation against experimental results. Additional contributions by refining the pressure coefficient calculations have been provided and compared to both wind tunnel and on-site experiments. Then, some analyses contrasting natural ventilation and an air-conditioning system in terms of mould growth, energy consumption, thermal comfort and acceptability of air for a specific case study are presented.

In the sequence, the solar energy conversion of photovoltaic cells has been studied and a whole energy photovoltaic system simulation for crystalline modules has been implemented into PowerDomus. A method to integrate the photovoltaic system and the building structure has also been presented. The validation of the photovoltaic models has been made comparing distinct photovoltaic simulation software and the influences of photovoltaic systems on the hygrothermal performance of buildings in terms of mould growth and degree-hours of comfort.

To conclude, the integration of natural ventilation strategies to a solar powered mechanical ventilation system is presented. Comparative analyses between a hybrid ventilation system and natural ventilation have been carried out in terms of thermal comfort, indoor air quality and energy consumption. Results have reported the possibilities of using solar-hybrid ventilation systems to enhance thermal comfort levels and to increase indoor air quality by adopting more elaborated ventilation control strategies.

Keywords: HVAC Systems, Natural Ventilation, Photovoltaic Systems, Hybrid Ventilation, Building Simulation.

Resumo

Nos últimos anos, sistemas de climatização de expansão direta ou indireta eram considerados as melhores estratégias para prover conforto térmico e qualidade do ar em ambientes de edificações. Atualmente, com a necessidade da redução do consumo de energia, soluções alternativas vêm sendo elaboradas. Dentre várias estratégias utilizadas, citar-se a ventilação natural que, em muitos casos, é capaz de reduzir o consumo de energia e proporcionar condições de conforto aceitáveis. Outra opção disponível e atrativa é a utilização de fontes renováveis para suprir a demanda excessiva de energia de sistemas de climatização. Levando-se em conta o potencial brasileiro para o uso tanto da ventilação natural quanto da energia solar, este trabalho demonstra a viabilidade da utilização destes dois recursos de forma conjugada em uma única estratégia de ventilação híbrida fotovoltaica, integrando o estado da arte de modelos matemáticos de ambas as áreas em um software de simulação higrotérmica e energética de edificações - PowerDomus.

Primeiramente, abordam-se os princípios físicos que regem a ventilação natural e modelos empíricos de ventilação cruzada e unilateral. Apresentam-se ainda os processos de implementação e validação desses modelos, através de comparações com resultados experimentais. Disserta-se a respeito da influência do parâmetro “coeficiente de pressão” e discutem-se as contribuições de dois métodos distintos para o cálculo deste parâmetro na estimativa do fluxo de ar através de aberturas. De modo a demonstrar as diferenças entre os dois métodos, comparam-se resultados experimentais tanto em túnel de vento quanto em campo, verificando-se as diferenças em termos de risco de crescimento de mofo, consumo de energia, conforto térmico e aceitabilidade do ar entre um sistema de climatização de expansão indireta e um sistema composto somente por ventilação natural.

Na sequência, estuda-se passo a passo o processo de conversão da energia solar em energia elétrica até a implementação de um modelo capaz de simular sistemas fotovoltaicos de células mono e poli-cristalinas. Propõe-se ainda uma metodologia para integrar o modelo fotovoltaico à estrutura da edificação dentro do software PowerDomus. Neste ponto, apresenta-se um estudo verificando as influências do acoplamento de um conjunto de painéis solares no comportamento higrotérmico da edificação em termos de risco de crescimento de mofo e aumento/diminuição das horas de conforto em seu interior.

Finalmente, descreve-se a integração de estratégias de ventilação natural a um sistema de ventilação mecânica com fornecimento de energia através de um módulo fotovoltaico. Apresenta-se uma análise comparativa entre o sistema de ventilação híbrida fotovoltaica e um sistema somente com ventilação natural em termos de conforto térmico, qualidade do ar e consumo de energia. Resultados demonstraram os benefícios do uso da ventilação híbrida fotovoltaica com o intuito de melhorar os níveis de conforto e a qualidade do ar através de adoção de estratégias de controle mais elaboradas.

Palavras-chave: Sistemas de Climatização, Ventilação Natural, Sistema Fotovoltaico, Ventilação Híbrida, Simulação de Edificações.

1 Introduction

1.1 Problem Statement

New strategies for improving indoor air quality, thermal comfort and building energy efficiency are progressively attracting attention of academic and industry researchers. The development of methodologies to reduce energy consumption associated to thermal comfort and indoor air quality (IAQ) standards are constantly in evidence and those strategies become of paramount importance regarding the present and the future global energy savings context.

1.2 Motivation

Associated to thermal comfort and indoor air quality concepts, energy consumption is another important issue related to HVAC (Heating, Ventilating and Air-Conditioning) systems performance. Energy efficiency in buildings is an important issue due to the growth of energy costs, energy consumption and environmental impacts, especially those related to global warming. According to the IEA - International Energy Agency - (2004) and Salsbury (2005), in the United States and other developed countries, about one third of all energy use can be attributed to buildings.

Presently, research works on the design of efficient buildings are growing fast and, in many countries, projects of commercial and residential buildings must contain improvements on energy saving strategies. Efforts existing to improve the energy efficiency of buildings are discussed by Karlsson and Moshfegh (2006), where a computational fluid dynamics (CFD) model was applied to simulate and evaluate changes on energy demand when different control strategies and changes in the building material are used. The aim is to save energy while maintaining the occupants' thermal comfort and acceptable indoor air quality.

In order to reduce energy consumption of HVAC systems, natural and mechanical ventilation systems can be used to reduce CO_2 concentration and make small variations on the indoor temperature when necessary. Although ventilation is essential for the maintenance of good IAQ, as presented by Fordham (2000), there is evidence to suggest that energy loss through uncontrolled or unnecessary air infiltration is excessive. Therefore, it is important to quantify present energy use, so that possibilities for energy conservation may be investigated. The objective of this section is to present some studies in order to verify the need for development of new strategies to reduce energy consumption and improve indoor air conditions, *e.g.*, the natural ventilation potential in Brazil.

Usually, the indoor air of buildings are treated by HVAC systems. However, these systems are costly, energy consuming, pollutant and sometimes may not ensure better indoor air conditions for the occupants. The energy waste of heating and cooling equipment is discussed below in order to emphasize the need for hybrid techniques to improve the indoor air conditions.

Analyzing the service and residential sectors of the world economy, the first consists of buildings used for commercial or public purposes, while the second consists of both single-family dwelling and apartments. Primary energy use is defined by Schipper and Meyers (1992) to be the sum of energy utilized by end-user (known as delivered energy) and the energy lost in the production and delivery of energy products. According to Orme's estimation (Orme, 2001), the aggregated total annual (1994) primary energy use for 13 industrialized countries (Belgium, Canada, Denmark, Finland, France, Germany, The Netherlands, New Zealand, Norway, Sweden, Switzerland, United Kingdom and United States of America) is 114 EJ , shown in Figure 1.1. Non-industrial (*i.e.* service and residential) buildings can be seen to be very significant users of primary energy. Furthermore, the residential sector of developed countries uses almost twice the primary energy compared to the service sector.

In Figure 1.2, the estimated aggregated totals of the space heating and cooling energies for those 13 countries are presented, which relies on hot water and space cooling use.

Finally, Figure 1.3 summarizes the ways in which delivered space conditioning is dissipated. The arrows in Figure 1.3 indicate that both of the heating air change and conduction losses are associated with a fraction of the heating equipment losses. Their sum together with the equipment loss is then equal to the delivered energy supplied for heating. Considering the building stock of the 13 countries collectively studied by Orme (2001), the total annual loss of delivered heating energy due to air change is estimated to

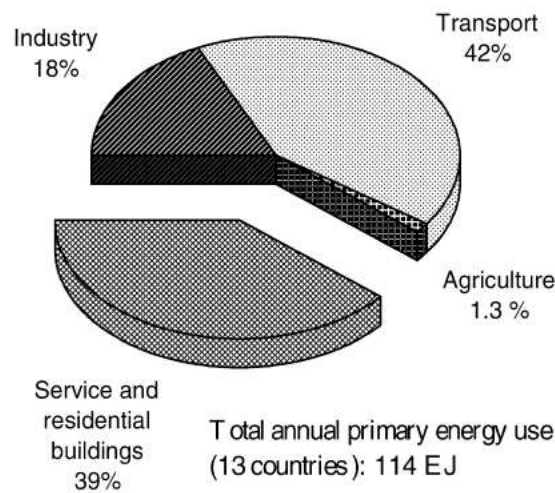


Figure 1.1: The approximate service and residential sector shares of primary energy use of 13 industrialized countries (Schipper and Meyers, 1992).

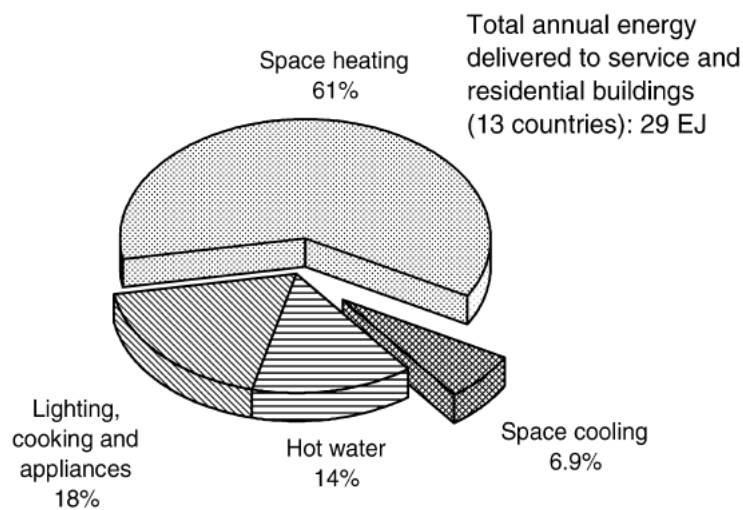


Figure 1.2: End use shares of delivered energy use in the service and residential sectors (Schipper and Meyers, 1992).

amount 48% of delivered space conditioning energy (including heating equipment losses).

In Brazil, when energy consumption is associated to HVAC systems, the situation is analogous. However, according to both world (published by the IEA - in 2007) and Brazilian (presented in the Brazilian Energy Balance - 2009) generation structures, the evident advantage is that Brazil has a predominance of renewable sources, specially hydro power (greater than 70% of total offer). Figure 1.4 presents a detailed comparison between the world and Brazil electricity supply according to primary generation source.

In 2004, 45.2% of the delivered electric energy in Brazil was used by the commercial, residential and public sectors, with residential dwellings being responsible for 22.3%, that

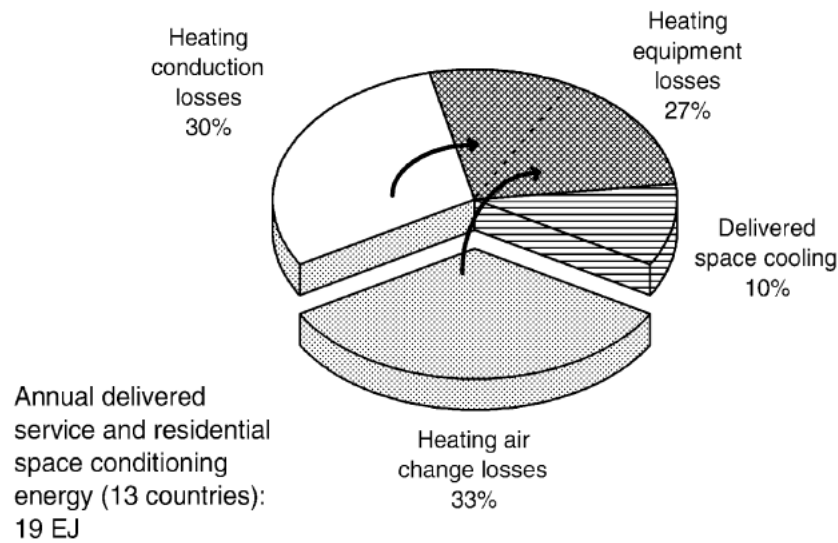


Figure 1.3: Dissipation of space conditioning energy in the service and residential sectors (Schipper and Meyers, 1992).

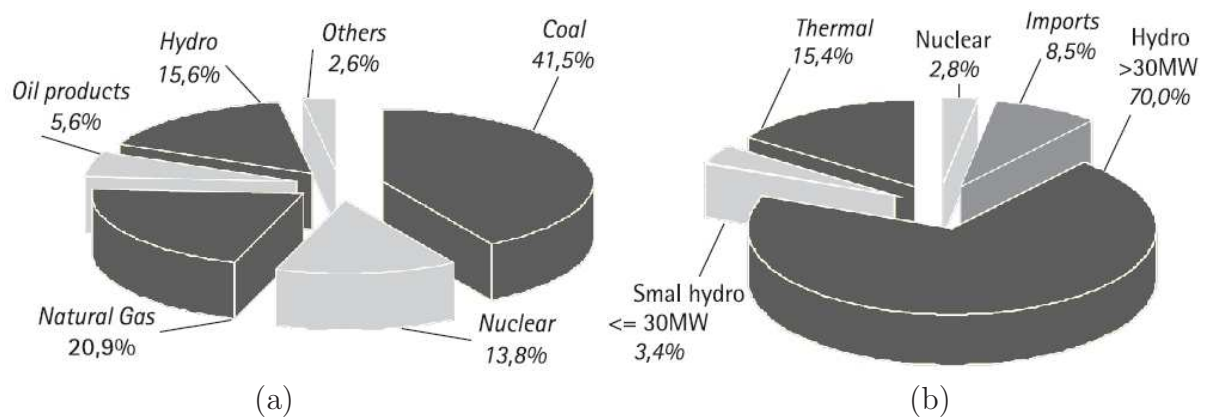


Figure 1.4: Electricity - Supply according to primary generation source: (a) World (IEA, 2007) and (b) Brazil (EPE, 2009).

also seems to be significant users of primary energy (Ordenes *et al.*, 2007). In 1992, the HVAC systems were responsible for just 7% of the energy consumption, with a growing saturation potential of 6% (Lamberts *et al.*, 2004). In the last years, it has been noticed that the energy consumption in the residential sector of Brazil has been growing fast (EPE, 2009), considering that the total energy consumption is almost three times higher than eighteen years ago. Following these steps, the Brazilian electric potential will be insufficient, becoming unavoidable the constructions of new thermoelectric and hydroelectric plants with consequent environment impact.

Comparing 2007 and 2008 electrical energy demand by sector, Brazilian's residential sector presents an increase of 5.2% in the electrical energy consumption due specially to

income improvements and grid connection. Commercial sector also demonstrated strong increase of 6.8%, while industries have small increase (2.4%) (EPE, 2009). Figure 1.5 shows the Brazilian electricity consumption by sector from 2004 to 2008. It can be verified that in 2008 public, residential and commercial sectors are responsible for 45% of total electrical energy demand, which means more than 690.82 *GJ*.

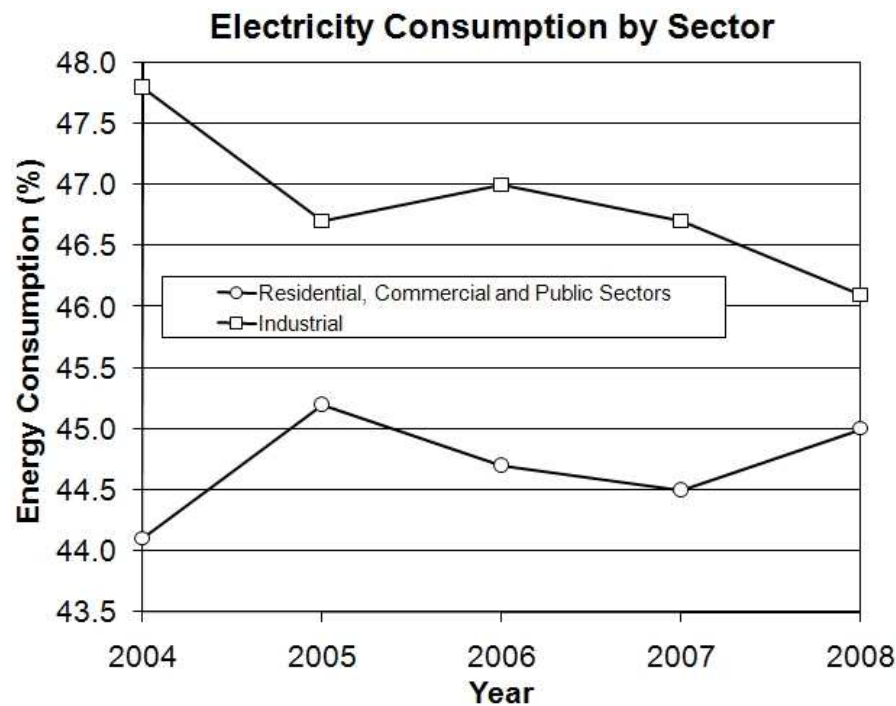


Figure 1.5: Brazilian electricity consumption by sector.

Climate changes have also contributed to the need for controlling better indoor climate. Increases of the average temperature of the Earth's near-surface air and oceans in recent decades, due to the global warming effect, are responsible for the development of powerful HVAC projects in order to decrease the supply air temperature or to increase the supply airflow than what was necessary a few years ago. Even in environments where there was no necessity of air-conditioning systems, nowadays they could be used, specially in Europe after the heat wave of 2003.

Trying to avoid the excessive energy usage of HVAC systems and adopting new strategies for improving indoor air conditions, studies using natural and mechanical ventilation have been carried out. A few years ago, hybrid ventilation control has been adopted by ASHRAE (ASHRAE, 2005*a*) as the highest research priority topic in order to reduce energy consumption of buildings. Following this way, the IEA (International Energy Agency) (through Annex 35 - (IEA, 2002)) also contributed to integrate natural and mechanical ventilation systems in order to reduce energy consumption by using alternative

HVAC strategies.

Additionally, according to the RESHYVENT project (Van der Aa and 't Veld, 2004), dwellings represent about 25–30% of all energy used in European Union, where ventilation losses and fans accounts for almost 10% of total energy use. When using hybrid ventilation systems, the expected energy saving on long term within European Union is approximately 64 PJ/year for residential buildings, giving a reduction of 3.6 Mton CO₂ – eq./year. In order to implement hybrid ventilation, more knowledge of the working principles and the techniques of these systems are crucial.

In this way, the need to reduce energy consumption of buildings is evident as well as the advances on building structures and the development of renewable technology strategies to improve the indoor air conditions. Following, some studies where the main objectives are the maintenance of acceptable thermal comfort conditions, better indoor air quality to the occupants and energy savings in buildings are presented.

1.3 Literature Review

The estimation performed by the International Energy Agency (IEA, 1998) about the energy resources usage that, without new policy initiatives, fossil fuels will account for more than 90% of total primary energy demand in 2020, is changing. As described in the previous section, based on the environmental impacts and on the increasing energy demand, different strategies to expand the world energy supply avoiding natural resources degradation are appearing. The importance of newer technologies (*i.e.* geothermal, photovoltaic, small-scale hydro, solar thermal electric and wind) is increasing, and according to Painuly (2001), they have grown proportionally more rapidly than any other electricity supply technology.

In terms of buildings, many of those renewable technologies can be adopted in order to reduce the residential, private and public sectors energy demand. Moreover, the improvements on the indoor air quality and thermal comfort can also be considered as objectives when the environmental impacts caused by HVAC systems are taken into account.

Based on the scope of this document, this section presents an overview of recent studies that are providing better results on the optimization of indoor climate and energy savings. A short review about each strategy is presented explaining the different approaches of this work. Detailed information and specific literature reviews will be presented in the following chapters.

1.3.1 Natural Ventilation

This work discusses the natural ventilation modeling as a requirement for the hybrid ventilation study. In this way, natural ventilation concepts have been studied and classified according to two configurations: ventilation through a unique aperture (single-sided ventilation) and through multiple ones (cross ventilation).

As it will be discussed in Chapter 2, many types of natural ventilation models are available in the literature. Considering the experimental difficulties on the obtention of empirical models able to describe the airflow through openings where non-linear effects caused by the turbulence are verified, some well established empirical models are available (de Gids and Phaff, 1982; British Standards, 1999; ASHRAE, 2005*b*; Larsen and Heiselberg, 2008). Some limitations of these methods are verified when the wind incident angle is almost perpendicular to the opening normal, in these cases, these models present more differences when compared to experimental results.

More detailed models can also be found in the literature (Papakonstantinou *et al.*, 2000; Jiang *et al.*, 2003), however, in this case, the whole-energy and hygrothermal analysis of natural ventilated environments become too costly and time-consuming.

1.3.2 Renewable Technology Integration

As presented before, many types of renewable technologies can be associated to buildings and contribute to the sector's energy demand reduction. Compared to others renewable technologies, during the last years, the integration of off-grid photovoltaic systems in buildings has progressed and new components have been successfully implemented in architecture. Photovoltaic panels can be used as a cover material or be integrated on roofs and façades. When semi-transparent collectors are adopted, they can be used to cover an atrium, contributing to reduce the energy consumption of lighting systems. Beyond the aesthetic aspect, the aim of building integration is to reduce the pay back time of PV systems. The fast development of PV cells technology and the consequent increases on cells efficiency can also be pointed as one of the main aspects to reduce the PV systems pay back time (Guiavarch and Peuportier, 2006).

Some examples of how PV technology could be applied to a building environment are presented below, showing the high potential of alternative strategies to deal with the indoor air climate and improve energy saving by using natural energy resources.

Renewable energy sources particularly the photovoltaic one are proven to be both clean and economical due to new advanced technological and efficient cells. The essential problem facing photovoltaic utilization as renewable energy source is solar array sizing, load matching and economic utilization via maximum solar energy tracking controllers and power tapping at all times (Sharaf *et al.*, 2000).

Recent studies show that photovoltaic electricity is most suitable for ventilation and air-conditioning applications mainly due to the matching of the supply and demand loads with time of the day (Sharaf *et al.*, 2000; Chow, 2010). In the early nineties, the application of building-integrated solar electrical systems were considerably expensive due to the high initial cost of PV (Photovoltaic) cells, but nowadays, this technology is becoming cheaper and seems to be a good strategy to reduce the use of energy provided from fossil fuel resources. Examples of photovoltaic utilization are presented in the sequence.

In the Brazilian context, some studies in order to motivate the use of PV systems are being developed. One example is the work presented by Silva and Beyer (2008), which associates the PV technology to a HVAC system providing a cost analysis and a design methodology of PV systems using the EnergyPlus simulation software. According to Silva and Bayer results, considering the whole HVAC system as energy demand for the PV system and high thermal loads for the indoor environment are not economically viable and low costs and small PV systems are considered the correct choice for the Brazilian economy.

Two low-cost photovoltaic schemes for ventilation and air-conditioning loads have been presented by Sharaf *et al.* (2000). Both schemes can provide an effective way to use renewable energy sources to reduce consumption via demand side-energy management. One of the PV interfaces has been proposed to a magnet motor drive for air-conditioning mechanical unit and it is highly suitable for residential and small commercial buildings, while the second PV scheme has been proposed for large commercial buildings and small industrial electricity generation.

In the work presented by Friling *et al.* (2009), the main objective was to identify a model capable of representing the cell operating temperature of a photovoltaic panel. Based on a test reference module which provides the opportunity of changing physical parameters, the ventilation speed and the type of airflow, the preferable set-up has been distinguished and data have been collected. Their analysis has revealed that it is necessary to use non-linear state space models in order to obtain a satisfactory description of the PV module temperature, and in order to be able to distinguish the variations in the set-up.

While the work proposed by Sharaf *et al.* (2000) presents generic available configurations of the entire PV system, some more specific works, as the one proposed by Friling *et al.* (2009), are based on the study of physical principles of Building-Integrated Photovoltaic (BIPV) systems. The wide range of works involving photovoltaic technology associated to building (Norton *et al.*, 2010; Román *et al.*, 2008; Fung and Yang, 2008; Friling *et al.*, 2009; Cheng *et al.*, 2009; Chel *et al.*, 2009) and the importance attributed to replace the fossil fuel by renewable energy resources are motivating the research in this specific area. Another example of a different approach in the BIPV research is the work presented by (Wang *et al.*, 2006), who decided to evaluate which will be the best building integration configuration based on four typical building photovoltaic integration strategies for the Tianjin city, China. BIPV configurations with ventilated air-gap, non-ventilated (closed) air-gap, closeroof mounted, and the conventional roof with no PV and no air gap has been studied by using one-dimensional transient models. Results evaluating the heating loads across the different roofs in order to select the appropriate PV building integration method have been presented.

CFD models are also adopted in parametrical studies of BIPV systems. When PV systems have a secondary purpose, *e.g.*, heat water, CFD simulation can be used to estimate the best parameters of the secondary system. In (Corbin and Zhai, 2010), an experimentally validated computational fluid dynamics (CFD) model of a novel building integrated photovoltaic-thermal (BIPV/T) collector is studied to determine the effect of active heat recovery on cell efficiency and to determine the effectiveness of the device as a solar hot water heater. In their results a new correlation is developed relating electrical efficiency to collector inlet water temperature, ambient air temperature and insolation that allows cell efficiency to be calculated directly.

However, the potential usage of PV technologies in buildings are growing fast and more advanced projects focusing the PV potential in reducing the environmental impacts caused by human activities have been developed, *e.g.* (Yun *et al.*, 2007), where a ventilated photovoltaic façade, which works as a pre-heating device in winter and a natural ventilation system in summer and reduces PV module temperature has been presented. They analyzed many parameters (*i.e.* climate, room depth, lighting loads, U-value, glazing type, shading device and the overall energy performance of the ventilated PV façade) to show how a PV wall can be used to reduce building energy consumption and improve indoor thermal comfort by using the PV façade as a hybrid ventilation system for better summer and winter periods.

According to the literature review presented above, it can be seen many approaches on the PV research. However, this work is focused on the implementation of a building-integrated photovoltaic model and on the evaluation of the PV array effects on the building hygrothermal behavior. Additionally, in Chapter 7, the PV system will be associated to a hybrid ventilation system.

1.3.3 Hybrid Ventilation

For many years natural and mechanical ventilation systems have been developed in a parallel way. Mechanical ventilation has been developed from constant airflow systems through systems with extensive heat recovery and demand-controlled airflows to energy-optimization low-pressure ventilation systems. Over the same period natural ventilation has been developed from being considered only as a largely uncontrolled system using air infiltration through cracks and airing through windows, to a demand-controlled ventilation system with cooling capabilities. Naturally, the next step in this process is the development of ventilation concepts that utilize and combine the best features of each system to create a new type of ventilation - Hybrid Ventilation (IEA, 2002). Following, some works focused on hybrid ventilation are presented.

In Jreiliry *et al.* (2007), two different hybrid ventilation control strategies, one using CO_2 sensors and other based on the detection of presence of occupants, have been simulated and compared in terms of indoor air quality, thermal comfort, CO_2 levels and energy consumption for residential buildings. Results show that the use of hybrid ventilation system does not bring major changes to summer thermal comfort and energy consumption for heating when compared to the reference system, in which the zones air change rates are defined as fixed values during occupied periods. However, the differences are important when the exposure of the occupants to CO_2 and electrical energy consumption of fans are considered, where the electrical energy consumed by the fan can be reduced by 90% when compared to reference system, a classical mechanic extract ventilation system.

Experimental work using hybrid ventilation has also been developed, as the one presented by Niachou *et al.* (2008), where three-single family building apartments were studied in two urban street canyons located in high-density residential areas. In order to study natural, mechanical and hybrid ventilation, a number of 114 ventilation experiments were conducted by using the single tracer gas (N_2O) decay method and the multitracer gas decay method with two tracer gases, N_2O and SF_6 . In the case of hybrid ventilation, a number of 12 fan-assisted natural ventilation configurations were investigated and re-

sults show that in spite of the reduced wind speeds due to the canyon effect, appreciable ventilation rates can be obtained with natural ventilation, especially when cross ventilation with two or more windows is presented. According to Niachou, for single-sided ventilation or under calm conditions, hybrid ventilation has only a slight advantage over natural, either in terms of air-exchange rates or if air-exchange efficiencies.

The present work deals with hybrid ventilation associating both mechanical and natural ventilation. In order to reduce the energy consumption of the mechanical ventilation, a building-integrated photovoltaic model will be adopted supplying the fan energy demand. Pollutant concentration will not be discussed in this work, where the main idea is to reduce energy consumption and optimize thermal comfort, even when natural ventilation is used. A more detailed analysis of the photovoltaic hybrid ventilation system is presented in the next section.

1.3.4 Photovoltaic Hybrid Ventilation

As presented by Fossa *et al.* (2008), many research works on BIPV are focused on the analysis of PV modules when coupled to the building structure. Through experiments and parametrical analysis, capable of defining new possibilities to increase the PV cells efficiency, *e.g.* by reducing the modules temperature, most of research works on the BIPV integration are based on enhancing the PV cells efficiency when coupled to the building structure, emphasizing the system design.

The PV analysis performed in this work describes the opposite idea when compared to the work presented by Fossa *et al.* (2008). Here, the influences of the BIPV system on the environment and consequent effect on the occupants' thermal sensation is verified. In this way, the last part of this work presents a hybrid ventilation strategy able to improve the occupants' thermal sensation and reduce energy consumption of mechanical ventilation systems.

When the hybrid control strategy automatically detects the need of mechanical ventilation, the power supplied to the fan will be provided by an auxiliary PV system, avoiding the grid energy use. The control strategy of the hybrid ventilation system verifies if there is airflow increase/decrease necessity considering the natural ventilation, based on the following priorities: thermal comfort, relative humidity at the internal surfaces (in order to avoid mould growth and improve indoor air quality) and indoor air quality standards.

Associating PV to a hybrid ventilation system, the renewable technology could be

adopted to increase electric energy savings. In this way, an intelligent control system for an HVAC device, capable of distinguishing when it is possible to use natural resources for cooling or heating the indoor air temperature, to increase the air change rate according to pre defined standards and finally to use better the energy when the demand is lower, will be presented.

1.4 Brief Methodology Description

This work is based on the utilization of a whole-building energy simulation software - PowerDomus, which is an object-oriented program that has been developed to predict the hygrothermal performance of multizone buildings considering both vapor diffusion and capillary migration transport mechanisms. A lumped formulation for temperature as well as for water vapor is adopted in each building zone. In its energy balance, loads such as from conduction, convection, short-wave solar radiation, inter-surface long-wave radiation, infiltration and HVAC system related loads are considered.

In this way, mathematical models presented in this work have been implemented and tested into PowerDomus, enhancing the software functionality. Comparisons to specific simulation software (for photovoltaic verification) and results found in the literature (natural ventilation models) provided the validation of the methods implemented into the software. The implementation generalizations for whole-building simulation have quickly been pointed to provide a better understanding of the results obtained during the verification and validation procedures.

1.5 Escape of the Present Work

The main objectives of this work are:

- Analyze the capability aspects of empirical natural ventilation models available in the literature and propose a more precise pressure coefficient calculation method in order to provide better prediction of the airflow rate in single-sided and cross ventilation cases.
- Implement both natural ventilation and pressure coefficient calculation models into PowerDomus, providing an advanced module able to calculate, through the evaluation of the boundary condition applied to buildings and the CAD (Computer-Aided

Design) interface, the airflow at each opening (doors or windows) in an specific project;

- Study and evaluate thermal comfort, indoor air quality, and mould growth models and implement all these model in the thermal analysis module of PowerDomus;
- Evaluate the most disseminated photovoltaic models available in the literature and integrate the PV energy conversion calculation method into the combined heat and moisture transport model (available in PowerDomus) in order to evaluate the effects of building-integrate photovoltaic systems on the building hygrothermal behavior;
- Integrate both natural and mechanical ventilation in a hybrid ventilation strategy capable of identifying the occupants' necessity in terms of thermal comfort, indoor air quality and standard ventilation rates. The hybrid ventilation will provide integration between mechanical ventilation and photovoltaic ventilation systems, reducing the energy consumption of the HVAC system.

1.6 Dissertation Structure

In order to present the research development sequence, the structure of the dissertation is divided as follows:

Chapter 2 - Natural Ventilation: Modeling

In this chapter, fundamentals of natural ventilation, such as wind and buoyancy effects, are described and empirical models for cross and single-sided ventilation are studied in order to understand air exchanges in indoor environments and how it affects the indoor thermal comfort of the occupants. Two distinct methods to calculate the pressure coefficients are presented and discussed.

Chapter 3 - Natural Ventilation: Validation Procedures

The natural ventilation models are coupled to a whole building and energy simulation software. Several cross and single-sided natural ventilation simulations through openings are performed. The simulations are then compared to experimental results carried out in a full-scale wind tunnel and in an on-site three storey office building.

Chapter 4 - Comparative Analysis: Natural Ventilation versus Air-Conditioning Systems

Chapter 4 starts presenting some thermal comfort models that are used to evaluate the occupants' thermal sensation. A mould growth model capable of calculating the favorable conditions for mould growth is also presented and discussed. A case study is then proposed in order to compare the effects of natural ventilation on the occupants thermal comfort and its advantages over traditional cooling systems.

Chapter 5 - Building-Integrated Photovoltaic Systems: Modeling

Chapter 5 shows the model used to simulate photovoltaic cells, since the basic calculation of PV cells temperature until the whole system description. Chapter 5 also describes the whole building and energy simulation models of photovoltaic panels when they are coupled to building surfaces and the PowerDomus heat and moisture transport through the building envelope models.

Two methods to include energy demand for the photovoltaic systems are presented. One treats general AC or DC electrical appliances, while other considers the central HVAC system components.

Chapter 6 - Building-Integrated Photovoltaic Systems: Verification Procedures

Here the photovoltaic model verification is demonstrated in terms of comparisons to the PV system itself and the building-integrated photovoltaic system. Results in terms of radiation that reaches the panel surface, energy conversion and energy delivered to the storage system are compared and discussed. In order to verify the influences of building integrated photovoltaic systems on the hygrothermal behavior of buildings, a case study based on the building test structure presented in Chapter 4 are performed and results are presented by analyzing the sensible and latent heat fluxes, vapor flows, temperature and relative humidity on the indoor roof surface, indoor air temperature and relative humidity and mould growth risk on the surfaces, where the PV array will be mounted.

Chapter 7 - Comparative Analysis: Natural Ventilation versus Photovoltaic Hybrid Ventilation

Chapter 7 starts presenting an introduction and definitions about hybrid ventilation technology. After, the Brazilian potential for natural ventilation and building-integrated photovoltaic systems applications are addressed and a evaluation of the worldwide venti-

lation requirements are discussed. The Brazilian standards for indoor air quality are also described.

In the sequence, the combination of an air-handling unit and natural ventilation used to control a new hybrid ventilation algorithm is presented. To finish, a case study using the hybrid ventilation technique is proposed and simulation results comparing natural hybrid ventilation strategies are presented.

Chapter 8 - Final Remarks

The last chapter emphasizes the contributions of this work and provides some discussions about the main aspects of natural ventilation empirical models, building-integrated photovoltaic simulation and photovoltaic hybrid ventilation. Future works and important considerations about the implementation and the software adopted during this work are also presented.

2 Natural Ventilation: Modeling

Healthy indoor climate conditions and, at the same time, energy efficient and environmentally friendly building is a clear challenge. This is valid for existing buildings as well as for early-stage design processes. Creating better indoor air conditions to the occupants is certainly the main aspect when health and productivity are taken into account. Full air conditioned systems were in the past considered as the ultimate choice, but today a more balanced view is found in many countries and among many people (der Aa and 't Veld, 2004). Nowadays, the combination of natural ventilation and air-conditioning systems are essential to reduce building energy consumption.

In fact, building air renewal can be achieved by either using natural driving forces or mechanically driven systems. This chapter describes the different types of natural ventilation strategies explaining how ventilation in buildings has changed during the last decades in order to follow new and strength economic requirements.

Ventilation in buildings is today, in most developed countries, considered as an essential aspect in each building project. Whereas in the past, the primary purpose of ventilation was to provide acceptable indoor air quality - and thus being viewed as energy loss, nowadays there is a growing interest in ventilation as part of an energy efficient strategy for achieving thermal comfort in summer. Usually, in the developed economies, buildings account for half of the fossil fuel consumed, so they must be designed or adapted to reduce energy consumption by a very large ratio (Fordham, 2000). In this way, one option to reduce energy consumption of commercial and residential buildings is the use of natural resources as natural ventilation in order to reduce or increase indoor temperature and relative humidity, providing acceptable indoor air quality to the occupants.

This chapter is divided into 6 sections:

- i)* natural ventilation modeling state-of-art - where single-sided and cross ventilation empirical models are evaluated according to the literature review;
- ii)* physical fundamentals - explanation about the physical principles of natural ven-

tilation;

iii) pressure coefficient calculation - ways to calculate the main coefficient when natural ventilation is caused by the wind effect;

iv) cross ventilation model implemented into PowerDomus software;

v) single-sided ventilation models implemented into PowerDomus;

vi) implementation - where the main difficulties to generalize the models for a building simulation software are addressed.

2.1 State-of-Art

Natural ventilation can be classified according to two configurations: ventilation through a unique aperture (single-sided ventilation) and through multiple ones (cross ventilation). If the modeling of cross ventilation is currently well defined (British Standards, 1999), that of single-sided ventilation is widely discussed since early 80's because of the complexity for existing models to reproduce the airflow through just one aperture in a building zone. Differently from the cross-ventilation, in single-sided ventilation the turbulence of the wind and variations in the pressure gradients induced by e.g. wind gusts strongly affect the airflow through an opening (Larsen, 2006). Since those parameters are unsteady, the airflow in single-sided ventilation is much more difficult to evaluate.

In 1982, the first most relevant model to calculate natural single-sided ventilation in buildings was presented by de Gids and Phaff (1982). They proposed an empirical expression to calculate the airflow through an opening based on three parameters: air speed, temperature variation and opening area.

Seventeen years after the presentation of the Gids and Phaff model, the British Standards (British Standards, 1999) published formulae to calculate the airflow in a single-zone with just one opening. In 2005, the American Society of Heating, Refrigerating and Air-Conditioning Engineers (ASHRAE, 2005*b*) proposed another expression to calculate the airflow in a single-sided ventilation residential building. That expression was the first one to take into account the wind incidence angle.

Finally, in 2006, based on de Gids and Phaff's model, Larsen concluded that a more precise design expression found from wind tunnel measurements could be used to predict single-sided ventilation airflows. From Larsen's experimental work (Larsen, 2006), it has been noticed that the wind prevails on the windward side and that the temperature

difference stands out on the leeward side of the building.

Recently, more advanced analysis to calculate the airflow through openings has been performed. Based on the evolution of computational hardware and on advances of CFD (Computational Fluid Dynamics) software, new methods to study the airflow through single-sided openings started to be developed (Papakonstantinou *et al.*, 2000; Jiang *et al.*, 2003). However, in the case of natural ventilation, the CFD approach requires the modeling of large computational domain and the use of high-order turbulence models such as Reynolds Stress Models (Emmel *et al.*, 2007) in order to represent correctly the airflow around the buildings. Actually, new strategies to accelerate the CFD calculation are being studied considering potential advances on the computational hardware programming (Zuo and Chen, 2009), but when the whole building hygrothermal and energy analysis are necessary, the use of CFD become complex and time consuming so that empirical expressions are still widely used when the use of building simulation software is necessary.

In the sequence, physical fundamentals of natural ventilation in buildings are addressed before the detailed description of the models discussed above. Implementation structures have also been shown in this chapter.

2.2 Physical Fundamentals

Natural ventilation is driven by pressure differences created by either temperature differences (thermal buoyancy), wind on the building or a combination of these two. The derivation of these pressure differences is made in the following sections.

From the pressure differences, an airflow rate through the opening(s) can be calculated. This calculation depends on the type of natural ventilation (cross- or single-sided ventilation) and other factors as building geometry and surrounding. A detailed presentation of the different expressions for calculation of flow rates is made in the following.

2.2.1 Thermal Buoyancy

When natural ventilation is driven only by thermal buoyancy, the pressure difference is created by density gradient between the warm and the cold air stream. The exchange of air between inside and outside will happen through one or more openings in the outer wall. The pressure difference increases with the vertical distance between the openings or, if only one opening exists, the height of the opening itself.

The air pressure (in Pa) - at a single point located at height H (in m) above the reference (floor level) - for both internal “ i ” and external “ e ” sides, can be expressed as shown in Equations 2.1 and 2.2.

$$P_i = P_{i,0} - \rho_i g H \quad (2.1)$$

$$P_e = P_{e,0} - \rho_e g H \quad (2.2)$$

where ρ is the air density (in kg/m^3) and g is the gravity acceleration expressed in (m/s^2).

The pressure difference between internal and external air can then be found by:

$$\Delta P = P_{e,0} - P_{i,0} - (\rho_e - \rho_i) g H \quad (2.3)$$

Whether the air enters or exits a building at a certain height depends on the position of the opening compared to the neutral plane in the building (where the difference ΔP is zero), see Figure 2.1. Above this plane an overpressure exists in the building because of the warmer indoor air in relation to the outdoor one ($T_i > T_e$) that will generate an outgoing airflow. Below it, there will be an underpressure in the building compared to outside which will make the airflow into the building. At neutral plane ($H = H_0$) where $\Delta P = 0$, Equation 2.3 becomes:

$$P_{e,0} - P_{i,0} = (\rho_e - \rho_i) g H_0 \quad (2.4)$$

From the Clapeyron equation of state, considering $P_e \cong P_i$, it can be found that

$$\frac{\rho_e - \rho_i}{\rho_i} \cong \frac{T_i - T_e}{T_e} \quad (2.5)$$

where T is the temperature expressed in K . The Equation 2.3 can therefore be rewritten as:

$$P_{e,0} - P_{i,0} \cong \rho_i g H \frac{T_i - T_e}{T_e} \quad (2.6)$$

Likewise the pressure in the height H_1 where $\Delta P \neq 0$ can be found as

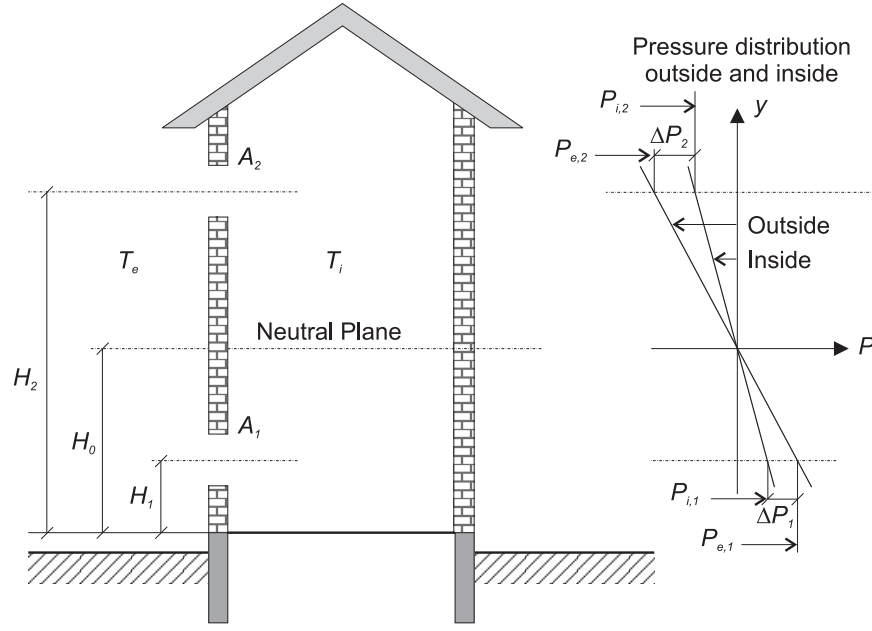


Figure 2.1: Pressure difference around the neutral plane in a building ventilated only by thermal buoyancy (Larsen, 2006) - case of $T_i > T_e$.

$$\Delta P_{H=H_1} = P_{e,0} - P_{i,0} - \rho_i g H_1 \frac{T_i - T_e}{T_e} \quad (2.7)$$

Replacing Equation 2.6 into Equation 2.7, the pressure difference in H_1 can be expressed simply by the internal and external temperatures, the gravitational acceleration and the density of air. Positive values of the pressure difference in Equation 2.8 (H_1 below the neutral plane) show that the pressure outside the building is higher than inside.

$$\begin{aligned} \Delta P_{H=H_1} &= \rho_i g H_0 \frac{T_i - T_e}{T_e} - \rho_i g H_1 \frac{T_i - T_e}{T_e} \\ &= \rho_i g (H_0 - H_1) \frac{T_i - T_e}{T_e} \end{aligned} \quad (2.8)$$

From this equation it can be seen that the pressure difference increase with increasing height difference (*i.e.* the distance from the neutral plane) or the temperature difference.

2.2.2 Wind

When natural ventilation is driven only by wind, the pressure difference depends on the wind speed and direction. The wind will then create an overpressure at the windward side of the building and an underpressure at the leeward and parallel sides of the building. The pressure created by the wind on the building is described in Equation 2.9. It is calculated by multiplying a dimensionless pressure coefficient (C_P) with the dynamic

pressure, where U_z - the air speed at z meters height - is obtained by Equation 2.19. The C_P -coefficient is function of the shape of the building, the wind direction and the surrounding terrain. Two methods to calculate the pressure coefficient are presented in Section 2.3.

$$P_{wind} = C_P \frac{1}{2} \rho_e U_z^2 \quad (2.9)$$

From Equation 2.9 the pressure difference between the inside and outside of the building can be calculated as

$$\Delta P_{wind} = C_P \frac{1}{2} \rho_e U_z^2 - P_i \quad (2.10)$$

where the reference air speed U_{10} (in m/s) used in the previous expressions is the velocity at 10 meter height.

If the pressure difference across the building is needed, the difference in C_P -values on the windward and leeward sides are used instead as shown in Equation 2.11 and by using this expression P_i disappears from the calculation of the pressure difference.

$$\begin{aligned} \Delta P_{wind} &= (C_{P, windward} - C_{P, leeward}) \frac{1}{2} \rho_e U_z^2 \\ &= \Delta C_P \frac{1}{2} \rho_e U_z^2 \end{aligned} \quad (2.11)$$

2.2.3 Combination of Thermal Buoyancy and Wind

Most often the pressure differences in natural ventilation will be created as a combination of thermal buoyancy and wind. The total pressure across an opening is found as a summation of the pressure created by buoyancy (Equation 2.8) and wind (Equation 2.11) as follows.

$$\begin{aligned} \Delta P &= \Delta P_{wind} + \Delta P_{buoyancy} \\ &= \left(C_P \frac{1}{2} \rho_e U_z^2 - P_i \right) + \left(\rho_e g (H_0 - H_1) \frac{T_i - T_e}{T_i} \right) \end{aligned} \quad (2.12)$$

2.3 Pressure Coefficient Calculation

As presented in Section 2.2.2, the pressure created by the wind on the building is described in Equation 2.9. The C_P coefficient is determined by the shape of the building, the wind direction and the surrounding terrain. In the sequence, two models to calculate the distribution of C_P are presented. The first one considers an unique value for the whole surface whereas the second one calculates the C_P value at any location on the surface.

2.3.1 Mean C_P Equation

According to (ASHRAE, 2005a), the distribution of C_P on a low-rise building associated to the variation of the incidence angle can be estimated through the curve presented in Figure 2.2. According to (Deru and Burns, 2003), there are several correlations for the wind pressure coefficient derived from wind tunnel experimental data in order of increasing complexity and accuracy, as those proposed by (Walton, 1982), (Swami and Chandra, 1988), and the COMIS group (Feustel and Rayner-Hooson, 1990). These correlations are potentially inaccurate in situations that introduce turbulence to the flow; for example: high terrain roughness or local shielding, irregular shaped buildings (non-rectangular or rectangular with aspect ratios far from a cube) or buildings with overhangs or fins. The model developed by Swami and Chandra (1988) was selected as the best fit for the needs of this work:

$$C_P = C_P(\beta = 0) \ln \left[\begin{array}{l} 1.248 - 0.703 \sin \left(\frac{\beta}{2} \right) - 1.175 \sin^2 \beta + 0.131 \sin^3(2\beta G) \\ + 0.769 \cos \left(\frac{\beta}{2} \right) + 0.07 G^2 + 0.717 \cos^2 \left(\frac{\beta}{2} \right) \end{array} \right] \quad (2.13)$$

assuming that:

$$G = \left(\frac{L_1}{L_2} \right) \quad (2.14)$$

This expression calculates, which will be called Mean C_P Equation, the surface pressure coefficient normalized to the pressure coefficient at zero incidence angle as a function of the wind incidence angle (β) within a $[0^\circ, 180^\circ]$ domain, where values higher than 180° are obtained by symmetry, and the natural logarithm of the side ratio (ratio of the lengths of adjacent walls L_1 and L_2). For vertical walls, Swami and Chandra (1988) recommended using a value of 0.6 for the pressure coefficient at zero incidence. Note that the values

obtained by Equation 2.13 lie in Figure 2.2 grey area.

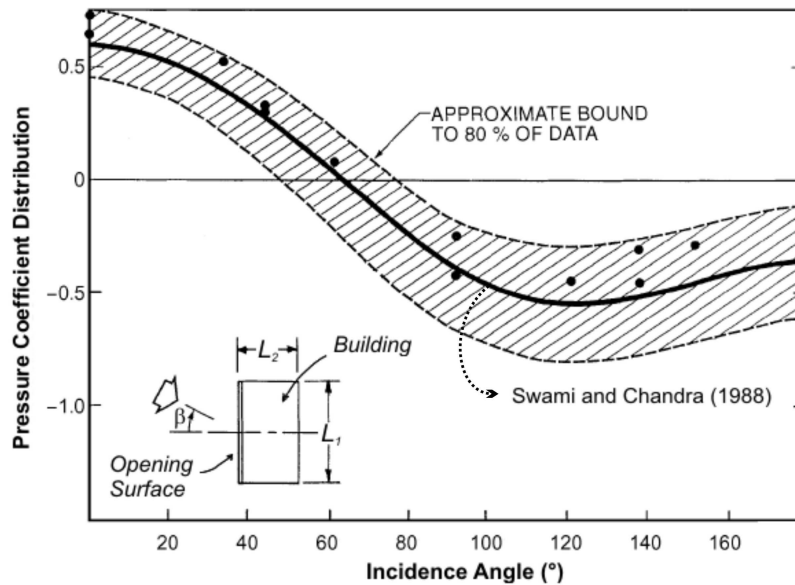


Figure 2.2: Variation of surface-averaged wall pressure coefficients for low-rise buildings (ASHRAE, 2005a).

2.3.2 CPCALC Model

As the main algorithm of CPCALC+ (software for calculating wind pressure coefficients on the envelope of a building which has been used for airflow modeling), the idea of the CPCALC algorithm was initiated within the European Research Programme PAS-COOL (Passive Cooling of Buildings) of the Commission of the European Communities, Directorate General for Energy (Grosso, 1993; Grosso *et al.*, 1994). In 1992 it was developed at the Lawrence Berkeley Laboratory (Feustel and Rayner-Hooson, 1990; Grosso, 1992) within the COMIS workshop on infiltration and ventilation, and being upgraded within the IEA-ANNEX 23 on multizone airflow modeling (IEA, 1996).

CPCALC and CPCALC+ were developed in order to fulfill the requirements of multizone airflow models which need a detailed evaluation of the wind pressure distribution around buildings. Scientists and professionals using this program, and who do not have the possibility to test a scale model of their building in a wind tunnel, do not need to extrapolate C_P data from tables usually yielding wall-averaged C_P values (Liddament, 1986).

The CPCALC model uses the following input variables: β is the wind incidence angle ($^\circ$), α_R is the wind speed profile (see Table 2.1) (Counihan, 1975), sbh is the surround building height (m), pad is the plan area density (%), the building height (m), the wall

azimuth ($^\circ$) and the coordinates x and y of the middle of the opening related to the origin of the building (m). Finally, L_1 and L_2 represent the frontal and side aspect ratios of the building (m).

Table 2.1: Reference values for the wind velocity profile exponent.

Terrain Roughness	α_R
Level surfaces, surfaces of water basins, grass land	0.10
Flat open country with few, very small, and scattered obstructions	0.15
Rolling or level surfaces broken by numerous obstructions such as trees or small houses	0.22
Heterogeneous surface with obstacles larger than one story	0.28
Low density suburban areas	0.34
Medium-high density urban areas	0.40
Very high density inner city areas	0.45

Based on these input data, the CPCALC algorithm is able to calculate the pressure coefficient value at any point on building's surface, in this case, at the center of the opening. More information about the CPCALC algorithm can be found in Annex 1 of this document.

2.4 Cross-Ventilation

Since cross-ventilation is much more used and also simpler to calculate than single-sided ventilation the knowledge of the airflow in this type of ventilation is more thorough. Here the flows induced by either thermal buoyancy, wind or a combination are presented and the theory with airflows driven by thermal buoyancy can also be applied in single-sided ventilation. In this section, standards presented in (British Standards, 1999) have been adopted to define the cross-ventilation airflow formulation.

2.4.1 Airflow Driven by Thermal Buoyancy through More than One Opening

Airflows driven by thermal buoyancy occur as soon as there are openings at different heights in the building. In this case it is of no importance whether the openings are on different walls in the building and therefore this is also valid for single-sided ventilation with more than one opening.

The general way to calculate pressure driven airflows (in m^3/s) through openings presented in (British Standards, 1999) is written in the Expression 2.15. This equation is based on the cross-ventilation problem presented in Figure 2.3, where the cross section of the building has been presented. In the simplest case where just two windows represent the cross-ventilation profile, Equations 2.15 and 2.16 should be simplified.

$$Q_V = C_D A_b \sqrt{\frac{2 \Delta T g H_d}{T_M}}, \quad (2.15)$$

where the discharge coefficient for window openings C_D is often within the range between 0.6 and 0.75 (Larsen, 2006), ΔT is the temperature difference between inside and outside (K), g is the gravity acceleration (m/s^2), H_d is the height difference between the two openings (m), T_M is the mean temperature between the indoor and outdoor air and A_b is the total opening area (in m^2) that can be calculated as presented in Equation 2.16.

$$\frac{1}{A_b^2} = \frac{1}{(A_1 + A_3)^2} + \frac{1}{(A_2 + A_4)^2} \quad (2.16)$$

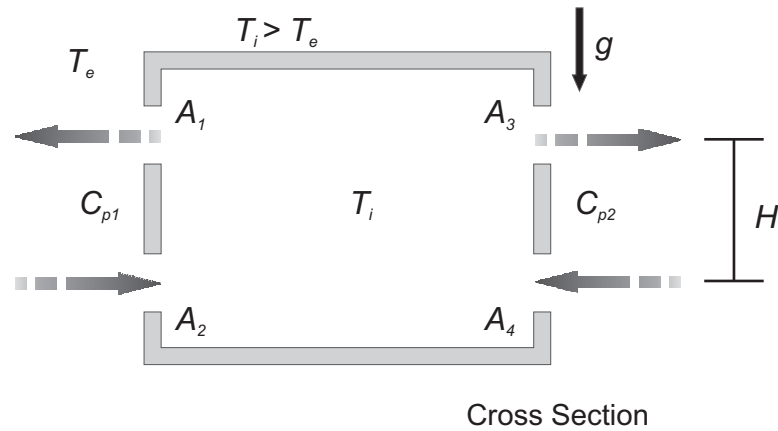


Figure 2.3: Cross-ventilation driven by temperature difference only.

2.4.2 Airflow Driven by Wind

To calculate the airflow rate caused by wind in the cross-ventilation problem presented in Figure 2.4, the following equation should be used (British Standards, 1999).

$$Q_V = C_D A_w U_{z=BH} \sqrt{|C_{P,1} - C_{P,2}|} \quad (2.17)$$

where A_w is the total opening area and it can be calculated as presented in Equation 2.18.

$U_{z=BH}$ is the wind velocity at the building's height and $C_{P,1}$ and $C_{P,2}$ are the pressure coefficients that can be evaluated according to the methods presented in Section 2.3 for openings 1 and 2.

$$\frac{1}{A_w^2} = \frac{1}{(A_1 + A_2)^2} + \frac{1}{(A_3 + A_4)^2} \quad (2.18)$$

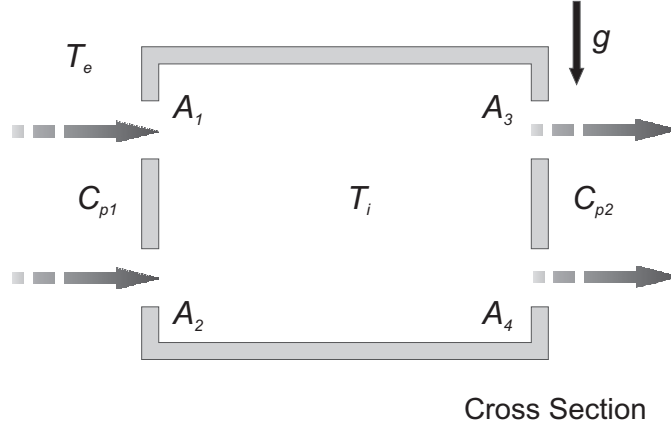


Figure 2.4: Cross-ventilation driven by wind only.

The wind velocity at the building's height is calculated using Counihan's expression (Counihan, 1975):

$$\frac{U_z}{U_{10}} = \left(\frac{z}{10} \right)_R^\alpha \quad (2.19)$$

where α_R depends on the terrain roughness (see Section 2.3).

2.4.3 Airflow Driven by Wind and Thermal Buoyancy

In this case, the expressions for cross-ventilation driven by thermal buoyancy and wind are combined to give the resultant airflow. According to (British Standards, 1999), the resultant airflow should be calculated based on the problem presented in Figure 2.5.

In this case, if the inequation

$$\frac{U_{z=BH}}{\sqrt{\Delta T}} < 0.26 \sqrt{\frac{A_b}{A_w} \frac{H}{\Delta C_P}} \quad (2.20)$$

is satisfied, the airflow should be calculated through Equation 2.15. Otherwise, the Equation 2.17 should be used.

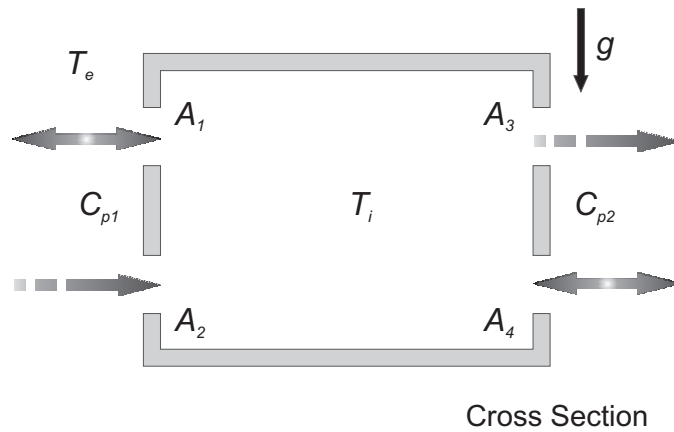


Figure 2.5: Cross-ventilation driven by wind and thermal buoyancy.

2.5 Single-Sided Ventilation

In the calculation of single-sided ventilation, it is not possible to only account for average wind velocity and pressure difference as often done for cross-ventilation. In single-sided ventilation, the turbulence in the wind and variation in the pressure gradients induced by *e.g.* wind gusts strongly affect the airflow through an opening (Larsen, 2006). Since these parameters are unsteady, the airflow in single-sided ventilation is much more difficult to calculate. In the sequence, four models to calculate the airflow for single-sided ventilation environments are presented.

2.5.1 de Gids and Phaff (1982)

In 1982, de Gids and Phaff presented an approach to calculate the airflow in single-sided ventilation zones, where the air change resulting from opening a window in a room while maintaining the internal door closed was the subject of investigation (de Gids and Phaff, 1982). Measurements have been carried out in different locations, all located on the first floor of buildings situated in an urban environment and surrounded by buildings up to 4 floors high. From the measurements, de Gids and Phaff found this expression which describes the flow rate (in m^3/s):

$$Q_V = \frac{A_o}{2} \sqrt{C_1 U_{10}^2 + C_2 H_o \Delta T + C_3}, \quad (2.21)$$

where A_o is the opening area (in m^2), H_o is the opening height (in m), U_{10} is the reference velocity at 10 meter height (m/s) and ΔT is the mean temperature difference between

inside and outside (K).

The coefficients of this model are (de Gids and Phaff, 1982): the dimensionless coefficient depending on the wind effect ($C_1 = 0.001$), the buoyancy constant ($C_2 = 0.0035$) and the turbulence constant ($C_3 = 0.01$).

2.5.2 British Standards (1999)

Seventeen years after the presentation of the de Gids and Phaff model, the British Standards published a formulae to calculate the airflow in a single-zone with just one opening, presented in Equation 2.22.

$$Q_V = 0.025 A_o U_{10} + C_D \frac{A}{3} \sqrt{\frac{\Delta T g H_o}{T_M}} \quad (2.22)$$

where A_o is the opening area (m^2), U_{10} is the wind speed measured in open country at a standard height of 10 m (m/s), ΔT is the temperature difference between inside and outside the building (K), C_D (adopted equal to 0.63) is the opening discharge coefficient, T_M is the mean temperature between inside and outside the building (K), g is the gravity acceleration (m/s^2) and H_o is the opening height (m).

2.5.3 ASHRAE (2005)

According to the American Society of Heating, Refrigerating and Air-Conditioning Engineers (ASHRAE, 2005c), the airflow in a single-sided ventilation residential building can be expressed as:

$$Q_V = C_V A_o U_{10} + C_D A_o \sqrt{\frac{2 g \Delta H_{NPL} \Delta T}{T_i}} \quad (2.23)$$

where the airflow rate is expressed in m^3/s , C_V is the effectiveness of the opening, C_V is assumed to be 0.5 to 0.6 for perpendicular winds and 0.25 to 0.35 for diagonal winds), A_o is the opening area (m^2), U_{10} is the wind speed at a 10-meter height, C_D is the discharge coefficient, g is the gravitational acceleration (m/s^2), ΔH_{NPL} is the height from midpoint of lower opening to neutral plane level (m), ΔT is the average indoor-outdoor temperature difference for time interval of calculation (K) and T_i is the indoor temperature (K).

The airflow model presented in Equation 2.23 is used when $T_i > T_e$, if the opposite situation occurs replace T_i on the denominator by T_e . If the building has more than one

opening, the outlet and inlet areas are considered equal.

According to ASHRAE (ASHRAE, 2005c), estimation of ΔH_{NPL} is difficult for naturally ventilated buildings. If one window or door represents a large fraction (approximately 90%) of the total opening area in the envelope, then the NPL (neutral plane level) is at the mid-height of that aperture, and ΔH_{NPL} equals one-half the height of the aperture. For this condition, flow through the opening is bidirectional. Finally, interfacial mixing occurs across the counterflow interface, and the orifice coefficient can be calculated according to the following equation:

$$C_D = 0.40 + 0.0045 |T_i - T_e| \quad (2.24)$$

In the cases where enough other openings are available, the airflow through the opening will be unidirectional, and mixing cannot occur. A discharge coefficient of $C_D = 0.65$ should then be used.

2.5.4 Larsen (2006)

Based on Gids and Phaff's model (de Gids and Phaff, 1982), Larsen (Larsen, 2006) concluded that a more precise design expression found from wind tunnel measurements can be used to predict airflows from single-sided ventilation. From Larsen's experimental results, Larsen noticed that the wind prevails on the windward side and that the temperature difference stands out on the leeward side of the buildings. As a result, Larsen (2006) proposed a new model to describe the airflow from single-sided ventilation, which is presented in Equation 2.25.

$$Q_V = A_o \sqrt{C_1 C_P U_{10}^2 + C_2 \Delta T H_o + C_3 \frac{\Delta C_{P,opening} \Delta T}{U_{10}^2}} \quad (2.25)$$

where C_P is the pressure coefficient calculated through the curve presented in Figure 2.2, U_{10} is the air speed at the reference height of 10 m (m/s), H_o is the opening height (m), the constants C_1 , C_2 and C_3 are defined in Table 2.2, and $\Delta C_{P,opening}$, which represents the variations on the pressure coefficient, is calculated according to Equation 2.26.

$$\Delta C_{P,opening} = 9.1894 \cdot 10^{-9} \beta^3 - 2.626 \cdot 10^{-6} \beta^2 - 0.0002354 \beta + 0.113, \quad (2.26)$$

Table 2.2: Constants C_1 , C_2 and C_3 (Larsen, 2006).

	C_1	C_2	C_3
Windward	0.0015	0.0009	-0.0005
Leeward	0.0050	0.0009	0.0160
Parallel	0.0010	0.0005	0.0111

where β is the wind incidence angle ($^\circ$).

The windward, leeward and parallel flows are defined as following:

- Windward, $285^\circ \leq \beta \leq 360^\circ$ or $0^\circ \leq \beta \leq 75^\circ$;
- Leeward, $105^\circ \leq \beta \leq 255^\circ$;
- Parallel, $75^\circ < \beta < 105^\circ$ or $255^\circ < \beta \leq 285^\circ$.

It is also seen that the value of the constants C_1 , C_2 and C_3 depends on the wind direction. This is due to the fact that the flows in the three cases (windward, leeward and parallel) are very different one from each other and therefore also have different weighting of the terms including wind pressure, thermal forces and fluctuating forces. Contrary to what was expected, C_1 does not have the largest weight factor at windward side, but it remains the most dominating factor in this case. In the case where the opening is in the leeward side of the building, the fluctuating term prevails. This is also the case in the parallel wind situations, but here the difference is not as high as in the leeward case.

2.6 Implementation

The implementation aspects are discussed here in order to clarify the main difficulties when natural ventilation models were included into the PowerDomus software code. First, a general idea about the PowerDomus code structure are reported and, in the sequence, the employed algorithms and strategies are also reported.

PowerDomus is an object-oriented software, which has been developed in C++ language and its structure is divided into classes. Those classes represent each part of a building project. For instance, a building structure is divided into zones, e.g. rooms, bathrooms, dinning rooms, and each zone is divided into surfaces, and each surface is divided into regions, and each region corresponds to an specific part of a building wall,

e.g. openings and shared surfaces. Following this structure, a simple class in PowerDomus is composed by a set of classes and the main class, which represents the PowerDomus project file, corresponds to a set of building structures.

To generalize the ventilation models presented above into the source code of PowerDomus software, a new natural ventilation module had to be created and some considerations had to be taken:

- PowerDomus considers time intervals for opening which are set by the users, these intervals corresponds to the time period where the openings are declared open.
- Each opening is configured on a building wall, which is part of a bigger structure called building zone;
- According to the natural ventilation models definitions, just openings on vertical surfaces have to be taken into account;
- Just openings placed on external surfaces are taken into account, those natural ventilation methods are not able to estimate the airflow between building zones;
- The user is able to add and configure more than one opening in each wall;
- The user defines the position of an specific opening according to the PowerDomus CAD (Computer Aided Design) interface;
- The single-sided natural ventilation model can be set by the user, the options are presented in Section 2.5, if there are more than one opening and their intervals coincide, the software must be able to define if a single-sided or cross ventilation model will be used;
- The pressure coefficient calculation method can also be selected by the user, the options are presented in Section 2.3;

2.6.1 Important Considerations

In order to attend the considerations presented above, new classes have been created in order to identify some simulation parameters. For the C_P calculation, the values of L_1 and L_2 are illustrated in Figure 2.6. To calculate L_1 and L_2 a list must be created before the simulation. If there are two or more buildings in a project, it is essential to identify the maximum width and length of each building to define these dimensions.

Before the implementation of the natural ventilation module, PowerDomus was not able to identify how many buildings are available in its projects; it was only capable of verifying if one surface is adjacent to another, which purpose is to avoid superposition of walls during the hygrothermal calculation through building surfaces.

However, to calculate the parameters L_1 and L_2 , a new algorithm was proposed. The general idea was the development of a search method that can find adjacent zones to a selected one and finally the whole building. To solve this problem, a recursive method was implemented. It works searching all shared walls of a zone, if no shared wall is found, than the building architecture is composed just by a single zone. In the other case, if adjacent walls are available, a list of adjacent zones are created and the recursive method is called again in each adjacent zone until no more different shared zones are available. Finally, a list of zones are provided and that list characterize the building.

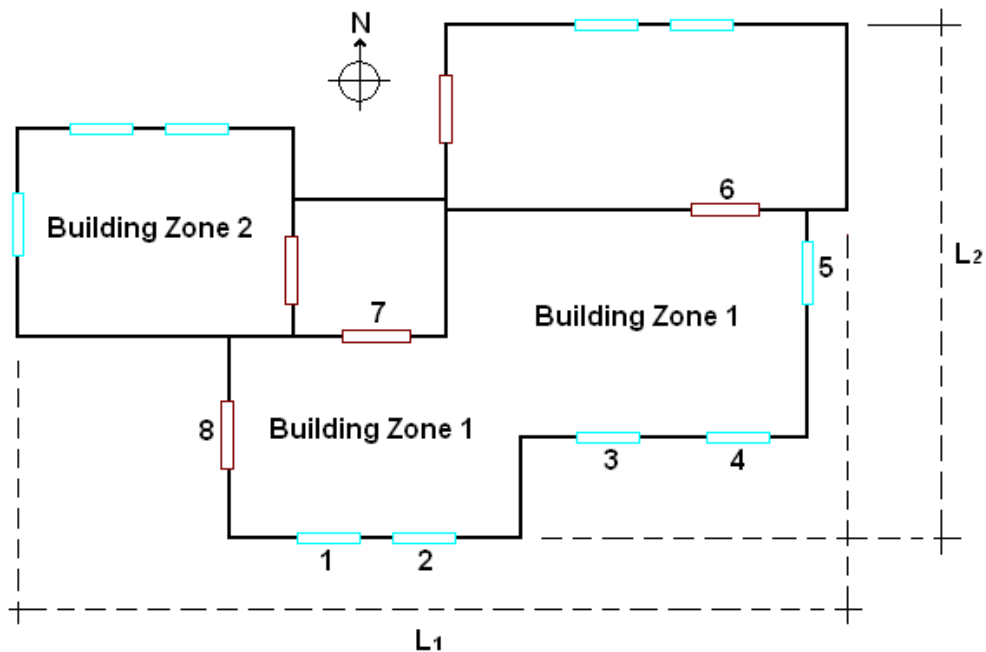


Figure 2.6: Example of natural ventilation model usage.

Considering the “Building Zone 1” in Figure 2.6, 8 openings are identified. However, as discussed before, the implemented natural ventilation models do not take into account the airflow between zones, in this way, for the natural ventilation calculation, just the openings from 1 to 5 will be considered.

If two or more openings are configured as “open” at the same simulation time interval, the software will identify their orientation and recognize if a cross or a single-sided ventilation model will be used. Before the simulation starts, a new class is created based

on setting pointers to the already created opening classes. This new class is called “*Openings_at_same_orientation*”, it is created as a sub-class in each building zone to accelerate the search process responsible to identify which ventilation model will be used during the simulation.

The “*Openings_at_same_orientation*” class consists of a set of linked lists; each list is a group of openings with the same orientation and is filled at each time step. If two or more lists are created during a step-time, it means that more than one opening is configured at the same simulation time interval and, in this way, the cross ventilation model should be used. Contrarily, if just openings in one list are available, the single-sided natural ventilation model selected by the user will be adopted.

To clarify this explanation, let’s consider that openings from 1 through 5 in the building presented in Figure 2.6 are open at the same time step. According to the implemented rules, two lists will be created, one with openings from 1 to 4 facing South, and other list with opening 5, facing East. In this case, the software will consider the cross ventilation case because two lists were created.

Nevertheless, when openings are created in the design process, some important considerations must be assumed to assure that the ventilation models will work properly. One important variable that must be carefully analyzed is the opening area, which is discussed in the following.

When openings are created at the design stage, as presented in Figure 2.6 “Building Zone 1”, the openings’ areas should be taken into account considering some specific situations. According to the models presented in Sections 2.4 and 2.5, the airflow through openings are provided by two main effects: thermal buoyancy and wind. If single-sided ventilation is considered, it is noticed that those models are well adapted to use the correct opening area, dividing the area for both outgoing and into (the building) airflows. However, for cross ventilation situations, the parameter A_b and A_w have to be calculated (see Section 2.4) and adaptations must be done to avoid calculation mistakes. Those adaptations are discussed bellow.

2.6.2 Cross Ventilation - Thermal Buoyancy Effect

The thermal buoyancy effect is basically based on the indoor and outdoor temperature difference (pressure difference), but considering that openings are positioned at the building surface according to the user needs, the airflow must be analyzed.

As it can be seen in Figure 2.7, in the PowerDomus source code, a neutral plane level is calculated to establish the airflow direction profile. In this example, the neutral plane level is calculated based on the vertices' coordinates "A" and "B", which are the higher and lower vertices of the openings set as open at the same time interval.

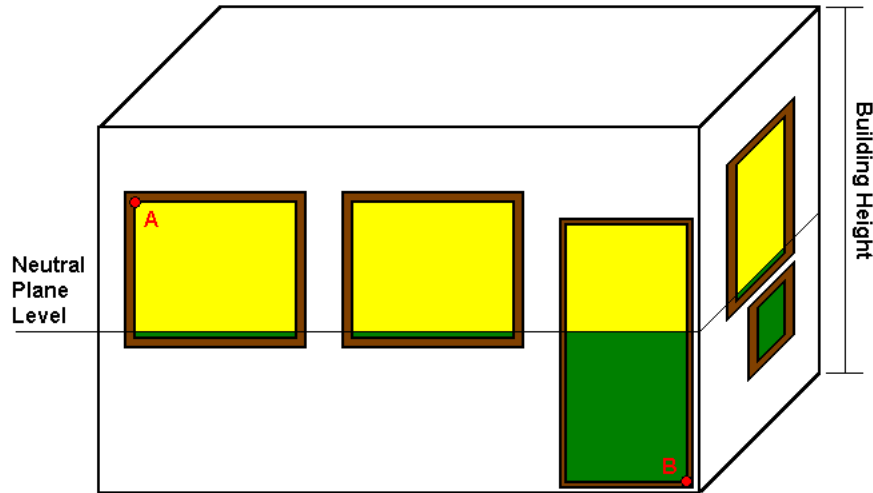


Figure 2.7: Determination of the neutral plane location.

This rule must be considered whenever the software identifies a cross ventilation caused by the thermal buoyancy effect.

2.6.3 Cross Ventilation - Wind Effect

If the wind effect prevails in the cross ventilation, the main variable that defines the airflow through openings is the pressure coefficient C_P . Here, the example presented in Figure 2.6 will be used again to explain the rules for general cross ventilation caused by the wind.

In Figure 2.6, when openings 1 to 5 are considered as "open" at the same simulation time interval, the software finds two directions: the windows from 1 to 4 that face South and the window 5 that faces East. After PowerDomus number of directions identification procedure (at the same simulation time interval), two variables are created: *i*) the mean C_P values of each list and *ii*) the airflow direction.

According to Section 2.3, PowerDomus can calculate the C_P value by two methods: *i*) Mean C_P , which calculates a mean C_P value for the entire surface; and *ii*) CPCALC, which calculates the C_P value for the geometric center of a specific opening.

Following the example, if the Mean C_P method was chosen, windows 1 and 2 will have

the same C_P value, and another value will be calculated for windows 3 and 4, because they are positioned on different surfaces. Finally, a third value will be calculated for window 5. After the calculation of the pressure coefficients, a surface-averaged C_P value will be obtained according to the direction. In the example described here (Figure 2.3), a mean C_P value will be obtained for windows 1 to 4 and compared to the one obtained for window 5. If the window 5 C_P value is higher than the mean value obtained for the other windows, window 5 will represent the airflow into the building and the other windows will be responsible for the outgoing airflow. If the opposite occur ($C_{P\text{window } 5} \leq C_{P\text{other windows}}$), the airflow direction will be also inverted.

If the CPCALC method was chosen, each window will have a C_P value. In this case, the mean C_P for windows 1 to 4 is also calculated and compared to the pressure coefficient of window 5. Finally, the same rules to define the airflow direction are applied.

When more than 3 directions are identified by the software, just the one with higher mean pressure coefficient will represent the incoming airflow; the other directions will then define the outgoing airflow.

2.7 Chapter Remarks

Based on the literature review, natural ventilation physical principles and their respectively mathematical representation have been described in this chapter. Each term, wind and thermal buoyancy, has been carefully studied in order to define generic specifications for whole building simulation. Finally, the definition of implementation rules and important considerations have have been pointed.

At this point, both cross and single-sided ventilation models were defined and are ready to be implemented. Next chapter described the validation of the above described natural ventilation models and their generalization tho whole hygrothermal and energy simulation.

3 Natural Ventilation: Validation Procedures

The main idea of this chapter is to show the validation procedures of the ventilation models implemented into the PowerDomus software comparing the airflow rate estimation of the cross ventilation model proposed by the the British Standard (British Standards, 1999) and Gids and Phaff (1982) and Larsen (2006) single-sided ventilation models to results obtained from wind tunnel and on-site experiments. The two methodologies for evaluating the wind pressure coefficient have also been analyzed here considering that the C_P value is necessary as an input parameter for both cross and single-sided ventilation models. In the sequence, the wind tunnel and on-site configuration have been presented. Results are presented and discussed in the last section.

This chapter is divided into two main sections: *i*) Experiments, where software parameters and building structures are discussed in order to test the main characteristics of each natural ventilation model; and *ii*) validation procedures and validation results, where comparisons between simulations performed into PowerDomus and experimental results found in the literature have been shown.

3.1 Experiments

Here the experiments, that have been chosen to analyze and compare the cross and single-sided ventilation models showed in the previous sections, are presented. Two types of experiments are addressed: *i*) wind tunnel experiment; *ii*) on-site experiment. The wind tunnel experiment presents results for both cross and single-sided ventilation whereas the on-site one is dedicated to the validation of the single-sided ventilation model.

3.1.1 Wind Tunnel Experiment

The wind tunnel experiment has been carried out in a full-scale wind tunnel at the Japanese Building Research institute (BRI) by Larsen (Larsen and Heiselberg, 2008) to investigate the airflow through openings in single-sided and cross ventilation situations. The building's dimension were $5.56m \times 5.56m \times 3.00m$, which means that scale effects were avoided. The opening's width and height were $0.86 m \times 0.15 m$ for both windows in the cross-ventilation case, they were positioned $0.54 m$ away from the right edge and $0.925 m$ from the top (see Figure 3.1 (a)). For the single sided case, the openings dimensions were $0.86 m \times 1.40 m$ of width and height, respectively. In this case, it was positioned at $0.54 m$ away from the right edge and $0.69 m$ away from the top of the building (see Figure 3.1 (b)). The internal room height was $2.4 m$, the thickness of the walls was $0.10 m$ and the room volume was $68.95 m^3$.

The experiment consisted of varying the wind speed in the tunnel ($1, 3$ and $5 m/s$) with a turbulence intensity less than 5% while imposing a temperature difference of $0, 5$ and $10 K$ between the internal and external air. The temperature difference was created with four electric heaters placed inside the building (Larsen *et al.*, 2003). The wind speed profile created in this wind tunnel was almost uniform, which resulted in a wind profile that differs from outdoor conditions as it was not able to reproduce the atmospheric boundary layer. The building was also rotated between 0° and 345° ; using either a 15° or a 30° step to obtain measurements for different wind angles. A total of 159 different cases was studied. The air-change rate was measured with the tracer gas decay method.

The building was designed into the PowerDomus program in order to simulate the wind tunnel experiment. Because of the constant conditions as wind speed, wind incident angle and indoor and outdoor temperatures, specific weather files have been developed in order to reproduce the experiment conditions. The building structures designed into PowerDomus are presented in Figures 3.1 (a) and 3.1 (b). Adiabatic and impermeable conditions has been configured for the floor and a purely conductive heat transfer model has been considered for the other surfaces.

3.1.2 On-Site Experiment

The building selected for the on-site experiment is the Institute of Meteorology and Physics of the Atmospheric Environment, which is a three-storey, naturally ventilated, office building referred as the NOA (National Observatory of Athens) building in the

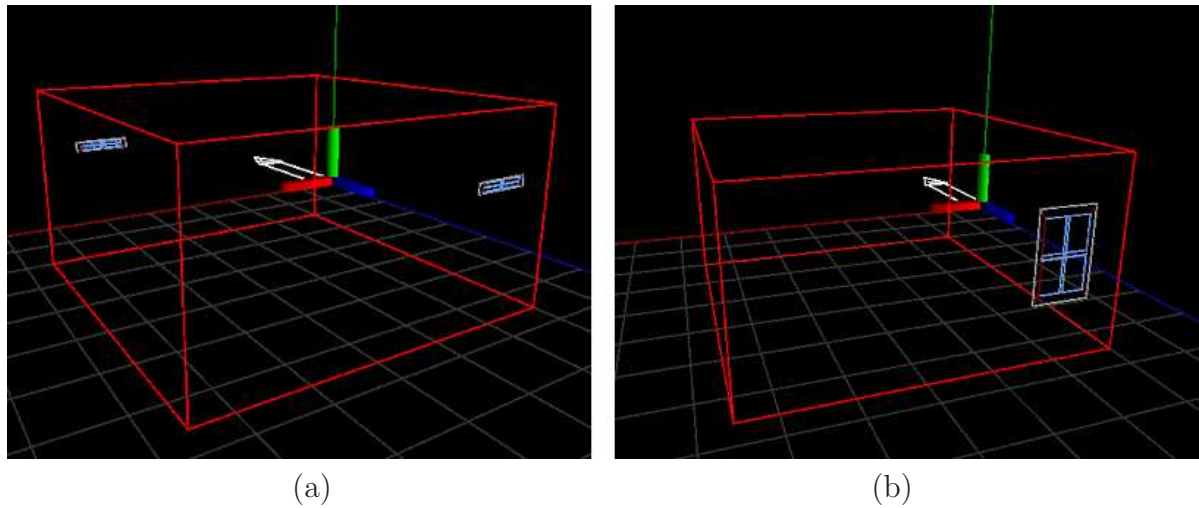


Figure 3.1: Experiments designs performed into the PowerDomus software for the wind tunnel: (a) cross ventilation case and (b) single-sided ventilation case.

sequence. Each floor is about 4.50 m high and the dimensions are $10.20\text{ m} \times 16.30\text{ m}$ of length and width respectively. Ventilation experiments were held at the first floor (IEA, 1996). The selected office room (see Figure 3.2) was isolated from the rest of the building. The room has a 13.59 m^2 floor area, while its length is equal to 3.00 m .

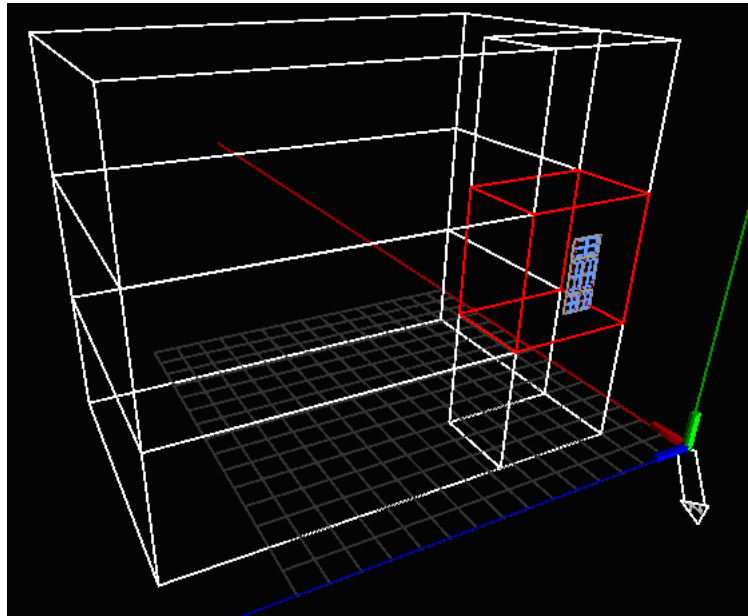


Figure 3.2: Experiment design performed into the PowerDomus software for the on-site single-sided ventilation case.

The only external window, which is shown in Figure 3.3 (Dascalaki *et al.*, 1999), is located on the west wall and is divided into five parts; each part can be opened separately providing the different opening configurations. The dimensions of each part of the opening are presented in Table 3.1, the total window area is 2.50 m^2 and its angle from the North

orientation is 315° .

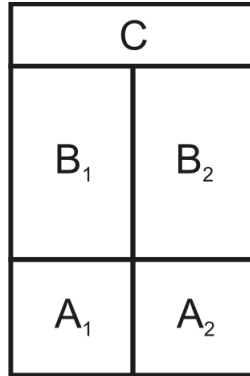


Figure 3.3: Window parts for the on-site experiment.

Table 3.1: Window dimensions for the on-site experiment.

Window Part	Height (m)	Width (m)	Opening Area (m ²)
A_1, A_2	0.65	0.53	0.34
B_1, B_2	1.13	1.13	0.60
C	0.62	1.06	0.66

Airflow rates across the openings have been performed according to the single tracer gas decay technique. Fourteen different experiments have been taken into account. The mean climatic conditions for each experiment are given in Table 3.2; more detailed information about this experiment can be found in (Dascalaki *et al.*, 1999).

Table 3.2: Opening configuration and mean climatic conditions for single-sided ventilation experiments in the NOA building.

Experiment	T_i	T_e	U_{10}	β
$A_1 + A_2$	31.4	31.3	6.8	40
$B_1 + B_2$	31.8	32.6	3.0	70
C	32.1	30.6	5.0	30
$A_2 + B_2$	31.8	32.5	6.7	50
$A_1 + A_2 + B_1 + B_2$	31.5	30.5	1.7	50
$B_1 + B_2 + C$	29.2	28.8	1.6	45
All	31.0	30.2	3.6	12
$A_2 + C$	31.7	31.2	5.4	30
$B_2 + C$	31.8	30.7	4.9	70
$A_1 + A_2 + C$	31.0	30.8	4.2	50
$A_1 + B_1 + C$	28.8	27.6	2.0	35
$A_2 + B_2 + C$	31.6	30.1	5.0	20
$A_1 + A_2 + B_1 + C$	31.0	29.6	3.1	35
$A_1 + A_2 + B_2 + C$	31.0	28.2	3.4	37

where T_i is the indoor temperature ($^\circ C$); T_e is the outdoor temperature ($^\circ C$), U_{10} is the wind speed at 10 m high (m/s) and β is the wind incidence angle ($^\circ$).

3.2 Validation Results

This section presents the comparisons among the results obtained by using the PowerDomus software and the experimental data obtained for both wind tunnel and on-site experiments. In the sequence, simulation parameters are addressed and results of each simulation case are discussed.

3.2.1 Wind Tunnel Simulations

3.2.1.1 Cross Ventilation

Figure 3.4 presents the results of wind tunnel cross ventilation experiments of Larsen (2006) and the predictions of the British Standard (1999) model implemented in the PowerDomus software.

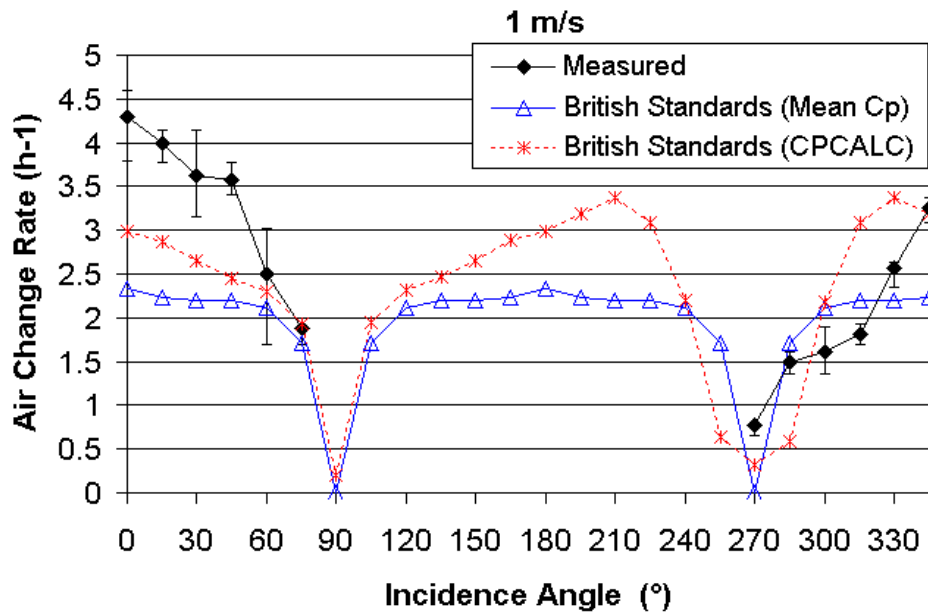


Figure 3.4: Comparisons between the experimental and simulation results performed for the wind tunnel - cross ventilation case.

Among the six different experiments (three different wind velocities and three distinct temperature differences) performed by Larsen (2006), only one is presented here (wind velocity of 1 m/s , isothermal case). In fact, as shown by Equation 2.17, the airflow rate is a linear function of the wind velocity so that results for other velocities can be easily interpolated from the presented ones. The experimental results clearly showed the linear behaviour. Moreover, because of the fact that the openings are located at the same height, there is no thermal buoyancy effect; in this way, the negligible air change rate variations

caused by temperature differences have not been treated in this case with high wind velocities. Results obtained by the model are the same for distinct temperature differences for the present configuration. The experimental results showed also that tendency with a slight variation probably due to the precision of the experimental measurements. The experimental results presented in Figure 5 are the airflow rate averages obtained from three distinct temperature differences results.

Results show that the British Standard (Mean C_P) model is not capable of predicting the variation of the airflow rate according to the wind direction. The British Standard (CPCALC) model tends to better follow this variation. One particular drawback of the Mean C_P -based model occurs when the wind is parallel to the openings. In this case, this model predicts no flow (the C_P difference between the openings is null) whereas the CPCALC-based model is able to detect a small but notable airflow.

However, it can be seen that the two models present almost the same mean relative difference of about 30% considering the whole set of data (Table 3.3).

Table 3.3: Relative differences (%) for the wind tunnel experiment - cross ventilation case.

Model	Relative Difference (%)
Mean C_P (A)	32.46
CPCALC (A)	31.11

3.2.1.2 Single-Sided Ventilation

In order to illustrate the behavior of each single-sided ventilation model and to analyze the effect from different wind speeds (1, 3 and 5 m/s), temperature differences (0, 5 and 10°C) and incidence angles (varying from 0 to 345°) on the airflow rate, 27 simulations using the PowerDomus software have been performed.

As simulation parameters, for the pressure coefficient calculation through the Mean C_P method an $\alpha_R = 0.10$ has been adopted, which is the value when there are no obstructions affecting the wind. For the CPCALC method, the same $\alpha_R = 0.10$ has been used and for the plan area density and surrounding building height the values of $pad = sbh = 0$, have been adopted because there are no obstructions inside the wind tunnel.

The results, presented in Figures 3.5, 3.6 and 3.7, represent the air-change rates as a function of the incidence angle and the temperature difference of 5°C. Each line represents one of the selected wind speeds. On the other hand, Larsen's model does present the expected angular dependency. For the lower wind velocity, wind and temperature gradient

effects are about the same so that the third term of Equation 2.21 really affects the results. In particular, the influence of the non-symmetrical term C_P is visible for the incidence angle in $120^\circ \leq \beta \leq 240^\circ$. For higher wind velocity, the first term of Equation 2.21, and $f(\beta)$ term, predominates so that the obtained air change rate becomes more symmetrical, at least when the Mean C_P method is used.

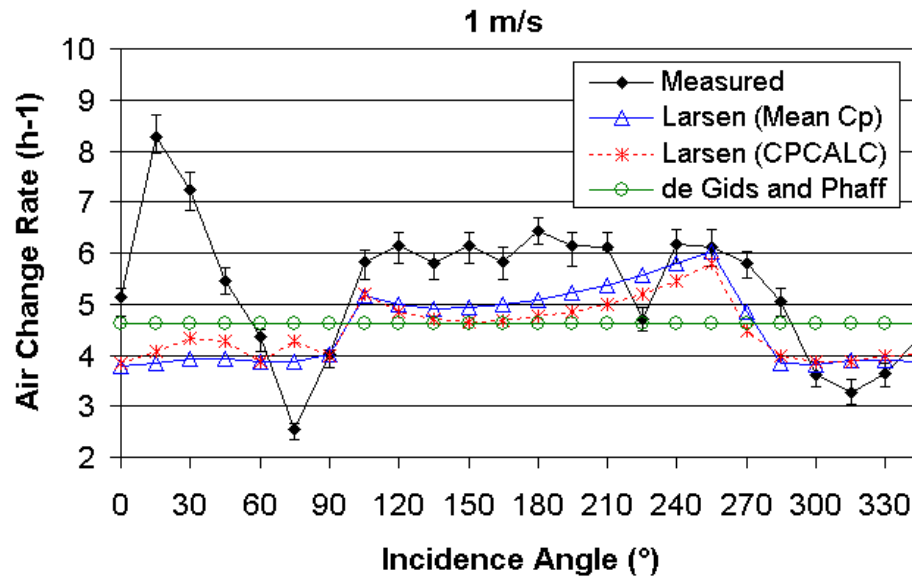


Figure 3.5: Comparisons between the experimental and simulation results performed into the PowerDomus software for the wind tunnel case with wind speed of 1 m/s - single-sided ventilation case.

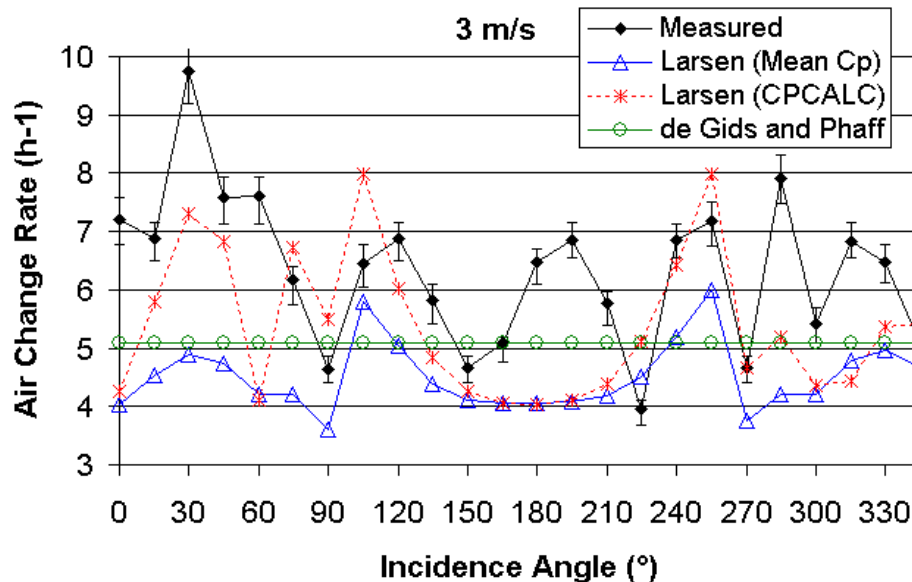


Figure 3.6: Comparisons between the experimental and simulation results performed into the PowerDomus software for the wind tunnel case with wind speed of 3 m/s - single-sided ventilation case.

Analyzing the results for the de Gids and Phaff model, it is noticed that there are

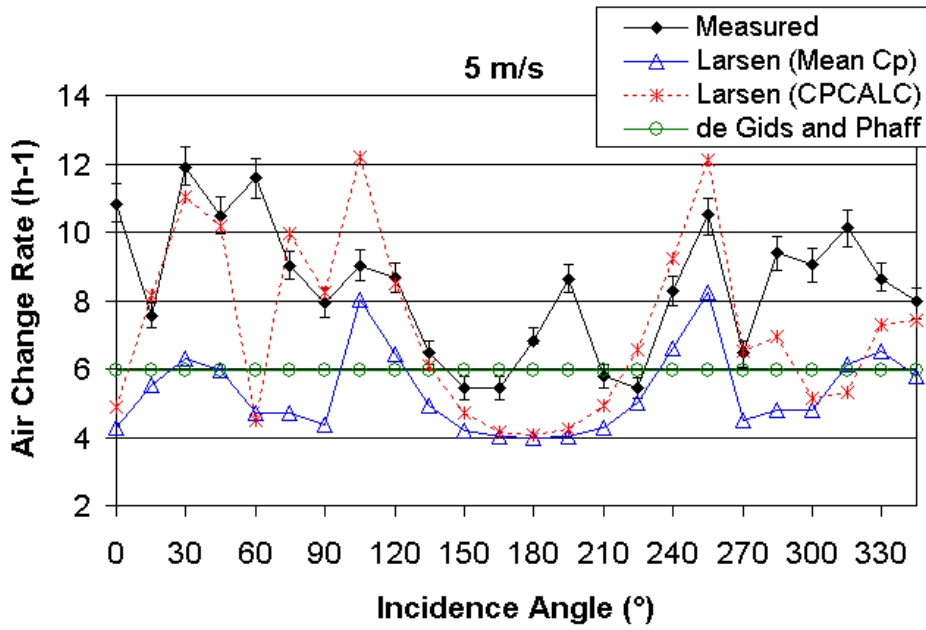


Figure 3.7: Comparisons between the experimental and simulation results performed into the PowerDomus software for the wind tunnel case with wind speed of 5 m/s - single-sided ventilation case.

no variations on the air change rates when the incidence angle changes. This happens because the model does not take into account the incidence angle in its calculation. In this way, a constant single value is obtained for each wind speed.

The differences noticed between the Larsen (Mean C_p) and Larsen (CPCALC) models are caused by the calculation of the pressure coefficient. While the Mean C_p method calculates the wall mean pressure coefficient, the CPCALC method estimates the C_p value for the geometric center of the opening. As a consequence, the C_p values calculated by the CPCALC method are higher when the wind incidents directly on the window (angle in the interval of $270 \leq \beta \leq 360^\circ$) than for angles between $0^\circ \leq \beta \leq 90^\circ$. The Mean C_p method is not able to represent this actual behavior.

The relative differences for the windward, leeward and parallel incidence angles have been presented in Table 3.4 and the relative differences calculations consider the three wind speed values (1.3 and 5 m/s). It is noticed for the windward and leeward incidence angles, the Larsen's model by using the CPCALC calculation presents slightly better results than the two others. When the parallel incidence angle is analyzed, the Mean C_p method has a difference higher than the others. This represents the model difficulty to calculate the pressure coefficient in angles near 90° .

Table 3.4: Relative differences (%) for the wind tunnel experiment - single-sided ventilation case.

Model	Windward	Leeward	Parallel
Larsen (Mean C_P)	34.25	20.85	22.38
Larsen (CPCALC)	24.99	19.75	7.68
de Gids and Phaff	29.89	20.39	14.68

3.2.2 On-Site Simulations

The comparisons of the on-site experiment and the simulations performed by PowerDomus are compared in this section. According to (Dascalaki *et al.*, 1999), the building is located in an open urban environment on top of a hill across from the Acropolis of Athens, consequently, the simulation parameter $\alpha_R = 0.28$ has been chosen for the pressure coefficient calculation by the Mean C_P and by the CPCALC methods. For the last one, the $pad = sbh = 0$ have also been used. Figure 3.8 shows the comparisons between the simulation and the measured results.

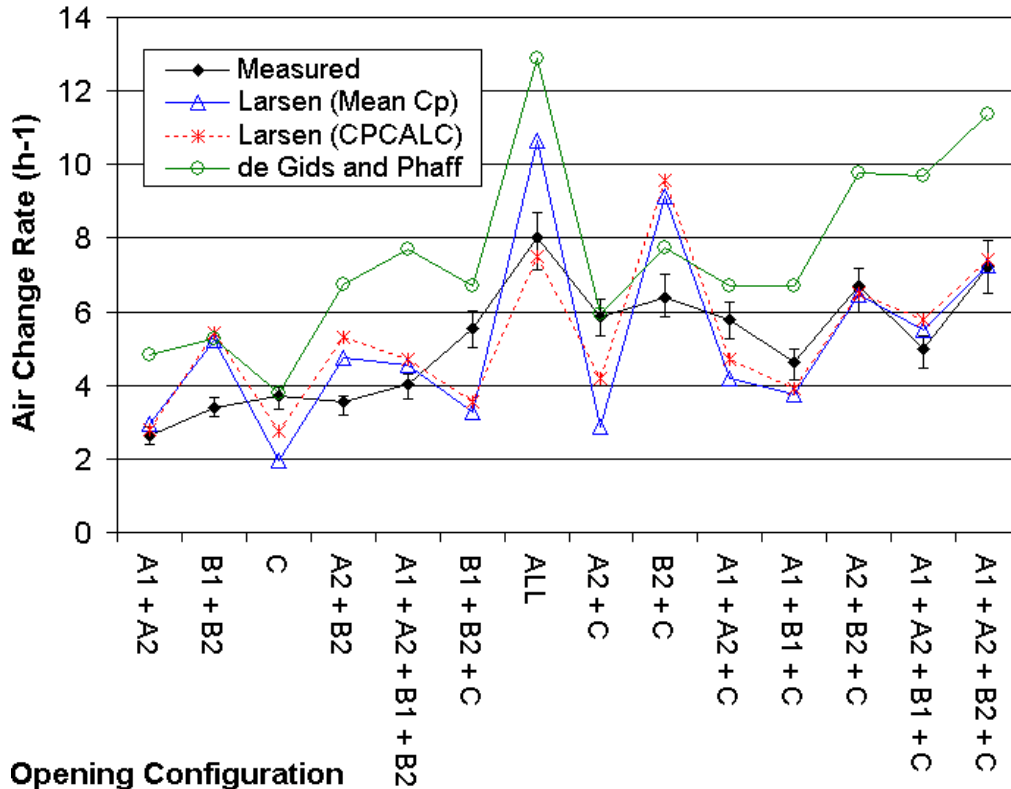


Figure 3.8: Comparisons between the experimental and simulation results performed into the PowerDomus software for the NOA Building case.

According to the results presented in Figure 3.8, it has been noticed that the Larsen model using the CPCALC method to calculate the pressure coefficient has provided the

best results. When the relative differences for all the obtained results are calculated, the graphical analysis is verified (Table 3.5).

It should be noticed that the wind incidence angle stayed around 90° during the experiments for which Larsen model already showed better prediction in the wind tunnel experiment. The slightly better results of Larsen (CPCALC) compared to Mean C_P essentially occur for 3 points (C , All , $A_2 + C$) where the angle is about 70° for which this model showed better prediction as well on the wind tunnel experiment. On the other side, the de Gids and Phaff model, which presented great results for the wind tunnel experiment, was not capable of providing good results in this case.

Table 3.5: Relative differences (%) for the NOA Building experiment.

Model	Relative Difference (%)
Larsen (Mean C_P)	27.71
Larsen (CPCALC)	24.03
de Gids and Phaff	49.06

3.3 Chapter Remarks

Several cross and single-sided natural ventilation simulations through openings were performed in the building hygrothermal and energy simulation software PowerDomus. The simulations have been compared to the experimental results carried out in a full-scale wind tunnel and in an on-site three storey office building.

Results showed that the use of the CPCALC algorithm actually improves the predictions, particularly in the case of single-sided configurations.

It has also been found that the current state-of-the-art empirical models for natural ventilation are capable of predicting the actual trends. However, the predictions still present a high difference of about 30%. More accurate empirical models are still needed to evaluate the air change rate by cross and single-sided natural ventilation.

4 Comparative Analysis: Natural Ventilation versus Air-Conditioning Systems

Considering modifications in the buildings in order to keep the indoor environment isolated from the outdoor climate, buildings have been gradually become a "pollutant trap", that is harmful to occupants, decreasing indoor air quality (IAQ) and productivity. Additionally, mould and mildew growth in internal surfaces have been noticed in hot and humid climates and consequentially health problems appear. This contributed to the Sick Building Syndrome phenomenon that showed up in the early eighties. After this, the optimization of building thermal comfort and improvement of indoor air conditions related to health became the main issues in the control of HVAC systems in order to ensure the required conditions to maintain the occupants' health. In the following, a review presents the main advances in the whole-building hygrothermal and energy combined simulation with HVAC systems to allow the analysis of energy consumption, thermal comfort and mould growth in building structures.

Mendes *et al.* (2003), presented the moisture effects on conduction loads using different levels of simplifications based on the model of Philip and De Vries, (1957), which have been implemented in the UMIDUS code (Mendes *et al.*, 1999) to simulate a single building element.

A need to develop good models to evaluate the integral performance of whole buildings, considering the presence of moisture within the porous elements, originated in late 2003 a new international research project (Annex 41) in the framework of the International Energy Agency (IEA/ECBCS) entitled "Whole Building Heat, Air and Moisture Response (MOIST-ENG)" (Hens, 2003). In the same context, other attempts to simulate the hygrothermal performance of non-conditioned buildings were presented by Rode in (Rode *et al.*, 2004), (Mendes *et al.*, 2003), (Holm *et al.*, 2002) and (Simonson *et al.*, 2002).

Despite the importance of the subject concerning moisture and its impact on the HVAC system performance, just a few publications can be found in the literature. Knabe and Le in (Knabe and Le, 2003) combined building simulation with a split air-conditioning system, considering the envelope hygrothermal effect by using the program TRNSYS-TUD. Cherem-Pereira (Cherem-Pereira, 2003) developed models for room air conditioners, integrating them to the Hygrothermal building simulation program PowerDomus (Cherem-Pereira and Mendes, 2003), considering adsorption and desorption effects. However, no work has mentioned the combined simulation of a central HVAC systems with a detailed hygrothermal model for the building envelope.

To model central HVAC systems, steady-state models have been largely presented such as in (Knabe and Le, 2003), (Hensen, 1991), (Chow *et al.*, 1997), (Lam *et al.*, 1997), (Corrêa, n.d.), (Cui *et al.*, 1999), (Nassif *et al.*, 2003), (Bourdouxhe and André, 1997). On the other hand, unsteady-state mathematical models have been presented by (Barbosa and Mendes, 2003) and (Novak *et al.*, 2004) to simulate secondary HVAC systems.

In order to verify the effects of the moisture buffer capacity on the energy consumption of buildings equipped with central HVAC systems, a model to simulate both the primary (chiller, cooling tower and pumps) and the secondary (cooling coil, humidifier, fan and mix-ing box) systems combined with a full hygrothermal model has been presented in (Barbosa and Mendes, 2008). The hygrothermal envelope model was based on the work presented by Mendes (Mendes *et al.*, 2002), which has a robust method to calculate simultaneously the temperature and moisture content distributions within the porous envelope and was conceived to preserve numerical stability.

By using the same envelope model presented by Mendes *et al.* (2002), the mould growth in building wall surfaces has been studied in this chapter. In buildings, mould fungi cause problems in different structures and materials: roofs, basements, floors and walls. In addition, health problems caused by mould spores presents in the air started to appear. According to (Sundell, 2007), researches on IAQ-health show that the probability of increasing health problems as asthma, and allergies are evident when mould growth appear on indoor wall surfaces.

Moulds are a heterogeneous group of multicelled organisms which reproduce asexually either by spore formation or by fragmentation. They can grow on a wide variety of substrates and are generally regarded as spoilage organisms. Mould fungi needs specific conditions to grow, according to Hukka and Viitanen (1999) model (Hukka and Viitanen, 1999). Mould grows usually at high humidity levels on wall surfaces when temperatures

are over 20°C .

The model proposed by Hukka and Viitanen (1999) corresponds to a generic mould growth index for building structures and the multidimensional effects of building elements has not been evaluated. In a more detailed analyzes, a Heat, Air and Moisture (HAM) transfer model based on driving potentials of temperature, air pressure and water vapor pressure gradients for consolidated porous materials has been presented by Santos and Mendes (Santos and Mendes, 2009). In their work, different climatic conditions have been used for hygrothermal analysis of specific corners (thermal bridges) to evaluate the conditions leading to mould growth in buildings. According to them, the moisture accumulation caused by air stagnation in corner is the main effect that describes them as the most susceptible regions to mould growth (Santos and Mendes, 2009). The mould leading conditions model used by them has been proposed by (Clarke, 1999), which defines six categories of mould growth under steady conditions.

By reducing the indoor air relative humidity and consequently the indoor wall surfaces relative humidity it is possible to reduce the possibility of mould growth in buildings structures. This effect is analyzed in this chapter by using the PowerDomus software and its generic computational algorithm developed to integrate models for HVAC systems and natural with hygrothermal building and mould growth models.

In this way, the mould growth problem in building structures is evaluated in this chapter based on the Mould Growth Risk Index (Hukka and Viitanen, 1999), showing that natural ventilation strategies can provided efficient mould growth control an be as efficient as HVAC systems, improving indoor air quality conditions.

This chapter is based in a case study where natural ventilation and an air handling units have been used to enhance comfort levels and reduce the potential of mould growth in building surfaces. In the next section an introduction describing the available types of HVAC systems is presented, followed by the description of primary and secondary HVAC components models. In Section 4.2, some thermal comfort models have been described, which have been adopted in order to correct evaluate the thermal conditions according to the air-conditioning strategy (natural ventilation or air-cooling). In the sequence, the Mould Growth Risk model has been introduced followed by the HVAC components parameters. Finally, Section 4.4 shows the case study addressing the building geometry and simulation parameters and, to conclude this chapter, results and chapter remarks are addressed.

4.1 HVAC System

According to Haines and Wilson, (2004), HVAC systems are designed to satisfy the environmental requirements of comfort in a specific building (or building zone) and in a particular geographic locale. Usually, HVAC systems can be classified into two methods of conditioning: *i*) radiant system; and *ii*) forced air systems. This work deals with forced air systems, which are widely used in the Brazilian context.

Forced air systems can be classified into four groups as follows:

- **Single Zone:** This type is identified for serving just one area of a building. In this case, all of the rooms in this area must have similar cooling and heating vents that are regulated by a common control system (usually a thermostat);
- **Multiple Zone:** In this type of HVAC system, each zone can have a different control scheme with separate indoor air control systems;
- **Constant Volume:** These systems are designed to provide to each zone a constant volume of flow rate. Temperatures are changed by switching the HVAC unit on or off;
- **Variable Volume:** Variable air volume (VAV) systems allow users to vary the amount of cooled or heated air delivered to each zone.

Moreover, forced air systems depend upon a number of factors like how large the area is to be cooled/heated, the total heat gains/losses inside the building environment and others. If the whole building is to be cooled/heated it is not economically viable to put window or split air conditioner in each and every room, in these cases, central air-conditioning plants are adopted.

When central systems are considered, they can be divided into two types: Direct Expansion and Indirect Expansion. In Direct Expansion systems, the air used for cooling/heating the indoor air is directly passed over the plant' coil. In indirect expansion systems, the heating/refrigeration system is used to first heat/chill the water or other fluid, which is then used to heat/chill the indoor air. However, many buildings have no central plant. This decision is, in part, influenced by the criteria presented in Table 4.1. Usually, central air-conditioning systems have a longer life than packaged equipment and can be operated more efficiently. The disadvantages include the cost of pumping and piping or, for the central AHU (Air-Handling Unit), longer duct systems and more fan

power. Recently, the idea cited by Haines and Wilson (2004), that each building must be evaluated separately, is being adopted.

Table 4.1: Criteria for HVAC system and equipment selection (Haines and Wilson, 2004).

Criterion	
1	Demands of comfort or process
2	Energy conservation, code requirements
3	First cost versus life-cycle cost
4	Desires of owner, architect, and/or design office
5	Space limitations
6	Maintainability/reliability

This work considers indirect expansion systems with constant airflow rate. The components of this type of systems, when just cooling is considered, can be separated into primary components (chiller, cooling tower, primary pumps and condensation pumps) and secondary components (cooling and dehumidifying coil, humidifier, fan and mixing box). In Figures 4.1 and 4.2, diagrams showing the primary and secondary systems are presented.

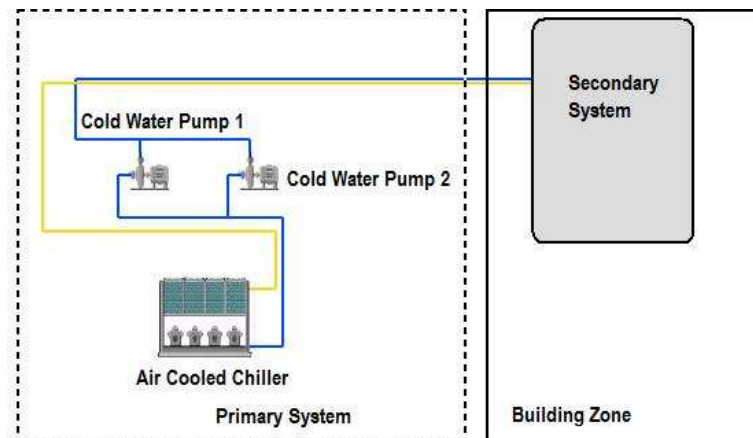


Figure 4.1: Central cooling system: primary components.

4.1.1 Primary System Components

In this section, the models of the primary components of the HVAC system used to compare natural ventilation and air-conditioning are presented.

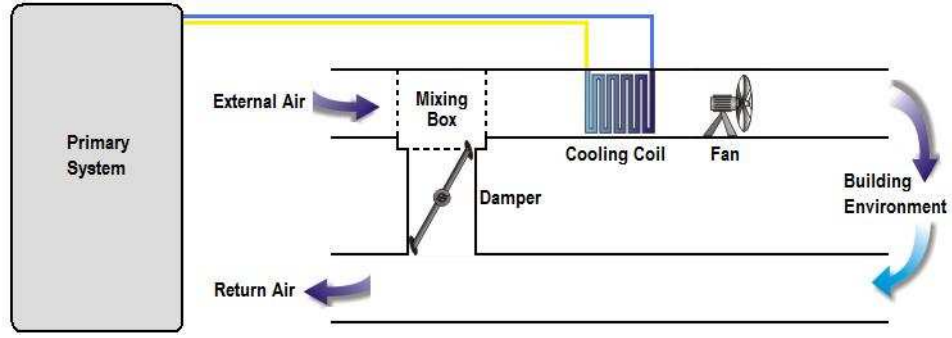


Figure 4.2: Central cooling system: secondary components.

4.1.1.1 Chiller Model

For the Chiller, a model based on regression functions that describe how the cooling capacity and the energy efficiency vary with operation conditions, as well as the power consumption varies with part-load ratio (Pacific Gas and Electric, 1996) is employed.

The chiller model can be described from Equation 4.1 to 4.3. Those equations represent the capacity (CAPFT) and efficiency (EIRFT) curves as a function of the chiller's evaporator leaving temperature and inlet condenser temperature and the efficiency curve (EIRPLR) of this air-cooled chiller as a function of the part-load ratio.

$$CAPFT = a_1 + b_1 T_{ev,out} + c_1 T_{ev,out}^2 + d_1 T_{cd,in} + e_1 T_{cd,in}^2 + f_1 T_{ev,out} T_{cd,in} \quad (4.1)$$

$$EIRFT = a_2 + b_2 T_{ev,out} + c_2 T_{ev,out}^2 + d_2 T_{cd,in} + e_2 T_{cd,in}^2 + f_2 T_{ev,out} T_{cd,in} \quad (4.2)$$

$$EIRPFPLR = a_3 + b_3 PLR + c_3 PLR^2, \text{ with } PLR = \frac{Q_{ev}}{Q_{ev,available}(T_{ev,out}, T_{cd,in})} \quad (4.3)$$

where,

- $T_{ev,out}$: the outlet evaporator water temperature ($^{\circ}C$);
- $T_{cd,in}$: the inlet condenser temperature (external air or condensing water) ($^{\circ}C$);
- PLR : the part-load ratio (-);

- $Q_{ev,available}$: the chiller cooling capacity available in full load conditions (W);
- a, b, c, \dots, f : the curve coefficients, which can be obtained experimentally or from catalogs.

Equation 4.1 is a biquadratic function that describes how the chiller cooling capacity varies at different outlet evaporator water temperatures and inlet condenser water temperatures. Equation 4.2 is also a biquadratic function that describes how the full load efficiency varies with water temperatures, while Equation 4.3 is a quadratic function that describes how the efficiency varies with part-load ratio.

Combining all three equations (Equations 4.1-4.3), the power at specified operating conditions can be evaluated by:

$$E_{comp}(T_{cd,in}, T_{ev,out}) = E_{ref} CAPFT EIRFT EIRPLR \quad (4.4)$$

The values of $CAPFT$, $EIRFT$ and $EIRPLR$ are dimensionless values, which are obtained in the following way:

$$CAPFT = \frac{Q_{ev,available}}{Q_{ev,rat}} \quad (4.5)$$

$$CAPFT = \frac{E_{comp,max} Q_{ev,rat}}{Q_{ev,available} E_{comp,rat}} \quad (4.6)$$

$$EIRPLR = \frac{E_{comp}(PLR)}{E_{comp,max}} \quad (4.7)$$

where,

- $Q_{ev,rat}$: the chiller cooling capacity at nominal conditions (W);
- $E_{comp}(PLR)$: the chiller compressor electric power at part-load conditions (W);
- $E_{comp,rat}$: the chiller compressor electric power at rating conditions (W);
- $E_{comp,max}$: the maximum chiller compressor electric power at full load conditions (W).

4.1.1.2 Pump Model

The pump model is based on the model presented in (Brandemuehl *et al.*, 1993). The model calculates pump power consumption and exiting fluid temperature for a given flow rate and entering fluid conditions. The model considers both variable and constant flow pumps. The pump power for variable flow is calculated from a regression of part-load power consumption as a function of part-load flow. The pump power consumption is determined by the following expression:

$$E_{pump} = FFLP E_{pump,rat} \quad (4.8)$$

where E_{pump} and $E_{pump,rat}$ are the actual pump/motor power at part-load conditions and full load power, respectively. The factor $FFLP$ is a polynomial function in function of the partial-load-ratio (PLR), in the following way:

$$FFLP = C_0 + C_1 PLR + C_2 PLR^2 + C_3 PLR^3 \quad (4.9)$$

The factor PLR is defined as the ratio between the actual volumetric flow and the rated flow $PLR = \frac{\dot{V}_{actual}}{\dot{V}_{rat}}$. The coefficients C_0, \dots, C_3 are obtained from data catalogs.

4.1.2 Secondary System Components

In the sequence, the models of the secondary components of the HVAC system used to compare natural ventilation and air-conditioning are presented.

4.1.2.1 Mixing Box Model

The model calculates the output air conditions for a mixing process based on the energy and mass conservation equations for the moist air. Applying the mass and energy conservation Equation 4.3 to the mixed humidity ratio and enthalpy are given as:

$$\dot{m}_{a,out} = \dot{m}_{a_1,in} + \dot{m}_{a_2,in} \quad (4.10)$$

$$w_{a,out} = \frac{\dot{m}_{a_1,in} w_{a_1,in} + \dot{m}_{a_2,in} w_{a_2,in}}{\dot{m}_{a,out}} \quad (4.11)$$

$$h_{a,out} = \frac{\dot{m}_{a1,in}h_{a1,in} + \dot{m}_{a2,in}h_{a2,in}}{\dot{m}_{a,out}} \quad (4.12)$$

where, \dot{m} , w and h are respectively air mass flow rate (kg/s), humidity ratio (kg water/ kg dry air) and enthalpy (kJ/kg) in the mixing box inlet and outlet.

4.1.2.2 Cooling and Dehumidification Coil Model

For the cooling and dehumidification coil model, the CCDET model (Brandemuehl *et al.*, 1993) has been used as presented in ASHRAE HVAC 2 Toolkit. The coil is modeled as a counterflow heat exchanger adapted for air-conditioning systems with at least four rows. Alternative models can be found in the literature such as in (Wang *et al.*, 2004) and (Ghiaus *et al.*, 2007). This model considers the external condensation at the coil surface.

This model demands geometric coil data such as the internal and external tube diameter, fin area, fin thickness etc. The model calculates the water temperature, air humidity ratio and temperature at the coil outlet, sensible heat transfer rate and the fraction of wet surface area.

4.1.2.3 Fan Model

The fan model calculates the fan power and leaving air conditions, as well the air temperature and humidity for a given flow rate and entering air conditions. The fan model used is based on the model presented in (Brandemuehl *et al.*, 1993).

The fan power consumption is then determined in the following way:

$$E_{fan} = FFLPE_{fan,rat} \quad (4.13)$$

where E_{fan} and $P_{W fan,rat}$ are the actual shaft power at part-load conditions and full load power, respectively. The factor $FFLP$ is a polynomial curve fit as a function of part-load ratio (PLR), in the following way:

$$FFLP = C_0 + C_1PLR + C_2PLR^2 + C_3PLR^3 \quad (4.14)$$

The factor PLR is defined as the ratio of the actual volumetric flow rate to the rated flow rate $PLR = \frac{\dot{V}_{actual}}{\dot{V}_{rat}}$. The coefficients C_0, \dots, C_3 are obtained from supplied catalogs data.

In order to evaluate building occupants thermal sensation and health parameters of the indoor environment, the following section presents thermal comfort models, which can be used to analyze the performance of HVAC and/or natural ventilation systems.

4.2 Thermal Comfort

Thermal comfort can be defined as “that condition of mind that expresses satisfaction with the thermal environment” (ASHRAE, 2005*d*) but the definition and control of indoor conditions for reaching thermal comfort in buildings are difficult to be established. As thermal satisfaction depends on several parameters, research works on thermal comfort have been conducted and some comfort indices have been proposed over the last fifty years. An example is the thermal comfort index called effective temperature, which is computed by using indoor temperature and relative humidity and has been adopted by ASHRAE (ASHRAE, 2005*d*) for decades.

On the other hand, a quite disseminated index for evaluating indoor thermal comfort is the PMV (Fanger, 1970), which combines environmental variables and individual parameters. ASHRAE (ASHRAE, 2005*d*) adopts besides PMV another index, the ASHRAE Thermal Sensation, referred as ATS in the present document, which correlations are based on a 1600 students report about thermal comfort (Rohles, 1973). Both PMV and ATS indices have been proposed here to be studied and implemented into PowerDomus software.

4.2.1 ASHRAE Thermal Sensation Index (ATS)

The ATS index allows to evaluate, in an easier way, the thermal comfort sensation compared to the PMV index because it is just based on the air temperature, air humidity (or vapor pressure), sex and time exposure. In the analysis of this correlations others parameters have been considered constants as light clothing index and metabolic rate, low air velocity and finally the mean radiant temperature has been adopted equal to the air temperature. The result of simplifications is a simple formulae to evaluate thermal comfort which is shown in Equation 4.15 for both sexes and 1-hour exposure time:

$$ATS = 0.2448 T_i + 0.2480 P_V - 6.52775, \quad (4.15)$$

where T_i is the indoor air temperature (in $^{\circ}C$) and P_V is the vapor pressure (in kPa).

In the same way, as the PMV index, ASHRAE (ASHRAE, 2005*d*) adopts a thermal sensation scale for the ATS index, which is presented in Table 4.2.

Table 4.2: ASHRAE thermal sensation scale.

ATS	Thermal Sensation
+3	Hot
+2	Warm
+1	Slightly Warm
0	Neutral
-1	Slightly Cool
-2	Cool
-3	Cold

4.2.2 Predicted Mean Vote (PMV)

According to the literature, the Predicted Mean Vote (PMV) has been widely used as a standard in thermal comfort applications. The PMV index predicts the mean response of a large group of people according to the ASHRAE thermal sensation scale (see Table 4.2). Fanger (Fanger, 1970) related PMV to the imbalance between the actual heat flux from the body in a given environment and the heat flux required for optimum comfort at the specified activity by the following equation:

$$\begin{aligned}
 PMV &= F(T_{bs}, T_{cl}, T_{rm}, h_c, f_{cl}, M, W, P_V) \\
 PMV &= (0.303e^{-0.036M} + 0.028)\{(M - W) - 3.05 \times 10^{-3}[5733 - 6.99(M - W) - P_V]\} \\
 &= -0.42[(M - W) - 58.15] - [1.7 \times 10^{-5}M(5867 - P_V)] - [0.0014M(34 - T_{bs})] \\
 &= -\{3.69 \times 10^{-8}f_{cl}[(T_{cl} + 273)^4 - (T_{rm} + 273)^4]\} - [f_{cl}h_c(T_{cl} - T_{bs})],
 \end{aligned} \tag{4.16}$$

where T_{bs} is the dry bulb temperature ($^{\circ}C$) or just the indoor air temperature, T_{cl} is the mean temperature of the outer surface of the clothed body ($^{\circ}C$), T_{rm} is the mean radiant temperature ($^{\circ}C$) e h_c is the convective heat transfer coefficient (W/m^2K), which is calculated according to Equation 4.17. The clothing area factor f_{cl} corresponds to the body surface covered by clothes, it can be obtained through the clothing insulation I_{cl} (Fanger, 1970). The total metabolic rate M within the body is the metabolic rate required for the person's activity plus the metabolic level required for shivering. A portion of the body's energy production may be expanded as external work W .

$$h_c = 10.4\sqrt{v}, \text{ para } v < 2.6 \text{ m/s.} \quad (4.17)$$

The vapor pressure and the humidity ratio are related from the psychrometry by Equation 4.18:

$$w = 0.622 \frac{P_V}{P_T - P_V}, \quad (4.18)$$

where P_T is the local barometric pressure (kPa). The term P_V is the partial vapor pressure (kPa), which can be related to the dry bulb temperature T_{bs} and the relative humidity ϕ (%) as presented in Equation 4.19:

$$P_V = \phi P_{SAT}(T_{bs}). \quad (4.19)$$

The correlation for the water vapor saturation pressure P_{SAT} can be found in (ASHRAE, 2005d) and the cloth surface temperature T_{cl} can be calculated iteratively according to the following Equation:

$$T_{cl} = 35.7 - 0.032M - 0.18I_{cl}(3.4f_{cl} \times ((T_{cl} + 273)^4 - (T_{rm} + 273)^4) + f_{cl}h_c(T_{cl} - T_{bs})). \quad (4.20)$$

Combining Equations 4.16 e 4.20, the PMV index can be described as a function of four environmental variables (indoor temperature: T_{bs} , relative humidity: ϕ , mean radiant temperature: T_{rm} and air speed: v) and two individual parameters (metabolic rate: M and clothing index: I_{cl}), as described in Equation 4.21:

$$PMV = G(T_{bs}, \phi, T_{rm}, v, M, I_{cl}) \quad (4.21)$$

After estimating the PMV by using Equation 4.16 or any other method, the Predicted Percentage of Dissatisfied (PPD) with a condition can also be estimated. (Fanger, 1982) related the PPD to the PMV as follows:

$$PPD = 100 - 95e^{-0.03353PMV^2 + 0.2179PMV^2}. \quad (4.22)$$

4.2.3 Acceptability of Air

Usually, thermal comfort indices are used to define parameters in air-conditioning projects. However, another important concept in HVAC projects is the acceptability of air. In order to enhance PowerDomus thermal comfort analysis, an acceptability of air model has been implemented.

Based in Fang *et al.* (1988), where a model to predict perceived air quality, based on experimental data, the impact of temperature and humidity on perception has been studied by correlating acceptability with the thermodynamic property “enthalpy” which is related to the energy content of the moist air. Through highly significant linear relations found in this experiment, a model that includes three factors - air pollution, temperature and humidity to determine perceived air quality has been proposed. This model has been implemented into PowerDomus thermal comfort module as presented in Equation 4.23.

$$ACE = a h_i + b, \quad (4.23)$$

where h_i is the indoor moist air enthalpy (kJ/kg), and the coefficients a and b are defined according to the indoor air pollution level. When a particular case for no pollutant is considered, Fang *et al.* (1988), adopts the values of $a = -0.033$ and $b = 1.662$.

The model presented in Equation 4.23 provides that at low enthalpy (low temperature and/or humidity), the pollution level is the key factor that influences the perception of air quality, while air pollution becomes less important for the perceived air quality when enthalpy of the air increases. Beyond a certain level of enthalpy, for instance at $28^\circ C$ and 70% of relative humidity, temperature and humidity are the key factors that determine the perceived air quality, in this case, the air is perceived as unacceptable whether it is clean or not.

The ACE index varies from -1 when unacceptable air conditions are provided to $+1$ for clearly acceptable air.

4.2.4 Acceptable Thermal Conditions in Naturally Conditioned Spaces

The Adaptive Comfort Standard (ACS) proposed by ASHRAE (ANSI/ASHRAE, 2004) is presented in this section in order to determine the comfort level in naturally ventilated spaces.

For the purposes of this standard, occupant-controlled naturally conditioned spaces are those spaces where the thermal conditions are regulated primarily by the occupants through the action of opening/closing windows. Field experiments have shown that occupants' thermal responses in such spaces depend in part of the outdoor climate and may differ from thermal responses in buildings with centralized HVAC systems, primarily because of the different thermal experiences, changes in clothing, availability of control, and shifts on occupants' expectations. This optional method is intended for such spaces.

According to the standard in order to apply this method, the space must be equipped with operable windows that open to the outdoors and that can be readily opened and adjusted by the occupants of the space. There must be no mechanical cooling system for the space (e.g., refrigerated air-conditioning, radiant cooling, or desiccant cooling). Mechanical ventilation with unconditioned air may be utilized, but opening and closing of windows must be the primary means of regulating the thermal conditions in the space. The space may be provided with a heating system, but this optional method does not apply when the heating system is in operation. It applies only to spaces where the occupants are engaged in near sedentary physical activities, with metabolic rates ranging from 1.0 to 1.3 *met* (the 1.0 *met* reference value of 1 *kcal/(kg h)*, is used by convention and refers to a typical metabolism at rest of an average individual). The method is only applied to spaces where the occupants may freely adapt their clothing to the indoor and/or outdoor thermal conditions.

Allowable indoor operative temperatures for spaces that meet these criteria may be determined from Figure 4.3. This figure includes two sets of operative temperature limits - one for 80% acceptability and one for 90% acceptability. The 80% acceptability limits are for typical applications and shall be used when no other information is available.

The 90% acceptability limits may be used when a higher standard of thermal comfort is desired. Figure 4.3 is based on an adaptive model of thermal comfort that is derived from a global database of 21,000 measurements taken primarily in office buildings. The mean monthly outdoor temperature is the arithmetic average of the mean daily minimum and mean daily maximum outdoor (dry-bulb) temperature for the month in question.

The allowable operative temperature limits in Figure 4.3 may not be extrapolated to outdoor temperatures above and below the end points of the curves in this figure. If the mean monthly outdoor temperature is less than 10°C (50°F) or greater than 33.5°C (92.3°F), then no specific guidance for naturally conditioned spaces is included in this standard.

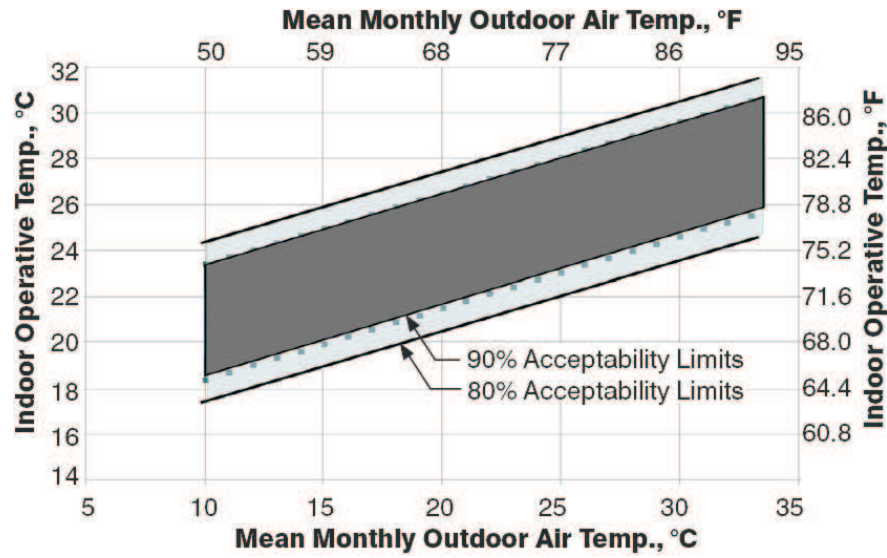


Figure 4.3: Acceptable operative temperature ranges for naturally conditioned spaces (ASHRAE, 2004).

The operative temperature (ASHRAE, 2005*d*), shown in Figure 4.3, can be defined as the average of the air temperature and the mean radiant temperature weighted, respectively, by the convective heat transfer coefficient and the linearized heat transfer coefficient as described below:

$$T_o = \frac{h_r T_{rm} + h_c T_a}{h_r + h_c} \quad (4.24)$$

The convective heat transfer coefficient, h_c , and radiative heat transfer coefficient, h_r ($W/(m^2 K)$), are evaluated at the clothing surface. T_{rm} is the mean radiant temperature ($^{\circ}C$) and T_a is the air temperature ($^{\circ}C$).

In cases where the occupants engaged in near sedentary physical activity (with metabolic rates between 1.0met and 1.3met), not in direct sunlight, and not exposed to air velocities greater than 0.20 m/s , the relationship can be approximated with acceptable accuracy by:

$$T_o = \frac{T_a + T_{rm}}{2} \quad (4.25)$$

4.3 Mould Growth Risk

Since PowerDomus models are able to calculate heat and moisture transfer through porous materials, models that involves wall surface temperature and humidity could be implemented into the software. The aim of this section is to present a mathematical model of mould growth risk that has been implemented into PowerDomus in the frame of the present work.

Over the past decades, mould and mildew growth has been attracting attention of academic and industrial researches, and consequentially greatly increased their understanding specially related to the associated potential health risks. Better understanding about this fungus can help with the removal of this micro organism and, thus, reducing health risk to humans and building structures deterioration.

Mould needs three factors to be able to grow: a food source, moisture, and a certain temperature range. If these three conditions are present, mould will be able to germinate and grow rather quickly. A common believe is that molds need physical water to be able to grow, but that is not the case. Mould need relative humidity be between 65% and 99% at the growing surface. Keeping the relative humidity below 50% will deter mould growth. Based on these factors, Hukka and Viitanen (1999) proposed a model for the growth rate of mould under different material surface conditions.

The scale applied to the present mathematical model comes from an existing standard based on the visual appearance of the surface under study. Some refinements have been made by Hukka and Viitanen and, as a result, the mould growth index (MGR) assumes the values presented in Table 4.3.

Table 4.3: Mould growth risk index description.

MGR	Growth
0	No growth
1	Some growth detected only with microscopy
2	Moderate growth detected with microscopy (coverage more than 10%)
3	Some growth detected visually
4	Visually detected coverage more than 10%
5	Visually detected coverage more than 50%
6	Visually detected coverage 100%

As a basis of their model, they have presented a regression equation for the response time t_m (in weeks) needed for the initiation of mould growth at constant material surface temperature and humidity:

$$t_m = e^{-0.68 \ln(T_{surf}) - 13.9 \ln(\phi_{surf}) + 0.14 W_{mat} - 0.33 SQ + 66.02}, \quad (4.26)$$

where T_{surf} is the surface temperature ($^{\circ}C$), ϕ_{surf} is the surface relative humidity (%), W_{mat} is the material constant (adopted here as 0.5) and SQ is the surface quality (adopted here as 0.5). According to Hukka and Viitanen (1999), both, material constant and surface quality index, have been experimentally obtained for resawn and original kiln-dried wood material. In this way, considering the necessity of experimental results for the obtention of different materials constants, the 0.5 value has been adopted.

As the mould index MGR is supposed to increase linearly in time (when time is measured in days), a differential interpretation of Equation 4.26 can be performed (see Equation 4.27). This extends the applicability of Equation 4.26 to transient conditions such that the relative humidity is constantly above the critical value defined by Equation 4.28 and the temperature lies between 0 and $50^{\circ}C$.

$$\frac{dMGR}{dt} = \frac{1}{7 e^{-0.68 \ln(T_{surf}) - 13.9 \ln(\phi_{surf}) + 0.14 W_{mat} - 0.33 SQ + 66.02}}, \quad MGR < 1, \quad (4.27)$$

$$\phi_{crit} = \begin{cases} -0.00267 T_{surf}^3 + 0.160 T_{surf}^2 - 3.13 T_{surf} + 100.0 & \text{when } T_{surf} \leq 20 \\ 80\% & \text{when } T_{surf} \geq 20 \end{cases}. \quad (4.28)$$

When interpreting the results of the model, all values of MGR below 1 indicate no growth. If growth proceeds above the initial stage ($MGR = 1$), Equation 4.27 is no longer valid. In this way, another regression model describing the response time (in weeks) needed for the first visual appearance of mould growth ($MGR = 3$) should be used (see Equation 4.29):

$$t_v = e^{-0.74 \ln(T_{surf}) - 12.72 \ln(\phi_{surf}) + 0.06 W + 61.50}. \quad (4.29)$$

If mould growth index is assumed to be between $MGR = 1$ and $MGR = 6$ on a constant rate in constant conditions, Equations 4.26 and 4.29 can be combined to give the growth rate on that range (Hukka and Viitanen, 1999). The result of this combination is a correction coefficient presented below.

$$k_1 = \begin{cases} 1 & \text{when } MGR < 1 \\ \frac{2}{\frac{t_v}{t_m} - 1} & \text{when } MGR > 1 \end{cases} \quad (4.30)$$

Taking into account the upper limit for mould growth defined by Equation 4.31, another correction coefficient may also be used in order to define the mould growth in fluctuating conditions. This coefficient is presented in Equation 4.32.

$$MGR_{sup} = 1 + 7 \frac{\phi_{crit} - \phi_{surf}}{\phi_{crit} - 100} - 2 \left(\frac{\phi_{crit} - \phi}{\phi_{crit} - 100} \right)^2 \quad (4.31)$$

$$k_2 = 1 - e^{2.3(MGR - MGR_{sup})} \quad (4.32)$$

Finally the complete model for mould growth in favorable conditions consists of:

$$\frac{dMGR}{dt} = \frac{1}{7 e^{-0.68 \ln(T_{surf}) - 13.9 \ln(\phi_{surf}) + 0.14 W - 0.33 SQ + 66.02}} k_1 k_2 \quad (4.33)$$

$MGR = 0$ at initial time has been adopted in the implemented algorithm.

According to Hukka and Viitanen (1999), instead of remaining on a constant level, the activity of mould can be regarded as decreasing during dry periods and a finite delay in growth can be clearly observed after the dry period. This delay does exist as soon as after 6 hours in dry conditions, but extending the dry period to 24 hours does not seem significantly affect it, if growth will initiate at all. After that, the delay occurs again. Following these relations, a mathematical description of the delay can be written by using the elapsed time from the beginning of the dry period ($t - t_1$) such as:

$$\frac{dMGR}{dt} = \begin{cases} -0.032 & \text{when } t - t_1 \leq 6 \text{ h} \\ 0 & \text{when } 6 \text{ h} \leq t - t_1 \leq 24 \text{ h} \\ -0.016 & \text{when } t - t_1 > 24 \text{ h} \end{cases} \quad (4.34)$$

4.4 Simulation Procedure

In order to compare natural ventilation and air-conditioning, in terms of mould growth risk, thermal comfort and energy consumption, an undirect cooling system model already implemented into PowerDomusDomus is presented in Sections 4.4.2.1 and 4.4.2.2. All the

parameters presented in these sections are related to the component models described in Sections 4.1.1 and 4.1.2.

4.4.1 Building Description

The building envelope considered in the case study presented in this chapter is a two-storey office building divided into two zones. Each zone has $8.0 \times 8.0 \times 3.0$ meters of length, width and height, respectively. The walls are divided into three layers of mortar (2 cm), brick (15 cm) and mortar (2 cm) with external and internal permeances of $9e^{-10} \text{ kg}/(\text{Pa m}^2 \text{ s})$ and $2e^{-10} \text{ kg}/(\text{Pa m}^2 \text{ s})$. The hygrothermal properties of each material are presented in Table 4.4.

Two $1.5 \text{ m} \times 1.0 \text{ m}$ double-glazed windows facing North, with unitary solar heat gain coefficient (at normal incidence), no internal shading device and a global heat transfer coefficient of $3 \text{ W}/\text{m}^2 \text{ K}$ have been distributed on the building façades. Additionally, a $2.10 \text{ m} \times 0.80 \text{ m}$ door is added to the building as shown in Figure 4.4. No ground contact has been considered, i.e., the building has been placed in the air to avoid simplifications on the heat and moisture transfer via the ground.

Table 4.4: Materials physical characteristics.

Material	ρ	λ	c_P	ε
Brick	0.749	1900	920	0.29
Mortar	0.720	2050	932	0.18

where λ is the thermal conductivity ($\text{W}/\text{m}^2 \text{ K}$); ρ the density (kg/m^3), ε is the porosity (-) and c_P the specific heat ($\text{J}/\text{kg K}$). Figure 4.4 shows the building geometric characteristics into the 3-D PowerDomus software interface.

Internal thermal gains from people, lighting and equipment from 8 am to 6 pm have been taken into account. During the occupation time (from 8 am to 6 pm), an individual vapor dissipation of 180 g of water at 37°C has been considered. This vapor capacity corresponds to the moisture generated by human beings when office activities are considered (IEA, 1991). The main idea is to stipulate that there is always someone in the ground floor during the occupation time.

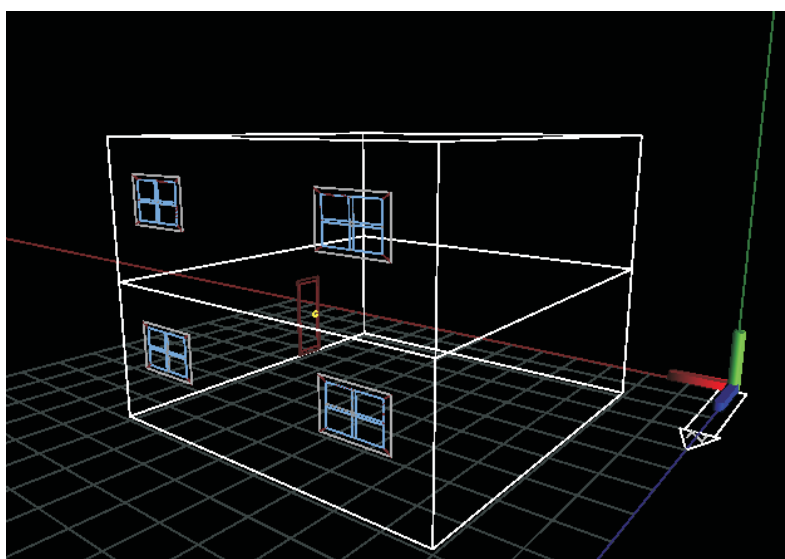


Figure 4.4: Two-storey office building geometric characteristics.

4.4.2 HVAC Parameters

4.4.2.1 Primary Systems (Plant) with Air Cooled Chiller (SP-AIR)

The primary system is composed of one air cooled chiller and two cold water circulation pumps. Table 4.5 presents the nominal data chiller obtained from catalog, while Table 4.6 shows the capacity ($CAPFT$) and efficiency ($EIRFT$, $EIRFPLR$) regression coefficients. Table 4.7 shows the nominal parameters pumps obtained from catalog data.

Table 4.5: Air-cooled chiller simulation parameters.

Nominal Parameters	Evaporator
Capacity (kW)	245.90
Temperature rise ($^{\circ}C$)	5.5
Water flow (l/s)	10.68
COP	3.05
Water leaving temperature ($^{\circ}C$)	7.0

4.4.2.2 Secondary System

The secondary system is composed of three components: mixing box, cooling coil and supply fan. For the mixing box, a constant air change rate of 30% in volume of the total supply airflow has been assumed. The largely used on-off based control system has been employed for all zones. The set-point controller is $24^{\circ}C$ with a hysteresis of $2^{\circ}C$, i.e., the

Table 4.6: Air-cooled chiller capacity and efficiency coefficients.

	A	B	C	D	E	F
CAPFT	1.08	3.5e-2	2.1e-4	-6.9e-3	-3.6e-5	-2.3e-4
EIRFT	0.64	-6.5e-3	4.6e-4	-1.7e-5	4.4e-4	-6.2e-4
EIRPLR	0.60	7.7e-2	3.4e-1	-	-	-

Table 4.7: Model parameters for the pumps.

Nominal Parameters	Pump 1	Pump 2
Required Power (<i>kW</i>)	0.6847	0.6847
Motor Efficiency (%)	70	70
Rotation(<i>rpm</i>)	1750	1750
Water flow (<i>l/s</i>)	5.34	5.34
Manometric Pressure (<i>m</i>)	9.15	9.15

temperature is kept between 23°C and 25°C . As it can be seen, no heating system is considered in this case.

Table 4.8 shows the cooling coil simulation geometric parameters for all building zones and Table 4.9 describes the fan simulation parameters for each zone.

4.4.3 Simulations and Reports

The Test Reference Year (TRY) of the city of Curitiba, South of Brazil (latitude: -25.52° ; longitude: -49.17° ; GMT: -3 h ; altitude: 934 m) has been used for one year simulation period. One year pre-simulation period has been adopted to avoid initial conditions effects.

Simulations have been performed using a 20-minute time step and changing three main parameters: *i*) the time that natural ventilation is used considering just one opening; *ii*) the pressure coefficient (C_P) calculation method; and *iii*) the use of natural ventilation or air-cooling system. Results are expressed in terms of: thermal comfort, indoor air quality and mould growth at the internal ceiling surface, for the ground level (Zone 1). According to these rules, the following simulations have been performed:

- Openings closed with no air-conditioning strategy;
- Openings closed using an air-conditioning system;

Table 4.8: Cooling coil simulation geometric parameters.

Coil Parameters	Zone 1
Height (<i>mm</i>)	457
Length (<i>mm</i>)	700
Width (<i>mm</i>)	198
Distance between face tubes (<i>mm</i>)	38.08
Row spacing (<i>mm</i>)	33.0
External tube diameter (<i>mm</i>)	15.87
Internal tube diameter (<i>mm</i>)	13.87
Fin thickness (<i>mm</i>)	0.190
Fins number per meter	314.9
Rows number	6
Tubes number per row	12
Circuits number	6
Fin thermal conductivity (<i>W/mK</i>)	230
Tube thermal conductivity (<i>W/mK</i>)	380
Water flow (<i>l/s</i>)	0.8

Table 4.9: Model parameters for the fan.

Parameters	Zone 1
Power (<i>kW</i>)	0.74
Efficiency (%)	80
Airflow rate (<i>m³/h</i>)	2879

- Natural ventilation configured for one opening from 8 *am* to 9 *am*;
- Natural ventilation configured for one opening from 8 *am* to 10 *am*;
- Natural ventilation configured for one opening from 8 *am* to 11 *am*;
- Natural ventilation configured for one opening from 8 *am* to 6 *pm*;

As presented in Section 4.2.4, when the selected air-conditioning strategy is natural ventilation, it is not correct to evaluate thermal comfort with the PMV index. In these cases, the model presented in Section 4.2.4 has been used. However, when an air-cooling system is selected, the idea is to evaluate the thermal comfort by using the PMV index.

It is clear that comparisons of two different thermal comfort indices are not possible, but, according to the simplification parameters presented in Section 4.2.4, some correlations can be made between PMV and ASHRAE (ANSI/ASHRAE, 2004) Adaptive

Comfort Standard for naturally ventilated environments. ASHRAE defines that the ACS model can be applied only to spaces where the occupants are engaged in near sedentary physical activities, with metabolic rates ranging from 1.0 *met* to 1.3 *met*. In this way, for the air-conditioning simulation, the values of 1.2 *met* and 0.66 *clo* have been set for the PMV metabolic rate and clothing index, respectively.

Another correlation that can be used is the percentage of people in the acceptability limits. In the ACS comfort zone presented in Figure 4.3, 80% and 90% of acceptability can be estimated. This consideration can also be found in the PMV index when the PPD is calculated. According to Figure 4.5, the values of 90% and 80% of people satisfied with the indoor thermal conditions can also be found (ASHRAE, 2005*d*).

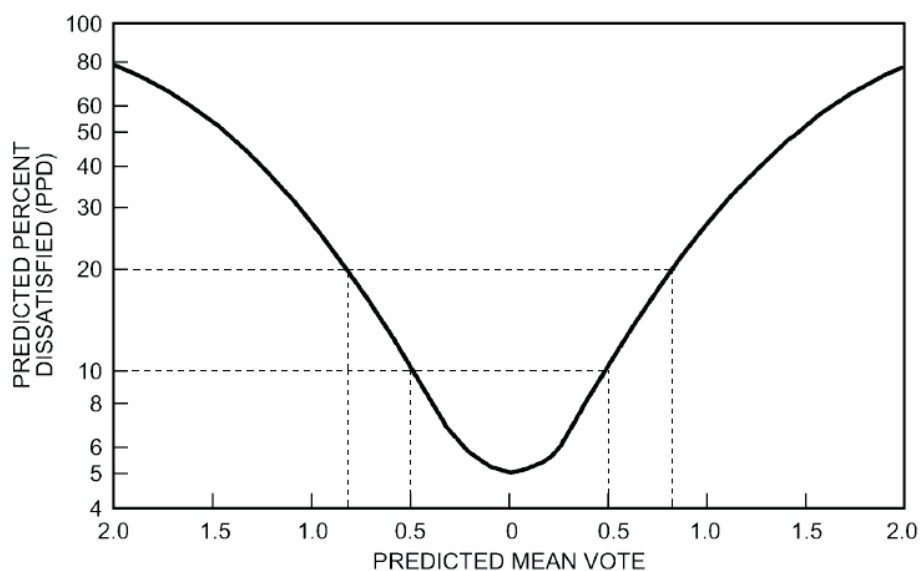


Figure 4.5: Correlation between PMV and PPD.
(ASHRAE, 2005*d*)

4.5 Results

This section presents the simulation results using the mathematical models for natural single-sided ventilation and the primary and secondary systems components integrated to a hygrothermal building model. The simulation parameters used were described in simulation procedure section.

4.5.1 Mould Growth Risk Analysis

The mould growth risk index have been analyzed for both natural ventilation and air-conditioning cases. The main idea is to assess the potential usage of natural ventilation to avoid the ideal conditions of mould spores growth.

Figure 4.6 presents the daily mean relative humidity of the internal ceiling surface for the whole year simulation period. As presented in Section 4.3, the critical value for relative humidity (φ_{crit}) is the main parameter for mould fungi development. As described before, even for temperatures under $20^{\circ}C$ critical values of indoor air relative humidity can potentially affect the indoor surfaces and, as consequence, proportionate mould growth.

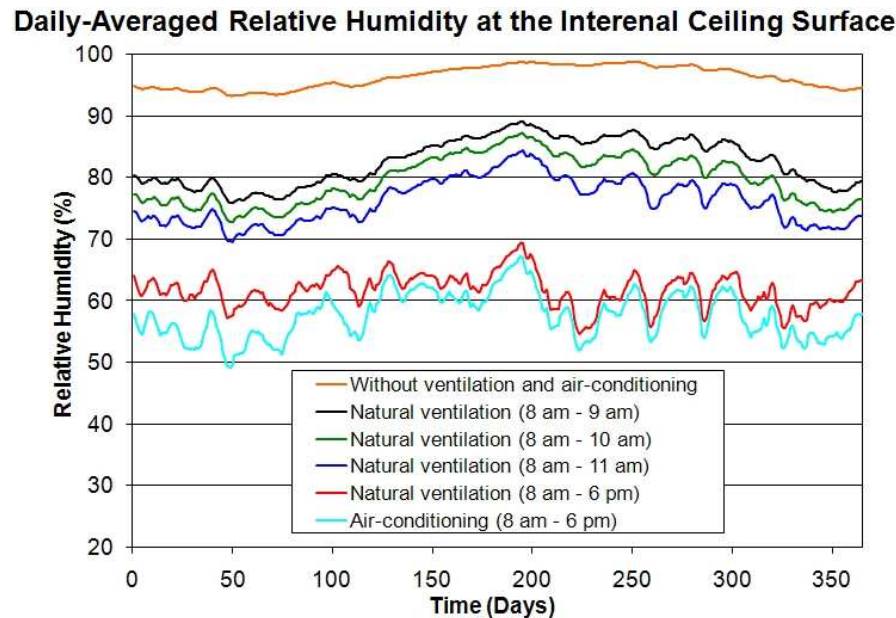


Figure 4.6: Daily mean relative humidity for the indoor roof surface.

As perceived in Figure 4.6, the effect of natural ventilation for the same time interval of air-conditioning system is similar and the roof surface relative humidity has been reduced. However, natural ventilation avoid energy consumption of air-conditioning equipment and improves the indoor air quality if outdoor air is cleaner than the indoor. When the air-conditioning system has been considered, an annual energy consumption of 28,885 kW has been noticed by adding the energy used by pumps, chiller and fan coil.

Figure 4.7 presents the mould growth on the indoor roof surface when neither natural ventilation nor air-conditioning system is considered during the whole year period. Mould spores found favorable growing conditions when the heat and moisture generated by people and equipment inside the building are not dissipated.

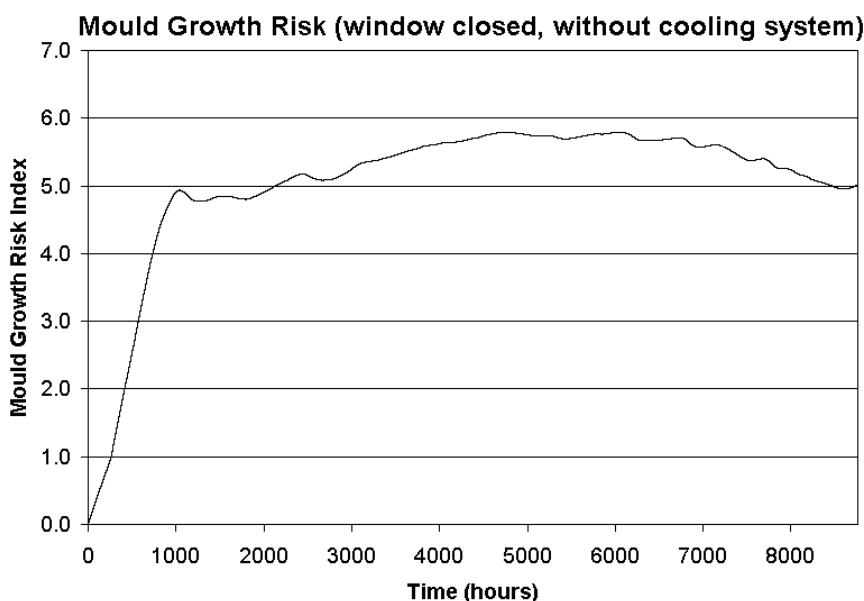


Figure 4.7: Mould growth risk for one year simulation.

Figures 4.8 to 4.10 describe the mould growth index for one year simulation period when the window open intervals are defined as 1, 2 and 3 hours.

Another simulation to evaluate the mould growth potential when the window is open during the occupation time (from 8 *am* to 6 *pm*) has been performed. In this case, no mould growth has been noticed for both pressure coefficient calculation methods. In Figure 4.8, it can be noticed that the winter period is responsible for the mould growth in the roof surface. In this case, minimum differences on the airflow rate can affect the mould growth were microscopically (Mean C_P) and visually (CPCALC) detected.

For a two-hour natural ventilation use period, a more significant difference can be seen (Figure 4.9). No growth from the CPCALC method has been verified, while some growth has been microscopically detected when the Mean C_P calculation method is used. These results report a 45-day period where mould fungi affect the indoor air quality, while for the Mean C_P calculation method there is practically no growth.

Finally, in cases that opening window time is 3 hours or more, results are almost equal when the pressure coefficient models are evaluated (see Figure 4.10). In this way, it confirms that for a more precise analysis when moisture transport is considered to evaluate natural ventilation and indoor air quality, it is necessary to use a more precise model to calculate the airflow rate through openings.

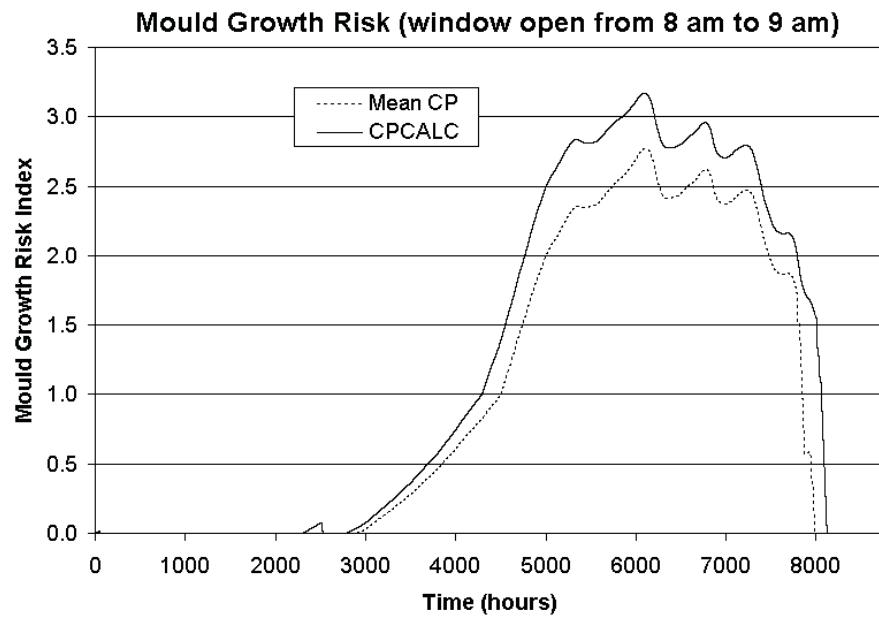


Figure 4.8: Mould growth risk for one year simulation (window open from 8 am to 9 am).

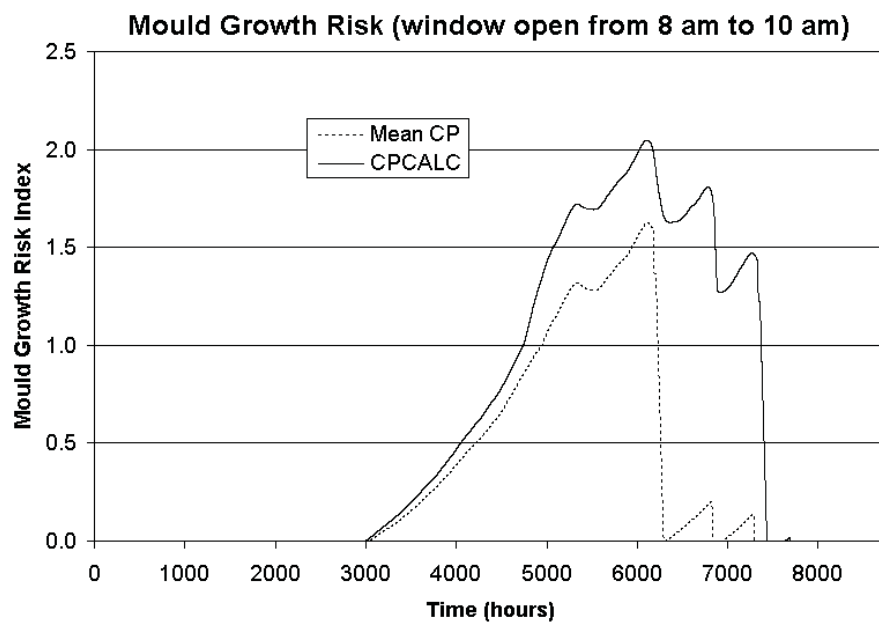


Figure 4.9: Mould growth risk for one year simulation (window open from 8 am to 10 am).

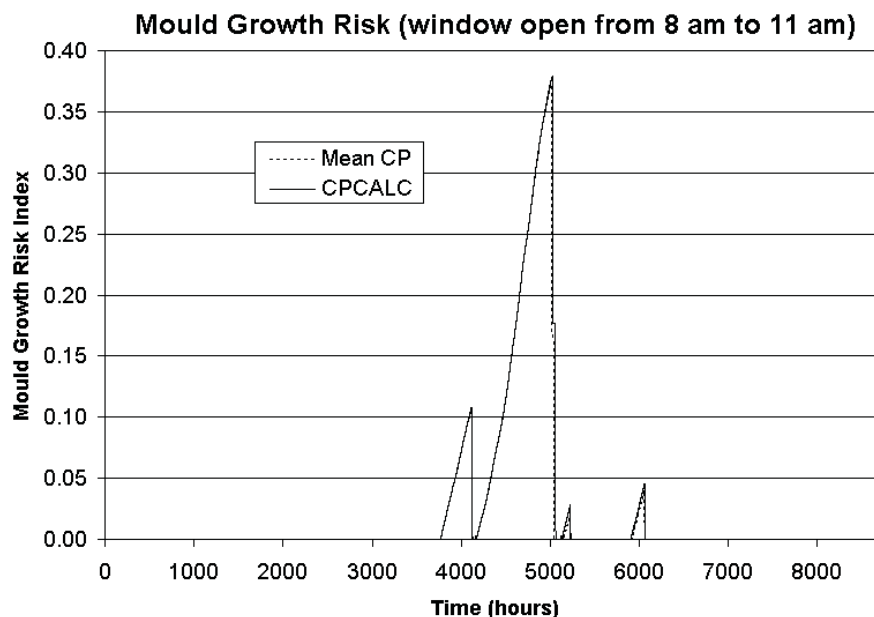


Figure 4.10: Mould growth risk for one year simulation (window open from 8 am to 11 am).

4.5.2 Thermal Comfort and Acceptability of Air

Besides mould fungi and energy consumption, thermal comfort and acceptability of air are important parameters that must be considered as building design criteria. As presented in the last section, the use of natural ventilation compared to air-conditioning system can avoid mould growth when the weather conditions are favorable and, additionally, reduce energy consumption. In the same way as mould growth risk, thermal comfort is equally important because is strongly related to occupants' healthy satisfaction and productivity. Therefore, a more balanced view between energy consumption, mould growth risk and thermal comfort has to be adopted.

This section treats the problem of thermal comfort and acceptability of air comparing both air-conditioning and natural ventilation strategies. The ACS (Adaptive Comfort Standard) index has been adopted to evaluate thermal comfort in natural ventilation cases. Simulations with opening window time of 1, 2, 3 and 10 hours have not shown significant variations on thermal comfort index when the two pressure coefficient calculation methods are compared.

Table 4.10 shows the percentage of time in different comfort zones (80% and 90%) under acceptable thermal comfort conditions. As seen in this case, the 10-hour of natural ventilation test period has presented the best results when thermal comfort is evaluated. In this case, differences no higher than 0.08% between CPCALC and Mean C_P algorithms

Table 4.10: Percentage of time within the comfort zone for both pressure coefficient calculation methods.

Open Window Interval	Percentage of Time within the Comfort Zone (%)			
	CPCALC		Mean C_P	
	80% Zone	90% Zone	80% Zone	90% Zone
8 am – 9 am	63.31	47.20	63.27	47.19
8 am – 10 am	63.47	47.49	63.41	47.51
8 am – 11 am	63.62	47.59	63.52	47.55
8 am – 6 pm	67.65	49.01	67.57	48.97

have been noticed. Based on these small differences, Figure 4.11 shows the distribution of a mean monthly operative temperature in the ACS comfort zone for the CPCALC pressure coefficient calculation method. No significant differences appear when this graphical visualization is applied to the Mean C_P strategy.

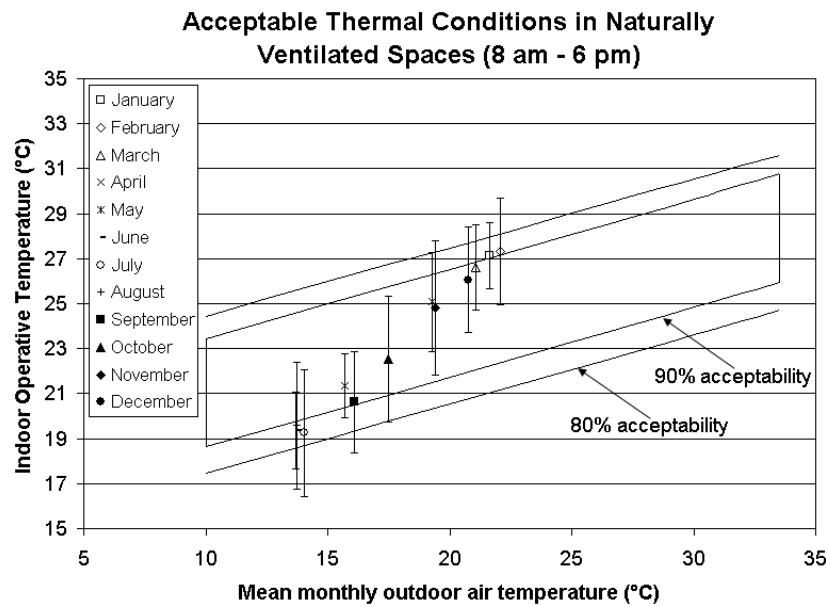


Figure 4.11: Comfort zone using natural ventilation from 8 am to 6 pm.

Comparing the results presented in Table 4.10 and Figure 4.11, it is noticed that for a long period of time occupants of the building are under acceptable thermal comfort levels. When the results for 1, 2 and 3 hours of window opening time are included into the comparative analysis, it can be concluded that occupants in these cases the indoor air will fall slightly warmer than in the 10-hour case, but with no significant changes on the percentage of time within the comfort zone boundaries.

According to the results presented in this chapter, it can be seen that another sim-

Table 4.11: Percentage of time within the comfort zone when air-conditioning system is considered.

Percentage of Time in the Comfort Zone (%)	
80% Zone	90% Zone
67.24	50.46

ulation considering windows closed and no air-conditioning system has been performed. When the results presented in Table 4.10 are extrapolated to the no HVAC case, it is clear that less hours within comfort levels occur.

When the air-conditioning simulation is considered and thermal comfort conditions are evaluated, the PMV (Predicted Mean Vote) index is considered. However, to compare two different comfort indices, the association of the PMV and ACS index cannot be made. So, the PPD (Predicted Percentage of Dissatisfied) is calculated and its antonymous is compared to the comfort zone of the ACS index, defining similar to the ACS comfort zone 80 and 90% of occupants satisfied with the indoor thermal conditions.

The percentage of time within the comfort zone when air-conditioning system is taken into account is presented in Table 4.11. Comparing the air-conditioning and 10 hours of natural ventilation use results, it can be seen that natural ventilation provides just 2.86% less time within 90% comfort boundaries than the air-conditioning systems. When the necessity is 80% of the occupants in acceptable comfort levels, the results are almost the same and natural ventilation provides 0.61% more time within comfort zone than air-conditioning system. These results means that, in one year period, natural ventilation has just 55 hours without 90% boundaries of comfort than air-conditioning system for the Curitiba city. When 80% boundaries are taken into account, the natural ventilation system provides 16 hours more of comfort than the air-conditioning system for one year period.

When the ASHRAE Thermal Sensation (ATS) is evaluate for the air-conditioning simulation case, the values for 90 and 80% of the occupants in acceptable thermal comfort conditions decrease compared to the PMV evaluation, see Table 4.12. It means that for ATS comfort index, occupants in the air-conditioning case are less 248 hours without comfort zone compared to the natural ventilation case for 90% of occupants within acceptable comfort levels and 391 less hours in comfort when the 80% of acceptability is considered. These results means that natural ventilation provides 13.42% and 15.33% more time, in acceptable comfort levels for a whole year period when 90 and 80% of

Table 4.12: Percentage of time within the comfort zone when air-conditioning system is considered (ATS index).

Percentage of Time in the Comfort Zone (%)	
80% Zone	90% Zone
57.28	42.43

occupants acceptance are respectively considered, than the air-conditioning system.

Not significant changes for acceptability of air have been noticed for both air-conditioning and natural ventilation strategies. However, it is important to present that slightly better results for the air-conditioning case has been obtained. This difference can be explained by the indoor air moist air enthalpy affected by the drying effect of the cooling coil.

4.6 Chapter Remarks

The present chapter aimed at evaluating an alternative to energy-consuming air-conditioning systems, *i.e.* the use of natural ventilation to provide healthy and comfortable conditions to building users. For the studied case of a building located in Curitiba (South of Brazil), it can be noticed that in both thermal comfort and mould growth analysis cases, natural ventilation can be used to improve indoor air quality and optimize thermal conditions for the occupants.

When acceptability of air has been compared between air-conditioning and natural ventilation strategies, no significant variations has been detected.

Some evaluations about the influences of the pressure coefficient calculation method on the mould growth risk have also been presented. According to the results, slight variations on the pressure coefficient value may provide significant changes in the mould growth profile and, in these cases, a more elaborated pressure coefficient calculation method should be used.

5 Building-Integrated Photovoltaic Systems: Modeling

In recent years, the whole world has been experiencing a growing electricity demand and a decrease of available resources to expand the generation system. Due to many facts as population and economic growth and access to cheaper electrical appliances, that have only recently become available, interests in the potential of renewable energy and passive technology integration has been taken place between academic and industrial researches.

Among different ways to generate electricity, the use of solar energy for the industrial, public and residential sectors has been discussed in many countries as one of the possible solutions to reduce global warming, since energy generated by fossil fuel combustion can be avoided. Electricity produced using the Sun's energy reduces the amount of energy used from non-renewable resources such as coal, gas, oil and nuclear, and energy is not wasted, e.g. as in transmission losses. In addition, there are significant environmental benefits resulting from reductions in air pollution from burning fossil fuels, reductions in water and land use from central generation plants, reductions in the storage of waste byproducts. In addition, the solar technologies produce energy with little noise and few moving parts.

Many technologies to convert solar energy into electricity have been proposed in literature, but the advances in the photovoltaic conversion are evident. The costs reduction, increasing efficiency reducing the needed area and generic applicabilities have been used as attractive issues for photovoltaic systems. In addition, the possibility of adapt photovoltaic systems to building structures without significant changes on the architect designs contributes to the use of this clean energy strategy. Moreover, when coupled to building structures, PV (photovoltaic) systems can reduce the peak electrical and cooling demands and save the building electricity expenditures. Figure 5.1 shows existing models of building-integrated photovoltaic systems, some added to existing buildings and others created during the building design stage.



Figure 5.1: Examples of building-integrated photovoltaic systems.

In this way, this chapter aims at describing models that can be used to simulate BIPV (Building-Integrated Photovoltaic) systems, showing how much energy can be saved adapting photovoltaic systems to the building structure. A whole-building energy simulation software has been used as the main tool for implementing photovoltaic models. In the sequence, an introduction about the technology and how BIPV has usually been employed has been presented. In the following, models for panel, storage system and converters have been addressed. Finally, the hygrothermal interactions between the building and the PV array have been discussed.

5.1 Solar Energy and Photovoltaic Simulation

The value of solar energy is recognized by engineers and architects but this technology has usually been avoided because of the highly visible collectors on roofs and also due to the high costs. It is clear that the solar power term is associated to freedom from fossil fuel dependence and consequently reduction of global warming, but some types of solar systems have not been used because of their unattractive appearance, changing building architectural designs. For this reason, photovoltaic (PV) modules, which convert sunlight directly into electricity, have been integrated into roofing or other building materials and surfaces as an alternative to traditional PV modules that are mounted above the roof on racks. The result is a photovoltaic system that is less noticeable.

Nowadays, the main drawback of BIPV systems are composed of PV modules and balance of system components, which include inverters, an electricity storage system and/or a grid-metered connection, fault protection, cabling, and wiring. Currently, according

to (Eiffert and Thompson, 2000), BIPV manufacturers are in early stages of technology development and do not have the capacity to take advantage of quantity purchases of materials and of large volume production in order to offer lower-priced BIPV components and systems. However, there has been a decline in the cost of PV technology over time due to technical advances. In addition, the industry and government foresee further cost as demand for PV technology increases internationally and manufacturing economies of scale increase.

Interests in the use of photovoltaic systems to reduce energy consumption of building air-conditioning systems have increased in the last two decades, *e.g.* in (Lai, 2006), where a prototype rooftop turbine ventilator powered by hybrid wind and photovoltaic energy has been developed. Lai (2006) describes a solution to enhance the ventilation rate by a rooftop turbine ventilator due to the poor indoor air quality in Taiwan and the national policy to explore the renewable energy.

As presented in (Khedari *et al.*, 2004), by using photovoltaic energy to power up fans, indoor thermal comfort can also be improved. Through experimental investigations of performance of a new type of photovoltaic-slat window, Khedari *et al.* (2004) have shown that it is possible to reduce indoor temperature, optimize thermal comfort in summer periods and improve daylighting by using a photovoltaic-slat window system compared to a commercial transparent slat window of the same size.

In order to contribute to technology advances and cost reducing of PV components, many countries have already adopted a clean energy policy, reducing taxes for people who adopt strategies that contributes to the reduction of global warming. In Brazil, following the laws for reducing energy consumption of electrical appliances, the government, supplied by academic researchers, created a new method to certificate buildings according to their energy demand (BRASIL, 2001). Through evaluations performed on the building envelop and also on the lighting and HVAC systems, it becomes possible to define a building energy efficiency level. In these rules, the use of clean energy strategies contributes to increase the building energy efficiency level and one of the accepted strategies is the use of solar energy systems (Ministério de Minas e Energia, 2009b).

According to (Ministério de Minas e Energia, 2009a), two methods are available to determine the building energy efficiency level: the prescriptive and the simulation methods. The prescriptive method is indicated to buildings that are already built, while the simulation method is usually indicated for building with uncommon structure design which are difficult to evaluate by the prescriptive method or buildings on the design stage. Follow-

ing the literature review, the whole-building energy simulation clearly brings benefits to enhance energy conservation through structural modifications, changes in building materials and inclusion of advanced low-cost energy systems, e.g. lighting and HVAC, without significant additional costs. Inspired on the simulation method, the main idea of this chapter is to include BIPV (Building-Integrated Photovoltaic) systems into the Power-Domus software and validate its results in terms of photocurrent generation comparing to others photovoltaic simulation software.

Actually, there are many algorithms and software capable of simulating photovoltaic systems through different calculation methods, some using simplified models where just the PV system is studied and some using more detailed models where the whole PV system components (storage, inverters, on-off grid connections) are studied. Considering that solar cells depend on the operative thermal conditions, the complexity of PV models analysis also increases according to the thermal analysis of solar panels. Among many PV simulation software, one should cite RETSCreen (CETC, 2004) and PVSYST (ISE, 2008), which are considered software packages - worldwide used - for the technical study, sizing, simulation and data analysis of photovoltaic systems.

However, when a more detailed analysis is required, and the integration of both building structure and photovoltaic panels must be verified, the software has to provide the whole-building and energy simulation reports. This is a reduced group of software such as EnergyPlus (Griffith and Ellis, 2004), TRNSYS (Solar Energy Laboratory, 2007) and ESP-r (Qiu *et al.*, 2009). In this way, the present work proposes an implementation of a photovoltaic module into a building hygrothermal and energy simulation software.

Considering the energy related importance of natural ventilation strategies on design of HVAC systems, the main idea of this chapter is to develop a photovoltaic simulation module to provide the required airflow rate when natural ventilation is not sufficient to maintain good indoor air quality and thermal comfort. Sometimes, natural ventilation is not enough to maintain the minimum ventilation rate and then mechanical ventilation should be used to reach the standard ventilation requirement rates of an specific environment. In this case, where electrical fans can be powered by solar energy through photovoltaic panels, the PV renewable energy strategy can be used to reduce energy consumption of HVAC systems.

When the necessity to enhance the ventilation potential of an HVAC system is evaluated, it is obviously detected that the highest demand for ventilation appears in summer periods. In agreement to this condition, the best performance of photovoltaic panels are

also at hot seasons. Therefore, the use of photovoltaic energy - to improve ventilation rates, in cases where the air-conditioning system could be avoided reducing energy demand - can be used as a method for saving energy. In the sequence, the PV model description is presented followed by the PV panels and the building structure integration procedures.

5.2 Array Modeling

It can be verified that most residential photovoltaic systems are used in conjunction with utility-supplied power and, in addition to the PV panels, an inverter, located near the electrical panel, converts the PV produced electricity into utility compatible alternating current (AC) electricity for the home. When storage systems are used, it can be possible to produce electricity for the home even when the utility power is disconnected or when the sun is not shining. Utility-provided electricity is used when the house demand is greater than what can be supplied by the photovoltaic system. BIPV systems can be sized on a small scale to produce a limited amount of energy or be large enough to power an entire home and send excess power produced during daylight hours back into the utility's lines. Typical residential PV systems commonly have a peak power production of between 1,200 and 5,000 W, AC - requiring 14 to over 93 m² area, depending on the efficiency of the photovoltaic technology used (Lai, 2006).

To simulate photovoltaic systems, a renewable energy module had to be created into the PowerDomus software. In this way, a component which models the electrical performance of a photovoltaic array has been implemented and presented in the sequence. This component may be used in simulations involving electrical storage batteries and direct load coupling. It employs equations for an empirical equivalent circuit model to predict the current-voltage characteristics of a single module. This circuit consists of a DC current source, diode, and either one resistors. The strength of the current source is dependent on solar radiation and the current-voltage characteristics of the diode are temperature-dependent. The results for a single module equivalent circuit are extrapolated to predict the performance of a multi-module array.

The model presented below is proposed for crystalline modules (either single crystal or polycrystalline technology). It is called "four-parameter" equivalent circuit. The values of these parameters cannot be obtained directly from manufacturers' catalogs. However, the four-parameter model will automatically calculate them from available data. To enhance the calculation precision, the main algorithm for PV calculation also includes an optional

incidence angle modifier correlation to calculate how the reflectance of the PV module surface varies with the angle of incidence of solar radiation. Based on well established PV simulation codes, the algorithm also determines the PV current as a function of load voltage.

5.2.1 Model Parameters

As cited before, the “four-parameter model” should be used for single crystal or polycrystalline photovoltaic cells. This assumes that the slope of the current-voltage curve at short-circuit conditions is zero. Another important consideration which has been chosen before simulation is whether or not the simulation should call the “incidence angle modifier” correlation. This correlation accounts for the increased reflective losses when radiation is incident on the module at large angles. If the incident angle modifier is not required, the input product transmittance-absorptance parameter for normal incident angle will be considered as the value of the product ($\tau\alpha$) for all angles of incidence. Otherwise, the $\tau\alpha$ product for other angles is calculated based on the normal value and on an empirical correlation as described in Section 5.2.6.

5.2.2 Mathematical Description of the Four-Parameter Model

The photovoltaic model for crystalline PV modules, which has been incorporated into PowerDomus, was developed largely by Townsend (1989) and also detailed by Duffie and Beckman (1991). The four-parameter equivalent circuit model is also available in TRNSYS PV component (Eckstein, 1990). The four parameter model assumes that the slope of the IV curve is zero at the short-circuit condition:

$$\left(\frac{dI}{dV}\right)_{v=0} = 0 \quad (5.1)$$

This is a reasonable approximation for crystalline modules. The “four parameters” in the model are:

- $I_{L,ref}$: reference photocurrent (A);
- $I_{o,ref}$: reference reverse saturation current (A);
- γ : diode curve fit factor (–);
- R_s : series resistance (Ω).

These are empirical values that cannot be determined directly through physical measurement. The model calculates these values from manufactures' catalog data and the calculations are discussed in the following. The four-parameter equivalent circuit is shown in Figure 5.2.

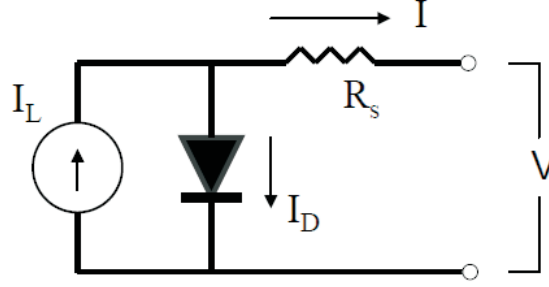


Figure 5.2: Equivalent electrical circuit in the four-parameter model.

During the whole-building and energy simulation, the array efficiency must be calculated at each time step. This value can be obtained dividing the amount of energy that reach the panel surface by the total energy converted into electrical power as shown in Equation 5.2:

$$\eta_c = \frac{E_p}{(G_T y_1 y_2)}, \quad (5.2)$$

where η_c is the collector efficiency, E_p the power at the array output (W), G_T , the total irradiance that reaches de panel surface (W/m^2) and y_1 and y_2 the array width and length (m).

5.2.3 Determining Performance under Operating Conditions

The current-voltage characteristics of a PV change with both insolation and temperature. The PV model employs these environmental conditions along with the four module constants $I_{L,ref}$, $I_{o,ref}$, γ , and R_s to generate an IV curve at each time step. The current-voltage equation of circuit shown in Figure 5.2 is as follows:

$$I = I_L - I_o \left[\exp \left(\frac{q}{\gamma \lambda_c T_c} (V + I + R_s) \right) - 1 \right], \quad (5.3)$$

where R_s , γ and λ_c are constants. The photocurrent I_L depends linearly on incident radiation:

$$I_L = I_{L,ref} \frac{G_T}{G_{T,ref}} \quad (5.4)$$

The reference insolation $G_{T,ref}$ is a model input parameter. It is nearly always defined as 1000 W/m^2 . The diode reverse saturation current I_o is a temperature dependent quantity:

$$\frac{I_o}{I_{o,ref}} = \left(\frac{T_c}{T_{c,ref}} \right)^3 \quad (5.5)$$

Equation 5.5 gives the current implicitly as a function of voltage. Once I_L and I_o are found from Equations 5.4 and 5.5, Newton's method is employed to calculate the PV current. In addition, an iterative search routine finds the current (I_{mp}) and voltage (V_{mp}) at the point of maximum power along the IV curve.

5.2.4 Calculating $I_{L,ref}$, $I_{o,ref}$, γ , and R_s

The needed parameter to complete the time step calculation process include several values which must be read from manufacturers' PV module catalogs. The manufacturers' values are used to determine the equivalent circuit characteristics $I_{L,ref}$, $I_{o,ref}$, γ , and R_s . These characteristics define an equivalent circuit that is employed to find the PV performance at each time step. This section describes the algebra and calculation algorithms used to solve for the four equivalent circuit characteristics.

Three of these values, $I_{L,ref}$, $I_{o,ref}$ and γ , may be isolated algebraically. The first step is to replace the current and voltage into Equation 5.3 at the open-circuit, short circuit, and maximum power conditions:

$$0 = I_{L,ref} - I_{o,ref} \left[\exp \left(\frac{q}{\gamma \lambda_c T_{c,ref}} V_{oc,ref} \right) - 1 \right] - \frac{V_{oc,ref}}{R_{sh}} \quad (5.6)$$

$$I_{sc,ref} = I_{L,ref} - I_{o,ref} \left[\exp \left(\frac{q I_{sc,ref} R_s}{\gamma \lambda_c T_{c,ref}} \right) - 1 \right] - \frac{I_{sc,ref} R_s}{R_{sh}} \quad (5.7)$$

$$I_{mp,ref} = I_{L,ref} - I_{o,ref} \left[\exp \left(\frac{q}{\gamma \lambda_c T_{c,ref}} (V_{mp,ref} + I_{mp,ref} R_s) \right) - 1 \right] - \frac{V_{mp,ref} I_{mp,ref} R_s}{R_{sh}} \quad (5.8)$$

where I_{sc} is the short-circuit current (A), V_{oc} is the open circuit voltage (V) and R_{sh} is

the module shunt resistance (Ω).

In each case, the “ -1 ” term may be dropped to simplify the algebra. This approximation has little influence on the right side of those equations since the magnitude of I_o is very small, generally of the order of 10^{-6} A. Some rearrangements then yield to the following three expressions, which isolate $I_{L,ref}$, $I_{o,ref}$ and γ :

$$I_{L,ref} \approx I_{sc,ref} \quad (5.9)$$

$$\gamma = \frac{q(V_{mp,ref} - V_{oc,ref} + I_{mp,ref} R_s)}{\lambda_c T_{c,ref} \ln \left(1 - \frac{I_{mp,ref}}{I_{sc,ref}} \right)} \quad (5.10)$$

$$I_{o,ref} = \frac{I_{sc,ref}}{\exp \left(\frac{q V_{oc,ref}}{\gamma k T_{c,ref}} \right)} \quad (5.11)$$

At this point, an additional equation is needed in order to determine the last unknown parameter. The fourth equation is derived by taking the analytical derivative of voltage with respect to temperature at the reference open-circuit condition. This analytical value is matched to the open-circuit temperature coefficient and a catalog specification:

$$\frac{\partial V_{oc}}{\partial T_c} = \mu_{voc} = \frac{\gamma k}{q} \left[\ln \left(\frac{I_{sc,ref}}{I_{o,ref}} \right) + \frac{T_c \mu_{isc}}{I_{sc,ref}} - \left(3 + \frac{q \varepsilon}{A_n k T_{c,ref}} \right) \right] \quad (5.12)$$

where:

$$A_n = \frac{\gamma}{N_{cells}}, \quad (5.13)$$

and N_{cells} is the number of individual cells in module.

The four-parameter model uses an iterative search routine in these four equations to calculate the equivalent circuit characteristics. The first step is to set upper and lower bounds for the series resistance parameter R_s : physical constraints require the R_s value to lie between 0 and the value such that $\gamma = Ns$. The initial guess for R_s is midway between these bounds. γ and $I_{o,ref}$ are found from Equations 5.10 and 5.11, respectively, while Equation 5.9 gives a trivial solution for $I_{L,ref}$. Equation 5.12 is used to compare the analytical and catalog values for μ_{voc} . When all other variables are held constant, the analytical value for μ_{voc} increases monotonically with series resistance (Townsend, 1989).

If the analytical voltage coefficient is less than the catalog value, the lower bound for R_s is reset to the present guess value. Likewise, the upper bound is set to the current value if the calculated μ_{voc} is too large. After resetting the upper or lower bound for R_s , a new guess value is found by averaging the bounds. This procedure is repeated until R_s and γ converge. Note that $I_{L,ref}$, $I_{o,ref}$, γ and R_s are assumed to be constant and calculated only on the first call in the simulation.

5.2.5 Module Operating Temperature (Thermal Model)

The PV calculation algorithm uses temperature data from the standard NOCT (Nominal Operating Cell Temperature) measurements to compute the module temperature T_c at each time step. The NOCT temperature ($T_{c,NOCT}$) is the module operating temperature at a 1 m/s wind speed, no electrical load, and a certain specified insolation and ambient temperature (Duffie and Beckman, 1991).

The NOCT conditions also depend on the type of the considered PV module. They can be entered by the user through the software interface or, for standard technologies, are assumed the values given in Table 5.1 (CETC, 2004).

Table 5.1: PV module characteristics of standard technologies.

PV Module Type	η_r (%)	$T_{c,NOCT}$ ($^{\circ}C$)
Mono-Si	13.0	45
Poly-Si	11.0	45
a-Si	5.0	50
CdTe	7.0	46
CIS	7.5	47

The values for insolation $G_{T,NOCT}$ and ambient temperature $T_{a,NOCT}$ are usually $800 W/m^2$ and $20^{\circ}C$. The NOCT data will be used to determine the ratio of the module transmittance-reflectance product to the module loss coefficient:

$$\frac{\tau\alpha}{U_L} = \frac{(T_{c,NOCT} - T_{a,NOCT})}{G_{T,NOCT}} \quad (5.14)$$

Assuming $\tau\alpha/U_L$ ratio is constant, the module temperature at any time step is:

$$T_c = T_a + \frac{(G_T T_{c,NOCT} - T_{a,NOCT})}{G_{T,NOCT} \left(1.0 - \frac{\eta_{c,ref}}{\tau\alpha}\right)} \quad (5.15)$$

where:

$$\eta_{c,ref} = \frac{I_{MR} V_{MR}}{G_{T,ref}} \quad (5.16)$$

$\eta_{c,ref}$ is a reference conversion efficiency of the module which varies with ambient conditions. V_{MR} is the reference maximum power Voltage (V) and I_{MR} is the reference current at maximum power (A). The value of $\tau\alpha$ may be either a constant or calculated from an incidence angle correlation, as described in the following section.

5.2.6 Incident Angle Modifier Correlation

The implemented algorithm includes an ‘‘incidence angle modifier’’ routine. If this routine is selected by the user, an empirical correlation determines the transmittance-reflectance product ($\tau\alpha$) of the module at each time step according to the sun position in the sky. This calculation is based on the module slope, on the angle of incidence and on the intensity of each radiation component (direct, diffuse, and ground-reflected). Considering the product $\tau\alpha$ for normal incidence angle as input parameter, using the incidence angle modifier will always produce a more conservative (and probably more accurate) estimate of system performance. For most locations, a given PV array will generate about 10% less energy over the course of an year when the incidence angle routine is enabled. $\tau\alpha$ at normal incidence is not usually included in the list of manufacturer’s parameters, although 0.9 is usually a good estimate (Solar Energy Laboratory, 2007).

Whether or not the modifier is used, the radiation incident on the PV Panel is always multiplied by $\tau\alpha$ to account for reflective losses before Equation 5.4 is used to determine the photocurrent. The expression for the incidence angle modifier (IAM), taken from (King *et al.*, 1997) is:

$$IAM = 1 - (1.098 \times 10^{-4})\xi - (6.267 \times 10^{-6})\xi^2 + (6.583 \times 10^{-7})\xi^3 - (1.4272 \times 10^{-8})\xi^4 \quad (5.17)$$

where,

$$IAM = \frac{\tau\alpha}{\tau\alpha_{normal}} \quad (5.18)$$

Here, ξ is the angle of incidence in degrees, with $\xi = 0^\circ$ indicating normal incidence. In Figure 5.3, the incidence angle modifier (IAM) variations as function of θ have been presented.

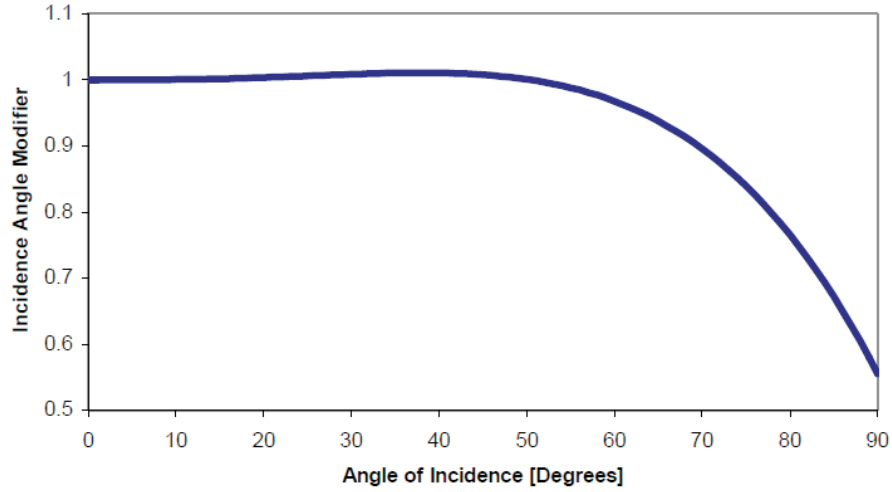


Figure 5.3: Incidence Angle Modifier of King *et al.*, 1997.

The angle of incidence for the beam component of the solar radiation is obtained directly the PowerDomus. However, the software does not calculate effective angles of incidence for the diffuse and ground-reflected radiation components. In this way, the photovoltaic module uses two additional correlations to find these effective angles of incidence. These correlations, developed by Duffie and Beckman (Duffie and Beckman, 1991), are:

$$\theta_{eff,diff} = 59.7 - 0.1388\omega + 0.001497\omega^2 \quad (5.19)$$

$$\theta_{eff,gnd} = 90 - 0.5788\omega + 0.002693\omega^2 \quad (5.20)$$

where ω is the slope of the PV array in degrees. In the case of PowerDomus application, this value will be equal to the surface slope. The total insolation on the array is found by summing the individual radiation components and multiplying them by their appropriate incidence angle modifiers:

$$G_{T,eff} = \tau\alpha_{norm}(G_{T,beam}IAM_{beam} + G_{T,diff}IAM_{diff} + G_{T,gnd}IAM_{gnd}) \quad (5.21)$$

5.2.7 Multi-Array Modules

The electrical calculations discussed for the four-parameter PV model deal only with a single module. The algorithm implemented into PowerDomus may be used to simulate arrays with any number of modules. An user friendly interface allows the user to define

the number of modules in series (N_{Series}) and modules in parallel ($N_{Parallel}$) for the entire array. The total number of modules in the array is the product of N_{Series} and $N_{Parallel}$. The single-module values for all currents and voltages discussed here above are multiplied by $N_{Parallel}$ or N_{Series} to find values for the entire array. This approach neglects module mismatch losses.

Finally, Figure 5.4 shows the energy conversion flowchart. According to Evans (1981), this structure is common to all types of PV applications.

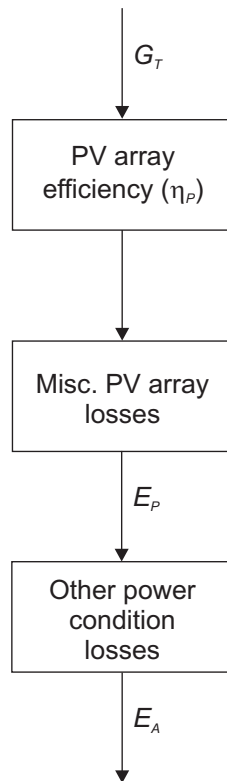


Figure 5.4: Flowchart for PV array model.

5.3 Battery

The main idea on the BIPV simulation in PowerDomus applications is to verify the hygrothermal influences of the array coupled to building structures. However, the simulation must consider the generation and storage of the converted energy. Considering that the main aspect of BIPV systems is that there is no storage system, a simplified storage model has been implemented in order to provide results in terms of energy demand and battery (charging and discharging) conditions. Additionally, this option will increase the simulation possibilities of the PowerDomus software.

In Figure 5.5, it can be verified how the energy converted by the PV array is used by the load when the charging conditions are enabled.

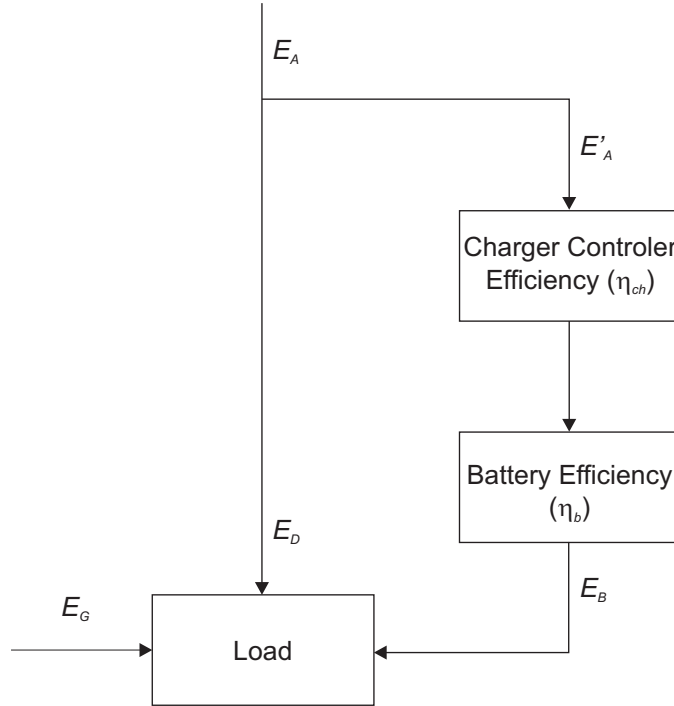


Figure 5.5: Flowchart for the battery model.

To enable the charging conditions, the amount of energy supplied by the PV array (E_A) must be greater than the building energy demand (E_D) at a time step level. As described in Equation 5.22, the available energy that will be used to charge the battery (E'_A) is the difference between the power supplied by the PV array and the demand (in W).

$$E'_A = E_A - E_D \quad (5.22)$$

5.3.1 Discharge Calculation Method

If not enough energy is supplied by the PV array, the battery will be gradually discharged, that is, the demand is higher than the energy converted by the PV array at a given time, the battery discharge process will start. Based on the Peukert Equation (Eq. 5.23) (Doerffel and Sharkh, 2006), which represents the battery discharge behavior, the battery capacity can be written as the amount of electricity (Ah) or the amount of energy (Wh) that a battery can attend to an external circuit.

$$C_{pk} = I^k t_h \quad (5.23)$$

where, C_{pk} is the capacity according to Peukert, at a one-ampere discharge rate (Ah), I is the discharge current (A), k is the Peukert constant and t_h is the discharge time (h). However, more commonly, manufacturers rate the capacity of a battery with reference to a discharge time. Therefore, the following equation should be used:

$$t_h = t_d \left(\frac{C}{I t_d} \right)^k \quad (5.24)$$

where t_d is the hour rating that the battery is specified against and C is the rated capacity at that discharge rate. Note that C_{pk} no longer appears in this equation. For an ideal battery, the constant k would be equal one, in this case the actual capacity would be independent of the current. For a lead-acid battery, the value of k is typically between 1.1 and 1.35. The Peukert constant varies according to the age of the battery generally increasing with age.

Within the battery parameters that must be set on by the user during the photovoltaic module configuration is the maximum discharge coefficient. It means that if the battery is discharged until its capacity reaches the maximum discharge coefficient, the battery will start to be recharged and the equipment will be connected to the grid in order to avoid battery damage. Usually, batteries manufactures provide this information on datasheets.

5.3.2 Charge Calculation Method

When the available energy delivered by the PV array is greater than the demand, the battery will be charged until it reaches 95% of its nominal capacity. This value can be changed on the software interface through the maximum charge coefficient. The amount of energy supplied to the battery during charge at each time step is described in Equation 5.25:

$$C = \eta_b * I_b \quad (5.25)$$

where η_b is the battery efficiency and I_b is the charging current (A). The charging current is limited by the battery maximum charging current (I_{max}) and by the charger controller efficiency (η_{ch}) according to Equations 5.26 and 5.27.

$$I_{max} = C * 0.30 \quad (5.26)$$

$$I_{ch} = E_B \eta_{ch} \quad (5.27)$$

Equation 5.26 represents the charge characteristic of a gel battery for constant charge current at 20 hour rate. More information can be found in Annex 3 of this document.

5.4 Load Calculation

Two ways of adding electrical equipment, considered in the PV system demand calculation, have been implemented. The first one allows the user to add equipment from a list of common residential and commercial building electrical appliances. In this way, a database of continuous (DC) or alternate (AC) current equipment have been created. It can be found a range of low- and high-power electrical appliances combined to the options of add and remove custom equipment characteristics provided by the users. The second way to increment the demand of the PV system is combined to the central HVAC system module, where air handling unit components can be entirely or more frequently partly powered by the PV modules. Both demand increasing ways affect the building internal gains.

5.4.1 General Demand

To simulate the equipment energy demand, inverters models have also been implemented and the efficiency for both AC and DC inverters must be set by the user. At each time step, the total energy demand will be calculated summing the equipment AC and DC demands. To provide these values of demand, the user must enter the time interval of each equipment on the PowerDomus schedule configuration menu. Each equipment will have a list of working time and during simulation the list will be checked out to determine the total energy demand at each time step.

The demand equations for AC and DC equipment are specified multiplying the power to the number of equipment (if the same) and dividing this product to the circuit voltage and the inverter efficiency, according to Equation 5.28.

$$E_{eq} = \frac{P_{eq} n_{eq}}{V_{circuit} \eta_{AC,DC}} \quad (5.28)$$

5.4.2 Integration to Central HVAC System

In order to provide different simulation conditions to the users, the PowerDomus PV module considers on its equipment demand components of the HVAC central system simulation. Based on the work proposed by Barbosa and Mendes, (2008), the main idea is to use a fan-coil unit powered by the building PV system and simulate how a mechanical ventilation system can enhance the energy savings when combined to natural ventilation strategies.

In the context of this work, only the fan model will be used to enhance ventilation capacity when natural ventilation does not provide acceptable indoor thermal comfort and ventilation rates. In the sequence, the fan model and its integration to the whole-building simulation have been presented.

5.4.3 Fan Model

Following Barbosa and Mendes (2008) work, this section presents a model that calculates the fan power and leaving air conditions, as well the air temperature and humidity for a given flow rate and entering air conditions. The fan model used is based on the model presented in (Brandemuehl *et al.*, 1993), which considers a constant pressure rise across the fan. This assumption is equivalent to assuming fixed supply air duct static pressure, which is common in many standard HVAC systems.

The fan model is characterized by the full-load power and the volumetric airflow rate at rating condition. Fan power consumption at part-load is determined by an empirical relationship as a function of the ratio of operating airflow rated airflow. The air temperature rise across the fan is calculated to account for shaft and motor power input, as necessary. The model assumes a constant air density across the fan.

The fan power consumption is then determined in the following way (Barbosa and Mendes, 2008):

$$E_{fan} = E_{fan,rat} FFLP \quad (5.29)$$

where E_{fan} and $E_{fan, rat}$ are the actual shaft power at part-load conditions and full-load power, respectively. The factor $FFLP$ is a polynomial curve fit as a function of part-load ratio (PLR) as presented in Equation 5.30:

$$FFLP = C_0 + C_1 PLR + C_2 PLR^2 + C_3 PLR^3 \quad (5.30)$$

The factor PLR is defined as the ratio of the actual volumetric flow rate to the rated flow rate, in the following way:

$$PLR = \frac{\dot{V}_{actual}}{\dot{V}_{rat}} \quad (5.31)$$

The coefficients C_0, \dots, C_3 are obtained from supplied catalogs data, scanning the volumetric flow from the point of the rated condition to a possible minimum value and obtaining the corresponding power values for a constant pressure.

5.4.4 Load and Building Hygrothermal Model Integration

The present HVAC model can be easily integrated to building simulation programs, even using a dynamic model for the analysis of a whole-building hygrothermal behavior. In the present work, a lumped formulation for calculating both room air temperature and humidity ratio is considered for each building zone.

Equation 5.32 describes the energy balance, for a building room submitted to loads of conduction, convection, short-wave solar radiation, inter-surface long-wave radiation, infiltration, ventilation and the sensible and cooling loads for the HVAC system.

$$\dot{E}_t + \dot{E}_g = \rho_{air} c_{P, air} V_{room} \frac{dT_i}{dt} \quad (5.32)$$

where \dot{E}_t is the energy transfer rate that crosses the room control surface (W), \dot{E}_g is the internal energy generation rate (W), ρ_{air} is the air density (kg/m^3), $c_{P, air}$ is the specific heat of air ($J/(kgK)$), V_{room} is the room volume (m^3) and dT_i is the room air temperature ($^{\circ}C$).

The term \dot{E}_t , on the energy conservation equation, includes loads associated to the building envelope (sensible and latent conduction heat transfer), furniture (sensible and latent), fenestration (conduction and solar radiation), openings (ventilation and infiltration) and HVAC systems. The term \dot{E}_g accounts for the internal heat gain from people,

equipment and lighting.

The sensible and latent loads associated to the combined heat and moisture transfer problem through the building zone porous walls are calculated as:

$$Q_{wall,S}(t) = \sum_{j=1}^m h_{c,j} A_{surf,j} [T_{j,x=L}(t) - T_j(t)] \quad (5.33)$$

$$Q_{wall,L}(t) = \sum_{j=1}^m L(T_{j,x=L}(t)) h_{m,j} A_{surf,j} [\rho_{v,n,j=L}(t) - \rho_{v,int}(t)] \quad (5.34)$$

In Equations 5.33 and 5.34, $A_{surf,j}$ represents the area of the j -th surface, h_c is the convective transfer coefficients for heat and h_m for mass, $T_j(t)$ the temperature at the j^{th} internal surface of the considered zone, L the vaporization latent heat and ρ_v the water vapor density.

The temperature and the vapor density distributions needed to determine the sensible and latent conduction loads given by Equations 5.33 and 5.34 are calculated by using the combined heat and moisture transfer model based on the Philip and DeVries theory (Philip and De Vries, 1957) and the method presented in (Mendes *et al.*, 2002), which solves the following set of partial different governing equations for each control volume within the porous building element:

$$\begin{aligned} \rho_0 c_{P,M}(T, \theta) \frac{\partial T}{\partial t} &= \frac{\partial}{\partial x} \left(\lambda(T, \theta) \frac{\partial T}{\partial x} \right) \\ &+ L(T) \rho_l \frac{\partial}{\partial x} \left(D_{TV}(T, \theta) \frac{\partial T}{\partial x} + D_{\theta V}(T, \theta) \frac{\partial \theta}{\partial x} \right) \end{aligned} \quad (5.35)$$

$$\frac{\partial \theta}{\partial T} = \frac{\partial}{\partial x} \left(D_T(T, \theta) \frac{\partial T}{\partial x} + D_\theta(T, \theta) \frac{\partial \theta}{\partial x} \right) \quad (5.36)$$

where ρ_0 is the solid matrix density, $c_{P,M}$ the mean specific heat, T the temperature (in K), t the time (s), λ the thermal conductivity, L the latent heat of vaporization ($= h_{LV}$), θ the volume basis moisture content, j_v the vapor flow, ρ_l the water density, D_{TV} the vapor phase transport coefficient associated to a temperature gradient ($m^2/(s K)$), $D_{\theta V}$ the vapor phase transport coefficient associated to a moisture content gradient (m^2/s), D_T the moisture transport coefficient associated to a temperature gradient ($m^2/s K$) and D_θ the moisture transport coefficient associated to a moisture content gradient (m^2/s).

Internally, the wall is exposed to convection and phase change, and externally ($x = 0$), it is exposed to solar radiation (αG_T), convection ($h_{c,e}(T_e - T(0))$) and phase change ($h_{m,e}(\rho_{v,e} - \rho_{v,x=0})$), so that the energy equation becomes:

$$-\left(\lambda(T, \theta) \frac{\partial T}{\partial x}\right)_{x=0} - (L(T) j_v)_{x=0} = h_{ext}(T_{ext} - T_{x=0}) + \alpha G_T + L(T) h_{m,ext}(\rho_{v,ext} - \rho_{v,x=0}) \quad (5.37)$$

The conservation governing equations are then discretized by using the control-volume formulation method with a central difference scheme and linearized vapor concentration difference at the boundaries in terms of temperature and moisture content. The resulting algebraic equations are solved using the MultiTriDiagonal Matrix Algorithm (MTDMA) as described in (Mendes and Philippi, 2004).

The building zone model has to be fed with the sensible and latent HVAC system cooling loads, while the HVAC model needs the zone leaving air psychrometric state and the airflow return rate.

In terms of water vapor balance, different contributions have been considered: ventilation, infiltration, internal generation, porous walls, furniture, HVAC system and people breath. In this way, the lumped formulation becomes:

$$(\dot{m}_{inf} + \dot{m}_{vent})(w_e - w_i) + J_b + J_{ger} + J_{porous\ surface} + J_{HVAC} = \rho_{air} V_{air} \frac{dw_i}{dt} \quad (5.38)$$

In the water vapor mass balance (Equation 5.38), the term \dot{m}_{inf} is the mass flow by infiltration (kg/s), \dot{m}_{vent} corresponds to the mass flow by ventilation (kg/s) and w_i and w_e are the internal and external humidity ratio ($kg\ water/kg\ dry\ air$), respectively. The term J_{HVAC} is calculated as:

$$J_{HVAC} = \dot{m}_{inf}(w_{inf} - w_{int}) \quad (5.39)$$

and the term $J_{porous\ surface}$ is calculated in the same way as the latent conduction load.

The room air temperature (T_i) is calculated by the energy conservation equation (Equation 5.32), while the supply air temperature (T_{inf}) is calculated by using the equations that compose the secondary system, in general applications it will be the models for

the mixing box, cooling and dehumidification coil, humidifier and fan. In this work, just the fan model will be used.

5.5 Integration of Photovoltaic Modules to the Building Structures

By using the PowerDomus software, the user can select any building zone external surface to add photovoltaic panels to the building envelope as building-integrated photovoltaic strategy. In this way, the wall layer materials will still be considered and additional calculations will be performed in order to simulate the whole-building and energy effect of photovoltaic panels by changing the boundary conditions on the external surface. The following sections describe how the PV modules affect the heat and mass transfer to a specific region on the building wall.

Based on two simulation parameters that are offered to the users, PowerDomus can simulate just the building energy calculation or the whole-building hygrothermal model, according to the user needs. Following this configuration, two options of building-integrated photovoltaic systems have also been implemented and both heat and mass transfer can be considered.

5.5.1 Energy Model

At the external free surfaces, the wall material is exposed to convection heat and mass transfers and phase change so that the boundary condition energy conservation equation has already been presented in Equation 5.37.

When photovoltaic solar panels are considered, an additional thermal resistance will be created in the external layer and the heat flux will be modified according to the photovoltaic panel efficiency (η_c). The amount of energy that was not converted into electrical energy by the silicon cells will be conducted as a heat ($E_{conducted}$) according to Equation 5.40.

$$E_{conducted} = (1 - \eta_c) \tau_{glass} \alpha_c G_{T,eff} \quad (5.40)$$

In Equation 5.40, τ_{glass} is the glass transmittance and α_c is the cell absorptance. Equation 5.41 shows the thermal resistance caused by the PV panel, where a correction for the

convective heat transfer coefficient is presented.

$$\frac{1}{\bar{h}_{c,e}} = \frac{1}{h_{c,e}} + \frac{e_{glass}}{\lambda_{glass}} \quad (5.41)$$

where $\bar{h}_{c,e}$ is the corrected convection heat transfer coefficient on the building external surface ($W/m^2 K$), e_{glass} is the glass thickness (m) and λ_{glass} is the glass thermal conductivity.

5.5.2 Moisture Model

When the mass transfer is taken into account under the photovoltaic panel, the panel itself is considered as an impermeable boundary condition for moisture transfer. In this way, Equation 5.42 which represents the mass balance at the surface and Equation 5.37 which represents the energy balance will then be modified under the panel region, where the mass transfer convection coefficient - h_m - will be neglected.

$$-\frac{\partial}{\partial x} \left(D_\theta(T, \theta) \frac{\partial \theta}{\partial x} + D_T(T, \theta) \frac{\partial T}{\partial x} \right)_{x=0} = 0 \quad (5.42)$$

Important considerations about the difficulties (additional uncertainties) on the integration of the PV array and the building structure can be made:

- There is a lack of information on the contact resistance between the panel and the building envelope;
- The unidimensional characteristics of the heat and moisture model implemented into PowerDomus neglect the heat flux between the region area without PV and the area covered by the PV array.

5.6 Chapter Remarks

This chapter described the coupling of photovoltaic panels into a whole-building and energy simulation software - PowerDomus. The whole system composed by panels, batteries, inverters and demand equipment connected to the PV systems have been illustrated. Two methods to include energy demand for the photovoltaic systems have been shown, one for general AC or DC electrical appliances and other considering the HVAC system components.

In the following chapter the photovoltaic validation will be performed and a zero-energy case study aiming at evaluating “near zero-energy approach” to provide better indoor air quality by reducing mould growth and optimize thermal comfort will be presented and discussed.

6 Building-Integrated Photovoltaic Systems: Verification Procedures

After the description of the photovoltaic module presented in Chapter 5, this chapter shows the verification procedures of the PV code implemented into the PowerDomus software. The verification is based on comparisons between PowerDomus and two other well established PV simulation tools: PVSYST (ISE, 2008) and TRNSYS (Solar Energy Laboratory, 2007).

The chapter is divided into two main parts: *i*) Photovoltaic system verification - where the PowerDomus PV module results are compared to simulations performed into PVSYST and TRNSYS tools; *ii*) hygrothermal effects of photovoltaic integration - where the influences of BIPV systems on the building hygrothermal behavior are discussed.

6.1 Photovoltaic System Verification

This section shows the verification procedures of the PV algorithm. Comparisons in terms of PV incident radiation and the amount of energy converted into electrical energy by the “four-parameter” calculation method have been described here. In the sequence, the total incident radiation on the PV panel surface is evaluated and compared to results gathered from PVSYST and TRNSYS tools.

6.1.1 Radiation

The amount of energy that reaches the PV panel surface is tested here. To perform this test, some parameters have to be selected in order to define configuration standards for comparison purposes among the three software. In this situation, no building structures are taken into account

The first parameter to be selected is a typical weather file that could be used by all programs. Here, the TMY2 weather file for Denver, USA, has been adopted (US Department of Energy, 2006). This weather condition has been considered because it has already been used as standard for building and energy simulation tests - BESTEST (Judkoff and Neymark, 1995).

After the definition of test climatic conditions, the photovoltaic panel has to be selected. Considered as the main characteristics of this radiation test, the verification of the solar radiation algorithm, any PV panel can be used since their thermal and energy characteristics be available. Table 6.1 shows the panel characteristics adopted here. More information can be found in Annex 2, where the panel technical brochure is presented.

Table 6.1: Photovoltaic panel electrical characteristics.

Electrical Characteristics	Values
Nominal Voltage	12 V
Maximum power (P_{max})	50 W
Voltage at P_{max} (V_{mp})	17.5 V
Current at P_{max} (I_{mp})	2.9 A
Warranted minimum P_{max}	45 W
Short-circuit current (I_{sc})	3.2 A
Open-circuit voltage (V_{oc})	21.8 V
Temperature coefficient of I_{sc}	$(0.065 \pm 0.015) \% / ^\circ C$
Temperature coefficient of V_{oc}	$-(80 \pm 10) mV / ^\circ C$
Temperature coefficient of power	$-(0.5 \pm 0.05) \% / ^\circ C$
NOCT	(Air $20^\circ C$; Sun $0.8 kW/m^2$; wind $1 m/s$) $47 \pm 2^\circ C$
Maximum series fuse rating	20 A
Maximum system voltage	50 V

The selected panel has also $0.839 m \times 0.537 m$ of length and width, respectively, and weights $6.0 kg$. It has 72 solar cells distributed in a 4×18 matrix connected in two parallel strings of 36. The construction characteristics are: a high-transmission tempered 3-mm glass out the front and white polyester at the rear part.

In this particular case, a specific number of panels has been tested. However, the algorithm is able to simulate different modules configurations. Figure 6.1 shows the radiation verification procedure, where two panels in parallel configuration have been simulated maintaining 12 V at the array output.

Another parameter that must be configured before the simulation is the PV array slope, as PowerDomus PV module considers just BIPV systems. Figure 6.1 presents the results of panels integrated at the roof surface (0° slope). It is clear that, in this particular

case, the reflected irradiance will be equal to zero and, according to Section 5.2.6 when a horizontal surface is considered, the third term of Equation 5.21 is neglected by the algorithm. The horizontal orientation has been adopted in order to avoid obstructions between the Sun and the PV array. A mean annual representation of the total solar radiation that reaches the horizontal surface in Denver (USA) is presented in Figure 6.1. It can be seen in Figure 6.1 that the Denver climate variations has been similarly adopted by the three software - PowerDomus, TRNSYS and PVSYST.

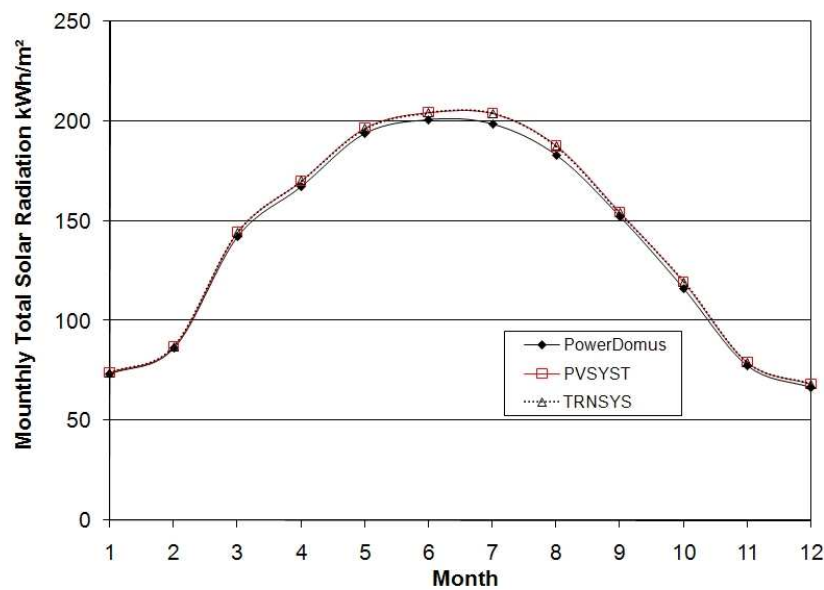


Figure 6.1: Total solar radiation comparisons between PowerDomus, PVSYST and TRNSYS software.

The differences presented in Figure 6.1 are explained by the numerical approximation found when the weather file was converted into the PowerDomus standard file type.

6.1.2 Array Generation

In order to test the “four-parameter” model, comparisons between PowerDomus and TRNSYS have been performed. In this section and in the following section, the PVSYST software has not been included in the comparative analysis because it does not include the “four-parameter” model. Energy conversion measurements at the PV array output have been reported and the same parameters that have been adopted in Section 6.1.1 were considered for the array generation analysis.

Figure 6.2 shows a comparison between PowerDomus and TRNSYS for the first week of January and for the first week of July, *i.e.*, winter and summer periods. In Figure 6.2, a good agreement between PowerDomus and TRNSYS results is verified when the array

output energy generation is compared.

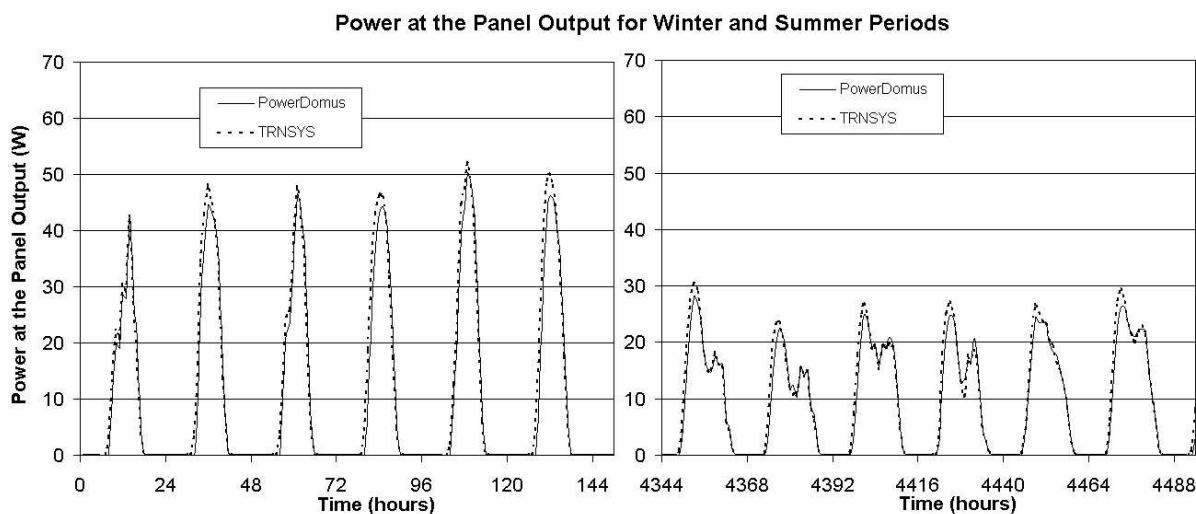


Figure 6.2: Energy conversion comparisons when incident angle modifier is not considered.

The differences between TRNSYS and PowerDomus, that have been illustrated in Figure 6.2, correspond to a yearly 6.09% more energy conversion for TRNSYS when compared to the the results presented for the PowerDomus simulation tool.

6.1.3 Incident Angle Modifier

The incident angle modifier correlation algorithm, which has been described in Section 5.2.6, has also been compared in terms of array output energy generation. Performing the same comparison as the one presented in Figure 6.2, where the algorithm has not been used, it is possible to evaluate the influences of the angle modifier correlation and its influences on the correction of the array converted energy.

Figure 6.3 reports the comparisons between TRNSYS and PowerDomus by using the same simulation parameters presented in Section 6.1.1. In terms of agreement, PowerDomus and PVSYST results show the same level presented when the incident angle modifier has not been adopted. However, it can be seen that a slight reduction on the energy conversion has been verified. The influences of the incident angle modifier when Denver climate conditions have been adopted are more relevant during cold seasons.

When the incidence angle modifier correlation is considered in both software, the differences between TRNSYS and PowerDomus, that have presented in Figure 6.3, present significant reduction. In this case, just a yearly 3.49% more energy conversion for TRNSYS is verified.

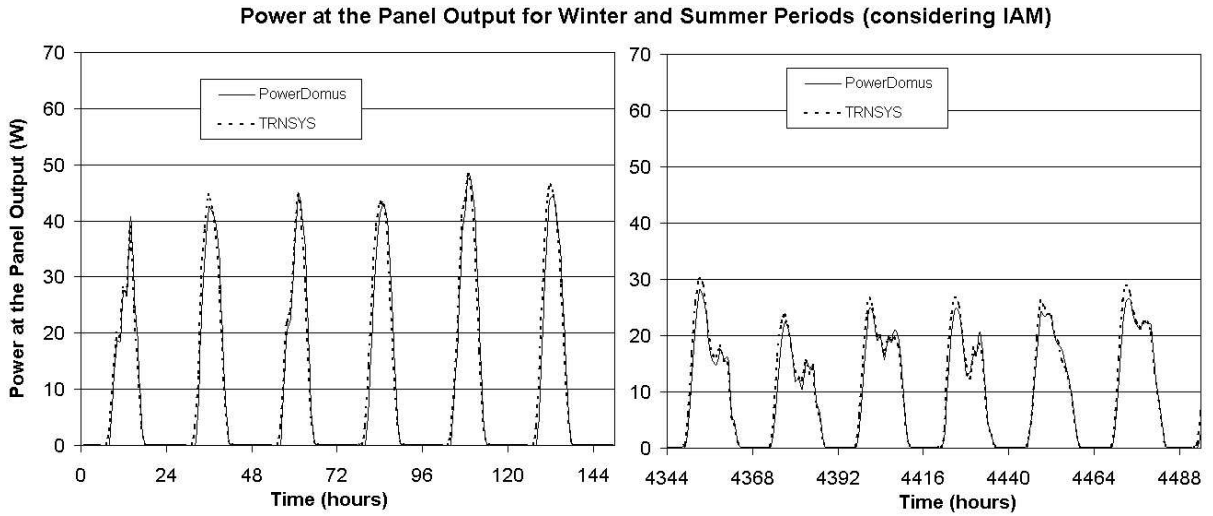


Figure 6.3: Energy conversion comparisons considering incident angle modifier.

Comparing the results presented in Figures 6.2 and 6.3, the monthly converted power differences between TRNSYS and PowerDomus in the PV array with and without considering the incident angle modifier correlation are presented in Table 6.2. The term IAM described in Table 6.2 means incident angle modifier correlation. Higher differences between the amount of energy converted by the PV panels are presented in the winter period and the converted power values provided by TRNSYS are always higher than PowerDomus.

Table 6.2: Monthly converted power differences between TRNSYS and PowerDomus when the incident angle modifier correlation is adopted.

Month	Differences(%)	
	without IAM	with IAM
1	6.75	2.74
2	6.04	2.21
3	5.70	2.55
4	5.91	3.32
5	5.19	3.11
6	4.97	3.62
7	4.75	4.05
8	6.04	4.85
9	6.15	3.97
10	7.92	4.81
11	7.18	3.27
12	7.78	3.77

6.2 Hygrothermal Effects of Photovoltaic Systems Integration

After both Radiation and energy conversion verification procedures, this section presents an analysis where the influences of the PV array on the building hygrothermal behavior are illustrated. Here, BIPV system integration analysis have been divided into four parts: *i*) building and photovoltaic system description; *ii*) simulation parameters; *iii*) simulation results by using a purely conductive heat transfer model, and *iv*) simulation results by using a combined heat and moisture transport model.

In order to facilitate the comprehension of this chapter, some terms have been adopted to describe the considerations about heat and moisture transport during the simulation procedures. While the first model (purely conductive heat transfer model) is based on Fourier's law and neglects any moisture desorption/adsorption effect, the second model (a combined heat and moisture transport model) considers the coupled heat and moisture transport through the building envelope, described by Equations 5.32 to 5.39.

6.2.1 Building and Photovoltaic System Description

In order to establish a sequence based on the previous chapters, the building structure described in Section 4.4.1 has been selected as the building reference to evaluate the hygrothermal integration of the BIPV system. Moreover, the same TMY2 data file of Curitiba - PR - Brazil (see Section 4.4.1) has been adopted (US Department of Energy, 2006).

To enhance the influences of the PV system over the building hygrothermal behavior, a 14×9 PV array configuration has been placed over the roof of the building, which means that almost all the roof area is covered by the PV array (88.75%). In this way, the additional layer on the roof surface of the first level is the orange highlighted area presented in Figure 6.4.

The panel glass properties are presented in Table 6.3. Moreover, the value of 0.95 for the cell solar absorptance has been considered.

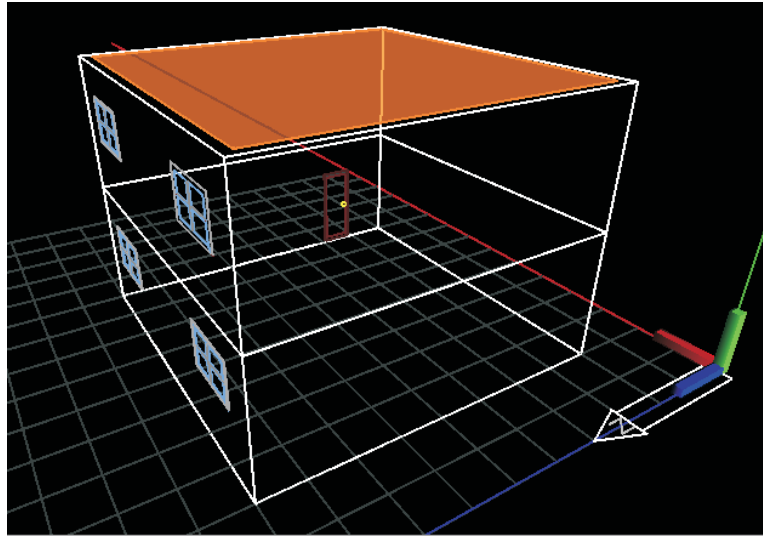


Figure 6.4: PV array representation on the two-storey office building.

Table 6.3: Glass characteristics.

Property	Value
Thickness (e)	0.003048 m
Thermal conductivity (λ)	1.0 W/m ² K
Transmittance (τ)	0.84

6.2.2 Simulation Parameters

Differently from the parameters presented in Section 4.4.3, simulations in this section do not take into account natural ventilation. In this way, the results presented in the following section are evaluated in terms of: *i*) degree-hours of comfort; *ii*) temperature and relative humidity at the internal ceiling surfaces; *iii*) indoor air temperature and relative humidity; and *iv*) mould growth risk at the internal ceiling surface.

In order to verify the influences of the PV array on the hygrothermal behavior at the internal ceiling surfaces, thermal comfort is not discussed in Sections 6.2.3 and 6.2.4. However, some analyzes are presented comparing hours of cooling and heating, which terms can be associated to thermal comfort. It is clear that, in conditions where infiltration and ventilation have not been considered and sensible and latent heat and vapor generation are available inside the building zones, the occupants' thermal comfort sensation will be depreciated. Moreover, the increase of roof solar absorptance, due to the small efficiency of solar cells, will contribute to depreciate the occupants' thermal comfort. In the case study presented in the sequence, thermal comfort will be evaluated in cases where both

natural and mechanical ventilation techniques have been adopted.

6.2.3 Results using a Purely Conductive Heat Transfer Model

This section and the following ones present the PV array influences on the building hygrothermal behavior. When just a purely conductive heat transfer model was adopted to solve the heat transfer through the building envelope, some considerations can be made according to the results presented in this section. Table 6.4 shows the yearly degree-hours of cooling and heating for building zones 1 (ground level) and 2 (first level) when the PV array is considered or not on the roof. The reference temperature range adopted on the calculation is $24 \pm 2^\circ C$.

Table 6.4: Yearly degree-hours of cooling and heating for building zones 1 and 2 when a purely conductive heat transfer through the building envelope model was adopted.

Zone	<i>degree-hours of cooling</i>		<i>degree-hours of heating</i>	
	without PV	with PV	without PV	with PV
1	32980.11	36152.97	878.00	678.91
2	18566.85	26671.68	8328.16	6031.77

Analyzing the results presented in Table 6.4 it can be verified that the effects of the PV array on the hygrothermal behavior of Zone 2 in terms of degree-hours of cooling increased 30.39% considering PV panels on the roof. On the other hand, a 27.57% decreasing on the degree-hours of heating is reported. Evaluating building Zone 1 (ground level), results present the same tendency when compared to Zone 2. In this case, 8.78% more degree-hours of cooling is reported when the simulations consider the PV array on the roof while a 22.67% less degree-hours of heating is obtained.

Figure 6.5 shows daily-averaged values of temperature at the internal ceiling surface for a whole year simulation period of building Zone 2 (first level). The building Zone 1 results have not been presented here because no significant differences were reported on the indoor air and ceiling surface temperatures when compared to the results presented in Figures 6.5. As expected, Zone 2 has presented more amplitude variations compared to Zone 1 in terms of internal ceiling surfaces and indoor air temperatures.

Temperature comparisons at the internal ceiling surface are presented in Figure 6.5, showing some peak differences of almost $8^\circ C$ higher when the PV panels are coupled to the building structure. This temperature increase is justified by the high solar ab-

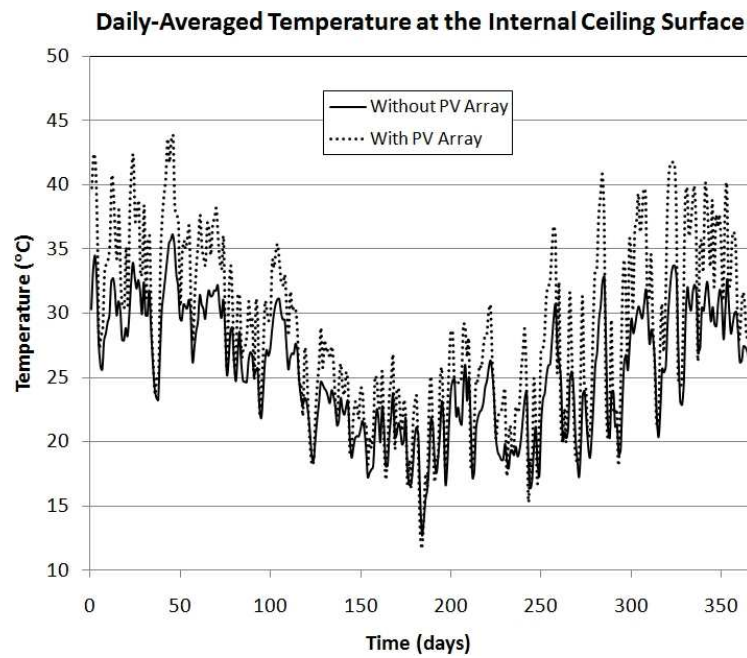


Figure 6.5: Daily-averaged values of temperature at the Zone 2 internal ceiling surface (with and without PV system) considering a purely conductive heat transfer model was adopted.

sorptance of PV cells and their low efficiency, where great amount of thermal energy is transmitted through the building envelope. The heat transport affects the indoor building surface temperature and consequently performs changes on the indoor air temperature, as presented in Figure 6.6.

In Figure 6.6, variations on the daily-averaged indoor air temperature of Zone 2 have been presented. It can be seen significant increases on the peak values when the PV array is considered. In these cases, increases of almost 3°C on daily-averaged values of indoor air temperature were noticed. In this way, even not considering the thermal comfort analysis, which will be performed in Chapter 7, previous remarks can be made over the increasing differences on the daily-averaged indoor air temperature, as they will significant affect the occupants' thermal comfort.

The daily-averaged indoor air and indoor ceiling surface temperatures of Zone 1 (ground level) present the same behavior as shown in Figures 6.5 and 6.6 for Zone 2. However, the panel influences on both daily-averaged internal ceiling surface and indoor air temperatures of Zone 1 are lower, and the averaged values of temperature are decreased of 5°C for the internal ceiling surface and 2.5°C for the indoor air.

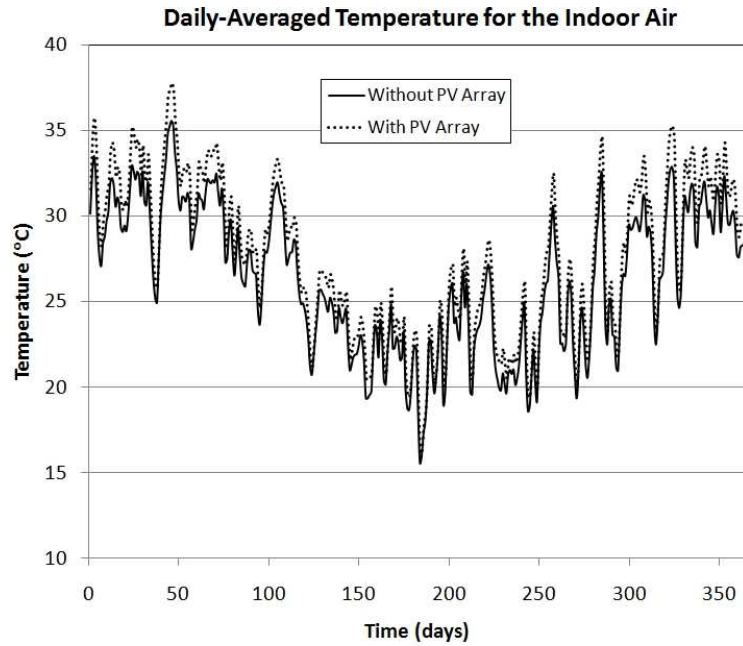


Figure 6.6: Daily-averaged values of indoor air temperature of Zone 2 (with and without PV system) considering a purely conductive heat transfer model was adopted.

6.2.4 Results using a Combined Heat and Moisture Transport Model

When the combined heat, liquid and vapor transport are considered through building materials, some additional results can be presented in order to compare the main significant effects of the PV array on the building hygrothermal behavior. In the hygrothermal analysis, Table 6.5 shows the results for building zones 1 and 2 in terms of degree-hours of cooling and heating.

Table 6.5: Yearly degree-hours of cooling and heating for building zones 1 and 2 when a combined heat and moisture transport model was adopted.

Zone	<i>degree-hours of cooling</i>		<i>degree-hours of heating</i>	
	without PV	with PV	without PV	with PV
1	20499.38	22587.16	4161.83	3664.12
2	8426.72	13052.75	20879.48	17594.62

As the results presented for the purely conductive heat transfer model, Table 6.5 describes the same thermal behavior when simulations considering a combined heat and moisture transport model to through the building envelope are carried out. However, for the results using the combined heat and moisture model for Zone 2, 35.44% degree-

hours more of cooling were reported when the PV array is considered and, consequently, 15.73% degree-hours less of heating were obtained. When Zone 1 is evaluated, 9.24% more and 11.96% less degree-hours of cooling and heating have been, respectively, obtained considering the PV system.

According to Figure 6.7 some changes on the internal ceiling surface temperature can be noticed, but the main changes are presented in Figure 6.8, where the relative humidity on the roof surface is presented. It can be seen that the inclusion of the photovoltaic system strongly affects the relative humidity at the internal ceiling surface. In this particular simulation, the PV array effect increases the relative humidity in winter period and the opposite effect is verified during the summer.

Analyzing the PV panels effects on the indoor air temperature, Figure 6.9 shows almost the same results when simulations with and without considering PV array are taken into account. Comparing the results presented in Figure 6.9 to the ones presented for the pure conductive heat transfer case (Figure 6.6), it can be seen almost no influences of the PV array on the indoor air temperature when moisture transport is considered.

The following results show the PV influences on the hygrothermal behavior of Zone 1 (ground floor). The changes verified at the internal ceiling surface for the first level slightly affect the indoor air conditions in terms of temperature and relative humidity.

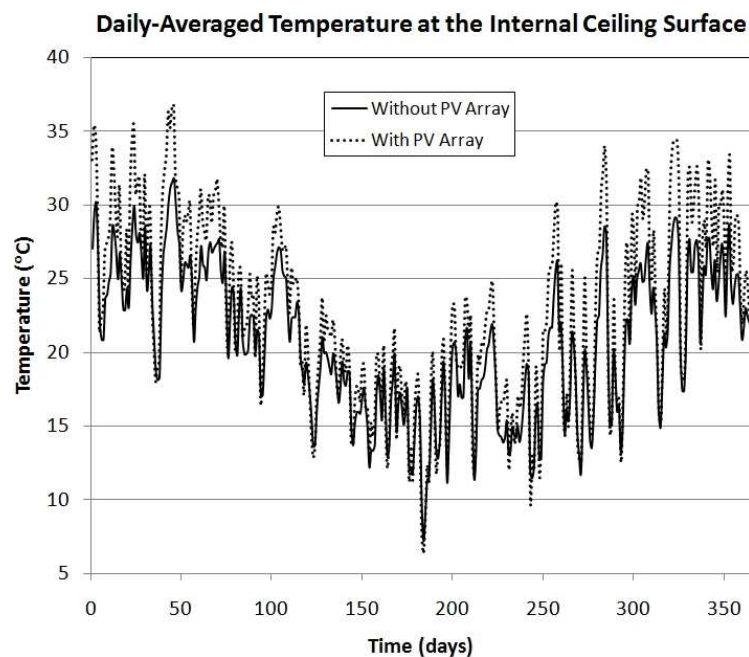


Figure 6.7: Daily-averaged values of temperature at the Zone 2 internal ceiling surface (with and without PV system) considering a combined heat and moisture transport model.

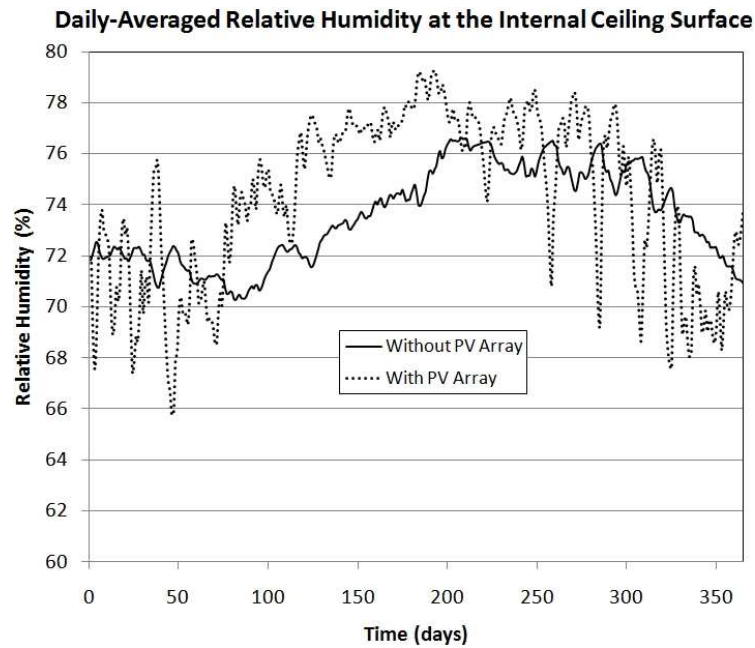


Figure 6.8: Daily-averaged relative humidity at the Zone 2 internal ceiling surface (with and without PV system) considering combined heat and moisture transport model.

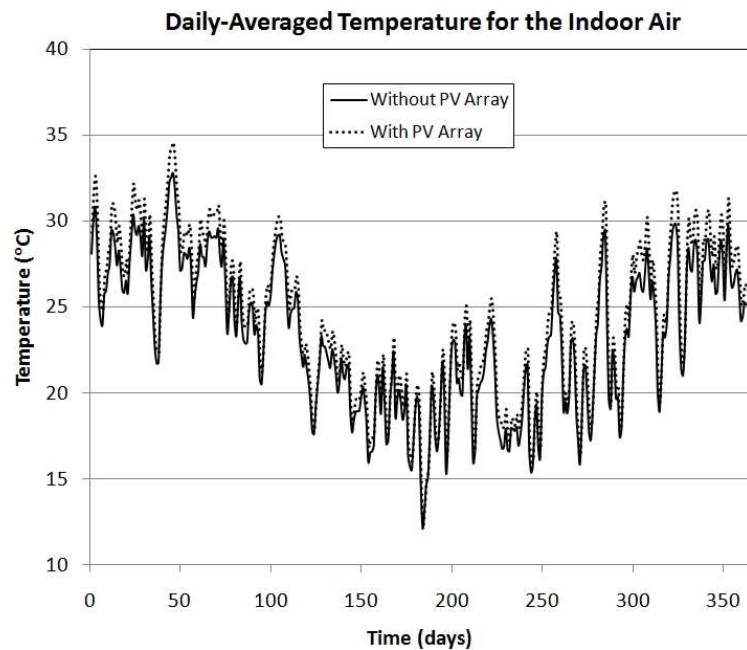


Figure 6.9: Daily-averaged values of indoor air temperature of Zone 2 (with and without PV system) considering combined heat and moisture transport model.

As not significant changes have been noticed, no significant changes are verified on the indoor air temperature. Figure 6.10 presents the most considerable changes in building Zone 1 (ground level), where no more than 1% relative humidity variations at the internal ceiling surface are presented. In this case, it can be concluded that the PV array coupled

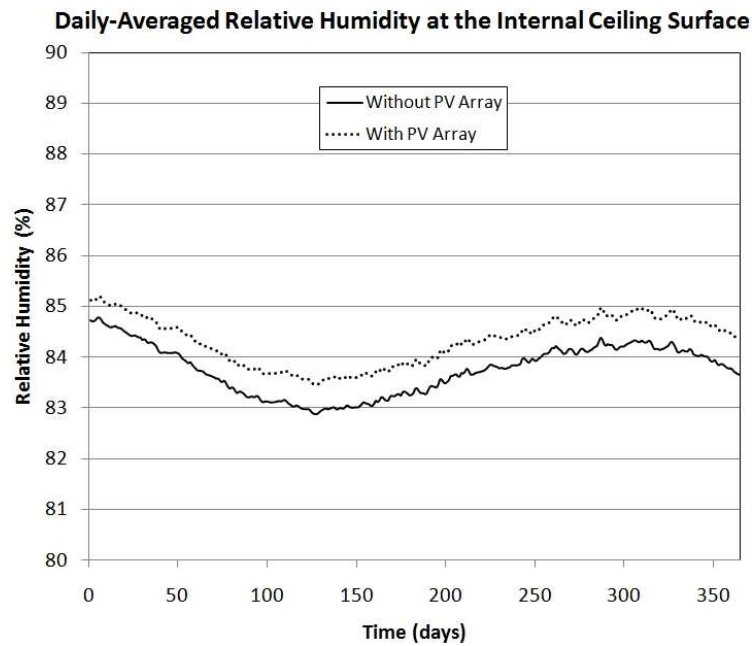


Figure 6.10: Daily-averaged relative humidity at the Zone 1 internal ceiling surface (with and without PV system) considering combined heat and moisture transport model.

to the roof of Zone 2 has almost no influences on the hygrothermal conditions of Zone 1.

When the results of these simulations, performed with combined heat and moisture transport model, are compared to those that consider pure conductive heat transfer through the building envelope, it is evident that the highest considerable differences between them have been verified for Zone 2 (first level). Other comparisons can be made by evaluating the mould growth index at the internal ceiling surfaces of zones 1 and 2.

Figures 6.11 and 6.12 show how the temperature and relative humidity variations at the ceiling surfaces affect the mould growth risk index during the whole year simulation period. The mould presence at the internal ceiling surface when the PV array is considered can be justified due to the increase on the internal ceiling surface temperature, internal heat and vapor gains from people and equipment and, associated to these factors, the impermeable condition found on the external ceiling surface, avoiding the drying effect, commonly found in cases without considering the PV coupled to the building.

Even with small influences on the Zone 1 hygrothermal behavior, the mould growth is affected by the PV system placed at the roof.

According to the daily-averaged temperature fluctuations presented in Figures 6.13 and 6.14, where simulations results for Zone 2 considering the PV array are presented and the purely conductive heat transfer model is compared to the combined heat and moisture

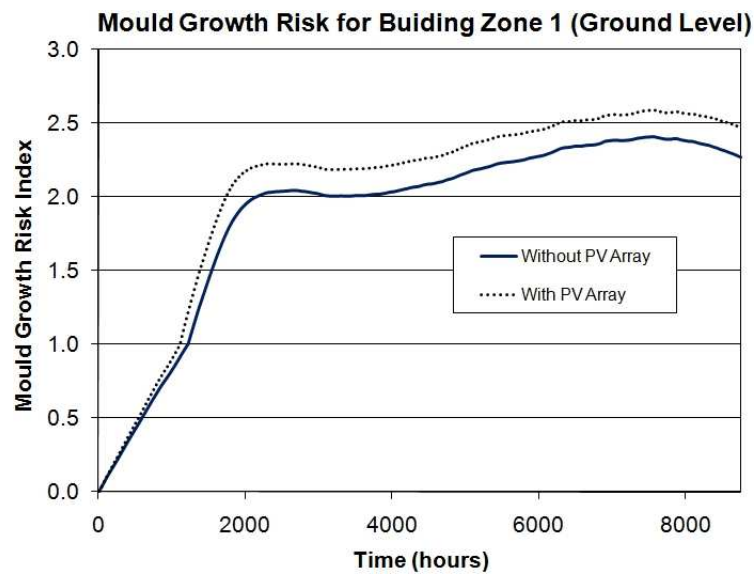


Figure 6.11: Mould Growth Risk at the internal ceiling surface of ground level.

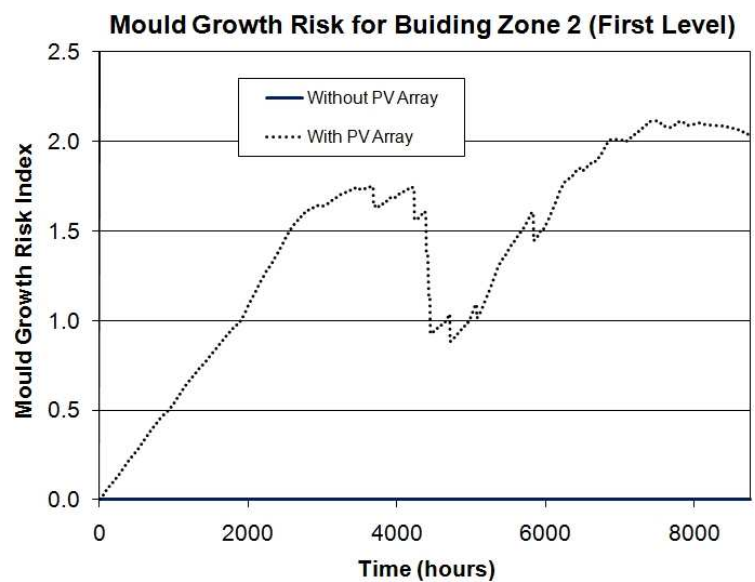


Figure 6.12: Mould Growth Risk at the internal ceiling surface of first level.

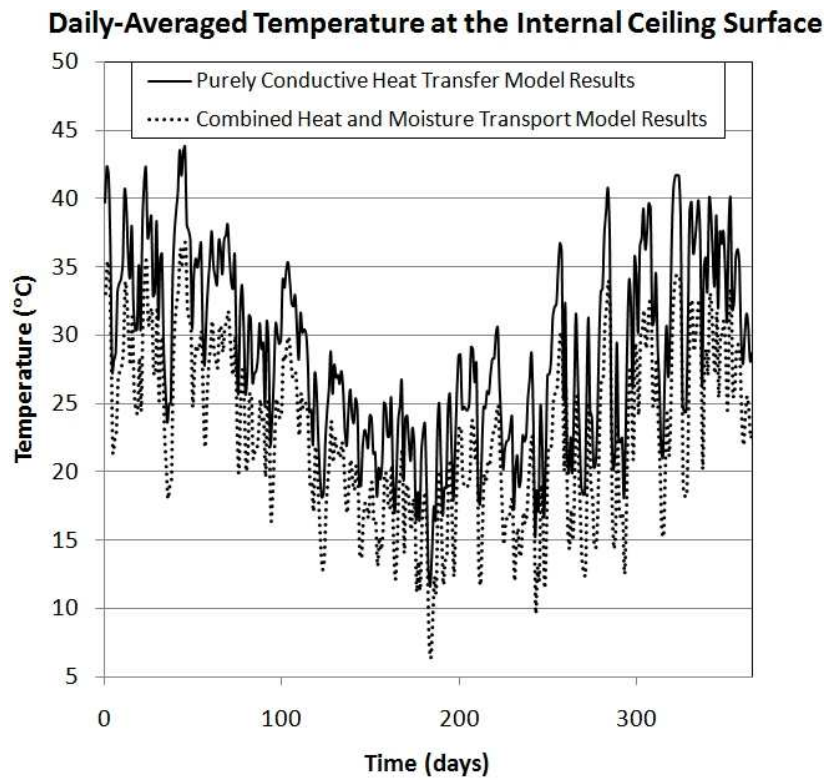


Figure 6.13: Daily-averaged values of temperature at the Zone 2 internal ceiling surface for both purely conductive heat transfer and combined heat and moisture transport models.

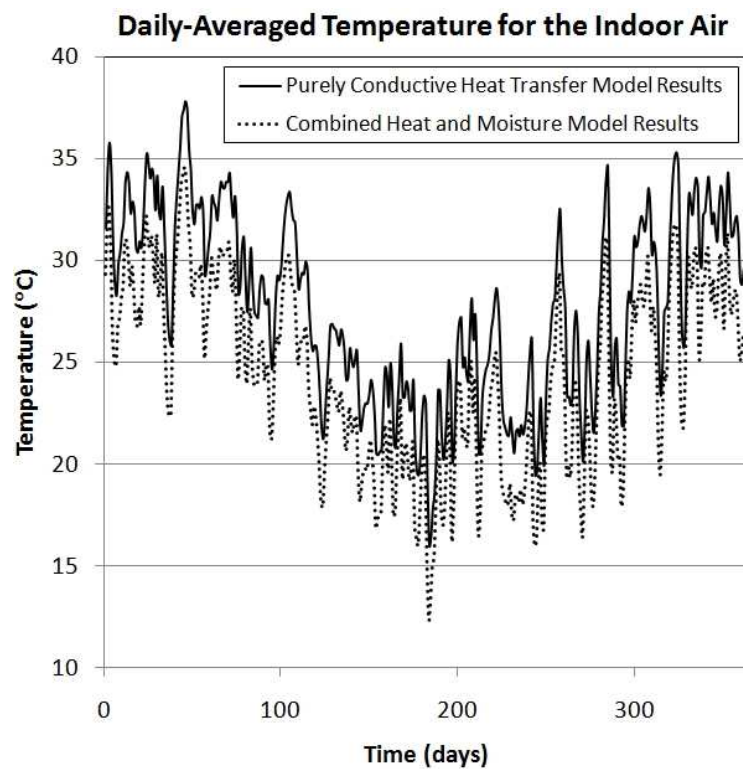


Figure 6.14: Daily-averaged values of indoor air temperature of Zone 2 for both purely conductive heat transfer and combined heat and moisture transport models.

transport model, it can be seen how important is the moisture transport on the study of building-integrated photovoltaic systems. As presented in these figures, variations of more than 5°C are noticed considerably affecting the occupants thermal comfort.

Results presented in Figures 6.13 and 6.14 also explain the difference of 5.05% more degree-hours of cooling when simulations considering the combined heat and moisture transport model were performed.

6.3 Chapter Remarks

This chapter was presented to describe the verification procedures of the photovoltaic module implemented into the PowerDomus software. The main changes on the hygrothermal performance of buildings when photovoltaic panels were coupled to building structures have been evaluated in terms of degree-hours of cooling and heating, indoor air temperature, temperature and relative humidity variations on the internal ceiling surface and mould growth.

Results were divided into two main sections: the first section described the Photovoltaic system verification, where the PowerDomus simulation results were compared to simulations performed in PVSYST and TRNSYS tools; in a second part, the evaluation of the PV influences on the building hygrothermal behavior was presented. By using the same building geometry adopted in this section which was presented in Chapter 4, simulations considering: *i*) pure conductive heat transfer through the building envelop, and *ii*) combined heat and moisture transfer model have been presented and discussed.

Some analyzes were performed in order to illustrate the importance of the moisture transport on the simulation of BIPV systems. As reported, the moisture transport analysis provides the evaluation of indoor air quality through the mould growth risk index calculation and its effect changes considerably the occupants thermal comfort sensation.

The next section aims at integrating natural ventilation and photovoltaic systems in a hybrid ventilation strategy capable of reducing energy consumption of HVAC systems and enhance thermal comfort and indoor air quality in typical Brazilian office buildings.

7 Comparative Analysis: Natural Ventilation versus Photovoltaic Hybrid Ventilation

This chapter describes an alternative way to enhance the natural ventilation potential of Brazilian buildings by using a hybrid photovoltaic ventilation strategy when thermal comfort parameters are not reached by the natural ventilation itself. Here the ventilation problem is treated as a condition to establish acceptable indoor thermal comfort to the occupants, while maintaining acceptable indoor air quality, and to reduce the energy consumption of buildings, avoiding the use typical cooling systems.

The potential usage of natural ventilation in Brazil and how it can be correlated to photovoltaic technology have been treated here, showing the Brazilian potential for BIPV (Building Integrated Photovoltaic) systems. The main idea of this chapter is to simulate a hybrid ventilation system - where a combined mechanical and natural ventilation strategy has been used to increase the indoor air quality, to improve the occupants' thermal comfort sensation and reduce mould growth risk on the indoor surfaces.

This chapter combines the use of an air handling unit model implemented into PowerDomus to the natural airflow models described in Section 2.1 in order to reduce energy consumption of buildings and optimize the indoor air quality. The development of a hybrid ventilation algorithm will be also presented.

In the sequence, an introduction and definitions about hybrid ventilation technologies are presented. Then, the Brazilian potential for natural ventilation and building-integrated photovoltaic systems applications are also addressed and a evaluation of the worldwide ventilation requirements and the Brazilian standards are described. The hybrid ventilation algorithm is presented in Section 7.5 and, in Section 7.6, a case study using the hybrid ventilation technique is proposed. Finally, simulation results are presented in Section 7.7 and final remarks about this chapter are addressed.

7.1 Hybrid Ventilation Systems

According to (IEA, 2002), the hybrid ventilation definition is: “*Hybrid ventilation can be described as systems that provide a comfortable internal environment using both natural and mechanical ventilation systems, but using different features of these systems at different times of day or season of the year. In hybrid ventilation, mechanical and natural forces are combined in a two-mode system where the operating mode varies according to the season, and within individual days. Thus the active mode reflects the external environment and takes maximum advantage of ambient conditions at any point in time*”.

The main difference between a conventional ventilation system and a hybrid system is that the latter has an intelligent control system that can switch automatically between natural and mechanical in order to minimize energy consumption.

Some benefits of hybrid ventilation systems are (IEA, 2002):

- Hybrid ventilation technologies fulfils the high requirements on indoor environmental performance and the increasing need for energy savings and sustainable development by optimizing the balance between indoor air quality, thermal comfort, energy use and environmental impact;
- Hybrid ventilation results in high user satisfaction because of the use of natural ventilation, the high degree of individual control of the indoor climates (including the possibility of varying the indoor climate - adaptive comfort) as well as a direct and visible response to user interventions;
- Hybrid ventilation offers an intelligent and advanced ventilation solution for the complex building developments of today, that is user transparent and sustainable.

In fact, when just the natural ventilation is considered, during a substantial part of the time, the stability of the flows is not the same as with mechanical ventilation and, in this case, restrictions in natural ventilation strategies appears. Considering environments where variations in natural ventilation airflow rate may result in pressure fluctuations and even flow direction changes, an additional strategy must be adopted to supply the minimum ventilation rates. Usually, this compensation is made by mechanical ventilation systems, *e.g.*, an operating room in a hospital or a laboratory where full mechanical ventilation might be the only solution (de Gids, 2007).

In the past, ventilation systems were in general only used for IAQ control and they

were classified into two categories (Wouters *et al.*, 1999): (constant air flow) mechanical ventilation systems and (manual controlled) natural ventilation systems. During the last two decades, interesting developments have been accomplished for both categories. There is a tendency for combining the best of both technologies: intelligent natural ventilation if appropriate, efficient mechanical ventilation if required. This tendency is valid also for ventilation concerning thermal comfort in summer.

Based on these characteristics, hybrid ventilation systems can be a reasonable solution for buildings located in urban areas, where natural ventilation is depreciated due obstructions.

In the following, some of the most disseminated strategies for improvement of indoor air conditions, thermal comfort and energy savings are discussed. Tests and implementations will be performed on the continuation of this work to show the efficiency of the following strategies in the Brazilian context.

7.2 Brazilian Potential for Natural Ventilation Applications

The potential use of natural ventilation becomes evident when some characteristics of the Brazilian country are discussed. Considering the country area, it clear that good wind resources can be found in many parts of the country, mainly along the coast cities. Usually, if places with high wind potential are near to the high demographic regions, the inclusion of natural ventilation strategies in each building design project may increase substantially. In Figure 7.1 (IBGE, 2000; CBEE, 1998), it is noticed that the Brazilian population are placed almost near the coast, which are the places with high wind power potential and, fortunately, higher potential for the use of natural ventilation as well.

7.3 Brazilian Potential for BIPV Applications

In the Brazilian context, it is noticed that residential, commercial and public buildings in urban areas correspond to over 45.0% of the electricity demand in the country (EPE, 2009). According to (Ordenes *et al.*, 2007) Brazil has a continuous increase of energy demand and a decrease of available resources to expand the generation systems. In this way, analyzing the Brazilian solar atlas presented in Figure 7.2, it is noticed a great potential in building-integrated photovoltaic (BIPV) systems.

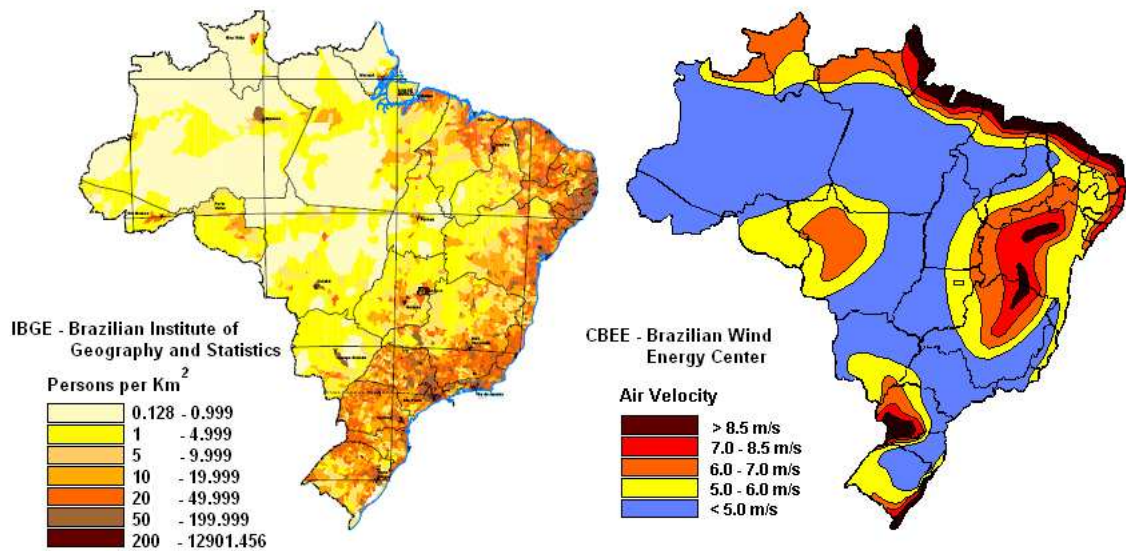
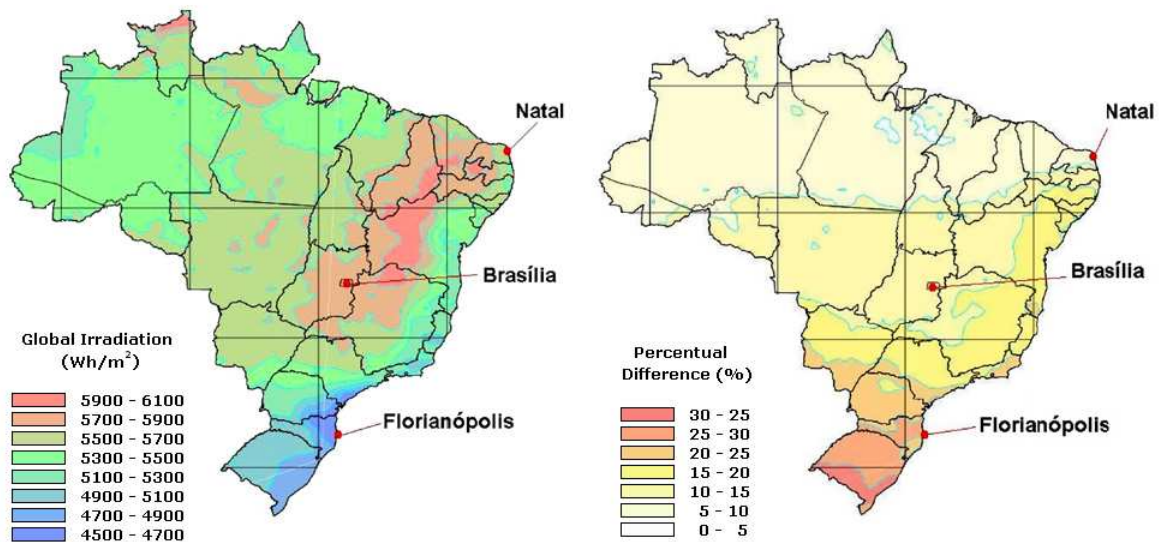


Figure 7.1: Demographic and wind energy potential maps for Brazil.

Figure 7.2: Brazilian solar atlas - yearly average of the daily global radiation and its percentage variation on horizontal plane (Ordenes *et al.*, 2007).

7.4 Ventilation Requirements

In this section, an overview of some current standards and regulations including solutions for equivalent functional requirements is presented. Here, ventilation requirement standards from Brazil, Canada, France, Italy, United Kingdom and United States of America are reported in order to present the air change rates for offices and dwellings used in some American and European countries.

Some of the information presented in this section have been included in this and in

the following sections will be used as parameters for the hybrid ventilation case study presented in this chapter.

7.4.1 Ventilation in Dwellings

Minimum ventilation rate standards for residential buildings are essential to provide occupant health and comfort and to remove and dilute pollutants. In residential buildings these are pollutants generated by cooking (moisture, NO_X) and washing (moisture), as well as in some cases tobacco smoke. In this way, guidelines for minimum ventilation rates are presented in Table 7.1 (Limb, 2001).

Table 7.1: Minimum ventilation criteria for dwellings.

Country and Reference	Ventilation Rates
Canada (NRCC, 1983)	$> 0.3 \text{ ach}$ 5.0 l/s .
France (Millet, 2001) (CSTB, 1988)	$< 50 \text{ m}^2$ up to 2 occupants Minimum: 17 l/s . Total: 17 l/s . $< 80 \text{ m}^2$ up to 4 occupants Minimum: 25 l/s . Total: 34 l/s . $> 80 \text{ m}^2$ up to 2 occupants Minimum: 34 l/s . Total: 50 l/s .
Italy (Standard UNI, 1995)	Naturally ventilated dwellings: 0.35 to 5.0 ach .
United Kingdom (British Standards, 1999)	Average Dwelling. Recommended: 12 l/s per person. Luxury Dwelling. Recommended: 18 l/s per person. Minimum: 18 l/s per person. Background ventilation $\approx 6000 \text{ mm}^2$ per room with minimum $\approx 4000 \text{ mm}^2$.
United States of America (ASHRAE, 2005c)	0.35 ach but no less than 7.5 l/s per person. Natural ventilation minimum area of openable window as 5% of floor area in each room.

Usually, minimum ventilation rate criteria are difficult to compare, mainly because the overall size and nature of typical dwellings and population densities vary from country to country, or even country wide, *e.g.*, is Brazil.

7.4.2 Ventilation in Offices

In office environments, the most common pollutants are the ozone (O_3) and odour. Sometimes, in ventilation systems, carbon dioxide is used as indoor air quality indicator. Although other specific pollutants may be present, this is becoming less important with legislative restrictions becoming even greater (Limb, 2001). Also the heat generated by office equipment, lighting and solar gains and the outside air, which can contribute to the pollutant load within office spaces, *e.g.*, traffic pollution, can be reported as important pollutants. Table 7.2 presents values of ventilation rate requirements for offices.

Table 7.2: Minimum ventilation criteria for offices.

Country	Minimum Ventilation Rate Criteria for Offices
Canada	8 to 30 l/s per person for commercial and factory buildings.
France	Requirements: for current teaching rooms the required value of fresh air is 4.26 l/s . For current offices it is 7.1 l/s per person and for meeting rooms 5.0 l/s (non-smoking) or 8.1 l/s (smoking).
Italy	Single offices and open space offices: 11.0 l/s per person. Meeting rooms and computers: 10.0 l/s per person. toilets: exhaust ventilation 8 <i>ach</i> .
United Kingdom	Offices (open plan) - Smoking: some. Recommended: 8.1 l/s per person. Minimum: 5.0 l/s per person. Offices (private) - Smoking: heavy. Recommended: 12.0 l/s per person. Minimum: 8.0 l/s per person.
United States of America	Office: 10.0 l/s per person. Reception spaces: 8.0 l/s per person. Telecommunications centres: 10.0 l/s per person. Conference rooms: 10.0 l/s per person.

7.4.3 Brazilian Standards for Indoor Air Quality

The Brazilian ventilation requirement standards have been recently modified and a more realistic expression to define the airflow rate in a building has been provide. According to ABNT (ABNT, 2008), it is indicated three levels of air flow rate values for ventilation systems. Each air flow rate value is calculated based on Equation 7.1.

$$Q_{V,eff} = P_Z F_P + A_Z F_A, \quad (7.1)$$

where Q_V is the air flow rate to be supplied to the zone (l/s), P_Z is the maximum number of people in the ventilated building zone, A_Z is the occupied area (m^2), F_P is the air flow rate per person (l/s) and F_A is the air flow considering the occupied area ($l/(s m^2)$).

The values of F_P and F_A can be obtained according to the use of the building and are defined in (ABNT, 2008). Values of F_P and F_A are provided in Table 7.3.

Table 7.3: Minimum ventilation rates according to the Brazilian Standard NBR 6401-08.

Environment Type	Density (people/ m^2)	Level 1		Level 2		Level 3	
		F_P	F_A	F_P	F_A	F_P	F_A
Stores	15	3.8	0.9	4.8	1.1	5.7	1.4
Offices (low density)	11	2.5	0.3	3.1	0.4	3.8	0.5
Banks (public area)	41	3.8	0.3	4.8	0.4	5.7	0.5
Fitness center (aerobic)	40	10	0.3	12.5	0.4	15.0	0.5

7.5 Hybrid Ventilation Strategy

Based on natural ventilation models and the standards for indoor air quality, this section presents an alternative strategy that can be used to change the indoor climate enhancing indoor thermal comfort of buildings. The hybrid ventilation strategy presented here integrates the use of photovoltaic energy to power up a fan and a three stage control system, capable of enhancing indoor air quality and thermal comfort while trying to reach ventilation standards.

The flowchart presented in Figure 7.3 describes the functionality of the hybrid ventilation algorithm. As it can be seen in Figure 7.3, the three stage algorithm has the following priorities:

1. *Thermal Comfort*: the algorithm determines the upper and lower limits of the acceptable thermal conditions in naturally conditioned spaces (ACS, see Section 4.2.4). Defining the instant thermal comfort condition based on the indoor operative temperature and mean monthly outdoor air temperature, the algorithm uses both indoor and outdoor air enthalpy to define if an additional airflow rate is necessary by turning the fan on.
2. *Relative humidity on the indoor wall surface*: when 80 or 90% of the occupants are considered within acceptable thermal comfort conditions, the algorithm improves

the indoor air quality by reducing the mould growth risk on the indoor building surfaces. Based on the 80% critical relative humidity presented in the definition of the mould growth risk index (see Section 4.3), it is possible to reduce the risk of mould development when the outdoor air is drier than the indoor air.

3. *Minimum ventilation rate:* Considering that the occupants are in acceptable thermal comfort conditions and the relative humidity of the indoor surfaces are under 80%, the algorithm is able to provide a previously defined ventilation rate.

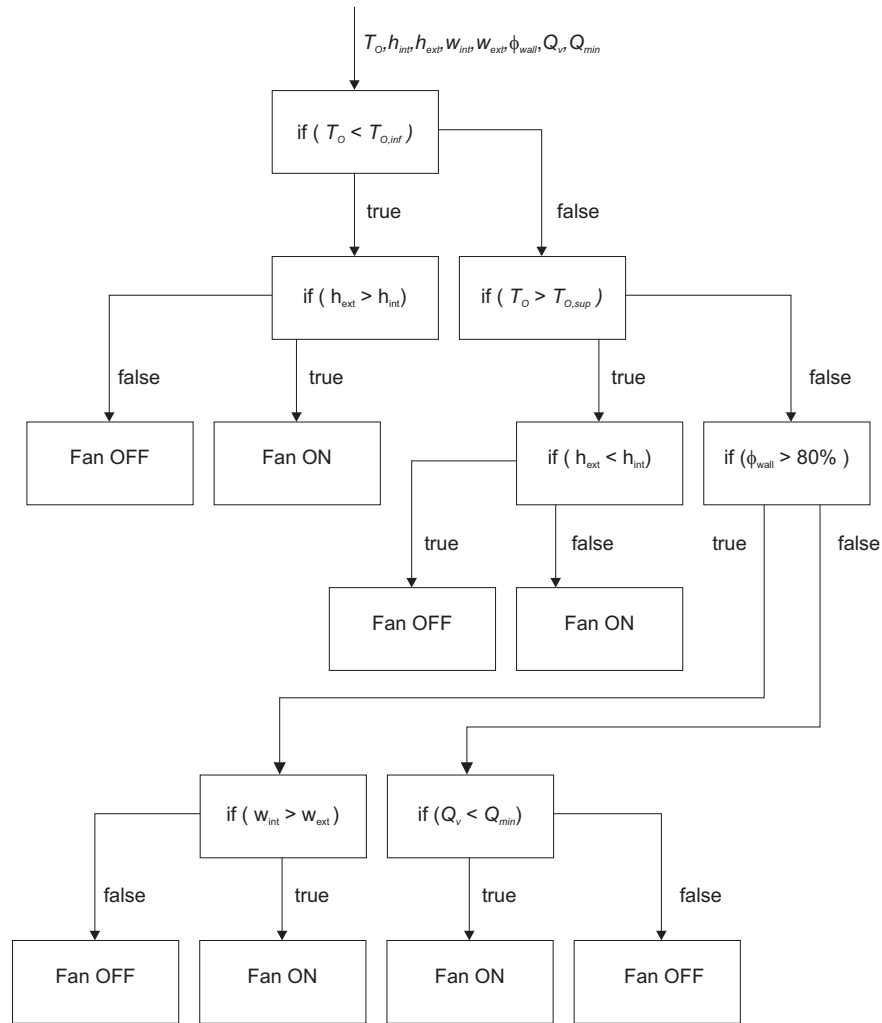


Figure 7.3: Hybrid ventilation algorithm flowchart.

Some considerations have to be taken into account before the use of this control strategy. The algorithm verifies constantly the airflow rate through the openings based on the empirical models presented in Chapter 2. The definition of the activities performed by the occupants on the indoor environment and the maximum number of people should be defined before simulation. Finally, the priority of the two first terms (thermal comfort

and relative humidity on the indoor wall surface) can be redefined. However, the minimum ventilation rate could take higher priorities only if a fan variable airflow rate is provided. In this case, the fan air flow rate is constant and defined according to the indoor air quality standards.

7.6 Case Study

This section presents a case study in order to test the hybrid ventilation algorithm presented in the above section. The idea is to use a pre-defined geometry and, considering the recent Brazilian ventilation standards, change some simulation parameters to check different control reactions on the hybrid ventilation system.

7.6.1 Building Description

Following the previous chapters, the building structure presented in Chapter 4 and 6 has also been adopted here. However, comparing the building structure in Chapter 6 to the one presented in Figure 7.4, differences on the size of the PV array are noticed. While in Chapter 6 the PV array had almost the same area as the roof of the buildings in order to enhance the hygrothermal influences of the PV modules on the indoor environment, here the PV system has been sized to provide sufficient energy to the hybrid ventilation fan.

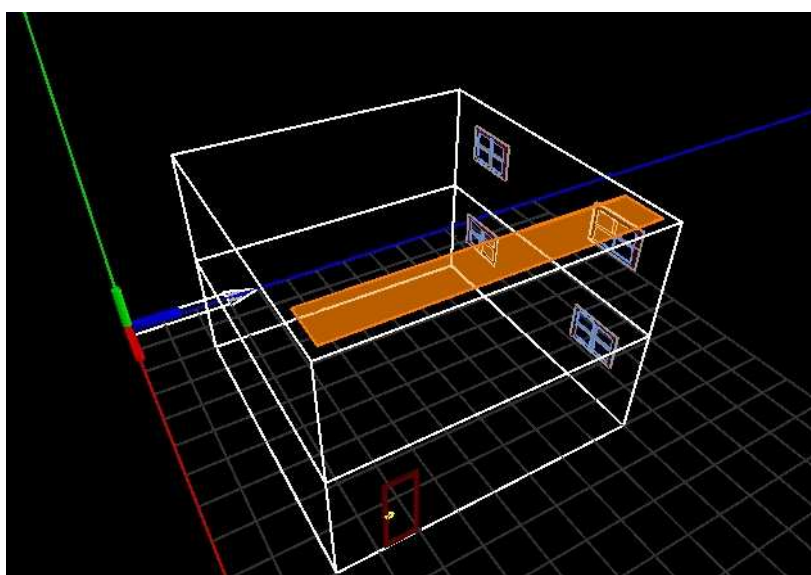


Figure 7.4: PV array representation on the top of the two-storey office building.

Table 7.4: Model parameters for the fan used in the hybrid ventilation strategy.

Parameters	Zone 1
Power (kW)	0.16
Efficiency (%)	51
Air Flow (m^3/h)	187.27

The Test Reference Year (TRY) of the city of Curitiba, South of Brazil (latitude: -25.52° ; longitude: -49.17° ; GMT: $-3 h$; altitude: $934 m$) has been used again here for a two-year simulation period. The first year has been considered as a warm up period to avoid initial conditions effects. The building envelope materials and dimensions are already presented in Section 4.4.1. More information about the BIPV system will be discussed in the following section.

7.6.2 BIPV System Description

System Energy Demand:

The building-integrated photovoltaic system has been sized according to the power supplied to the hybrid ventilation fan. Considering that the office building occupation period is from $8 am$ to $6 pm$, the worst case is when the window is closed all the time and the fan must be turned on during the whole occupation time. According to the data presented in Table 7.4, it can be seen that a $160 W$ with 51% efficiency means the necessity of $313.75 W$ to provide an air flow of $187.27 m^3/h$. Considering the worst case, the value $3.14 kW$ has to be supplied to the fan during one day period.

The $187.27 m^3/h$ air flow rate has been calculated according to the Brazilian standard for offices with low density of people. The Brazilian standard (ABNT, 2008) indicates three efficient air flow levels for ventilation systems. The calculation of the air flow rate can be made through Equation 7.1. In this case, the adopted parameters F_a and F_p are considered for level 2 and are 3.1 and 0.4, respectively.

Array Configuration:

After calculating the energy demand, both PV array and storage system can be estimated. The PV array can be basically defined as function of the energy demand and of the system voltage. Here, a $24 V$ system has been chosen. Usually, PV systems are configured as multiple of $12 V$ and the association of modules and batteries in parallel configuration can provide different system voltages (CETC, 2004).

Considering that this work is focused on the validation and implementation of PV systems into a building and energy simulation software and the influences of the PV array on the building hygrothermal behavior, the software does not have a presizing module for photovoltaic equipments. In this way, the PVSYST software has been used to define the necessary numbers of panels and batteries capable of supplying the fan energy demand during the whole year period (ISE, 2008).

The panel model selected in this case study has been already presented in Section 6.1.1 and its characteristics have also been shown in Table 6.1. More details about this panel can be found in the panel technical brochure (Annex 2).

As verified in Table 6.1, this type of module provides $12V$ at the array output. In order to have a $24V$ at the array output, two panels in series must be considered. According to the PVSYST presizing module, it is suggested to use 11 modules in parallel. However, as the PV array has been placed on the roof of the building and not at a vertical wall and additionally the fan will not be turned on during the all the occupation period, 9 panels in parallel configuration have been considered. In this case, 9 modules in parallel configuration can provide $900W$ peak power.

Storage System:

When the storage system is taken into account, it must provide the same voltage compared to the array configuration in order to avoid conversion losses. In this way, a $12V$ battery with $225.0Ah$ nominal capacity (C20) has been considered.

When the PVSYST presizing module is evaluated, a $443Ah$ suggested capacity is presented. Considering the battery characteristics, the association of two batteries in series two batteries in parallel configuration will provide $24V$ output and $450Ah$ of total capacity. This suggested system can provide $1.1kWp$ for a 4-day autonomy period.

Actually, the storage system can be more detailed as it is described in this section. However, the main idea in this chapter is to present the hybrid ventilation technique, which depends of the PV system. More detailed information can be found in Annex 2, where the constant charge voltage, operating temperature and self-discharge curves are presented.

7.6.3 Simulations Parameters and Reports

Simulations have been performed and three main parameters have been changed: *i*) the time that natural ventilation is used considering just one opening; *ii*) the use of hybrid ventilation system; and *iii*) the use of air-cooling system. Results are expressed in terms of thermal comfort, mould growth at the internal ceiling surface and energy consumption. According to these rules, the following simulations have been performed:

- Openings closed with no air-conditioning strategy;
- Openings closed using an air-cooling system;
- Simulations performed with and without hybrid ventilation:
 - Hybrid ventilation from 8 *am* to 6 *pm* when necessary;
 - Natural ventilation configured for one opening from 8 *am* to 9 *am*;
 - Natural ventilation configured for one opening from 8 *am* to 1 *pm*;
 - Natural ventilation configured for one opening from 8 *am* to 6 *pm*;

Following the Brazilian ventilation standards for indoor air quality, 11 people have been considered on the ground level of the office building. The results presented for the building zone at the ground level during the occupation time (from 8 *am* to 6 *pm*), an individual moisture generation (at 37°C) of 180 *g/hour*. Additionally, a heat gain of 2050 *W* to account for the office equipment has also been added.

7.7 Results

This section presents the comparisons between hybrid ventilation system and natural ventilation strategy. Furthermore, hybrid ventilation and traditional cooling systems, shown in Chapter 4, are also compared.

7.8 Natural Ventilation Comparisons

First, simulations performed with and without hybrid ventilation are presented in terms of thermal comfort. Here, the thermal comfort index ACS for naturally ventilated

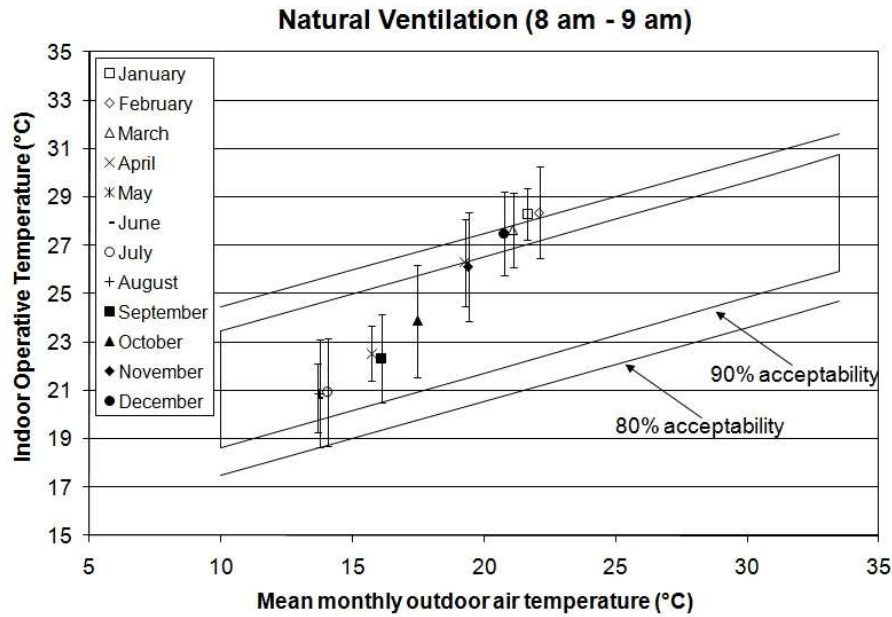


Figure 7.5: Comfort zone using just natural ventilation from 8 *am* to 9 *am*.

environments is discussed. In Figures 7.5 and 7.6, results of thermal comfort zone for 1 hour of natural ventilation, with and without hybrid ventilation are presented.

As it can be verified when Figures 7.5 and 7.6 are compared, even for the hotter months (January and February), the mean values for thermal comfort are within the 80% comfort limits. This behavior is verified for the 5 and 10 hours of natural ventilation; in this way, the graphical representation of the comfort zone for these cases will not be presented.

This case has been selected because it is the worst case in terms of indoor air quality, where a considerable amount of humidity and energy is provided inside the environment and just one-hour-period of natural ventilation is not enough to provide acceptable conditions to the occupants. Mould growth and humidity at the wall surfaces will be discussed in the sequence, where influence of the hybrid ventilation will be more evident.

Tables 7.5 and 7.6 shows the percentage of hours in comfort for one-year period, for natural ventilation cases considering or not hybrid ventilation.

Comparing the results presented in Tables 7.5 and 7.6, it can be seen how hybrid ventilation can enhance comfort levels even with high values of heat and moisture generation inside the building.

For the air-conditioning case, it maintains 80% of the occupants 75.23% of the whole year period in acceptable thermal conditions. When the 90% criteria is taken into account,

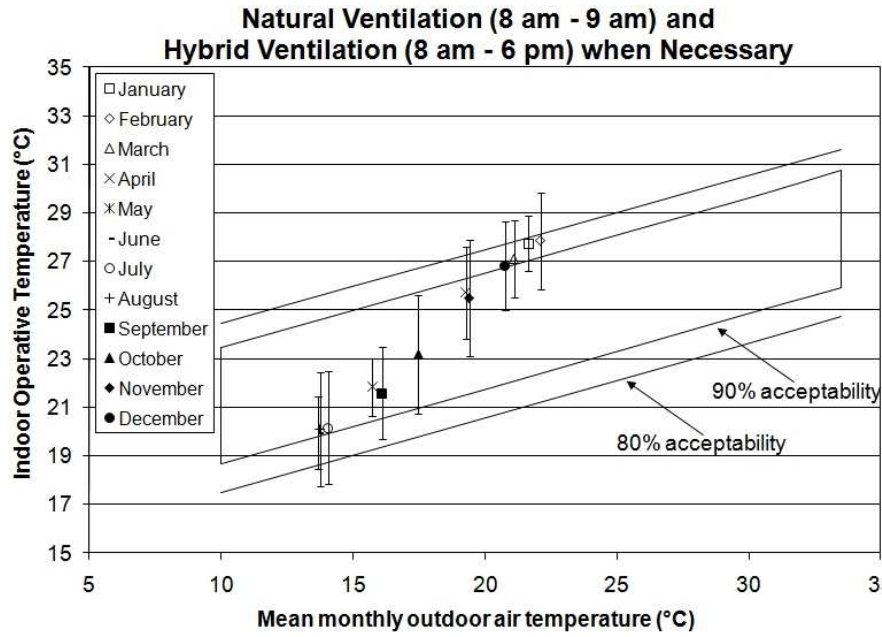


Figure 7.6: Comfort zone using natural ventilation from 8 *am* to 9 *am* and hybrid ventilation when necessary.

Table 7.5: Percentage of time within the comfort zone without hybrid ventilation.

Case	Percentage of Time in the Comfort Zone (%)	
	80% Zone	90% Zone
Natural ventilation (8 <i>am</i> - 9 <i>am</i>)	26.07	17.06
Natural ventilation (8 <i>am</i> - 1 <i>pm</i>)	41.10	28.51
Natural ventilation (8 <i>am</i> - 6 <i>pm</i>)	54.79	39.23

the air-conditioning system can provide 53.63% of the year period in acceptable thermal conditions. As it can be verified, considering the 80% of occupants in acceptable thermal comfort conditions, the HVAC system contributes significantly to enhance the percentage of time within the comfort limits. However, the amount of energy used by the HVAC system depreciates the verified results.

In terms of energy consumption, Tables 7.7 and 7.8 show the data compilation of hybrid ventilation and air-conditioning simulation cases. When just natural ventilation is considered, no energy consumption is reported. The term “NV” in Tables 7.7 and 7.8 means natural ventilation.

Table 7.8 shows no energy consumption in December, *i.e.*, just natural ventilation has been considered by the controller.

Table 7.6: Percentage of time within the comfort zone when hybrid ventilation is considered (8 am - 6 pm).

Case	Percentage of Time in the Comfort Zone	
	80% Zone	90% Zone
Natural ventilation (8 am - 9 am)	45.28	33.30
Natural ventilation (8 am - 1 pm)	50.09	36.91
Natural ventilation (8 am - 6 pm)	57.68	42.38

Table 7.7: Monthly energy demand.

Case	Monthly Energy Demand (<i>kWh</i>)					
	January	February	March	April	May	June
Window closed	100.26	90.56	100.26	97.03	100.26	90.35
NV (8 am - 9 am)	100.26	90.56	98.80	91.71	87.22	83.99
NV (8 am - 1 pm)	100.26	88.37	88.27	82.21	55.82	47.16
NV (8 am - 6 pm)	85.45	75.54	83.26	73.03	32.13	9.29

The yearly energy consumption of all cases is summarized in Table 7.9. The HVAC system monthly energy demand is not presented because the main idea of Tables 7.7 and 7.8 is to show the self tuning of the hybrid ventilation controller, presenting different energy consumption values, according to the window open time.

Finally, the results are discussed in terms of mould growth and indoor roof relative humidity. First the internal ceiling surface relative humidity of the building zone at the ground level is discussed. According to previous analysis, this is the building surface with the highest amount of accumulated moisture. In this case, the relative humidity of the internal ceiling surface has been adopted as input control parameter for the hybrid ventilation technique.

Figure 7.7 shows the mould growth risk index for the whole year period when just natural ventilation is considered. As it can be seen in this figure, it is difficult to reduce mould growth just considering natural ventilation and the possibility of letting the window open during an extended time is not always possible due to outdoor conditions.

An alternative solution to this problem is the use of the hybrid ventilation techniques presented in this chapter. In Figure 7.8 the results for the mould growth index are presented when hybrid ventilation technique is used. As it can be verified, the hybrid ventilation technique presents considerable reduction on the mould growth index.

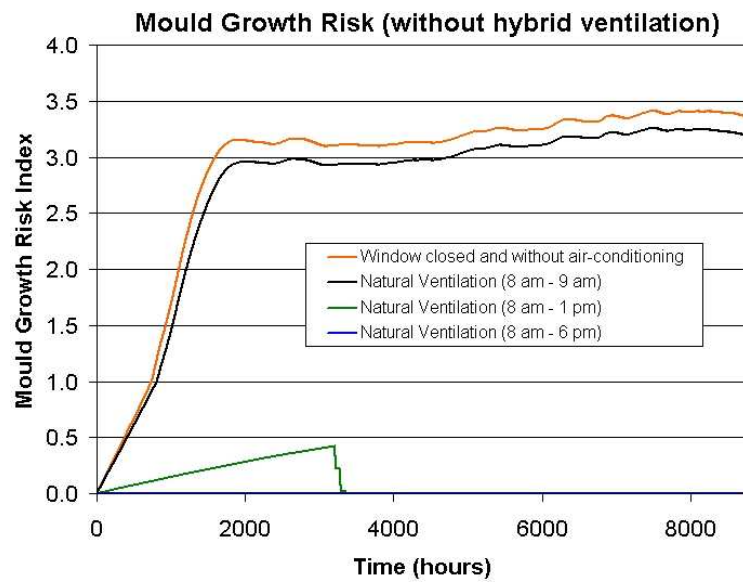


Figure 7.7: Mould growth risk when just natural ventilation is considered.

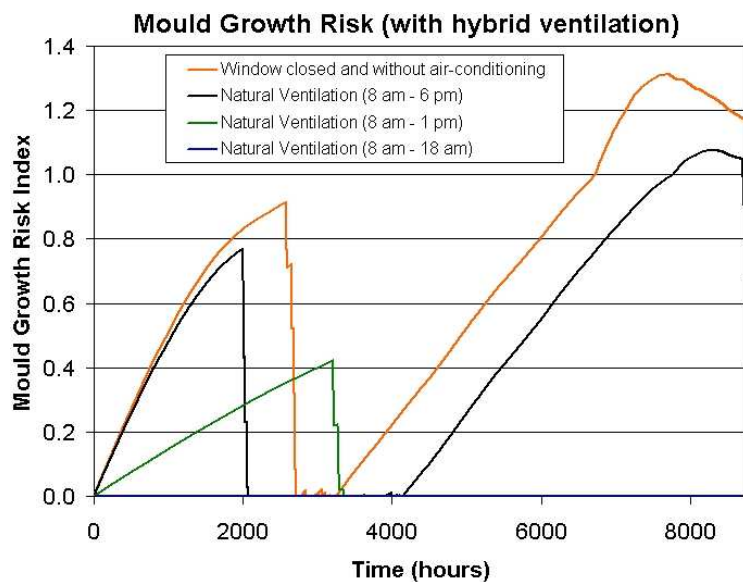


Figure 7.8: Mould growth risk when hybrid ventilation is considered.

Table 7.8: Monthly energy demand from January to June.

Case	Monthly Energy Demand (<i>kWh</i>)					
	July	August	September	October	November	December
Window closed	84.72	88.89	85.45	95.67	96.82	0.00
NV (8 <i>am</i> - 9 <i>am</i>)	82.11	86.28	83.88	95.36	96.30	0.00
NV (8 <i>am</i> - 1 <i>pm</i>)	47.99	50.81	51.54	60.51	69.90	0.00
NV (8 <i>am</i> - 6 <i>pm</i>)	21.39	14.08	19.51	33.80	54.15	0.00

Table 7.9: Annual energy demand.

Case	Annual (<i>kWh</i>)
Window closed	1030.27
NV (8 <i>am</i> - 9 <i>am</i>)	996.47
NV (8 <i>am</i> - 1 <i>pm</i>)	742.84
NV (8 <i>am</i> - 6 <i>pm</i>)	501.63
HVAC (8 <i>am</i> - 6 <i>pm</i>)	36166.55

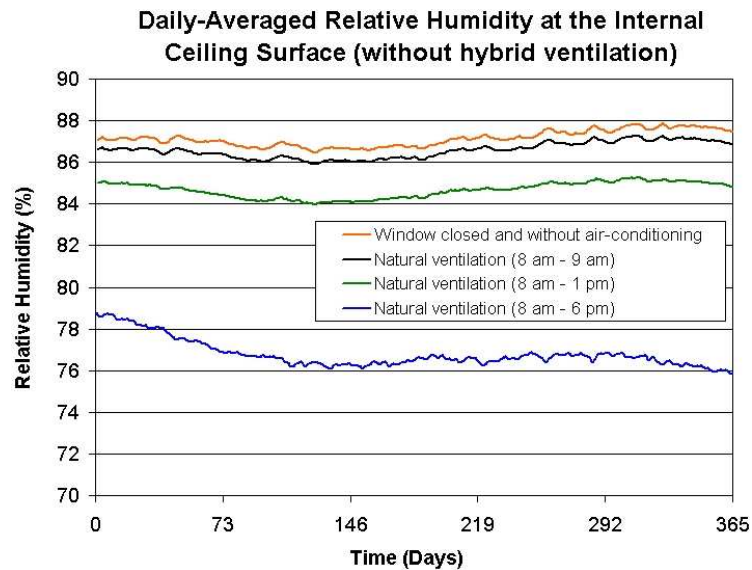


Figure 7.9: Daily-averaged values of relative humidity at the internal ceiling surface when just natural ventilation is considered.

A more detailed analysis can be made through the evaluation of the internal ceiling relative humidity. Figure 7.9 and 7.10 present the daily-averaged values of relative humidity at the internal ceiling surface obtained from simulations with and without considering PV hybrid ventilation.

Those figures show that the hybrid ventilation algorithm keeps the internal ceiling

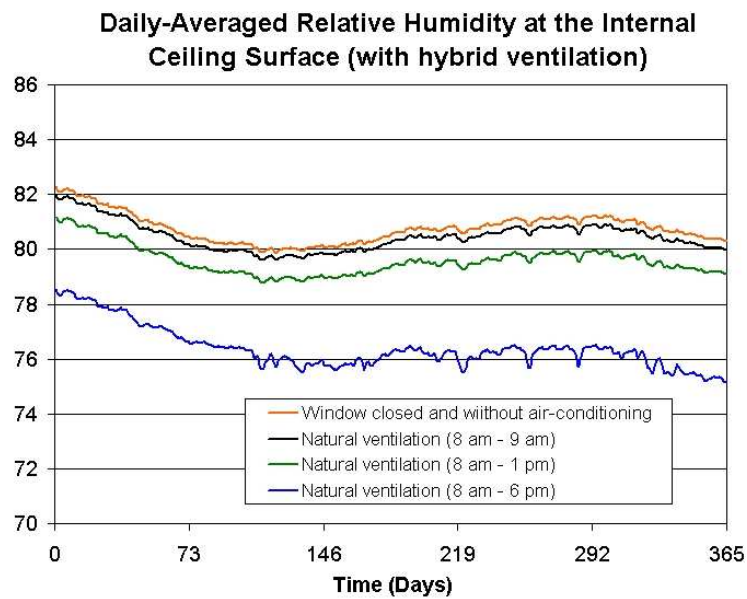


Figure 7.10: Daily-averaged values of relative humidity at the internal ceiling surface when hybrid ventilation is considered.

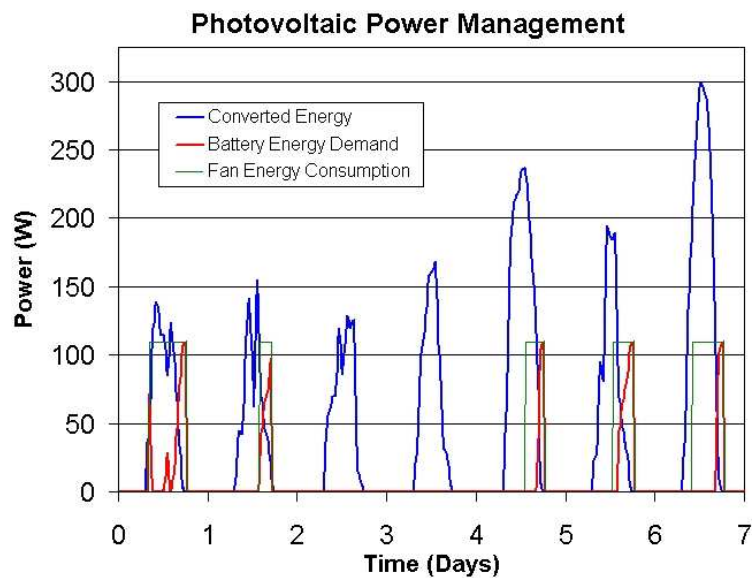


Figure 7.11: Simulation results for the first week of July (PV power management).

surface as dry as it can be by using the outdoor drier air when necessary. The indoor surface relative humidity decreases when the outdoor air humidity ratio is smaller than the indoor air humidity ratio.

Figure 7.11 shows how PowerDomus PV module provides the reports for the photovoltaic system, where the energy demand, energy converted and the energy used from the storage system for the first week of July period are presented. As it can be verified in

Figure 7.11, low energy conversion due to low solar radiation during the winter period has forced the battery energy consumption to supply the fan energy demand.

7.9 Chapter Remarks

This chapter 7 has shows the integration of the photovoltaic module and natural ventilation in a new hybrid ventilation strategy. The Brazilian context was considered in order to illustrate the national potential usage of hybrid BIPV ventilation. Standards for indoor air quality have been presented and the hybrid ventilation strategy was tested and compared to traditional air-cooling system and common natural ventilation cases.

In order to represent the results in a more detailed way, three parameter have been evaluated: thermal comfort, indoor surface relative humidity and ventilation standards. As it can be seen, results can be improved by using advanced ventilation techniques capable of providing better indoor air conditions to the occupants.

8 Final Remarks

This chapter presents the main contributions of this dissertation. Each chapter has been reviewed and their main aspects are presented in order to establish a synchronous presentation of the studied topics. Additional information about the work developed during the doctoral period is presented in Annex 3, where a publication list is shown.

8.1 General Overview

Chapter 1 introduced the problematic related to the excessive energy usage of HVAC systems. Studies using natural and mechanical ventilation were shown and an introduction to hybrid ventilation control was presented in order to illustrate its potential to reduce energy consumption of buildings. Additionally, the efforts of academic and industrial research around the world were presented, citing Brazilian government rules to include building energy efficiency in the agenda.

After describing the objectives of this work, natural ventilation physical principles and empirical models for cross and single-sided natural ventilation were presented in Chapter 2. Two methods developed for the pressure coefficient calculation have also been reported and the correlation between both cross and single-sided ventilation models and also a generic implementation method were shown.

Chapter 3 aimed at validating the implementation of natural ventilation models performed in a whole building and energy simulation software - PowerDomus. Results were compared to wind tunnel and on-site experiments and the precision of both Mean C_P and CPCALC pressure coefficient calculation methods were evaluated.

Chapter 4 showed how natural ventilation can be used to enhance indoor thermal comfort conditions and improve the indoor air quality of buildings. Simulations showed that, in some cases, it is possible to enhance thermal comfort to the same levels when compared to traditional cooling systems.

An introduction of photovoltaic modeling has been presented in chapter 5, where a widely adopted method to calculate the photovoltaic conversion of single crystal or polycrystalline technologies known as 'four-parameter model' has been presented. In this chapter, the implementation of a generic photovoltaic module into the PowerDomus software has been performed. This module consists of upgrading the PowerDomus CAD interface in order to show the PV system configuration and implement the mathematical description of the PV array coupled to the building materials. Here, the concept of BIPV (Building-Integrated Photovoltaic) systems was presented.

In chapter 6 comparisons between PowerDomus and another two photovoltaic simulation tools have been performed to validate the PV module implementation. Moreover, results for the whole building hygrothermal simulation have also been presented, and the influences of the PV systems on the building hygrothermal behavior were discussed.

Finally, chapter 7 was responsible to show the integration of the photovoltaic module and natural ventilation in a new hybrid ventilation strategy. The Brazilian context was considered in order to show the Brazilian Potential usage of a hybrid BIPV photovoltaic ventilation. Standards for indoor air quality were presented and the hybrid ventilation strategy was tested and compared to a traditional air-cooling system.

In the sequence, important considerations about the two main points (natural ventilation and building-integrated photovoltaic systems) discussed in this work are presented.

8.2 Natural Ventilation

As described in this work, it can be seen that natural ventilation modeling is widely discussed by academic and industrial researchers. Differently from cross-ventilation modeling, single-sided ventilation empirical models usually give an idea of the flow behavior, and could not exactly represent the flow rate through openings. The difference between models and experimental data can be justified by the turbulence of the wind and variations on the pressure gradients that strongly affect the airflow through an opening. Since those parameters are unsteady, the airflow for single-sided ventilation is much more difficult to be evaluated.

The results of cross and single-sided natural ventilation models can be improved by the pressure coefficient calculation method. However, even with specific pressure coefficient values considered for each opening, the results are considerably different from experimental results. Discussions about the measurements of the airflow through openings are found in

the literature. This point was not treated in this work, which is focused in the numerical approach of natural ventilation. However, it is important to emphasize the difficulties of experimental works to estimate the natural ventilation airflow, specially for single-sided ventilation cases.

The obtention of a new natural ventilation empirical model is a challenge for researchers and a need for building simulation software users. Due to the implementation of natural ventilation models into PowerDomus, the usability aspects of the software have been enhanced.

8.3 Building Integrated Photovoltaic systems

This work presented the initial development of a building-integrate photovoltaic module into the PowerDomus software. It was focused on the interactions between the PV array and the building structure, showing the influences on the hygrothermal effect differences of a building with and without an integrated PV system. Additionally, the development of a new zero-energy hybrid ventilation technique has been presented using the concepts of natural and mechanical ventilation. The mechanical ventilation energy supply has been performed by a photovoltaic system, and results have shown that it is possible to maintain acceptable indoor air quality and thermal comfort with no use of traditional air-conditioning systems.

During the development of the PowerDomus PV module, it has been noticed that many considerations should be made in order to simulate the PV system. This consideration refers to the losses of the entire system and a detailed study in order to evaluate more precise values for the losses should be made. In this way, standard values can be applied in the software to make it more user friendly.

It is also important to emphasize that the PV module can now be easily associated to the energy demand of PowerDomus central HVAC systems and other equipment of an specific building zone. This point was treated in this work showing the integration of a fan energy demand and the PV system, providing the hybrid ventilation strategy. The fan was configured on the PowerDomus HVAC central system module and automatically associated to the PV system energy demand.

8.4 Photovoltaic Hybrid Ventilation

Considering the photovoltaic hybrid ventilation system, some considerations about the strategy could be pointed out. As presented, the strategy is based on three main parameters: *i*) thermal comfort; *ii*) relative humidity at the internal building surfaces; and *iii*) standard airflows. In order to control the fan power supply, the way how the input parameters should be obtained in a practical implementation of this controller were not defined. The acquisition of these parameters is a challenge in terms of cost and precision.

Additionally, some considerations can be made in terms of usage aspects of PV hybrid ventilation. In this work, the case study presented in Chapter 7 showed the use of PV hybrid ventilation strategy during the occupation period in a typical Brazilian office building. However, to enhance the hybrid ventilation effects in the occupants's thermal comfort sensation, some additional strategies, *e.g.*, night ventilation, could be adopted to provide better thermal conditions. Considerations about the fan noise generation has not been addressed here, and more a detailed study about this effect should be performed.

8.5 Further Works

In this section, we suggest some additional work on the topics treated in this dissertation:

- Considering that the predictions of natural ventilation models still present a high difference, the development of a more accurate empirical model are still needed and suggested to evaluate the air change rate by cross and single-sided natural ventilation.
- The next step on airflow modeling into PowerDomus program can be the integration of a multizone airflow model. Here it can be suggested the COMIS algorithm, developed in the Lawrence Berkeley Laboratory (Feustel and Rayner-Hooson, 1990; Feustel, 1998);
- The development of an advanced control strategy capable of minimizing the errors of the PV hybrid ventilation strategy, should be considered. The three parameters: thermal comfort, relative humidity at the internal building surfaces and standard airflows rates can be used to define control laws using the same priority level, *e.g.*, through the implementation of model-based predictive controllers (MBPC);

-
- In this work, photovoltaic conversion of single crystal or polycrystalline technologies were presented. It is clear that other types of PV structures are available and additional models could be implemented into the software, e.g. amorphous silicon photovoltaic panels. Following this way, it is important to enhance the software equipment database as new products are in constant development;
 - The next step in the PowerDomus photovoltaic module development is the study of detailed battery models and a way to facilitate the system configuration through the addition of a PV presizing system scheme. As most of the PowerDomus users are interested in the building hygrothermal influences performed by the PV array integration, the idea is to follow the user friendly interface and provide an PV auto-sizing model according to the energy demand associated to the PV system;
 - In this work the usage potential BIPV technology in Brazil was presented. However, the study performed in this work is just based of geographical physical variables, not taking into account the costs. In this way, an evaluation of the available technology found in Brazil and a detailed cost analysis is important to be carried out.

References

- ABNT (2008). *Instalações de ar condicionado - Sistemas centrais e unitários - Parte 3: Qualidade do Ar Interior*. Associação Brasileira de Normas Técnicas.
- ANSI/ASHRAE (2004). *ANSI/ASHRAE Standard 55-2004 - Thermal Environmental Conditions for Human Occupancy*. American Society of Heating, Refrigerating and Air Conditioning Engineers. Atlanta, GA.
- ASHRAE (2005a). *Handbook of Fundamentals; Chap. 16 - Airflow Around Buildings*. American Society of Heating, Refrigerating and Air Conditioning Engineers. Atlanta, GA.
- ASHRAE (2005b). *Handbook of Fundamentals; Chap. 27 - Ventilation and Infiltration*. American Society of Heating, Refrigerating and Air Conditioning Engineers. Atlanta, GA.
- ASHRAE (2005c). *Handbook of Fundamentals; Chap. 27 - Ventilation and Infiltration*. American Society of Heating, Refrigerating and Air Conditioning Engineers. Atlanta, GA.
- ASHRAE (2005d). *Handbook of Fundamentals; Chap. 8 - Physiological Principles and Thermal Comfort*. American Society of Heating, Refrigerating and Air Conditioning Engineers. Atlanta, GA.
- Barbosa, R. M. and N. Mendes (2003). Dynamic simulation of fan-coil systems. In: *17th International Congress of Mechanical Engineering (COBEM'2003)*. São Paulo, Brazil.
- Barbosa, R. M. and N. Mendes (2008). Combined simulation of central HVAC systems with a whole-building hygrothermal model. *Energy and Buildings* (40), 276–288.
- Bourdouxhe, J. P. and P. André (1997). Simulation of a centralized cooling plant under different control strategies. In: *Proc. of the Second Building Simulation Conference (IBPSA '97)*. Vol. 1. Eindhoven, Netherlands. pp. 95–102.
- BP SOLAR (2007). BP 350 high-efficiency photovoltaic module using silicon nitride multicrystalline silicon cells. Technical report. BP. [<http://www.bp.com>], accessed in January, 2010.
- Brandemuehl, M. J., S. Gabel and I. Andresen (1993). Hvac2 toolkit: A toolkit for secondary hvac system energy calculation. Technical report. American Society of Heating, Refrigerating and Air Conditioning Engineers (ASHRAE). Atlanta, GA, USA.

- BRASIL (2001). Lei n. 10295, de 17 de outubro de 2001. Dispõe sobre a Política Nacional de Conservação e Uso Racional de Energia. Lex: Diário Oficial da União. Technical report. Governo Federal. Brasília.
- British Standards (1999). *Code of Practice for Design of Buildings: Ventilation Principles and Designing for Natural Ventilation*. 1 ed.. British Standards Institution. BS5925.
- CBEE (1998). Wind Power Potential in Brazil. Technical report. CBEE - Brazilian Wind Energy Center. [<http://www.eolica.com.br>], accessed in April, 2008.
- CETC, CANMET Energy Technology Centre (2004). *Clean Energy Project Analysis: RETScreen® Engineering & Cases Textbook - Photovoltaic Project Analysis*. Minister of Natural Resources Canada. Varennes, Canada.
- Chel, A., G. N. Tiwari and A. Chandra (2009). Simplified method of sizing and life cycle cost assessment of building integrated photovoltaic system. *Energy and Buildings* (41), 1172–1180.
- Cheng, C. L., C. S. S. Jimenez and M. Lee (2009). Research of bipv optimal tilted angle, use of latitude concept for south orientated plans. *Renewable Energy* (34), 1644–1650.
- Cherem-Pereira, G. C. (2003). Modelagem de condicionadores de ar residenciais. Master's thesis. Pontifícia Universidade Católica do Paraná - Programa de Pós-Graduação em Engenharia Mecânica.
- Cherem-Pereira, G. C. and N. Mendes (2003). Room air conditioners: Determination of empirical cor-relations for predicting building energy consumption. In: *Proc. of the Eighth Building Simulation Conference (IBPSA '03)*. Vol. 1. Eindhoven, Netherlands. pp. 1–8.
- Chow, T. T. (2010). A review on photovoltaic/thermal hybrid solar technology. *Applied Energy* **87**, 365–379.
- Chow, T. T., J. A. Clarke and A. Dunn (1997). Primitive parts: an approach to air-conditioning component modeling. *Energy and Buildings* (26), 165–173.
- Clarke, J. A. (1999). A technique for the prediction of the conditions leading to mould growth in buildings. *Building and Environment* (34), 515–521.
- Corbin, C. D. and Z. J. Zhai (2010). Experimental and numerical investigation on thermal and electrical performance of a building integrated photovoltaic-thermal collector system. *Energy and Buildings* (42), 76–82.
- Corrêa, J. M. (n.d.). Dynamic analysis of Combined Whole Building and HVAC Systems (In portuguese). PhD thesis. Universidade Federal de Santa Catarina. Florianópolis, Brazil.
- Counihan, J. (1975). Adiabatic atmospheric boundary layer: A review and analysis of data from the period 1880-1972. *Atmospheric Environment* **9**(10), 871–905.
- CSTB (1988). Practical guidance to meeting the requirements of the thermal and ventilation regulations for residential buildings. Technical Report 2286. Centre Scientifique et Technique du Bâtiment. Exemples de solutions pour faciliter l'application du règlement relatif aux equipments et aux caracteristiques.

- Cui, J., T. Watanabe, Y. Ryu, Y. Akashi and N. Nishiyama (1999). Numerical simulation on simultaneous control process of indoor air temperature and humidity. In: *Proc. of the Sixth Building Simulation Conference (IBPSA '99)*. Vol. 2. Kyoto, Japan. pp. 1005–1012.
- Dascalaki, E., M. Santamouris, M. Bruant, C. A. Balaras, A. Bossaer, D. Ducarme and P. Wouters (1999). Modeling large openings with comis. *Energy and Buildings* **30**, 105–115.
- de Gids, W. and H. Phaff (1982). Ventilation rates and energy consumption due to open windows. a brief overview of research in the netherlands. In: *Proc. of the Third IEA Air Infiltration Center Conference*. Vol. 1. pp. 4–5.
- de Gids, W. F. (2007). Source book for residential hybrid ventilation development - contributed report 9. Technical report. Air Infiltration and Ventilation Centre - IEA Energy Conservation in Building & Community Systems Programme. Brussels, Belgium.
- der Aa, A. Van and P. O. 't Veld (2004). Reshyvent - a eu cluster project on demand controlled hybrid ventilation for residential buildings. Technical report. RESHYVENT Project.
- Deru, M. and P. Burns (2003). Infiltration and natural ventilation model for whole-building energy simulation of residential buildings. Technical Report NREL/CP-550-33698. National Renewable Energy Laboratory (NREL). Golden, Colorado, USA.
- Doerffel, D. and S. Abu Sharkh (2006). A critical review of using the peukert equation for determining the remaining capacity of lead-acid and lithium-ion batteries. *Journal of Power Sources* (155), 395–400.
- Duffie, J. A. and W. A. Beckman (1991). *Solar Engineering of Thermal Processes*. John Wiley Son, Inc.. New York.
- Eckstein, J. H. (1990). Detailed modeling of photovoltaic components. Master's thesis. Solar Energy Laboratory, University of Wisconsin. Madison.
- EIA (2004). Energy Information Administration. www.eia.doe.gov.
- Eiffert, P. and A. Thompson (2000). U.S. guidelines for the economic analysis of building-integrated photovoltaic power systems. Technical report. National Renewable Energy Laboratory (NREL). Golden, Colorado, USA.
- Emmel, M. G., M. O. Abadie and N. Mendes (2007). New external convective heat transfer coefficient correlations for isolated low-rise buildings. *Energy and Buildings* (39), 335–342.
- EPE (2009). Brazilian energy balance - 2009. Technical report. Empresa de Pesquisa Energética and Ministério de Minas e Energia - MME.
- Evans, D. L. (1981). Simplified method for predicting photovoltaic array output. *Solar Energy* **27**(6), 555–560.

- Fang, L., G. Clausen and P. O. Fanger (1998). Impact of temperature and humidity on the perception of indoor air quality. *Indoor Air* (8), 80–90.
- Fanger, P. O. (1970). *Thermal Comfort Analysis and Applications in Environmental Engineering*. McGraw-Hill Inc.. New York, USA.
- Fanger, P. O. (1982). *Thermal Comfort*. Robert E. Krieger. Malabar, FL.
- Feustel, H. E. (1998). Comis - an international multizone air-flow and contaminant transport model. Technical Report LBL-42182. Applied Science Division - Lawrence Berkeley National Laboratory. Berkeley, California, USA.
- Feustel, H. E. and A. Rayner-Hooson (1990). Comis fundamentals, technical report. Technical Report LBL-28560. Applied Science Division - Lawrence Berkeley National Laboratory. Berkeley, California, USA.
- Fordham, M. (2000). Natural ventilation. *Renewable Energy* (19), 17–37.
- Fossa, M., C. Ménézo and E. Leonardi (2008). Experimental natural convection on vertical surfaces for building integrated photovoltaic (bipv) applications. *Experimental Thermal and Fluid Science* (32), 980–990.
- Friling, N., M. J. Jiménez, H. Bloem and H. Madsen (2009). Modelling the heat dynamics of building integrated and ventilated photovoltaic modules. *Energy and Buildings* (41), 1051–1057.
- Fung, T. Y. Y. and H. Yang (2008). Study on thermal performance of semi-transparent building-integrated photovoltaic glazings. *Energy and Buildings* (40), 341–350.
- Ghiaus, C., A. Chicinas and C. Inard (2007). Grey-box identification of air-handling unit elements. *Control Engineering Practice* (15), 421–433.
- Griffith, B.T. and P.G. Ellis (2004). Photovoltaic and solar thermal modeling with the EnergyPlus calculation engine. Technical report. National Renewable Energy Laboratory. Denver, Colorado.
- Grosso, M. (1992). Wind pressure distribution around buildings - a parametrical model. *Energy and Building*.
- Grosso, M. (1993). Modelling wind pressure distribution on buildings for passive cooling. In: *Proceedings of the International Conference Solar Energy in Architecture and Urban Planning - Commission of the European Communities* (Florence, Ed.). pp. 17–21.
- Grosso, M., D. Mariano and E. Parisi (1994). Wind pressure distribution on flat and tilted roofs: a parametrical model. In: *Proceedings of the European Conference on Energy Performance and Indoor Climate in Buildings*. Lyon - France. pp. 24–26.
- Guiavarch, A. and B. Peuportier (2006). Photovoltaic collectors efficiency according to their integration in buildings. *Solar Energy* (80), 65–77.
- Haines, R. W. and C. L. Wilson (2004). *HVAC Systems Design Handbook*. McGraw-Hill Companies.

- Hens, H. (2003). Proposal for a new annex. whole building heat, air and moisture response (moist-eng). Technical report. Belgium.
- Hensen, J. L. M. (1991). On the thermal interaction of building structure and heating and ventilating system. PhD thesis. Eindhoven University of Technology.
- Holm, A., H. Künzle and J. Radon (2002). Uncertainty approaches for hygrothermal building simulations - drying of aac in hot and humid climates.. In: *Buildings VIII Conference*.
- Hukka, A. and A. Viitanen (1999). A mathematical model of mould growth on wooden material. *Wood Science and Technology* (33), 475–485.
- IBGE (2000). Brazilian Institute of Geography and Statistics. Technical report. IBGE - Geosciences Management, Geography Department. <http://www.ibge.gov.br>.
- IEA (1991). International Energy Agency - Annex 14: Condensation and Energy - Sourcebook. Technical report.
- IEA (1996). International Energy Agency - Annex 23: Multizone Airflow Modelling - Evaluation of COMIS Appendices. Technical report. Swiss Federal Institute of Technology - Lausanne, LESO.PB, Institute of Building Technology, Torino - Italy.
- IEA (1998). World energy outlook. Technical report. International Energy Agency. Paris.
- IEA (2002). IEA Energy Conservation in Buildings and Community Systems Programme - Annex 35: Hybrid ventilation in New and Retrofitted Office Buildings. Edited by Per Heiselberg. Technical report. Aalborg, Denmark.
- ISE (2008). PVSYST 5.06 - software for photovoltaic systems. [<http://www.pvsyst.com>], accessed in March, 2008.
- Jiang, Y., D. Alexander, H. Jenkins and ad R. A. Q. Chen (2003). Natural ventilation in buildings: Measurement in a wind tunnel and numerical simulation with large-eddy simulation. *Journal of Wind Engineering and Industrial Aerodynamics* **91**, 331–353.
- Jreijiry, D., A. Husaunndee and C. Inard (2007). Numerical study of a hybrid ventilation system for single family houses. *Solar Energy* **81**, 227–239.
- Judkoff, R. D. and J. S. Neymark (1995). *Building Energy Simulation Test (BESTEST) and Diagnostic Method*. Colorado National Renewable Energy Laboratory. NREL/TP-472-6231.
- Karlsson, J. F. and B. Moshfegh (2006). Energy demand and indoor climate in a low energy building - changed controle strategies and boundary conditions. *Energy and Buildings* (38), 315 – 326.
- Khedari, J., J. Waewsak, W. Supheng and J. Hirunlabh (2004). Experimental investigation of performance of a multi-purpose pv-slat window. *Solar Energy Materials & Solar Cells* (82), 431–445.
- King, D. L., J. A. Kratochvil and W. E. Boyson (1997). Measuring the solar spectral and angle-of-incidence effects on photovoltaic modules and irradiance sensors. In: *Proceedings of the 1994 IEEE Photovoltaics Specialists Conference*. pp. 1113–1116.

- Knabe, G. and H. Le (2003). Building simulation by application of a hvac system considering the thermal and moisture behaviors of the perimeter walls. In: *Proc. of the Seventh Building Simulation Conference (IBPSA '01)*. Rio de Janeiro, Brazil. pp. 965–972.
- Lai, C.M. (2006). Prototype development of the rooftop turbine ventilator powered by hybrid wind and photovoltaic energy. *Energy and Buildings* (38), 174–180.
- Lam, J. C., S. C. M. Hui and A. L. S. Chan (1997). Regression analysis of high-rise fully air-conditioned office buildings. *Energy and Buildings* (26), 189–197.
- Lamberts, R., L. Dutra and F. O. R. Pereira (2004). *Eficiência Energética na Arquitetura*. PW.
- Larsen, S. F., C. Filippín and G. Lesino (2003). Earth-to-air heat exchange through a buried pipe at a school in La Pampa (Argentina). In: *Proc. of the 20th Conference on passive and low energy architecture (PLEA 2003)*. Santiago, Chile. pp. 893–898.
- Larsen, T. S. (2006). Natural Ventilation Driven by Wind and Temperature Difference. PhD thesis. Aalborg University. Aalborg, Denmark.
- Larsen, T. S. and P. Heiselberg (2008). Single-sided natural ventilation driven by wind pressure and temperature difference. *Energy and Buildings* (40), 1031–1040.
- Liddament, M. W. (1986). Air Infiltration Calculation Techniques - an Applications Guide. Technical report. Air Infiltration and Ventilation Centre. Bracknell, U.K.
- Limb, M. J. (2001). A review of international ventilation, airtightness, thermal insulation and indoor air quality criteria. AIVC standads report. International Energy Agency - IEA: Air Infiltration and Ventilation Centre - AIVC.
- Mendes, N. and P. C. Philippi (2004). Multitridiagonal-matrix algorithm for coupled heat transfer in porous media: Stability analysis and computational performance. *Journal of Porous Media* 7(3), 193–211.
- Mendes, N., G. H. C. Oliveira, H. X. Araújo and L. S. Coelho (2003). A MATLAB-based simulation tool for building thermal performance analysis. In: *Proc. of the Eighth Building Simulation Conference (IBPSA '03)*. Vol. 1. Eindhoven, Netherlands. pp. 855–862.
- Mendes, N., P.C. Philippi and R. Lamberts (2002). A new mathematical method to solve highly-coupled equations of heat and mass transfer in porous media. *International Journal of Heat and Mass Transfer* 45(3), 509–518.
- Millet, J. R. (2001). Ventilation in the new french thermal regulation rt 2000. In: *AIVC 22nd Conference*. IEA - International Energy Agency: AIVC - Air Infiltration and Ventilation Centre. Brussels, Belgium.
- Ministério de Minas e Energia (2009a). Etiquetagem de eficiência energética de edificações. Technical Report 1. Eletrobrás - Procel; Equipe do Procel Edifica; Laboratório de Eficiência Energética em Edificações - LabEEE - UFSC. Brasília.

- Ministério de Minas e Energia (2009b). RTQ-C regulamento técnico da qualidade do nível de eficiência energética de edifícios comerciais, de serviços e públicos. Technical Report 2. Eletrobrás - Procel; Equipe do Procel Edifica; Laboratório de Eficiência Energética em Edificações - LabEEE - UFSC. Brasília.
- MK Battery (2009). The sealed battery specialists: Gel batteries - LIT GEL 102. Technical report. MK Battery. [<http://www.mkbattery.com/>], accessed in December, 2009.
- Nassif, N., S. Kajl and R. Sabourin (2003). Modélisation des composants d'un système cvca exis-tant. In: *VI Colloque Interuniversitaire Franco-Québécois, Thermique des systèmes*. Québec, Canada.
- Niachou, K., S. Hassid, M. Santamouris and I. Livada (2008). Experimental performance investigation of natural, mechanical and hybrid ventilation in urban environment. *Building and Environment* **8**(43), 1373–1382.
- Norton, B., P. C. Eames, T. K. Mallick, M. J. Huang, S. J. McCormack, J. D. Mondol and Y. G. Yohanis (2010). (article in press) enhancing the performance of building integrated photovoltaics. *Solar Energy*.
- Novak, P. R., N. Mendes and G. H. C. Oliveira (2004). Simulation and analysis of a secondary hvac system using matlab/simulink platform. In: *International Mechanical Engineering Congress*. USA.
- NRCC (1983). Measures for energy conservation in new buildings. Technical Report 22432. Associate Committee on the National Code - National Research Council of Canada. Ottawa.
- Ordenes, M., L. Marinoski, P. Braun and R. Rüther (2007). The impact of building-integrated photovoltaics on the energy demand of multi-family dwellings in brazil. *Energy and Buildings* (39), 629–642.
- Orme, M. (2001). Estimates of the energy impact of ventilation and associated financial expenditures. *Energy and Buildings* (33), 199–205.
- Pacific Gas and Electric (1996). Proceedings from the PG&E energy center DOE-2 lunch series: Chiller plant performance curves. Technical report. Pacific Gas and Electric. San Francisco, CA, USA.
- Painuly, J. P. (2001). Barriers to renewable energy penetration; a framework for analysis. *Renewable Energy* (24), 73–89.
- Papakonstantinou, K. A., C. T. Kiranoudis and N. C. Markatos (2000). Numerical simulation of airflow field in singlesided ventilated buildings. *Energy and Buildings*.
- Philip, J. R. and D. A. De Vries (1957). Moisture movement in porous material under temperature gradients. *Transactions of the American Geophysical Union* **38**(2), 222–232.
- Qiu, Z., T. Chow, P. Li, C. Li, J. Ren and W. Wang (2009). Performance evaluation of the photovoltaic double-skin facade. In: *Proc. of the 11th International IBPSA Conference (BS'2009)*. Glasgow, Scotland. pp. 2251–2257.

- Rode, C., A. Holm and T. Padfield (2004). A review of humidity buffering in the interior spaces. *Journal of Thermal Envelope and Building Science* **27**, 221–226.
- Rohles, F. H. Jr. (1973). The revised modal comfort envelop. *ASHRAE Transactions* **2**(79), 52.
- Román, E., V. Martinez, J. C. Jimeno, R. Alonso, P. Iban ez and S. Elorduizapatarietxe (2008). Experimental results of controlled pv module for building integrated pv systems. *Solar Energy* (82), 471–480.
- Salsbury, T. (2005). A survey of control technologies in the building automation industry. In: *Proc. of the 16th IFAC World Congress*. Prague, Czech Republic. pp. 331–341.
- Santos, G. H. and N. Mendes (2009). Heat, air and moisture transfer through hollow porous blocks. *International Journal of Heat and Mass Transfer* **52**, 2390–2398.
- Schipper, L. and S. Meyers (1992). *Energy Efficiency and Human Activity*. Cambridge University Press.
- Sharaf, A. M., M. M. AboulNaga and R. El Diasty (2000). Building-integrated solar photovoltaic systems - a hybrid solar cooled ventilation technique for hot climate applications. *Renewable Energy*.
- Silva, F. D. L. and P. O. Beyer (2008). Análise de uma simulação computacional de um ambiente climatizado alimentado pela rede elétrica convencional e por painéis solares fotovoltaicos. In: *Proc. of the Congresso de Ar Condicionado, Refrigeração, Aquecimento e Ventilação do Mercosul (MERCOFRIO'08)*.
- Simonson, C., M. Salonvaara and T. Ojanen (2002). The effect of structures on indoor humidity - possibilities to improve comfort and perceived air quality. *Indoor Air* (12), 243–251.
- Solar Energy Laboratory (2007). TRNSYS 16: a TRaNsient SYstem Simulation program - Mathematical Reference. Technical Report Volume 5. Solar Energy Laboratory, University of Wisconsin. Madison.
- Standard UNI (1995). Air-conditioning systems for thermal comfort in buildings. Technical Report 10339. UNI - Ente Nazionale Italiano di Unificazione. Milan, Italy.
- Sundell, J. (2007). The indoor environment in homes and health - what we have learnt, if any?. In: *Proc. of the Sixth International Conference on Indoor Air Quality Ventilation & Energy Conservation in Buildings*. Sendai, Japan.
- Swami, M. V. and S. Chandra (1988). Correlations for pressure distribution of buildings and calculation of natural-ventilation airflow. *ASHRAE Transactions* **4**(94), 244–266.
- Townsend, T. U. (1989). A method for estimating the long-term performance of direct-coupled photovoltaic systems. Master's thesis. Solar Energy Laboratory, University of Wisconsin. Madison.
- US Department of Energy (2006). Information resources - EnergyPlus energy simulation software. Technical report. Building Technologies Program from the US Department of Energy. [<http://apps1.eere.energy.gov/buildings/energyplus/>], accessed in December, 2006.

- Van der Aa, A. and P. Op 't Veld (2004). RESHYVENT - A EU cluster project on demand controlled hybrid ventilation for residential buildings. Technical report. RESHYVENT Project.
- Ventilnorte (2009). Ventiladores centrífugos de baixa pressão: Série at - transmissão por correia. Technical report. Ventilnorte. [http://www.ventilnorte.com/ventiladores_at_dd/ventiladores_at_dd.htm], accessed in July, 2009.
- Walton, G. N. (1982). Airflow and multiroom thermal analysis. *ASHRAE Transactions* **88**(2), 78–91.
- Wang, Y., W. Tian, J. Ren, L. Zhu and Q. Wang (2006). Influence of a building's integrated-photovoltaics on heating and cooling loads. *Applied Energy* (83), 989–1003.
- Wang, Y. W., W. J. Cai, Y. C. Soh, S. J. Li, L. Lu and L. Xie (2004). A simplified modeling of cooling coils for control and optimization of HVAC systems. *Energy Conversion and Man-agement* (45(18-19)), 2915–2930.
- Wouters, P., N. Heijmans, C. Delmotte and L. Vandaele (1999). Classification of hybrid ventilation concepts. In: *Proc. of the First International One day Forum on Natural and Hybrid Ventilation*. Sydney, Australia. pp. 2–23.
- Yun, G. Y., M. McEvoy and K. Steemers (2007). Design and overall energy performance of a ventilated photovoltaic façade. *Solar Energy* (81), 383–394.
- Zuo, W. and Q. Chen (2009). High-performance and low-cost computing for indoor airflow. In: *Proc. of Eleventh International IBPSA Conference*. pp. 244–249.

Annex 1: CPCALC Validation

This Annex presents a technical report of the Thermal Systems Laboratory, of the Pontifical Catholic University of Paraná, which had been developed in 2007 by professor Marc O. Abadie, from the University of La Rochelle, Laboratoire d'Étude des Phénomènes de Transfert et de l'Instantanéité, La Rochelle - France.

In this document a detailed explanation of the CPCALC algorithm is presented. Additionally, validation results are also reported.

CALCULATION OF VERTICAL WALL PRESSURE COEFFICIENT

Marc O. Abadie (August, 28th 2007)

1. Definitions

Most of the definitions, figures and tables presented in this section are directly extracted CPCALC+ final report (Grosso, 1995a).

1.1. CPCALC+

CPCALC+ is a program for calculating wind pressure coefficients on the envelope of a building for airflow modelling, developed within the European Research Programme PASCOOL (Passive Cooling of Buildings) of the Commission of the European Communities, Directorate General for Energy (Grosso, 1993, Grosso, Marino, Parisi, 1994). It has been developed at the Lawrence Berkeley Laboratory within the COMIS workshop on infiltration and ventilation (Feustel, 1990 and Grosso, 1992), and being upgraded within the IEA-ANNEX 23 on multizone airflow modeling. A modular framework allows for upgrading CPCALC by adding subroutines related to new application configurations. CPCALC+ includes new subroutines dealing with roofs as well as a WINDOWS Visual Basic User Interface.

CPCALC, and CPCALC+, were developed in order to fulfill the requirements of multizone airflow models which need a detailed evaluation of the wind pressure distribution around buildings. Scientists and professionals using this program, and who do not have the possibility to test a scale model of their building in a wind tunnel, do not need to extrapolate Cp data from tables usually yielding wall-averaged Cp values (Liddament, 1986).

1.2. Integration into PowerDomus

The motivation for calculating the pressure coefficients in PowerDomus comes from the Single Sided Ventilation model, developed by Larsen (2006) and integrated by Roberto Z. Freire in PowerDomus, that needs Cp values as input. Moreover, potential future PowerDomus developments may require this calculation, in the case of the implementation of an airflow network model to calculate the airflow between rooms for example.

As being developed for Natural Ventilation across vertical windows, the present work focuses on vertical walls only considering both windward and leeward façades. As a consequence, CPCALC+ parts regarding the (titled) roof are not included here. The program has been written in C++.

1.3. Input

- **Wind direction [wind_dir]:** see Figure 1
 - 0° for wind coming from North,
 - +90° for wind coming from East,
 - +180° for wind coming from South, and
 - +270° for wind coming from West.
- **Wind velocity profile exponent [a]:** see table 1.
- **Surrounding Building Height [sbh]:** averaged height of surrounding buildings (m).
- **Plan Area Density [pad]:** in %

The Plan Area Density is a parameter related to the layout pattern of the buildings surrounding the building under examination. Wind tunnel test data show that the radius of the built area surrounding the building, and affecting the wind pressure distribution on its envelope, is inversely proportional to the plan area density. The pad has to be evaluated within a radius ranging from 10 to 25 times the height of the considered building.

- **Building dimensions: Height [H]** in m
- **Wall azimuth [wall_azim]:** see Figure 2

- 0° for wall facing North,
 - $+90^\circ$ for wall facing East,
 - $+180^\circ$ for wall facing South, and
 - $+270^\circ$ for wall facing West.
- **Location of CP calculation:** see Figure 2
- The origin of (0, x, z) is taken as the point located at the lower left corner of the wall looking at this wall (wall normal coming to us).
- **Point horizontal coordinate [x]** in m
 - **Point vertical coordinate [h]** in m
 - **Length of the considered facade [L1]** in m
 - **Length of the facade adjacent to the considered facade [L2]** in m

1.4. Intermediate variables

- **Relative Building's Height [rbh]**

The relative building height is the ratio of the building's height to the averaged height of surrounding buildings.
- **Frontal Aspect Ratio [far]**

The frontal aspect ratio is the ratio of the length of the considered facade to its height.
- **Side Aspect Ratio [sar]**

The side aspect ratio is the ratio of the length of the facade adjacent to the considered one, to the facade's height.
- **Point dimensionless horizontal coordinate [xl]**

The point dimensionless horizontal coordinate is the ratio of the point horizontal coordinate to the facade's horizontal dimension.
- **Point dimensionless vertical coordinate [zh]**

The point dimensionless vertical coordinate is the ratio of the point vertical coordinate to the facade's vertical (=height) dimension.
- **Wind-to-wall angle [anw]**

The wind-to-wall angle is defined as the difference between the wind direction and the wall azimuth.

1.5. Pressure coefficients

- **Pressure coefficient reference value [z1]**
- **Correction coefficient for the Boundary Layer [z2]**
- **Correction coefficient for the Surrounding Area Density [z3]**
- **Correction coefficient for the Relative Height [z4]**
- **Correction coefficients for the Frontal Aspect Ratio [z5]**
- **Correction coefficients for the Side Aspect Ratio [z6]**
- **Correction coefficient for the Horizontal Distribution in relation to the wind angle [z7]**
- **Pressure coefficient at (xl, zh) [Cp]**

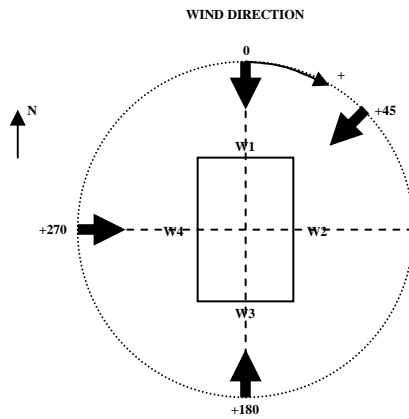


Figure 1: Wind direction.

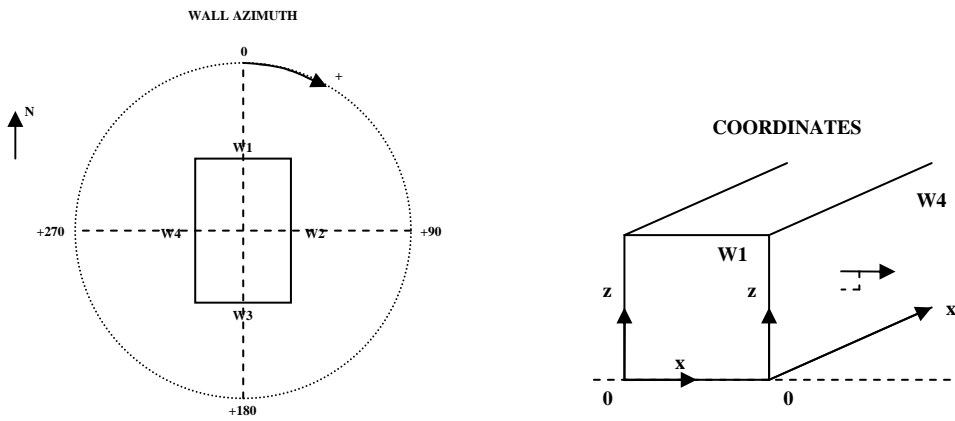


Figure 2: Wall azimuth and Point horizontal (x) and vertical (z) coordinates.

Table 1: Reference Values for the Wind Velocity Profile Exponent (alpha).

Terrain Roughness Type	alpha
Level surfaces, surfaces of water basins, grass land	0.10
Flat open country with few, very small, and scattered obstructions	0.14
Rolling or level surfaces broken by numerous obstructions such as trees or small houses	0.22
Heterogeneous surface with obstacles larger than one story	0.28
Low density suburban areas	0.34
Medium-high density urban areas	0.40
Very high density inner city areas	0.45

1.6. Limitations

The program CPCALC+ applies to rectangular-plan buildings with boundary conditions comprised in given variation ranges related to the Cp data on which the parametrical analysis was based. For each parameter, or for a combination of parameters, two levels of variation range are foreseen: the larger one is the maximum range outside of which the calculation can not be executed; the stricter one is the confidence range, outside of which results are given but the accuracy is not assured.

Table 2 shows the two-level variation range for the various parameters. However, no absolute values of Cp greater than 1 should be accepted, except for very high simultaneous values of the parameters PAD, FAR and SAR when the absolute Cp can reach values of 1.2-1.3.

Table 2: Application Range of CPCALC+ - Vertical Walls.

Parameter	Confidence Range		Maximum Range	
	Constant	Independent Variable	Constant	Independent Variable
a	$0.1 \leq zh \leq 0.9$	$0.10 \leq VeEXP \leq 0.33$	$0.0 \leq zh \leq 1.0$	$0.10 \leq VeEXP \leq 0.45$
pad	$0.07 \leq zh \leq 0.93$	$0.0 \leq PAD \leq 50.0$	$0.0 \leq zh \leq 1.0$	$0.0 \leq PAD \leq 50.0$
rbh	$0.07 \leq zh \leq 0.93$ $0.0 \leq PAD \leq 25$ (*)	$0.5 \leq RbH \leq 4.0$	$0.0 \leq zh \leq 1.0$ $0.0 \leq PAD \leq 25$ (*)	$RbH \geq 0.0$
far	$0.07 \leq zh \leq 0.93$ $0.0 \leq PAD \leq 12.5$ (*)	$0.5 \leq FAR \leq 4.0$	$0.0 \leq zh \leq 1.0$ $0.0 \leq PAD \leq 12.5$ (*)	$FAR \geq 0.0$ (#)
sar	$0.07 \leq zh \leq 0.93$ $0.0 \leq PAD \leq 12.5$ (*)	$0.5 \leq SAR \leq 2.0$	$0.0 \leq zh \leq 1.0$ $0.0 \leq PAD \leq 12.5$ (*)	$SAR \geq 0.0$ (#)

(*) If $RbH=1$ or $FAR=1$ or $SAR=1 \rightarrow 0.0 \leq PAD \leq 50.0$

(#) Varying in relation to specific combination of values for FAR, SAR, PAD, and position co-ordinates of the element

2. Validation

The first validation step of PowerDomus Cp routine has been performed by comparison with the results presented in the original work of Grosso et al. (1995b). Cp variations according to different parameters are presented.

A second validation step has been done comparing the results obtained by Wong and Chin (2002) for a more complex geometry for which the Cp value have been obtained by measurement and by the use of the CPCALC+ program. Additional calculations have been performed with the FORTRAN ESP-r routines.

A third validation has been performed comparing the Cp variation on different wall for three building shapes: a cube, a tall building, and a low building with large footprint. Comparisons were made with the wind tunnel data of Baines (1963) for a cubical building and a tall building with dimensions of 1:1:8 (length: width: height). The validation for a low - flat building 1:1:0.5 (length: width: height) is done using experimental data obtained from Architectural Institute of Japan(AIJ) report (1998).

A comparison exercise has been done comparing the results obtained by Larsen (2006) for isothermal natural cross ventilation.

2.1. Validation n°1

- Reference Cp

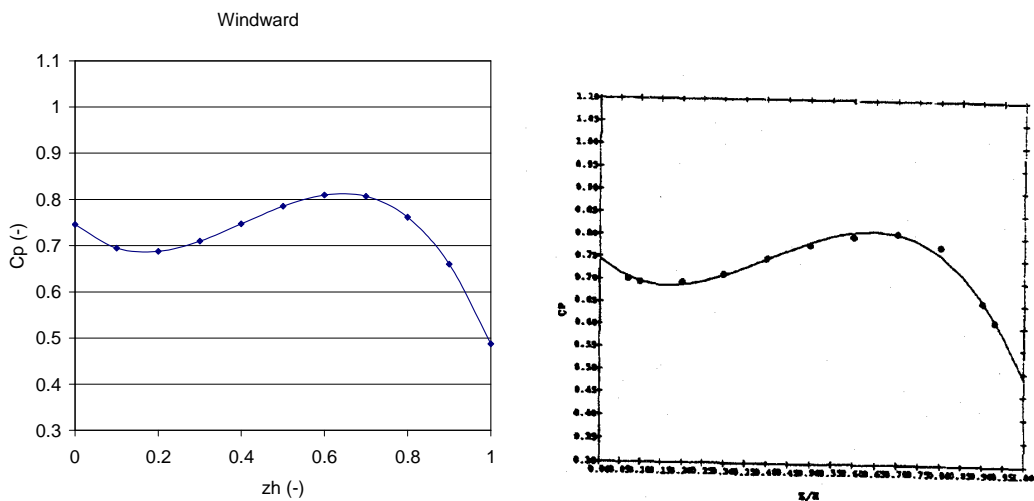


Figure 3: Reference Cp centerline profiles – Windward wall.

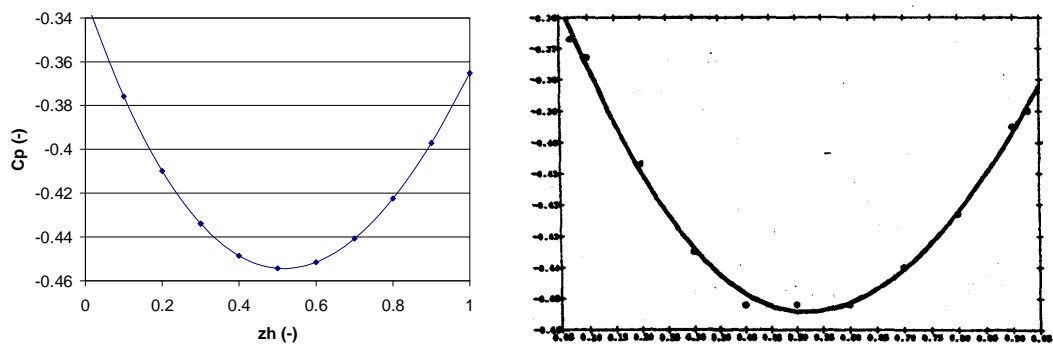


Figure 4: Reference Cp centerline profiles – Leeward wall.

- Cp correction for boundary layer profile

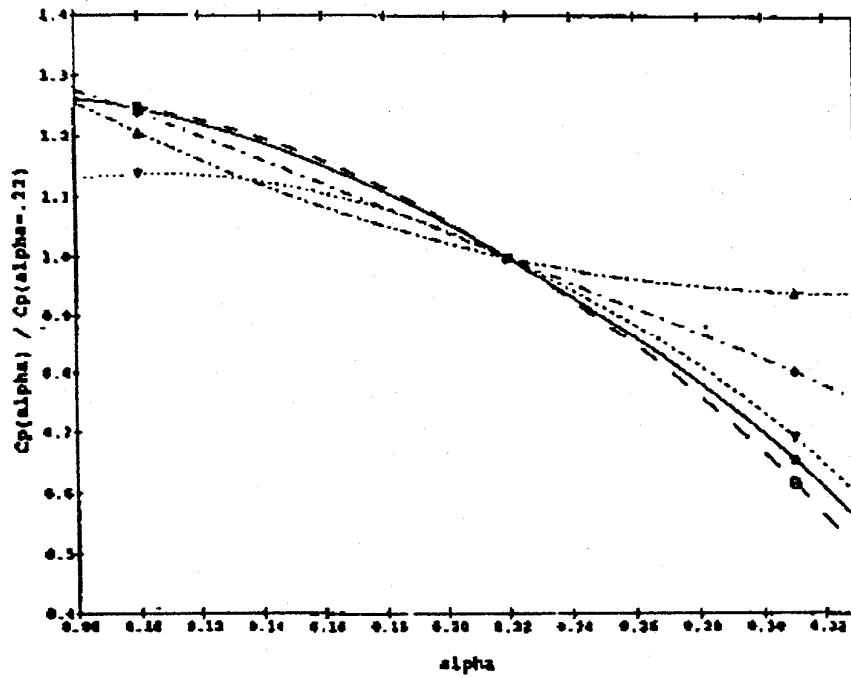
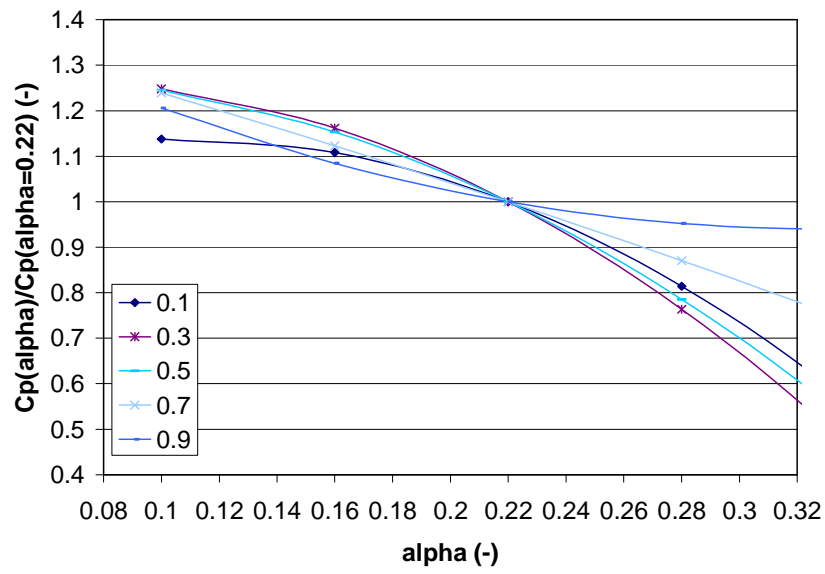


Figure 5: Cp correction for boundary layer profile – Windward wall.

- Cp correction for the Surrounding Area Density

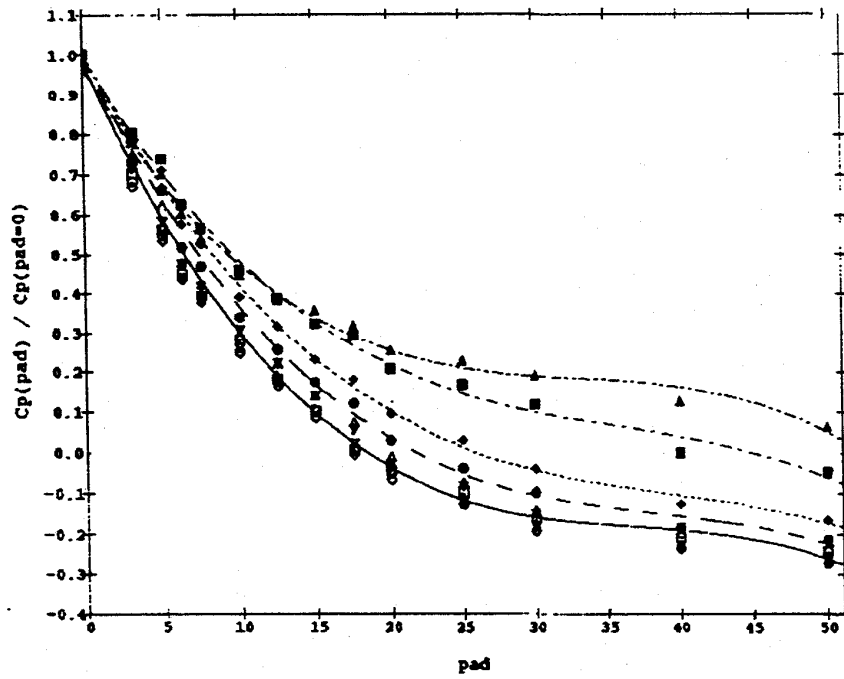
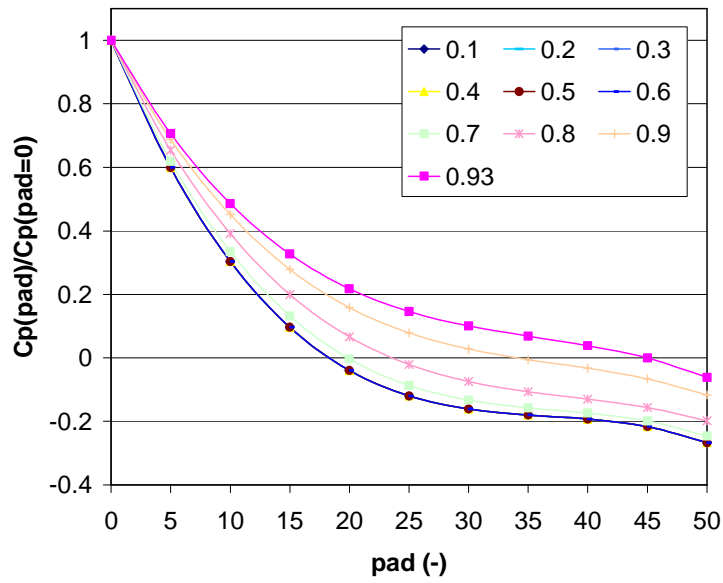


Figure 6: C_p correction for the Surrounding Area Density – Windward wall.

- **Cp correction for the Frontal Aspect Ratio**

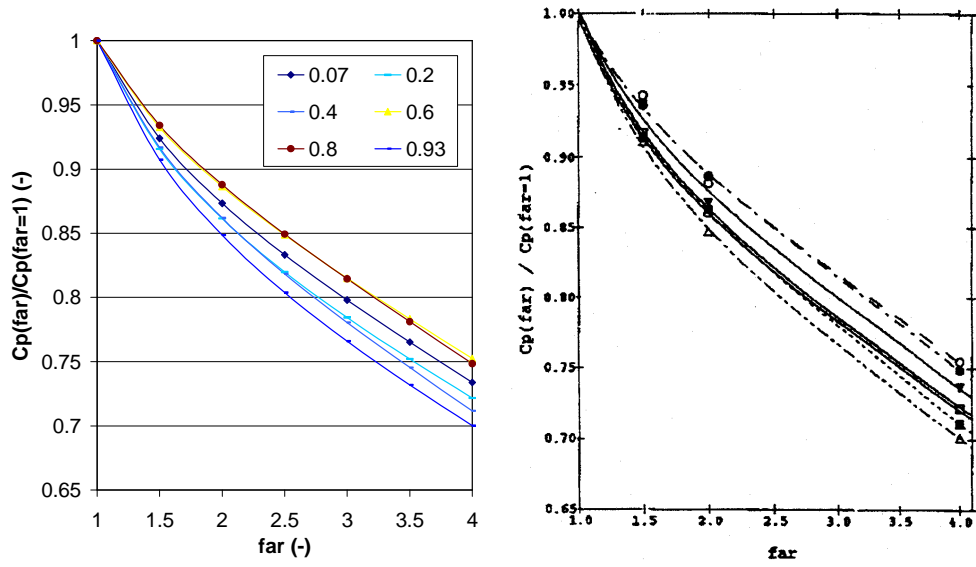
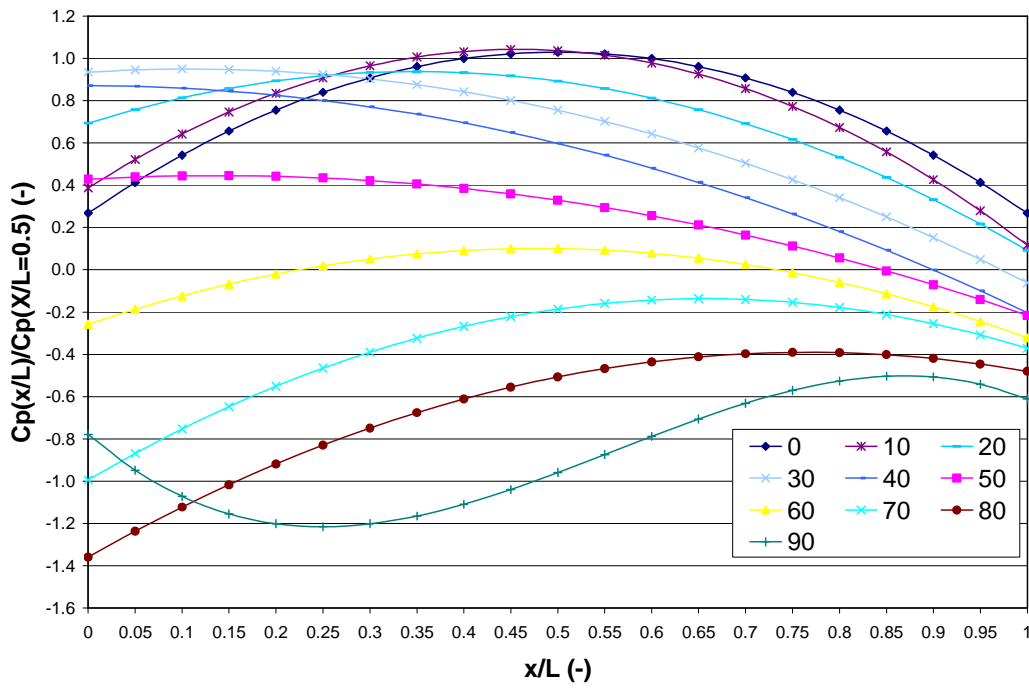


Figure 7: Cp correction for the Frontal Aspect Ratio – Windward wall.

- **Cp correction for the Horizontal Distribution in relation to the Wind Angle**



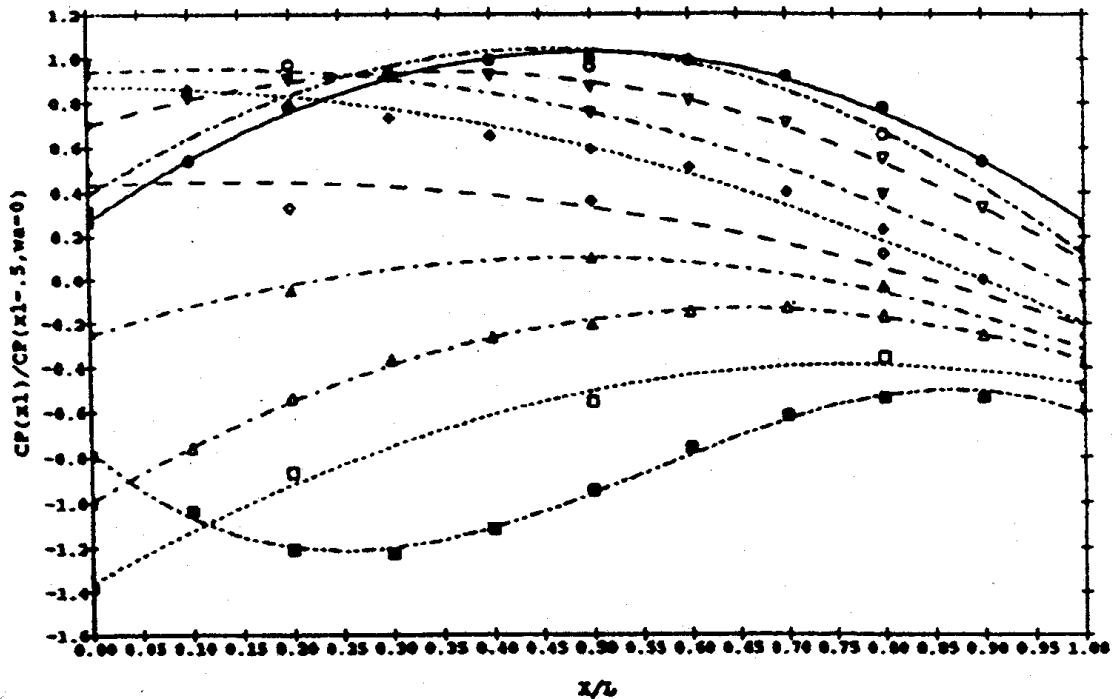


Figure 8: Cp correction for the Horizontal Distribution in relation to the Wind Angle – Windward wall.

2.2. Validation n°2

Figure 9 presents the studied geometry with the location of the sample points and other parameters.

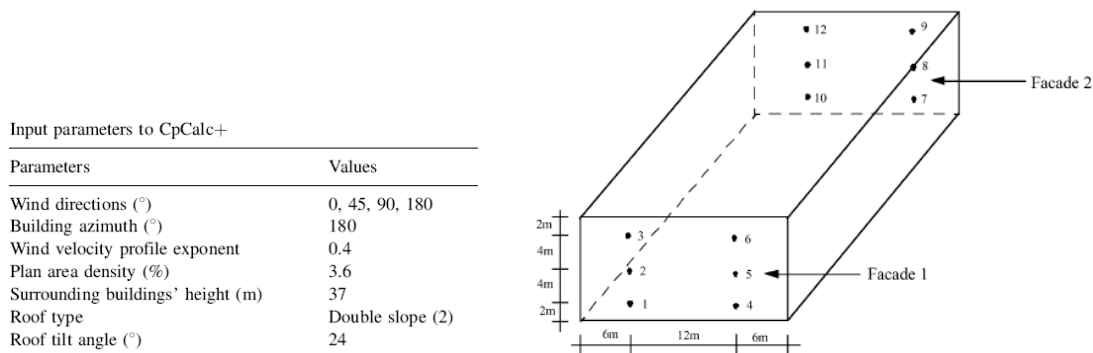


Figure 9: Geometry and CPCALC+ parameters.

Figure 10 presents the results obtained for wind to wall angle of 0°, 45° and 90°. First, for angles included in the dataset (i.e. 0° and 90°), the present routine gives the same results as that of ESP-r. For angles not included in the dataset (45° where data are only available for 40° and 50°), results differ only for the leeward wall. After investigation, an error of interpolation has been discovered in the ESP-r code. As ESP-r gives values very close to those of CPCALC+, a problem for leeward façade and intermediate angle might exist in the CPCALC+ program. Note that the results obtained in this case with the present program are more in line with the experimental data. To investigate this potential problem, Figure 11 has been generated using CPCALC+. The rule for windward wall is simple: it uses the nearest value (40 for 42, 50 for 45 and 47) that is different from ESP-r rule (the nearest higher value, always 50). For the leeward wall, the problem of linearization observed in ESP-r code seems to be present in the CPCALC+ thus all values are different from (even if they are close to) the 40° curve.

Conclusion: it seems more appropriate to always perform a linear approximation for both situations. The new results are presented in Figure 12.

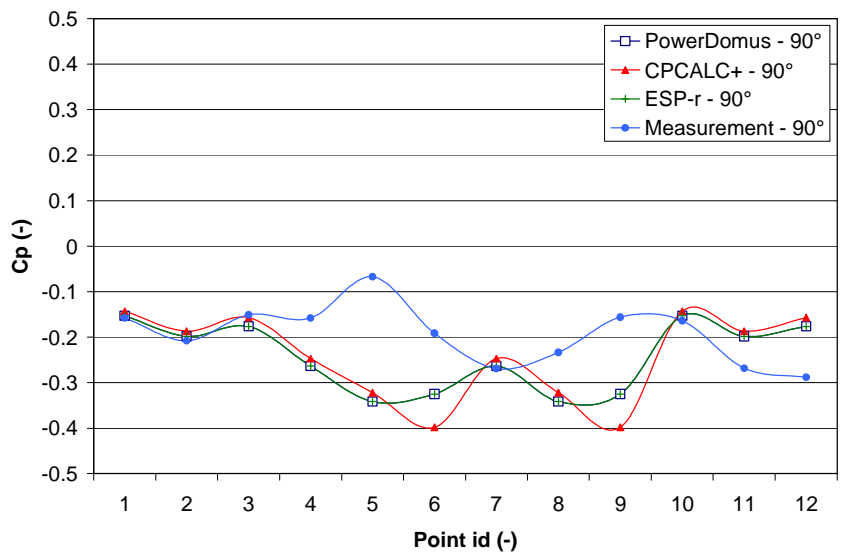
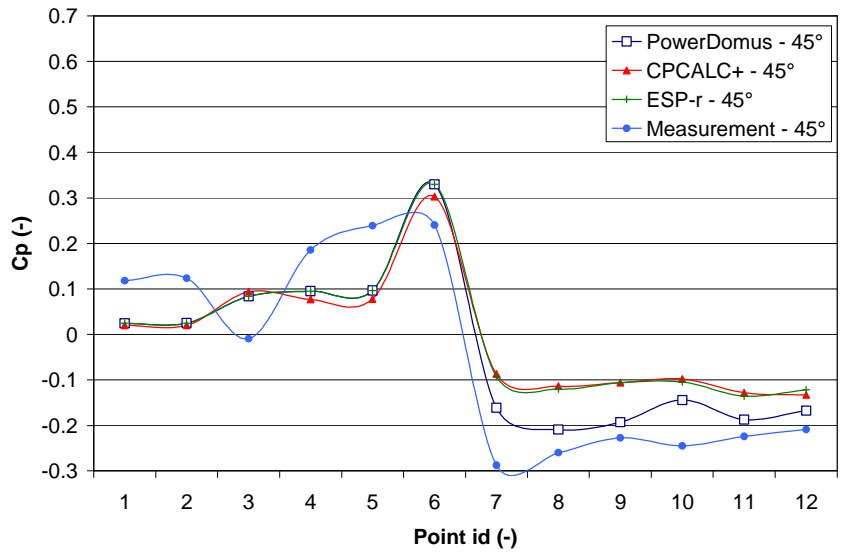
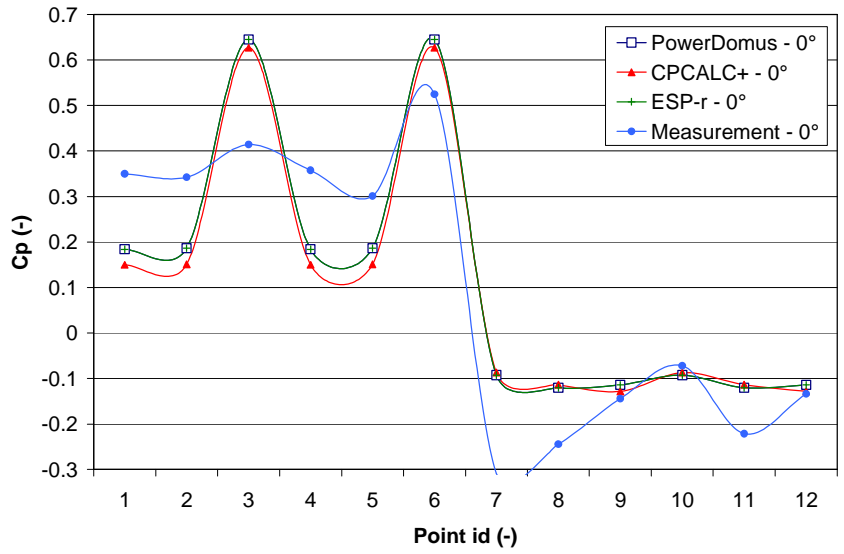


Figure 10: Cp values for wind to wall angle of 0°, 45° and 90°.

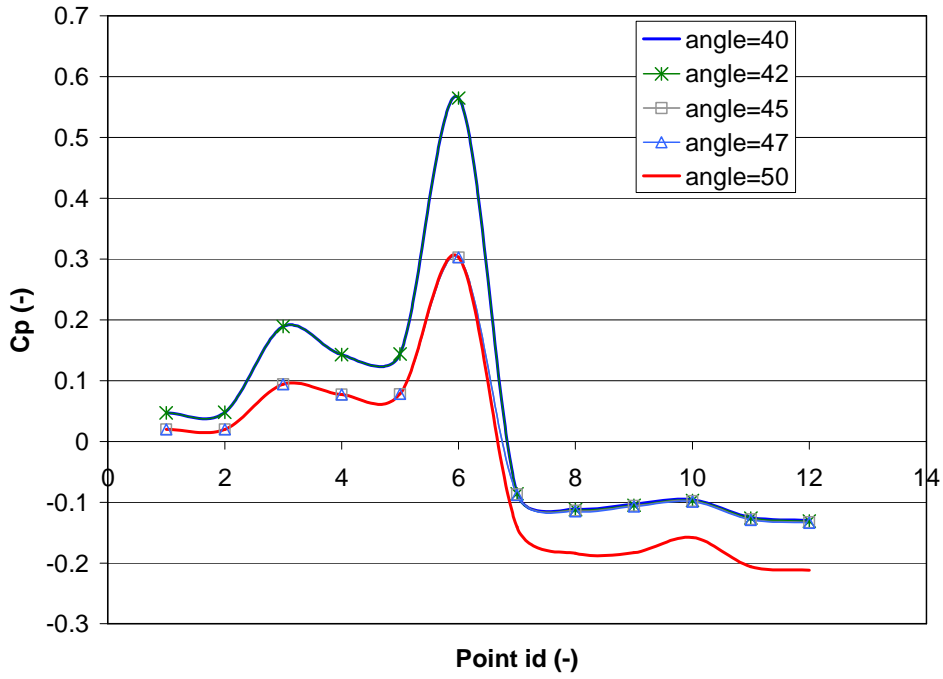


Figure 11: CPCALC+ variations with angle.

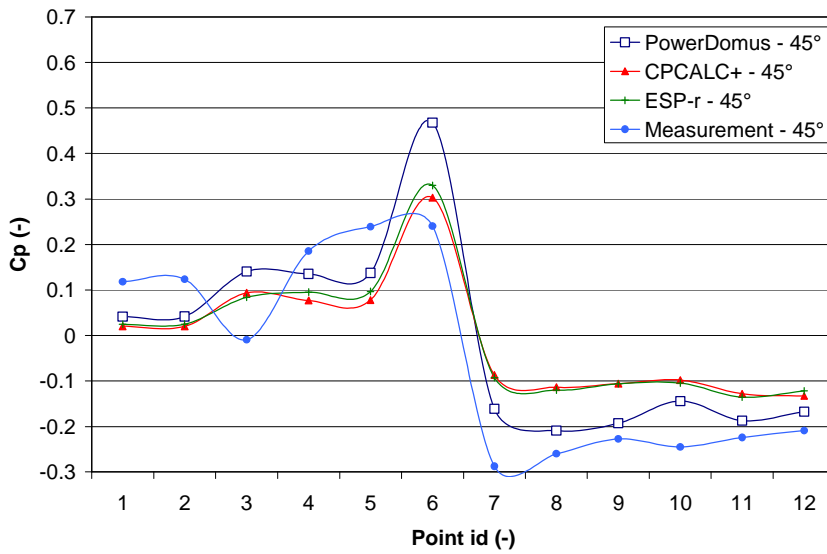


Figure 12: C_p values for wind to wall angle of 45° with the new calculation.

2.3. Validation n°3

Figure 13 to 15 presents the results for cubical, tall and low-flat buildings. The environmental parameters used here are: $a=0.25$, $pad=0$ and $sbh=H$ (H =building height). For sidewalls, the walls are considered with an angle of $+85^\circ$.

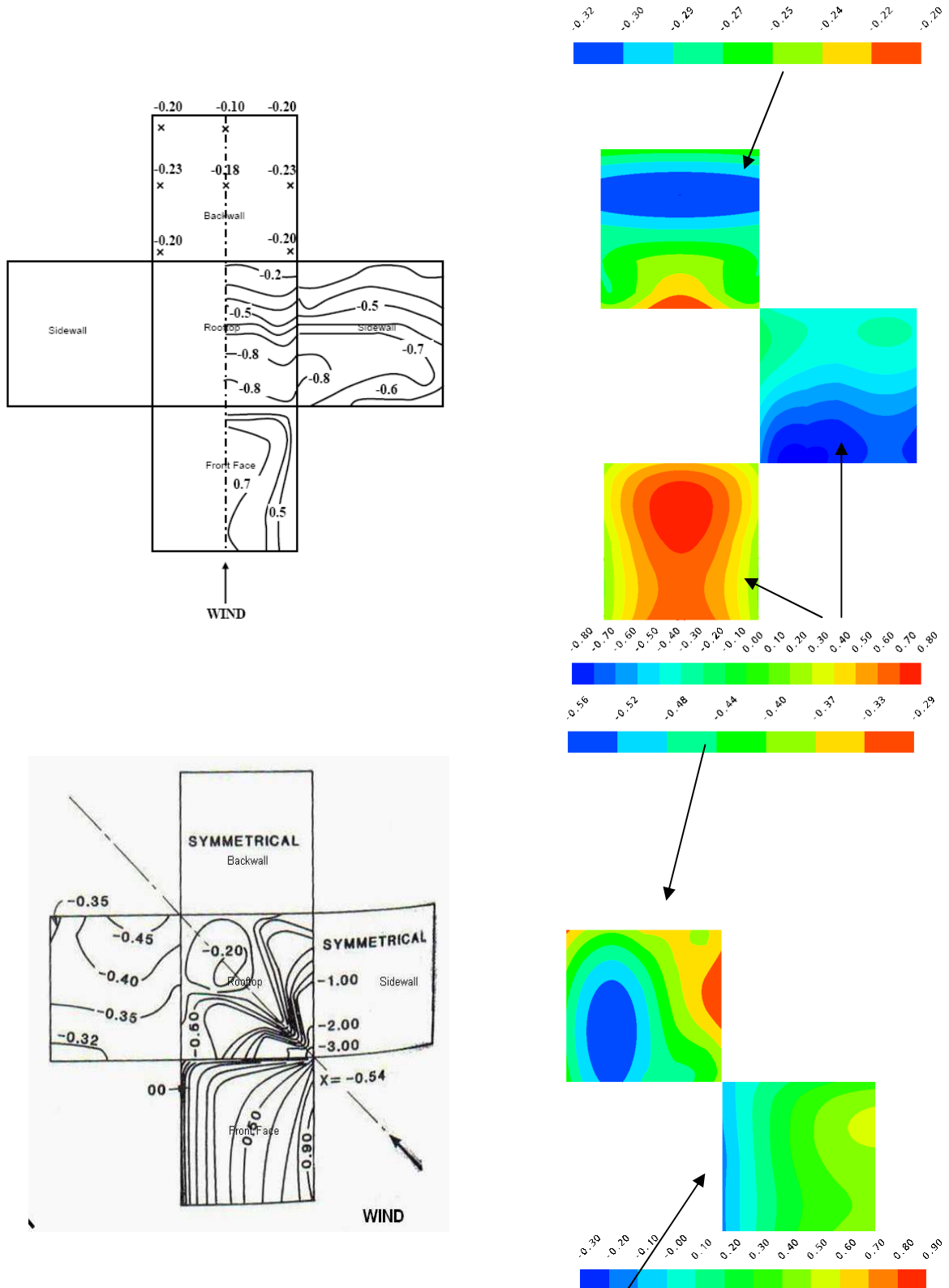


Figure 13: Wind-tunnel measurements (left) and present calculation (right) of the pressure coefficient on a cubical building for a shear inflow perpendicular to the building face (up) and with a 45° angle (down) after Baines (1963).

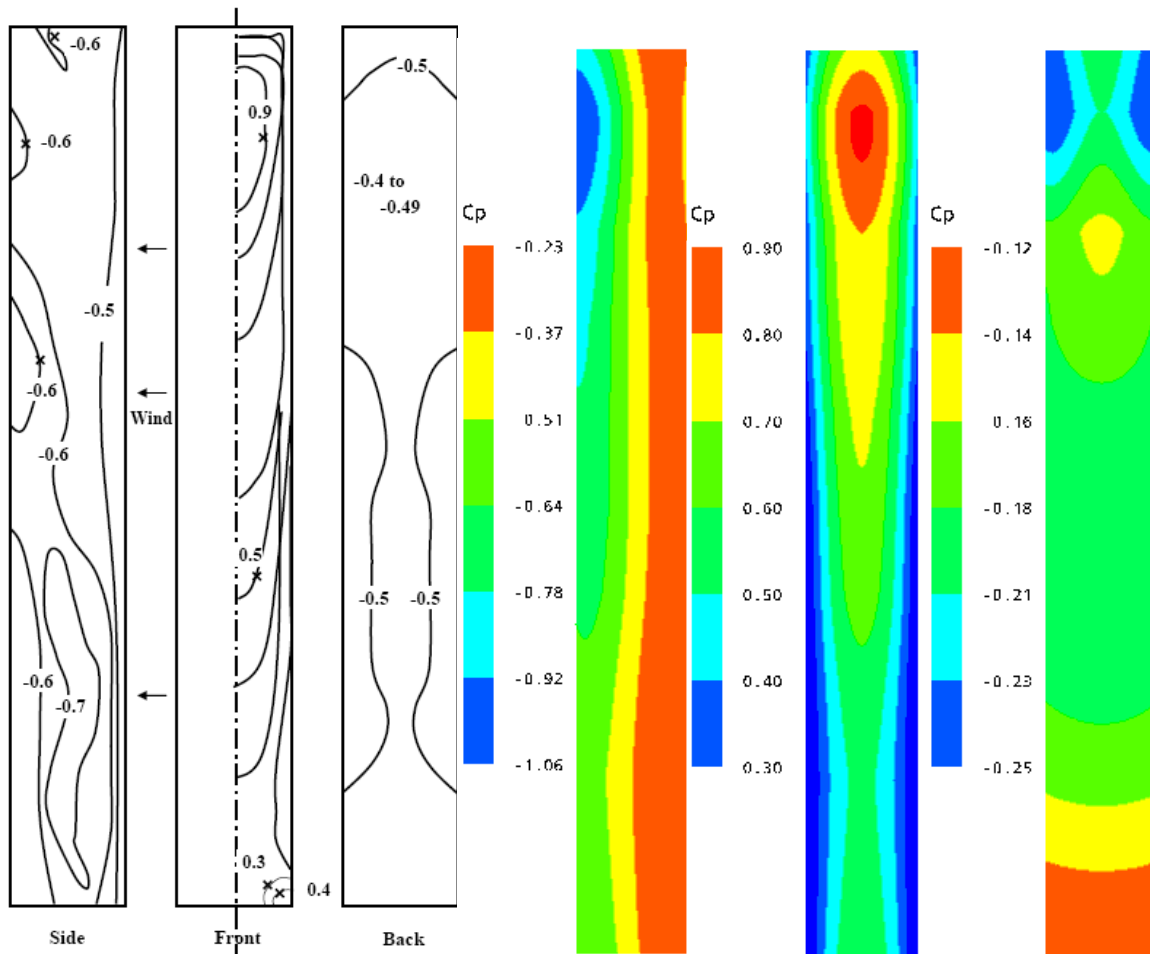


Figure 14: Wind-tunnel measurement after Baines (1963) (left) and present calculation (right) for a tall building for a shear inflow perpendicular to the building face (front).

In the case of a cubical building for normal wind (Figure 13), both the front and side wall C_p values are very well predicted. The model predicts higher values for the back wall (+40%). With an 45° wind-to-wall angle, results are less precise.

In the case of a tall building (Figure 14), only the windward wall C_p coefficients are predicted correctly both in value and location. For the back wall, C_p values are underestimated by a factor 2. The predicted values for the side wall are within a wider range but represent well the vertical distribution. Note that this building is normally out of the scope of the present model as it has a frontal and side aspect ratio of $1/8 \gg 0.5$.

To finish, same conclusions can be done about the predictions of the present model for the low-flat building than the cubical one (Figure 15). Note: Figure 16 presents the same experimental results with CFD predictions.

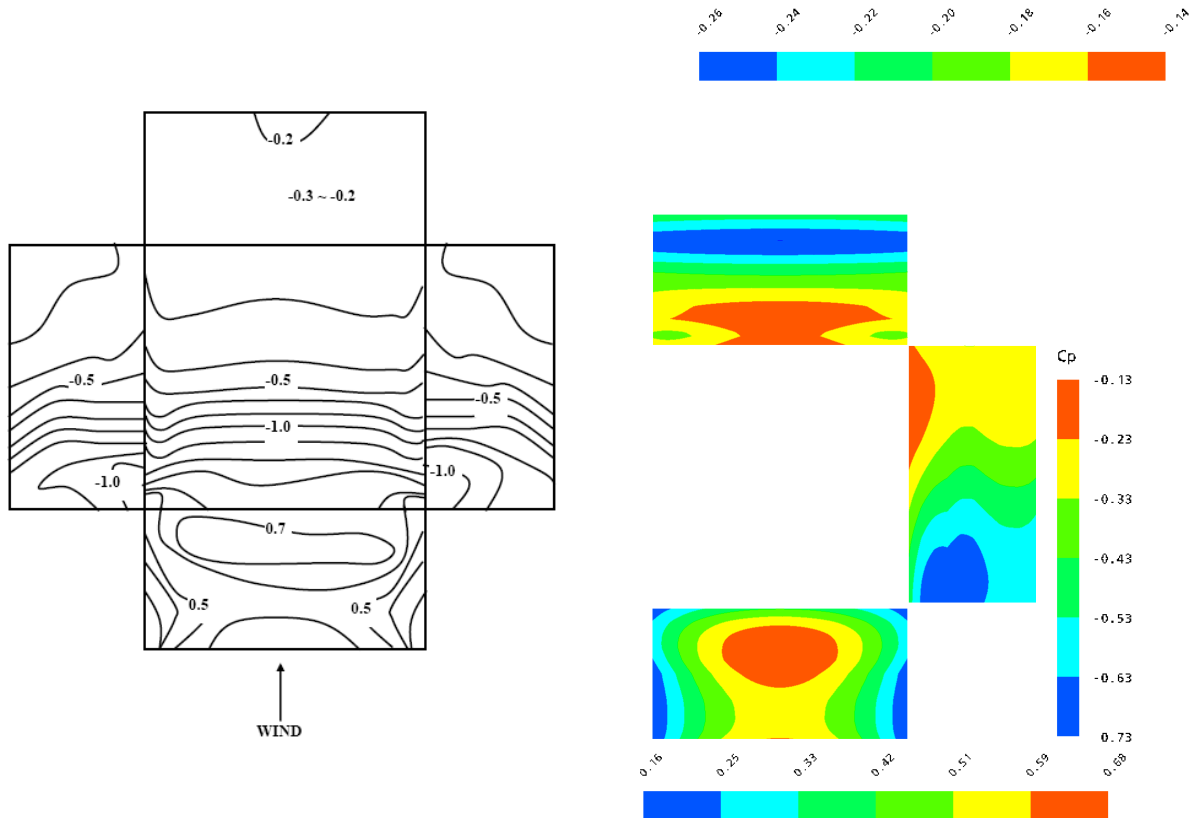


Figure 15: Wind-tunnel measurement after Baines (1963) (left) and present calculation (right) for a low-flat building for a shear inflow perpendicular to the building face (front).

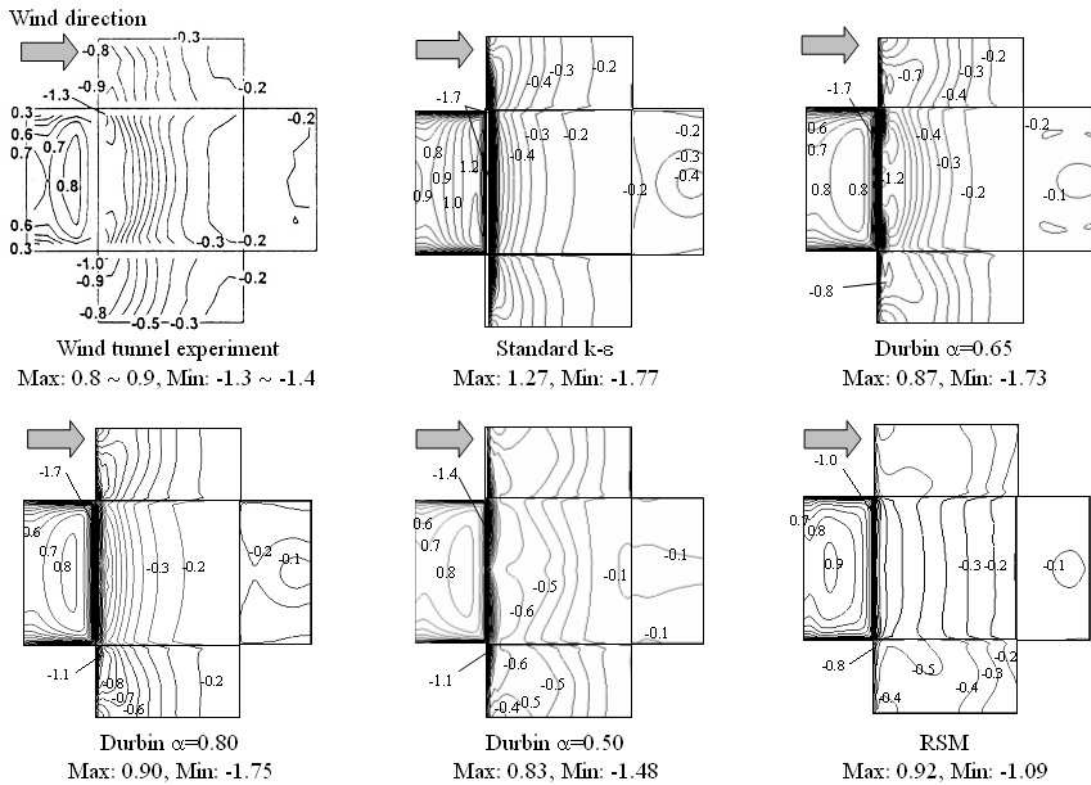


Figure 16: Wind-tunnel measurement after Murakami et al. (1996) and CFD simulations (Endo et al., 2005) for a low-flat building for a shear inflow perpendicular to the building face (front).

3. References:

- Architectural Institute of Japan, 1998: Numerical prediction of wind loading on buildings and structures.
- Baines, W.D., 1963: Effects of velocity distribution on wind loads and flow patterns on buildings. The symposium on wind effects on buildings and structure, Middlesex, England, National Physical Lab. 1, 197-225.
- Endo T., T. Kurabuchi, M. Ishii, K. Komamura, E. Maruta, T. Sawachi. 2005. Study on the numerical predictive accuracy of wind pressure distribution and air flow characteristics. Part 1: Optimization of turbulence models for practical use. International Conference "Passive and Low Energy Cooling for the Built Environment", May 2005, Santorini, Greece.
- Feustel, H.E., et al., "Fundamentals of the Multizone Air Flow Model - COMIS", International Energy Agency - Air Infiltration and Ventilation Centre, Technical Note AIVC 29, Coventry, Great Britain, May 1990.
- Grosso, M., "Wind Pressure Distribution around Buildings - a Parametrical Model", Energy and Building, Volume 18, No. 2, Elsevier, Sequoia S.A., Lausanne, Switzerland, 1992.
- Grosso, M., "Modelling Wind Pressure Distribution on Buildings for Passive Cooling", Proceedings of the International Conference Solar Energy in Architecture and Urban Planning, Commission of the European Communities, Florence, 17-21 May, 1993.
- Grosso, M., Marino, D., Parisi, E., "Wind Pressure Distribution on Flat and Tilted Roofs: a Parametrical Model", Proceedings of the European Conference on Energy Performance and Indoor Climate in Buildings, Lyon, France, November 24-26, 1994.
- Grosso M. 1995a. CPCALC+ CALCULATION OF WIND PRESSURE COEFFICIENTS ON BUILDINGS, PASCOOL Research Program Report, Turin, Italia.
- Grosso M., D. Marino, E. Parisi. 1995b. A wind pressure distribution calculation program for multizone airflow models. Building Simulation, Madison, Wisconsin, USA.
- Larsen T.S., 2006. Natural Ventilation Driven by Wind and Temperature Difference, PhD dissertation, Department of Civil Engineering, Allborg University, Denmark.
- Liddament, M. W., "Air Infiltration Calculation Techniques - an Applications Guide", Air Infiltration and Ventilation Centre, Bracknell, U.K., 1986.
- Murakami, S., A. Mochida, K. Kondo, Y. Ishida and M. Tsuchiya, 1996. Development of new k- ϵ model for flow and pressure fields around bluffbody. CWE96, Colorado, USA.
- Wong N.H., H.K. Chin. 2002. An evaluation exercise of a wind pressure distribution model. Energy and Buildings, 34, pp. 291-309.

Annex 2: Equipment Data

The last annex of this work presents all technical data adopted during the simulations performed into the PowerDomus software. Here, it will be found technical documents with technical characteristics of the following components:

1. *Fan Technical data and curves*: The fan technical specifications presented in this annex corresponds to the fan adopted for the hybrid ventilation strategy that have been showed in Chapter 7 (Ventilnorte, 2009).
2. *Panel Technical information*: The PV panels used in this document to perform photovoltaic simulations have been based on the technical information presented here (BP SOLAR, 2007).
3. *Battery Brochure*: The battery brochure has not been attached to this document due to copyright restrictions. However, the battery brochure can be found in the following reference: (MK Battery, 2009).

Série AT

Transmissão por correia

É possível com este tipo de ventiladores, usando várias relações de transmissão, obter uma grande gama de aplicações.

Ventiladores com turbina de pás inclinadas para a frente, cuja forma é estudada para permitir um alto rendimento, com baixa potência do motor e baixo nível de ruído.

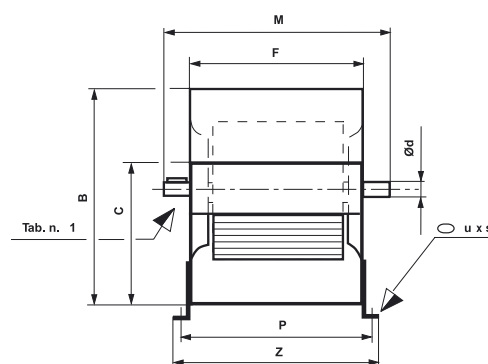
SIMPLEX

São designados pela sigla "SS"

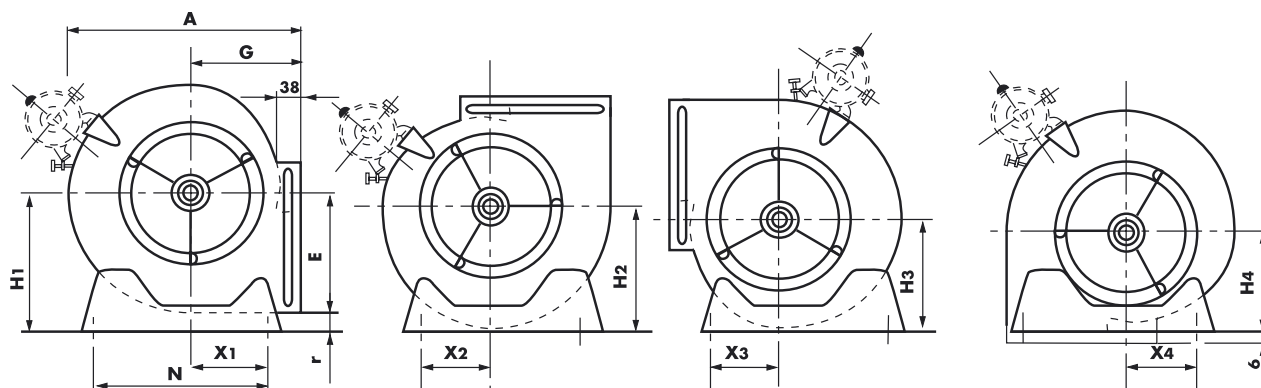
O ventilador SIMPLEX é o ventilador centrífugo tradicional.

As suas características principais são:

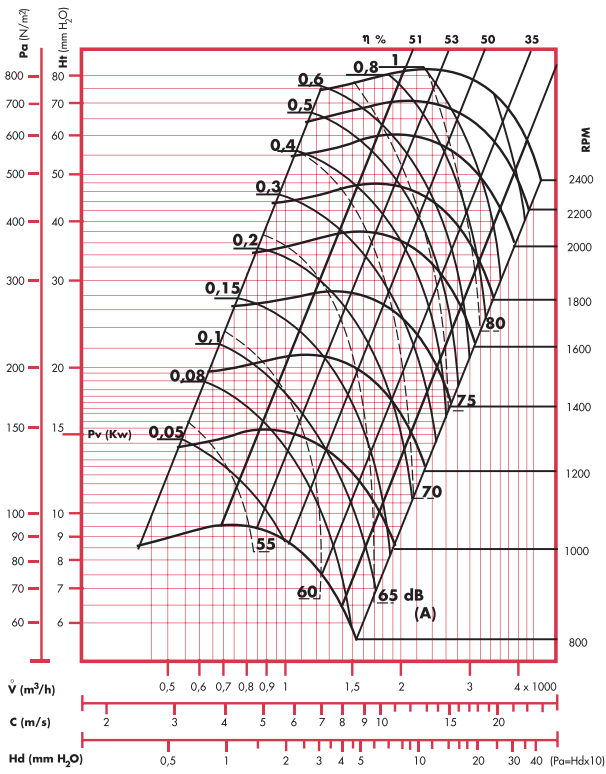
- Baixo nível de ruído
- Alto rendimento
- Facilidade de montagem
- Possibilidade de orientação da boca de descarga em 4 posições
- Disponibilidade de acessórios de montagem
- Pés com apoios anti-vibratórios
- Suporte de motor



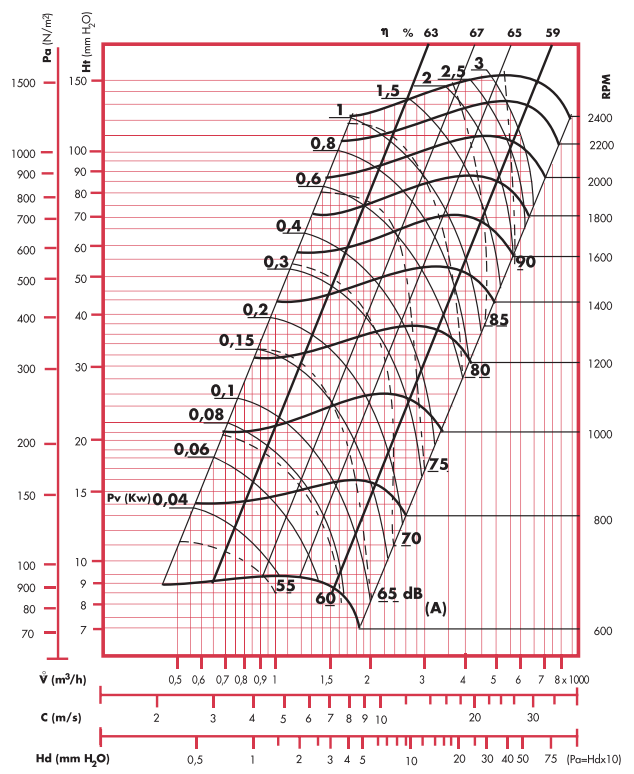
TIPO	A	B	C	E	F	G	H1	H2	H3	H4	M	N	X1	X2	X3	X4	P	Z	r	ød	u x s
AT 7-7	316	325	208	186	232	153	203	169	145	147	321	225	117	86	88	47	258	282	17	20	11 x 16
AT 9-7	380	387	262	215	232	185	253	199	177	179	321	300	119	124	123	120	258	282	38	20	11 x 16
AT 9-9	380	387	262	215	298	185	253	199	177	179	388	300	119	124	123	120	324	348	38	20	11 x 16
AT 10-8	425	443	289	249	265	203	287	227	198	197	355	340	136	132	135	132	291	315	38	20	11 x 16
AT 10-10	425	443	289	249	331	203	287	227	198	197	420	340	136	132	135	132	357	381	38	20	11 x 16
AT 12-9	491	521	341	294	309	230	332	266	232	224	420	408	161	153	161	153	335	359	38	25	11 x 16
AT 12-12	491	521	341	294	395	230	332	266	232	224	510	408	161	153	161	153	421	445	38	25	11 x 16
AT 15-11	569	609	404	342	373	264	380	309	272	258	510	495	197	211	201	200	399	423	38	25	11 x 16
AT 15-15	569	609	404	342	471	264	380	309	272	258	608	495	197	211	201	200	497	521	38	25	11 x 16
AT 18-13	684	739	478	415	430	314	457	376	340	307	567	608	262	283	278	288	456	480	42	25	11 x 16
AT 18-18	684	739	478	415	557	314	457	376	340	307	694	608	262	283	278	288	583	607	42	25	11 x 16



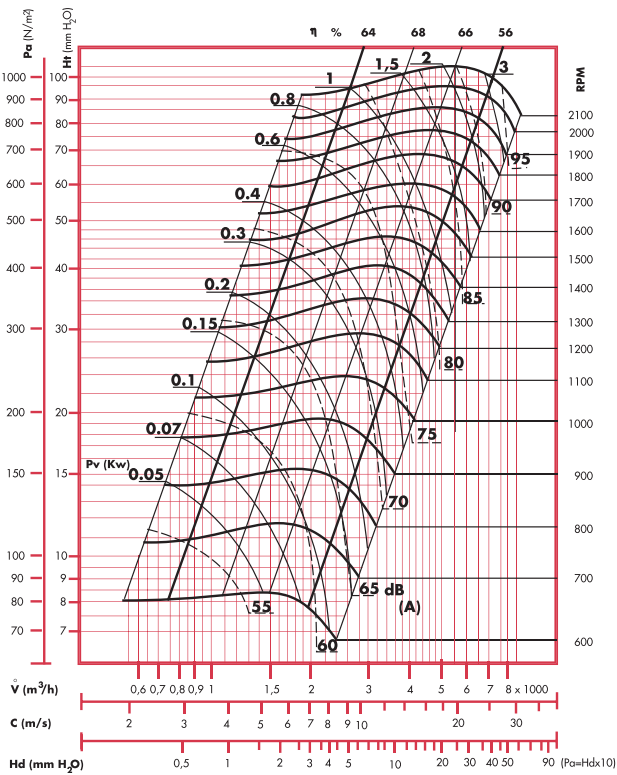
AT 7-7



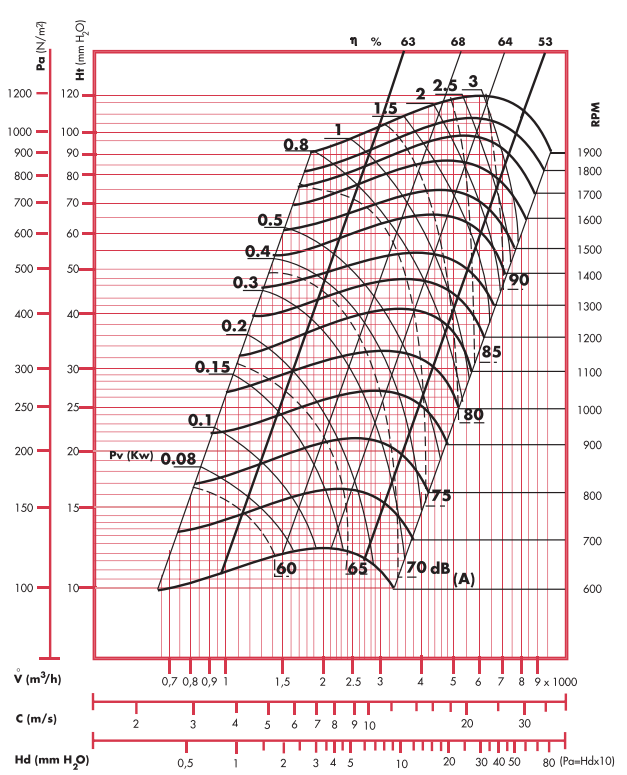
AT 9-7



AT 9-9



AT 10-8



High-efficiency photovoltaic module using silicon nitride multicrystalline silicon cells.

Performance

Rated power (P_{max})	50W
Power tolerance	$\pm 10\%$
Nominal voltage	12V
Limited Warranty ¹	25 years

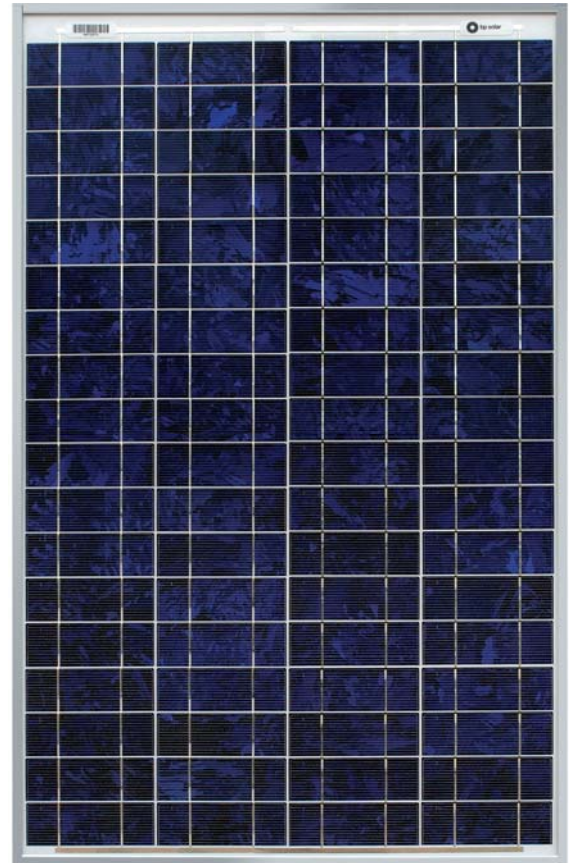
Configuration

J Clear universal frame and standard J-Box

Electrical Characteristics²

BP 350

Maximum power (P_{max}) ³	50W
Voltage at Pmax (V_{mp})	17.5V
Current at Pmax (I_{mp})	2.9A
Warranted minimum P_{max}	45W
Short-circuit current (I_{sc})	3.2A
Open-circuit voltage (V_{oc})	21.8V
Temperature coefficient of I_{sc}	$(0.065 \pm 0.015)\%/^{\circ}C$
Temperature coefficient of V_{oc}	$-(80 \pm 10)mV/^{\circ}C$
Temperature coefficient of power	$-(0.5 \pm 0.05)\%/^{\circ}C$
NOCT (Air 20°C; Sun 0.8kW/m ² ; wind 1m/s)	47 \pm 2°C
Maximum series fuse rating	20A
Maximum system voltage	50V (U.S. NEC & IEC 61215 rating)



Mechanical Characteristics

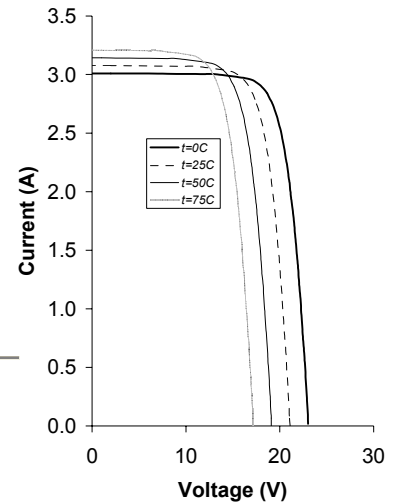
Dimensions	Length: 839mm (33")	Width: 537mm (21.1")	Depth: 50mm (1.97")
Weight	6.0 kg (13.2 pounds)		
Solar Cells	72 cells (42mm x 125mm) in a 4x18 matrix connected in 2 parallel strings of 36 in series		
Junction Box	J-Version junction box with 4-terminal connection block; IP 65, accepts PG 13.5, M20, ½ inch conduit, or cable fittings accepting 6-12mm diameter cable. Terminals accept 2.5 to 10mm ² (8 to 14 AWG) wire.		
Diodes	One 9A, 45V Schottky by-pass diode included		
Construction	Front: High-transmission 3mm (1/8 th inch) tempered glass; Back: White Polyester; Encapsulant: EVA		
Frame	Clear anodized aluminum alloy type 6063T6 Universal frame; Color: silver		

1. Module Warranty: 25-year limited warranty of 80% power output; 12-year limited warranty of 90% power output; 5-year limited warranty of materials and workmanship. See your local representative for full terms of these warranties.
2. This data represents the performance of typical BP modules, and are based on measurements made in accordance with ASTM E1036 corrected to SRC (STC.)
3. During the stabilization process that occurs during the first few months of deployment, module power may decrease by approx. 1% from typical P_{max} .

Quality and Safety

	Manufactured in ISO 9001-certified factories; conforms to European Community Directives 89/33/EEC, 73/23/EEC, 93/68/EEC; certified to IEC 61215
ESTI	Module power measurements calibrated to World Radiometric Reference through ESTI
	Listed by Underwriter's Laboratories for electrical and fire safety (Class C fire rating)
	Approved by Factory Mutual Research in NEC Class 1, Division 2, Groups C & D hazardous locations.

BP350 I-V Curves

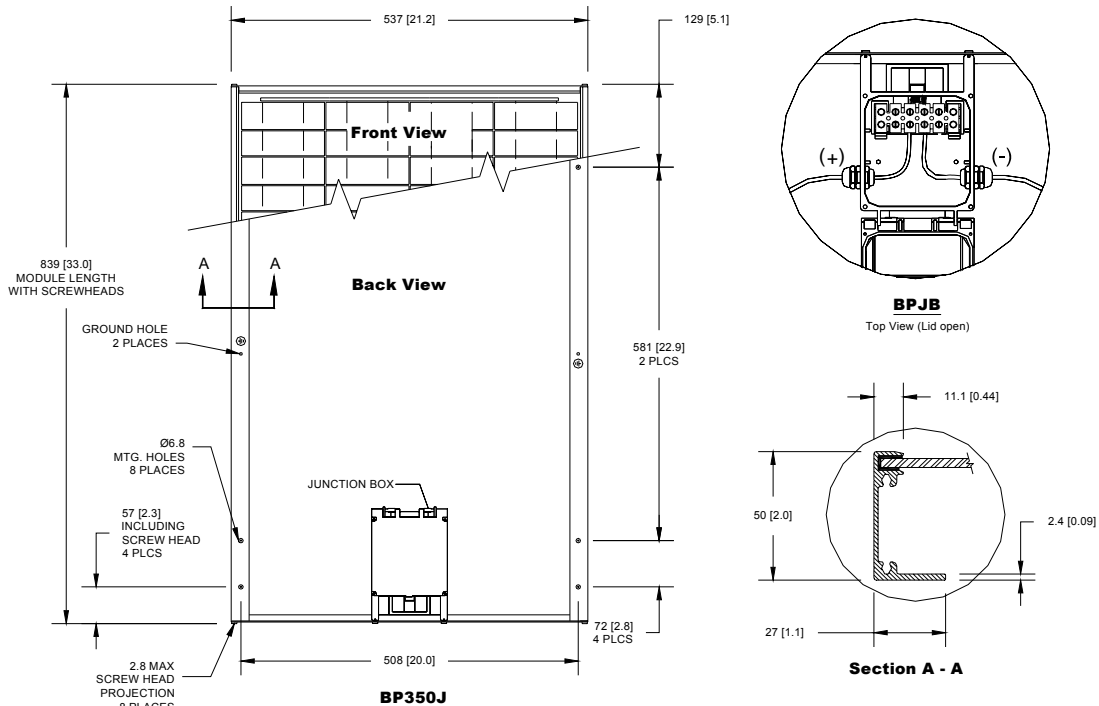


Qualification Test Parameters

Temperature cycling range	-40°C to +85°C (-40°F to 185°F)
Humidity freeze, damp heat	85% RH
Static load front and back (e.g. wind)	50psf (2400 pascals)
Front loading (e.g. snow)	113psf (5400 pascals)
Hailstone impact	25mm (1 inch) at 23 m/s (52mph)

Module Diagram

Dimensions in brackets are in inches. Un-bracketed dimensions are in millimeters. Overall tolerances $\pm 3\text{mm}$ (1/8")



Included with each module: self-tapping grounding screw, instruction sheet, and warranty document.

Note: This publication summarizes product warranty and specifications, which are subject to change without notice. Additional information may be found on our web site: www.bpsolar.com

